Catalized hydrogenation of cyanoboranes : from mechanistic investigation to the properties of cyclic BN compounds

Marion Beguerie

Université Fédérale
Toulouse Midi-Pyrénées

THÈSE

En vue de l'obtention du

DOCTORAT DE L'UNIVERSITÉ DE TOULOUSE

Délivré par :

Université Toulouse 3 Paul Sabatier (UT3 Paul Sabatier)

Présentée et soutenue par :
Marion BEGUERIE

le vendredi 27 octobre 2017

Titre :

Catalyzed hydrogenation of cyanoboranes:
from mechanistic investigation to the properties of cyclic BN compounds

Hydrogénation catalysée de cyanoboranes:
de l'étude du mécanisme à l'étude des propriétés de composés BN cycliques

---

École doctorale et discipline ou spécialité :

ED SDM : Chimie organométallique de coordination - CO 043

Unité de recherche :

Laboratoire de Chimie de Coordination - CNRS

Directeur/trice(s) de Thèse :

Sylviane Sabo-Etienne, Directrice de Recherche CNRS (directrice de thèse)
Gilles Alcaraz, Directeur de Recherche CNRS (co-directeur de thèse)

Jury :

Samuel Dagorne, SRCO, Directeur de Recherche CNRS, Strasbourg (Rapporteur)
Michael Hill, Professeur, University of Bath, UK (Rapporteur)
Blanca Martin-Vaca, Professeur, LHFA, Université Paul Sabatier Toulouse 3 (Examinatrice)
Hélène Olivier-Bourbigou, Directrice de département IFPEN, Solaize (Examinatrice)
Gilles Alcaraz, Directeur de Recherche, ISCR - CNRS, Rennes
Sylviane Sabo-Etienne, Directrice de Recherche, LCC - CNRS, Toulouse

“Personne ne sait tout mais tout le monde sait quelque chose”

Florence Nibart-Devouard

Acknowledgments

Ce travail a été possible grâce à la bourse du ministère de l'Ensègnement supérieur, de la Recherche et de l'Innovation.

First, I would like to thank the jury members for accepting to assess my Ph.D work. I thank Dr. Samuel Dagorne and Prof. Michael Hill acting as reviewers and Dr. Hélène Olivier-Bourbigou as well as Prof. Blanca Martin Vaca acting as examiners. I address a special thanks to Blanca who, beyond examining this work, supported me throughout the three years as my Ph.D godmother, a role that she took very seriously.

I would like to give all my gratitude to my supervisor Dr. Sylviane Sabo-Etienne, first for accepting me in the team and most importantly, for all what came after. I would like to thank her for her total implication in the project, for the motivating scientific discussions, but also for guiding me and giving me all the opportunities to make my Ph.D the rewarding experience I had imagined. Thank you for inspiring the next generations of women.

Merci au Dr. Gilles Alcaraz d'avoir participé à ma sélection pour ce projet et pour son implication dans le début du projet. Merci également de m'avoir méticuleusement formée au laboratoire.

Un grand merci au Dr. Sébastien Bontemps pour son attitude à la fois bienveillante et stimulante tout au long des trois ans. J'ai beaucoup appris grâce à nos discussions, sur le bore par exemple, toujours très ouvertes sur tout ce qu'il reste à découvrir. Merci aussi pour tous les conseils sur l'organisation de la pensée. Enfin, merci pour la confiance qu'il m'a donnée, qui m'a beaucoup aidée à mener à bien ce projet.

Merci beaucoup au Dr. Mary Grellier pour toute son aide. Que ce soit sur la théorie ou au laboratoire avec la boîte à gants, il a toujours répondu présent. Merci aussi pour ses conseils sur l'avenir. Enfin, merci pour sa bonne humeur, c'est toujours un plaisir de discuter.

Special thanks for my Ph.D twin brother Dr. Carlos Pinheiro. When I met you we were lab mates and I am very happy to count you as my friend today.

Sameh, merci pour tout. Nous avons travaillé côte à côte, au bureau et au laboratoire, toujours avec entraide, dans la bonne humeur et la motivation. On a partagé beaucoup de choses,mais surtout notre imagination et nos ambitions communes.

Merci à mes collègues de bureau, Elena et Paul, pour la bonne ambiance ainsi que pour le soutien pendant la rédaction de la thèse.

Thank you to all the other members of the O team: Emmanuelle Mothes, Dr. Gunnar Werncke, Julio Zamora Moreno, Vicky Corona, Dr. Yannick Escudié, Dr. Guanghua Jin, Dr. Aurélien Bethegnies, Sirine Layuni, Alexandre Mau, Dr. Paul Kläring, Cynthia Cuevas-Chavez, Nelson Nuñez, Sarah Desmons, Angelica Mejia Fajardo, Dan Zhang. I would like to thank you all, especially for the teamwork in the office and in the lab as well as for the great working atmosphere.

Un grand merci à Charlie Faradji avec qui je n'ai pas eu la chance de travailler en personne mais qui a commencé ce projet de recherche au cours de son stage de master.

I would like to warmly thank Prof. Jones for welcoming me in his team at the University of Rochester (New York, US) for a two months stay. I have learned a lot. I also would like to thank all the students of the team, Miles, Jing, Naveen, Hongmei and Ningyu for their excellent advices and kindness. I hope to see them or work with them in the future.

Merci à l'Institut des Sciences Chimiques de Rennes et au Dr. Véronique Guerchais de m'avoir accueillie dans son équipe pour une période d'environ deux mois. Merci en particulier à toutes les personnes qui m'ont guidée pour les mesures photochimiques, les Dr. Julien Boixel et Dr. Olivier Mongin, et merci au Dr. Corinne Lagrost pour les mesures électrochimiques ainsi que ses précieux conseils.

Je souhaite remercier les Dr. Iker Del Rosa et Dr. Chiara Dinoi avec qui nous avons collaboré pour les calculs théoriques. Merci pour votre grande implication et toutes les discussions qui ont joliment abouti.

Un grand merci à tout le personnel des services techniques du LCC et en particulier au Dr. Laure Vendier pour la DRX et à Francis Lacassin, David Paryl, aux Dr. Christian Bijani et Dr. Yannick Coppel pour la RMN. Je m'y suis toujours rendue avec plaisir.

Enfin, je remercie chaleureusement toute ma famille, mes amis, que j'ai la chance d'avoir dans ma vie et qui ont été là, pas seulement pendant ces trois années de doctorat, mais durant toutes ces années d'études, de construction de mon parcours et de ma vie. Je remercie Quentin pour avoir partagé chaque jour de cette expérience unique.

CONTENTS

AB	Amonia Borane
Ab	aminoborane
Bar(g)	Pressure gage
9-BBN	9-borabicyclo[3.3.1]nonane
$CNAr^{Dipp2}$	m-terphenyl isocyanide
COSY	COrrelation SpectroscopY
Cy	Cyclohexyl
Cyp	Cyclopentyl
DABCO	1,4-diazabicyclo[2.2.2]octane
dba	dibenzylideneacetone
DEPT	Distortionless Enhancement by Polarization Transfer
DMF	N,N-dimethylformamide
DOSY	Diffusion Ordered Spectroscopy
DFT	Density Functional Theory
HBcat	catecolborane
HBpin	pinacolborane
HMQC	Heteronuclear *Multiple* Quantum Coherence
HOMO	Highest Occupied Molecular Orbital
HSQC	Heteronuclear *Single* Quantum Coherence
HTM	Hole Transporter Materials
ICT	Internal Charge Transfer
Ipc(BH)	bis(4,6,6-trimethyl-3-bicyclo[3.1.1]heptanyl)boron
^{i}Pr	isopropyl
IR	InfraRed
LUMO	Lowest Unoccupied Molecular Orbital
NICS	Nucleus-Independent Chemical Shifts
PET	Photoinduced Electron Transfer
LED	Light Emitting Diode
Me	Methyl
NMR	Nuclear Magnetic Resonance
OLED	Organic Light Emitting Diode
OFET	Organic Field-Effect Transistor
PEPPSI™-IPr	Pyridine-Enhanced Pre-catalyst Preparation, Stabilization and Initiation
ppm	parts-per-million
$TBAPF_6$	Tetrabutylammonium hexafluorophosphate
^{t}Bu	tertiobutyl
THF	TetraHydroFuran

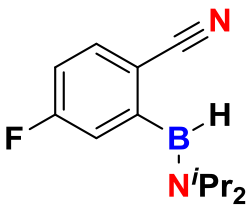

a1

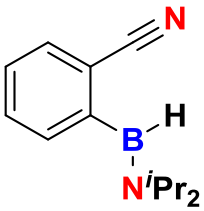

a2

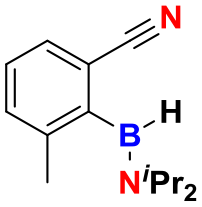

a3

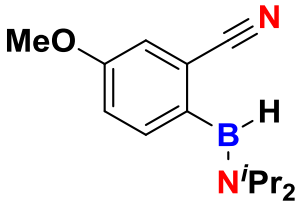

a4

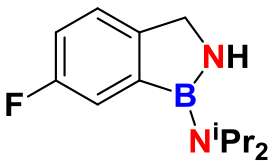

b1

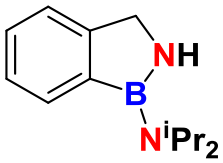

b2

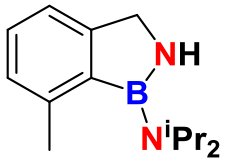

b3

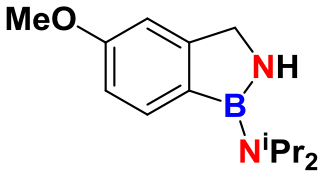

b4

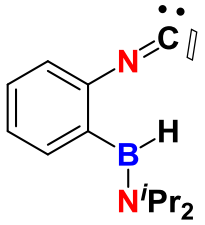

c

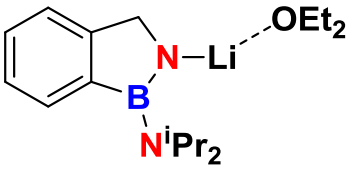

b2^{1}

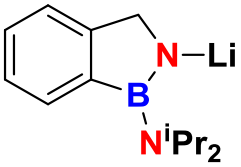

b2$^{1'}$

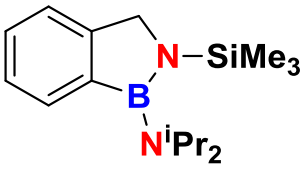

b2^{2}

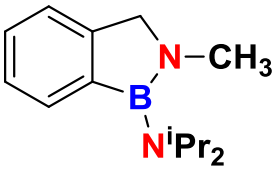

b2^{3}

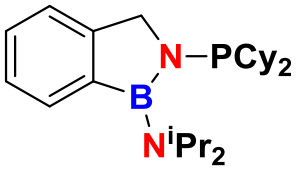

b2^{4}

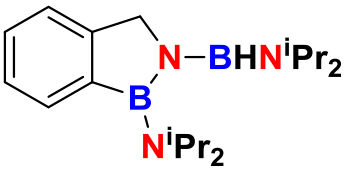

b2^{5}

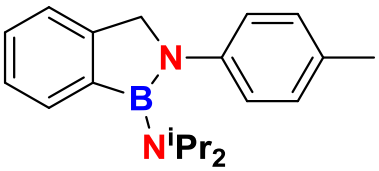

b2^{6}

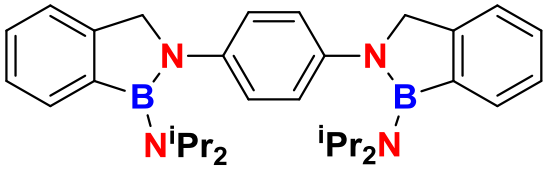

b2^{7}

List of compounds

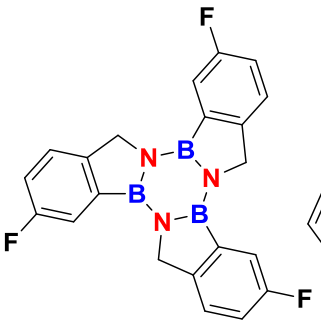

d1

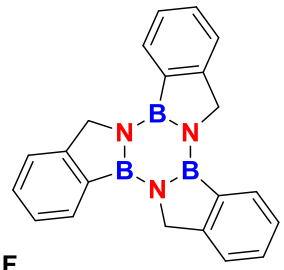

d2

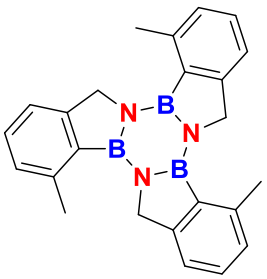

d3

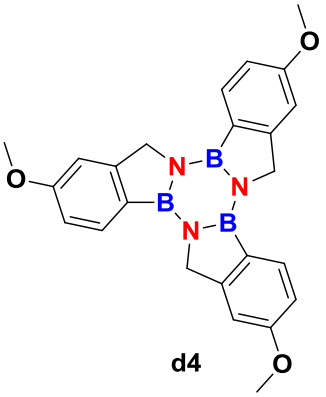

d4

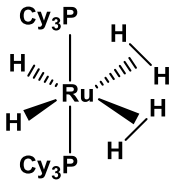

I

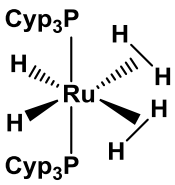

II

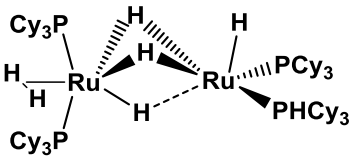

I-a

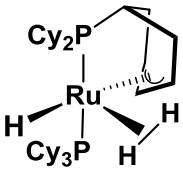

I-b

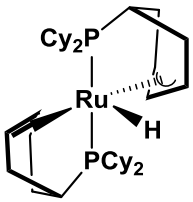

I-c

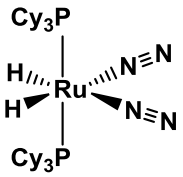

I-d

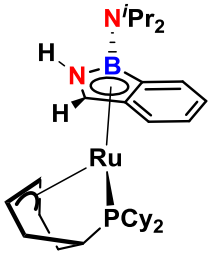

I-e

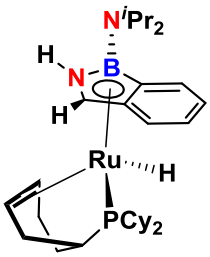

I-f

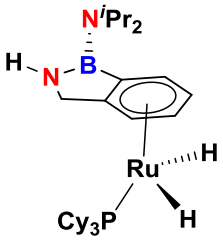

I-g

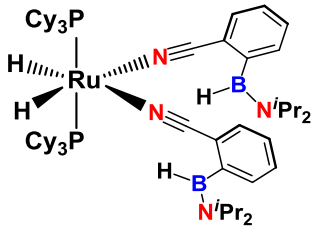

I-h

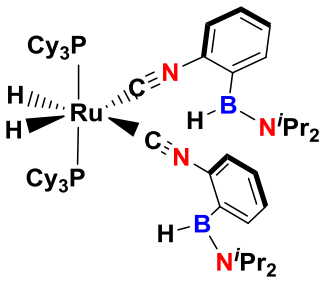

I-i

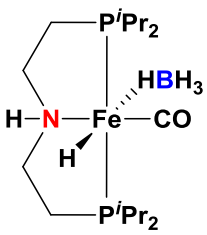

III-a

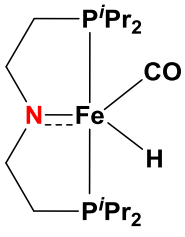

III-b

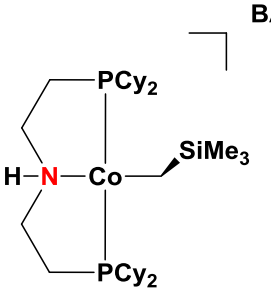

IV

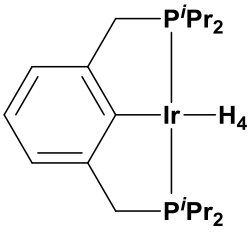

V

GENERAL INTRODUCTION

Catalysis is a naturally occurring process, in Nature and in a human body, partly responsible for life movement by constantly enabling efficient molecule transformations. Catalysis can be a selective process, breaking and making bonds with a low energy demand, reducing wastes and resource needs. For these reasons, it is a central principle in green chemistry and a key tool that organometallic chemists selected to address nowadays-societal challenges.

To name a few, it is necessary to diversify feedstocks to avoid depleting resources. In this respect, catalysts based on different elements, efficient biomass transformation, and inert molecules activation such as CO_2 or N_2 are needed. It is crucial to control wastes, to diminish pollution by designing selective and recoverable catalysts, recycling or biodegradable materials. A non-carbon emissive energy source such as H_2 is required to limit the greenhouse gas effect. Hence, catalysts enabling selective H_2O transformation for H_2 production as well as H_2 activation and transfer for the storage are of great importance. Besides, the discovery of environmentally friendly processes for known or new reactions is governed by catalysis. Thus, a fundamental understanding on the catalyst/substrate interaction and bonds activation are foundation to start answering the current challenges in coordination chemistry.

In this context, there is a growing interest for the development of very selective borane-mediated catalyzed transformations. The Suzuki-Miyaura coupling or the emerging versatile functionalization of C–H bonds via borylation enable efficient formation of a wide range of valuable products. One challenge in borane catalysis is also the control of B–H activation processes. On one hand, Lewis acid R_2B–H boranes meet the crucial challenge to reduce unsaturated functions with selectivity non-accessible otherwise, in mild conditions, while allowing a diversification of the catalytic systems. On the other hand, B–H bond catalytic activation within BNH compounds is placed at the center of attention for dihydrogen storage.

Despite sacrificial boron molecules are mostly produced, boron-containing compounds are indeed very attractive. In particular, the boron-nitrogen interaction endows the molecule with remarkable ability to release and transfer dihydrogen, with dynamic and optoelectronic properties as well as with interesting coordination chemistry on metal centers. Thus, the arousing interest in those old molecules called the development of synthetic methods. Strong efforts are made to access cyclic BN compounds along with their incorporation in electron-delocalized systems.

In this manuscript, we used the knowledge gained in B–H bond activation processes to allow the synthesis of uncommon boron containing molecules. In a previous study, the team showed that B–H bond activation of an aryl(phosphino)(aminoborane) with the bis(dihydrogen) complex $RuH_2(H_2)_2(PCy_3)_2$ led to the characterization of a unusual 3-center-2-electron coordination mode (σ-B–H) at a sp^2 boron (Figure 1). In another previous study, it was shown that $RuH_2(H_2)_2(PR_3)_2$ can selectively hydrogenate benzonitrile into benzylamine (Figure 1). Hence, in order to push the coordination study to a catalytic system, we have designed a new substrate in which the coordinative phosphine is replaced by a reactive nitrile function as depicted in Figure 1.

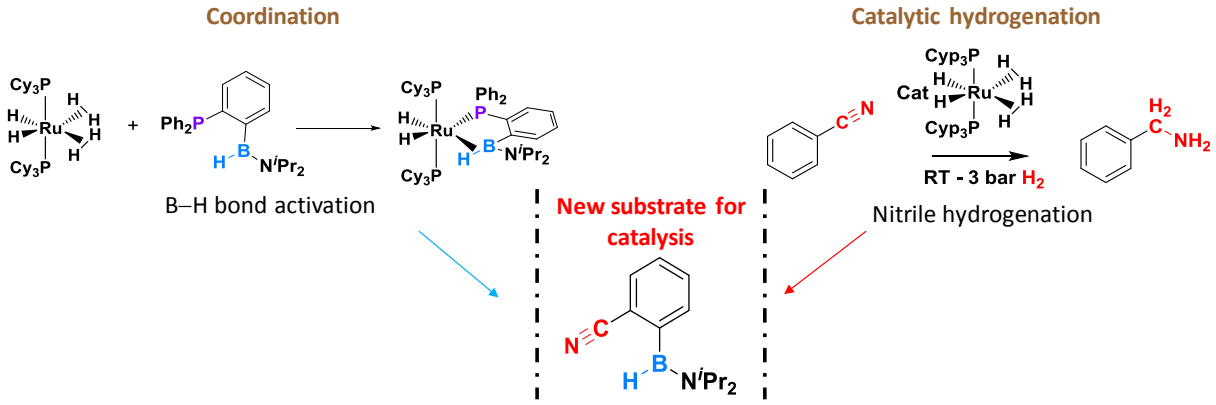

Figure 1: Previous work concerning B–H bond activation and nitrile hydrogenation with $RuH_2(H_2)_2(PR_3)_2$

After introducing the interest in BN containing molecules and addressing advances in CN bond reduction and B–H bond activation in chapter 1, the synthesis of a series of aryl(cyano)(aminoborane) will be presented in chapter 2. This new substrate was then exposed to a pressure of H_2 in the presence of $RuH_2(H_2)_2(PR_3)_2$ as catalyst precursor, that is to say, it was placed in conditions where both B–H and C≡N bonds could be activated. The net experimental result is:

- The cleavage of the B–H bond
- The hydrogenation of the C≡N bond
- The cyclization via B–N bond making

to yield the 1*H*-2,1-benzazaboroles represented in Figure 2. This catalytic reaction towards the synthesis of a series of 1*H*-2,1-benzazaboroles will be exposed in chapter 2. The described

transformation is situated at the crossroad of precedent studies using the bis(dihydrogen) ruthenium complex dealing in particular with:

- B–H bond activation leading either to agostic or bis $\sigma(B–H)$ -aminoborane complexes
- Catalyzed nitrile hydrogenation
- Catalyzed amine-borane dehydrogenation leading to cyclization

In the third chapter we will focus on the discovery of the elementary steps leading to the final 1*H*-2,1-benzazaboroles. The hydrogen transfer from the catalyst to the substrate as well as an investigation on the C≡N and B–H bond activation processes will be detailed.

As mentioned, boron and nitrogen containing molecules are of great interest in numerous fields. Thus, we will emphasize the synthetic potential of the newly formed 1*H*-2,1-benzazaboroles. Firstly, we will make use of the unique N–H moiety for this type of molecule. Nitrogen-functionalization and dehydrogenation of the heterocycle will be studied in chapter 4. Finally, we will demonstrate the cyclotrimerization of 1*H*-2,1-benzazaboroles to generate unprecedented planar borazines, BN analogues of truxene. The optoelectronic properties of such compounds will be detailed in chapter 5 and a discussion on the influence of the BN incorporation will be provided. The overall manuscript organization is depicted in Figure 2 with the 1*H*-2,1-benzazaboroles being the central point.

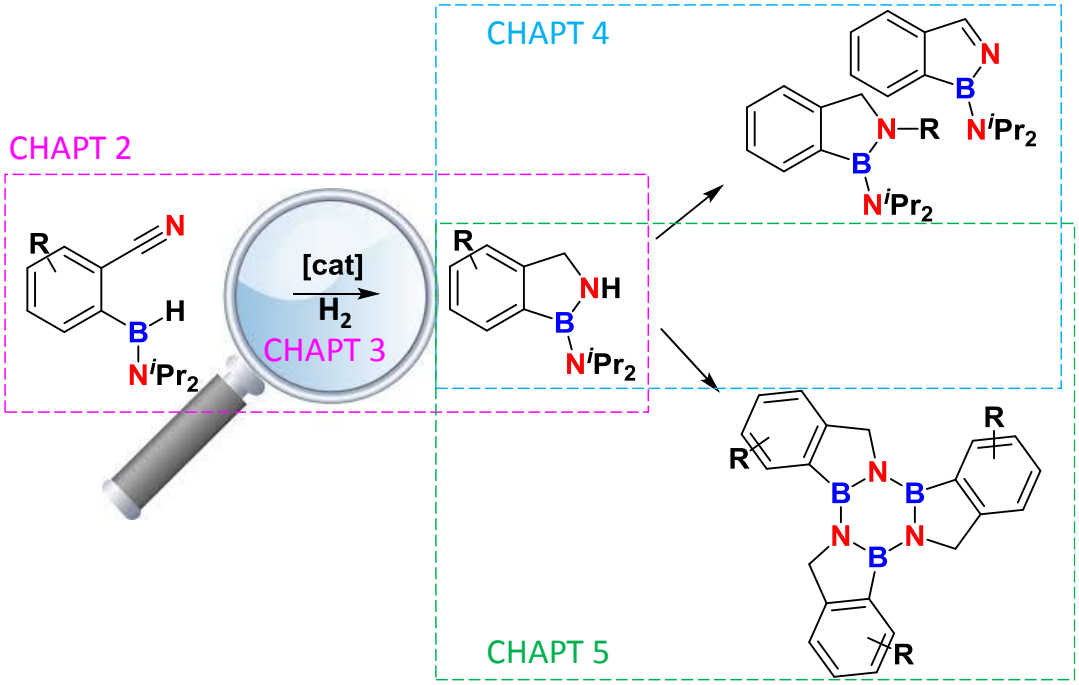

Figure 2: Overall organization of the manuscript

CHAPTER 1:

CYCLIC BN COMPOUNDS, B–H AND CN BOND ACTIVATION

CHAPTER 1: CYCLIC BN COMPOUNDS, B–H AND CN BOND ACTIVATION 9

CHAPTER 1: CYCLIC BN COMPOUNDS, B–H AND CN BOND ACTIVATION

This bibliographic chapter will be divided into two parts. The first section will highlight some applicative potential of BN compounds and detail the new interest in BN heterocycles. In the second part, B–N bond formation from B–H activation will be analyzed together with some key features of nitrile reduction. Mechanisms implying the activation of those two bonds will be emphasized. Then, we will focus on previous results concerning B–H and C≡N bonds activation with $RuH_2(H_2)_2(PR_3)_2$ complexes as an introduction to my Ph.D project that will be described in the next chapters.

I. Interest in BN compounds

I.1. Nature and properties of the B–N interaction

Boron is a scarce element on earth with 10^{-7}% in the earth's crust. It is rarer than ruthenium. Boron has been recognized as an element in 1824 by Jöns Jacob Berzelius and is still hard to isolate pure with nowadays-industrial processes. Most compounds found in nature are borate minerals such as borax often described as $Na_2[B_4O_5(OH)_4]\cdot 8H_2O$ in which boron is tri and tetra coordinated to oxygen. In nature, boron is also found bonding oxygen in the form of boric acid or borate as discovered in some natural bioactive boron-containing molecules.[1] Boron is also found bonding nitrogen in the form of natural cubic boron nitride, as recently discovered in the earth's mantle.[2] From borate minerals, a variety of boranes can be synthesized and are now widely used as reagents in organic and organometallic synthesis.

Boron is the first element and the only metalloid of the thirteen's row (electronic configuration $1s^2\ 2s^2\ 2p^1$). Trisubstituted sp^2 hybridized boranes possess a 2p vacant orbital, perpendicular to the substituents plane, which endows boron with strong Lewis acid character (Figure 1-1). Hence, in presence of a Lewis base, boron quaternaries *via* dative covalent bonding, resulting in a more stable sp^3 borane. Boron has a lower electronegativity than hydrogen, as a result the B–H hydrogen shows an hydridic character.

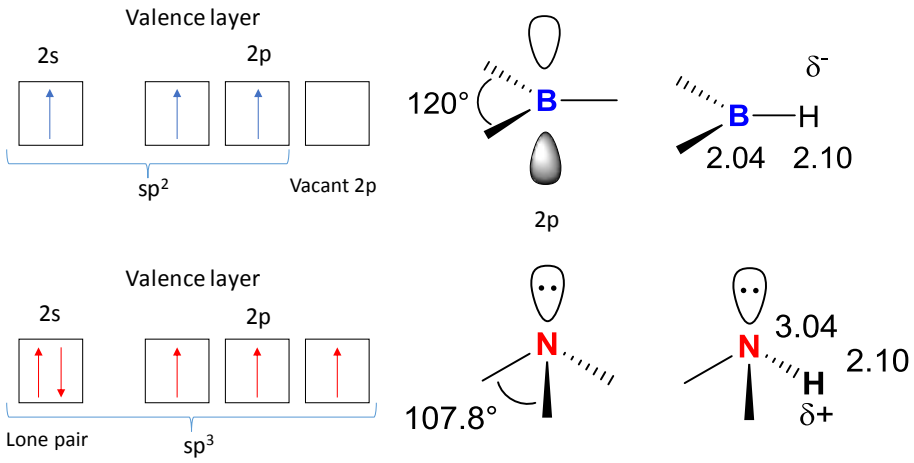

Figure 1-1: Hybridization and electronegativity at trigonal boron and nitrogen

Nitrogen is the first element of the fifteenth row (electronic configuration: $1s^2\ 2s^2\ 2p^3$). Mono, di or trigonal nitrogen species possess a lone pair likely to interact with electron deficient species such as sp^2 boranes (Figure 1-1). Trigonal nitrogen, relevant to the amine-borane and aminoborane chemistry, adopts a tetrahedral geometry, which is slightly distorted compared to Csp^3 due to the lone pair. Nitrogen has a greater electronegativity than hydrogen, as a result the N–H hydrogen shows a protic character.

I.1.1. Boron – Nitrogen interaction

Trisubstituted nitrogen, Lewis base, can react with trisubstituted boron, Lewis acid, to form amine-borane adducts (Figure 1-2). A dative covalent bond is formed between boron and nitrogen where the two electrons from the nitrogen lone pair interacts with the vacant orbital of the boron center. In this case, both atoms adopt a tetrahedral geometry and sp^3 hybridization. The simplest adduct with all substituents being hydrogens is called ammonia borane (AB). The bond dissociation energy (BDE) associated with this interaction is rather low with 113 kJ mol^{-1} for AB.[3] Bond lengths for such donor-acceptor compounds have been evaluated around 1.6 Å,[4] and precisely 1.58 (2) Å for $H_3N–BH_3$ by neutron diffraction.[5]

When boron and nitrogen are covalently linked, they form an aminoborane compound (Figure 1-2). The σ bond is much stronger than a dative covalent bond with a BDE of 456 kJ mol^{-1}.[3] In addition, the proximity of the nitrogen lone pair enables the interaction with the 2p orbital of

the boron resulting in π overlapping. This interaction is partial with the doublet not parallel to the 2p vacant orbital. In this respect, the covalent B–N bond is considered in between simple and double bonds that is to say it exhibits a double bond character (intermediate between the b and c configurations depicted in Figure 1-2). Strength of the π overlapping is governed by boron and nitrogen environment. More basic electron-donating substituted nitrogen and more acidic electron-withdrawing substituted boron favor boron-nitrogen π overlapping. Bond lengths give a good indication on the bond character. B–N simple and double bonds measure 1.51 and 1.31 Å, respectively.[6] Typical B–N bond lengths in aminoboranes will be expected within those values. This configuration stabilizes boron by lowering its Lewis acidity and prevents quaternarization.

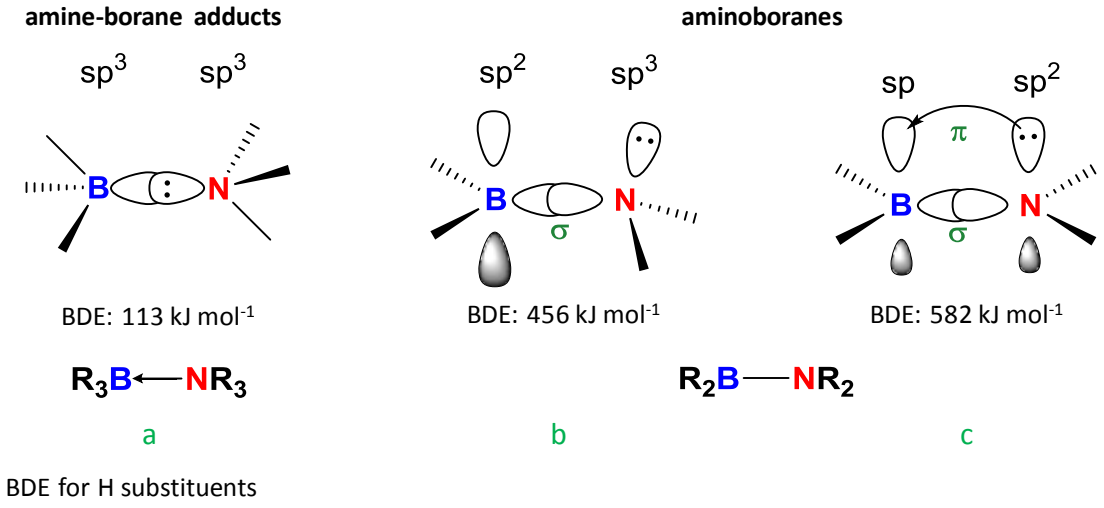

Figure 1-2: Amine-borane adducts (a) and aminoboranes (b,c) orbital configuration, BDE and developed representation

Throughout the manuscript, we will adopt a single bond B–N writing but remembering the double bond character.

Aminoborane (ab), NH_2BH_2, is the simplest molecule of the family with only hydrogen as substituents. Aminoborane is not known in the monomeric form. It can be produced from the dehydrogenation of AB and can be trapped on $RuH_2(H_2)_2(PR_3)_2$,[7] relevant to our work, and since then on other ruthenium, iridium and rhodium based metal complexes.[8-11] Otherwise, aminoborane readily dimerizes, trimerizes or oligomerizes as observed by NMR study throughout AB dehydrogenation.[12] Indeed, Lewis acid and Lewis basic centers coexist within the molecule favoring intermolecular reactions. Stabilization of the monomeric form can be

reached by decreasing Lewis acidity/basicity. This can be achieved either by reinforcing the B–N interaction and/or by adding bulky groups on boron and nitrogen atoms. Electron donating groups on nitrogen and electron withdrawing groups on boron have proven to strengthen the B–N bond by favoring pπ-nπ interactions.[13] For instance, Me_2NBH_2 dimerizes in organic solvents while $^{i}Pr_2NBH_2$, with bulkier and stronger donor substituents on nitrogen, is monomeric. $^{i}Pr_2NBH_2$ shows a deshielded triplet at 34.7 ppm in ^{11}B NMR compared to that of dimeric Me_2NBH_2 showing a triplet at 4.75 ppm.[14]

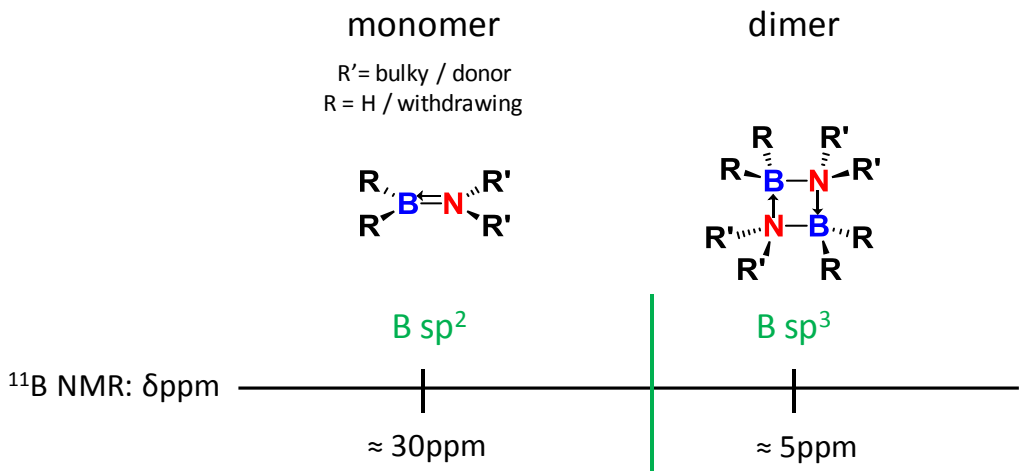

Figure 1-3: ^{11}B NMR generic values for monomeric and dimeric aminoboranes

On a general basis, downfield ^{11}B NMR signals refer to trigonal boron whereas upfield signals are assigned to electron richer tetragonal boron (Figure 1-3).

I.1.2. Comparison of BN and CC units

BN units are considered isoelectronic and isosteric to CC moieties. They both count 8 valence electrons shared by two atoms with the same connectivity. Amine-borane adducts are isoelectronic/isosteric to alkanes whereas aminoboranes are isoelectronic/isosteric to alkenes (Figure 1-4). Despite their electronic similarities, structural differences can be underlined such as the respective atomic radius as well as the electronegativity of the three elements.

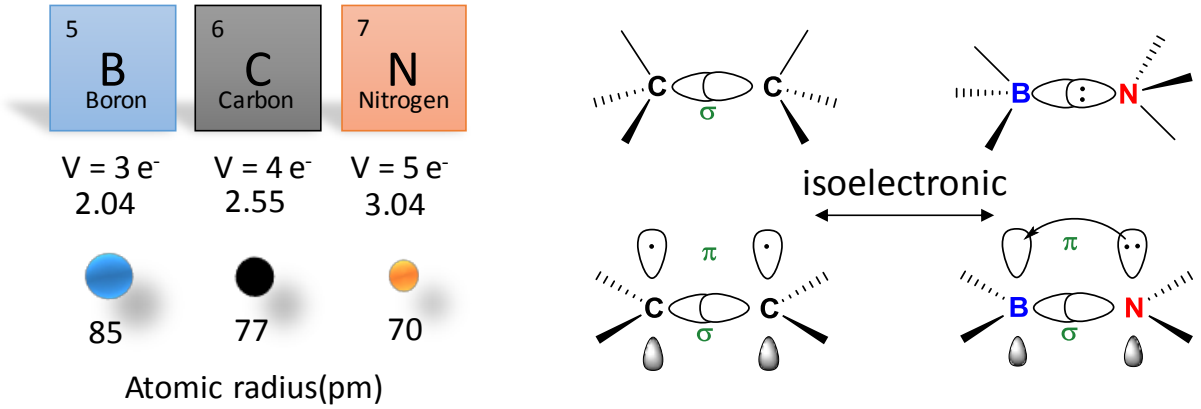

Figure 1-4: Comparison of BN and CC units

Most importantly, modifications in the bond properties are observed. One major distinction between BN and CC units is their polarity. Symmetric CC units are non-polar (μ = 0D)[15] whereas higher dipolar moment values are associated to BN units (AB: μ = 5.216 and ab: μ = 1.84 D).[16] One can note that significant reduced polarity is observed for the aminoborane. Based on that, incorporation of BN units in place of CC moieties in molecules can tailor their chemical behavior. Polarity within AB induces specific intermolecular interactions playing a role for hydrogen storage, as described in the next paragraph. A change in molecule solubility can also be noticed and used for cyclic aminoboranes to enhance *in vitro* aqueous solubility of synthetic biologically active compounds as recently described by Liu's research group.[17] The polar and weak BN interaction in amine borane adducts gives media dependent configuration and consequently interesting systems for dynamic applications such as sensing.

The reduced π overlapping in the BN moiety induces a change in electronic behavior when incorporated into electron-delocalized molecules. Thus, isoelectronic B–N to C=C bond is inserted into electron-delocalized systems to tailor optoelectronic properties of aromatic molecules and diversify the toolbox of molecules to find applications in materials science. Overall, BN containing molecules have broad potential in many challenging fields such as energy storage, catalysis, materials science and medicine. Examples relevant to my work described in this manuscript will be exposed.

I.2. Amine-borane adducts for dihydrogen storage

In the context of global warming, finding a non-carbon emissive energy source is necessary. Dihydrogen is a good candidate due to its high amount of energy available per kg. One technological challenge for the wide use of hydrogen-based energy is dihydrogen production from renewable resources. Production of dihydrogen from water is a very intense research area, particularly using solar energy for a photocatalytic water-splitting.[18] Another challenge is the safe storage of this gas, optimizing mass and volumetric H_2 content. Traditional physical-based solutions such as compression or liquefaction suffer from harsh pressure and temperature requirements. Material-based solutions, among which, hydrogen storage in chemical compounds represent an attractive option. Hydrogen rich BN species and particularly the simplest one, ammonia borane (AB), possess suitable properties for chemical hydrogen storage.[19-20] A general hydrogen storage principle with BN compounds is represented in Figure 1-5.

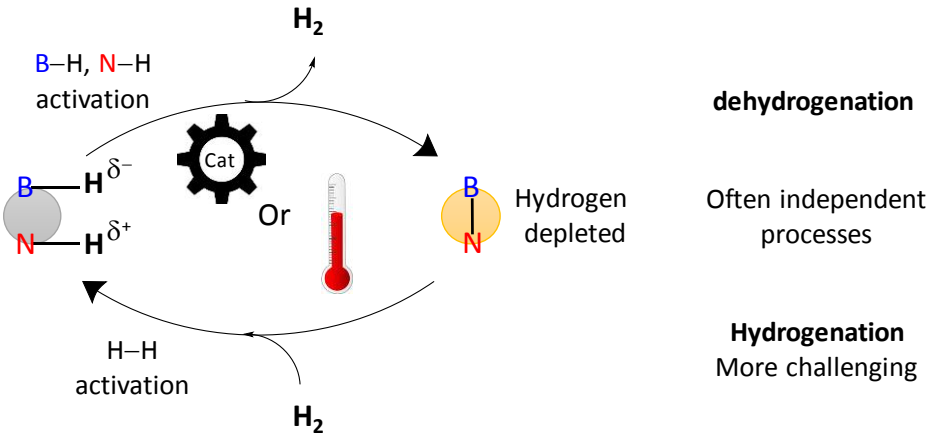

Figure 1-5: General principle of chemical hydrogen storage with BN compounds

AB is solid at room temperature unlike its carbon analogue ethane, which is gaseous in standard conditions. It is nonflammable and stable under standard conditions. AB has 19.5 wt% H_2 that meets the U.S. Department Of Energy hydrogen storage targets (5.5 wt% in 2020). Considering polarity differences within the molecule, AB exhibits a protic hydrogen (N–H) and a hydridic one (B–H). AB crystals present intermolecular dihydrogen bonding interactions $N–H^{\delta+}$.... $H^{\delta-}–B$ that have proven to play a role in the dehydrogenation process.[21] Hence, release of molecular H_2 is favored and the gas obtained is highly pure. AB dehydrogenation

occurs at relatively low temperature with or without transition metal complexes as catalyst. The use of transition metals allows to tune the rate, the temperature and the extent of H_2 realease.[22] According to the pathway, AB dehydrogenation results in hydrogen depleted borazines, polyborazylenes or polyaminoboranes formation.[23] Metal hydride complexes are often involved in the dehydrogenation of amine-boranes due to their ability to activate N–H and B–H bonds. Dihydrogen bonding also plays a crucial role in the metal mediated dehydrogenation.

While AB dehydrogenation is extensively studied, the regeneration of the remaining BNH solids, necessary for a large-scale development of AB as a hydrogen storage material, appeared to be much more challenging. So far, due to the high stability of BNH wastes, very few workable strategies for AB regeneration are documented. Ideally, the regeneration could occur starting from H_2 but hydrogen transfer strategy can also be developed. One noticeable example is the use of hydrazine (N_2H_4) in liquid NH_3 to transfer hydrogen to polyborazylene with up to 95% regeneration yield but N_2H_4 is in limited production worldwide.[24] To overcome this lack of reversibility, other systems involving the dehydrogenation of more sophisticated cyclic amine-boranes were investigated.[25] BN-methyl cyclopentane and BN-cyclohexane can be dehydrogenated in well-defined borazines for which *via*ble regeneration routes can be imagined.[26-27] The starting BN heterocycles can be recovered in good yields from borazines but those products do not meet DOE targets in terms of hydrogen content.[28]

Despite promising ability to release dihydrogen, AB used as a large-scale material for hydrogen storage remains uncertain mainly due to the absence of an efficient regeneration process. However, all these studies led to important advances in dehydrogenation systems and particularly on the comprehension of N–H and B–H bond activation. Thanks to fundamental studies and benchmark works in the field, dehydrogenation of BN compounds was extended to new purposes. For instance, catalyzed dehydrocoupling of amine-boranes led to well-defined polymeric backbones for polymers, pre-ceramic materials or precursors to white graphene.[29-31] Recently AB was used as hydrogen source in transfer hydrogenation of nitriles using a well-defined cobalt pincer catalyst.[32] Hence, B–H and N–H activation in amine-boranes and aminoboranes is still an area in expansion.

I.3. Amine-borane adducts in dynamic systems

Amine-borane adducts are used to build dynamic and reversible molecular assemblies.[33] Those systems are based on the modulation of the B–N interaction allowed by the rather weak dative covalent bond formed between the two atoms (Figure 1-2). In the presence of a stronger Lewis base, this bond can be cleaved and the nitrogen atom replaced by another electron donor. External factors have significant influence on the bond strength. For instance, the association/dissociation of the two atoms depends on the boron/nitrogen substituents, on solvent polarity or pH of the medium. In these systems, boron and nitrogen go from no interaction to fully quaternarized boron, depending on the conditions.

One noteworthy example of dynamic systems based on BN interaction is sugar sensing with boronic acids in the presence of tertiary amines or imines.[34-35] The simplified principle is presented in Figure 1-6.

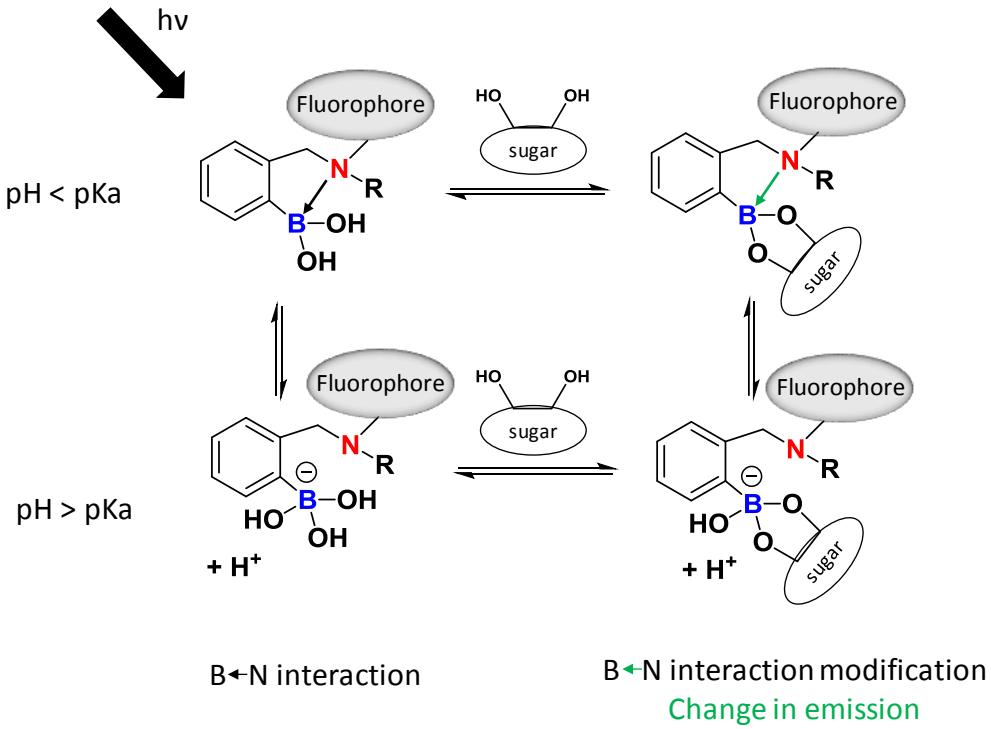

Figure 1-6: General principle of sugar sensing by boronic acid/amine chemosensors

Boronic acids are pH dependent and become boronates when pH > pKa. They are known to rapidly and reversibly bind diols and saccharides to form cyclic boronic or boronate esters.[36]

Upon saccharide binding, the interaction between boron and nitrogen changes since boron becomes more Lewis acidic. Although the B–N interaction is often represented, its nature is discussed in protic solvents due to the possible insertion of a molecule of solvent between the two atoms. However, it is clear than an interaction of some sort exists. A fluorophore, often an extended π conjugated system, is grafted to the molecule in order to convert the binding event into a macroscopic observation when irradiated (Figure 1-6). A sugar chemo sensor is created. Two main processes are responsible: Photoinduced Electron Transfer (PET) and the Internal Charge Transfer (ICT) related to fluorescence, which are both influenced by the B–N strength.

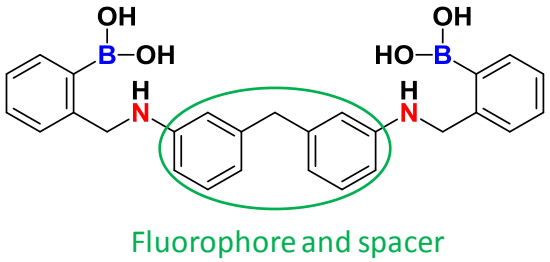

Figure 1-7: Diboronic acids/diamines selective chemical sensor for D-glucose

Those molecular systems allow selective sugar recognition. For instance, enhanced glucose or fructose selectivity has been reported by the preparation of correctly positioned diboronic acid.[37-38] The chemical sensor (Figure 1-7) described by James and coworkers,[37] selectively binds D-glucose at physiological pH. When irradiated at 263 nm, the sensor has a maximum emission at 405 nm shifted to 360 nm upon D-glucose binding.

I.4. Incorporation of B–N units into organic electron-delocalized systems

Organic-inorganic hybrid molecule synthesis is a strategy to increase structural diversity. One way to achieve it is the substitution of C=C units, by B–N moieties. Because of their structural resemblance and molecular properties distinctions, those molecules present promising mixed characteristics.

In aminoboranes, lone pair nitrogen electrons are only partially delocalized into the boron 2p vacant orbital in comparison to evenly distributed π electrons in the C=C bond. For instance, ethene BDE is 728 kJ mol^{-1} with 272 kJ mol^{-1} contribution from π overlapping and aminoborane BDE is only 582 kJ mol^{-1} with 121 kJ mol^{-1} contribution from π overlapping.[3] The decreased electron delocalization in B–N bond is used to tailor properties of carbon-based electron delocalized systems. The BN incorporation results in the modification of the HOMO-LUMO gap of the molecule, opening a wide field of applications in optoelectronic materials.

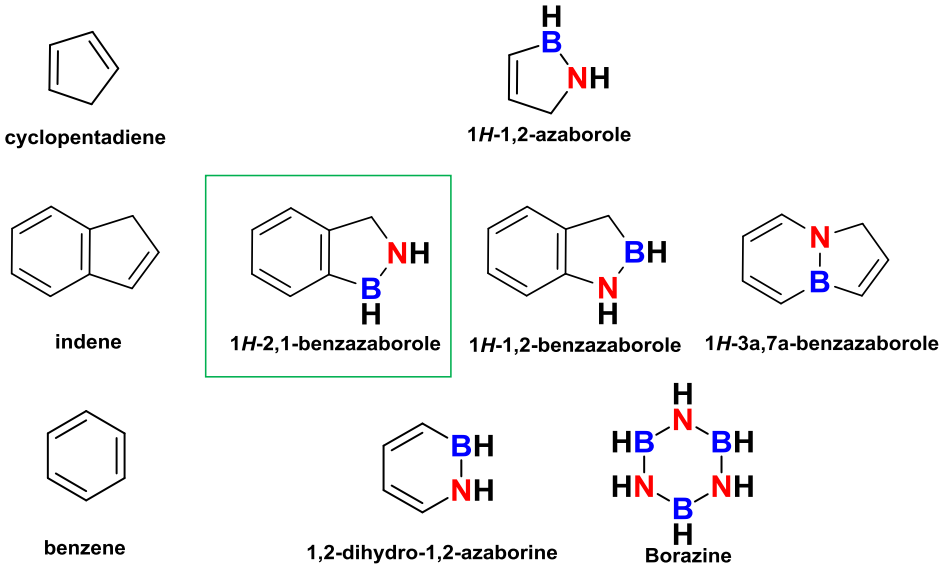

Figure 1-8: Carbon-based aromatic rings and their BN-based analogues

B–N units are generally installed into cyclic electron-delocalized systems that no longer needs to prove their broad field of applications.

I.4.1. Synthetic approach

Mostly encountered electron delocalized units are 5-and 6-member rings (Figure 1-8). The BN counterpart of cyclopentadiene, 1*H*-1,2-azaborole, is not isolated with hydrogenated B and N. Yet, Ashe and coworkers developed a ring closing metathesis synthetic route to obtain boron and nitrogen substituted azaborole heterocycles.[39] Later on, polymethylcyclopentadienyls have been synthesized using Sn-B exchange reaction strategies.[40]

Benzene ring fused with cyclopentene is known as indene. The two isomers 1*H*-2,1-benzazaborole and 1*H*-1,2-benzazaborole as well as 1*H*-3a,7a-benzazaborole are different BN

counterparts of indene (Figure 1-8). Herein, we will focus on the 1*H*-2,1-benzazaborole family. The parent version has not been isolated to date. However, substituted derivatives were obtained with substituents at the 1,2 or 3 positions as well as on the aromatic ring (Figure 1-9).

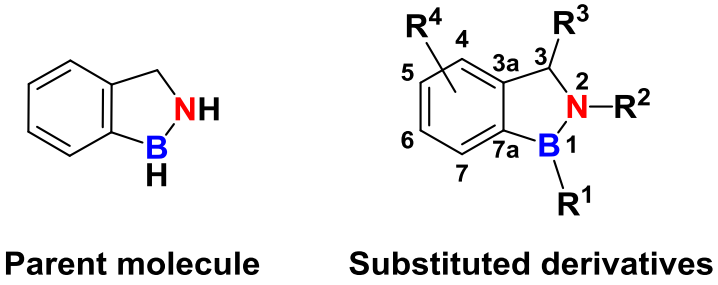

Figure 1-9: Parent and substituted derivatives of the 1H-2,1-benzazaborole family

Previously reported syntheses of substituted derivatives involve intramolecular cyclization from amines, aminoboranes or imines substituted benzene. The first 5-member rings containing boron and nitrogen were synthesized in the late 50's, in the chase for new heteroatomic compounds.[41-42] Based on those pioneering studies, Hawkins and Blackham used amines and boronic anhydrides or acids to produce 1*H*-2,1-benzazaborole systems but the data are not so well reported.[43-44]

A parallel study from Köster and coworkers demonstrated cyclization *via* B–C bond formation from aminoborane –RN–BH_2 under thermal treatment (Scheme 1-1-a).[45]

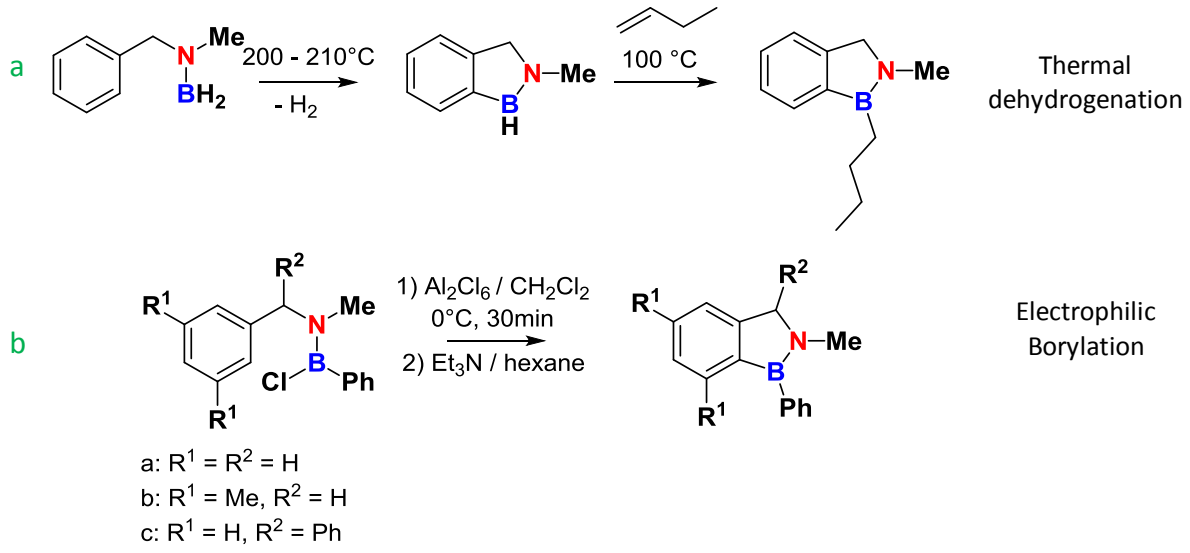

Scheme 1-1: Synthesis of 1H-2,1-benzazaboroles from aminoboranes by thermal dehydrogenation (a) and electrophilic borylation (b)

This process requires harsh conditions. It is applicable to compounds containing a B–H moiety and results in N-alkyl B–H substituted 1*H*-2,1-benzazaborole which can be used as hydroboration agents to obtain alkyl-B substituted products. Only 32 years later, another approach from aminoborane was proposed involving B–C bond formation from B–Cl bond (Scheme 1-1-b). The intramolecular electrophilic borylation was achieved with equimolar amounts of Al_2Cl_6 at 0°C with 75% yield.[46] This method afforded arene substituted 1*H*-2,1-benzazaboroles with methyl or phenyl groups at the 3, 6 and 7 positions.

Another pathway starting from (benzylimine)borane, has been proposed by two different groups (Scheme 1-2).

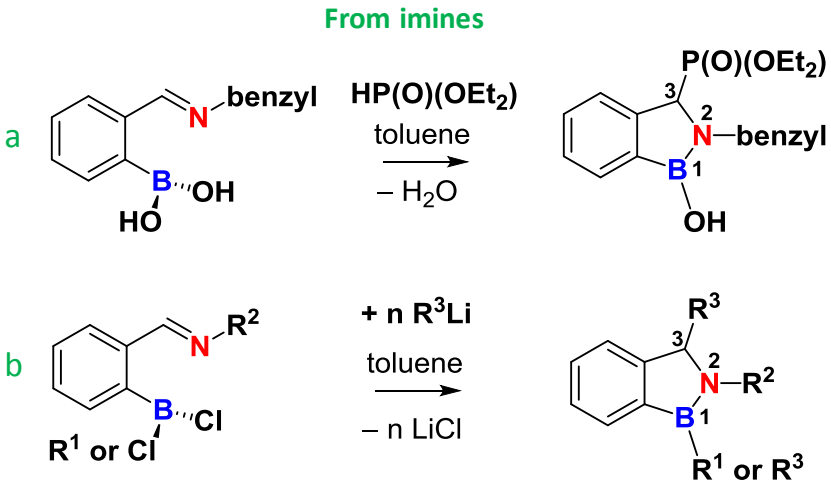

a: R^1 = R^3 = Me, R_2 = ^{t}Bu; **b**: R^1 = R^3 = Ph, R^2 = ^{t}Bu **c**: R^1 = Ph, R^2 = ^{t}Bu, R^3 = Me; **d**: R^1 = Ph, R^2 = R^3 = ^{t}Bu **e**: R^1 = R^3 = Me, R^2 = 2,6-^{i}Pr$_2$C$_6$H$_3$; **f**: R^1 = R^3 = Ph, R^2 = 2,6-^{i}Pr$_2$C$_6$H$_3$ **g**: R^1 = Ph, R^2 = 2,6-^{i}Pr$_2$C$_6$H$_3$, R^3 = Me

Scheme 1-2: Synthesis of 1H-2,1-benzazaboroles from imines

The 1,2,3 trisubstituted 1*H*-2,1-benzazaborole could be isolated from those methods.[47-48] The ring closing is triggered by nucleophilic addition on the sp^2 carbon of the imino group. Mlynarz and coworkers synthetic pathway gave solely the phosphite substituted 1*H*-2,1-benzazaborole by addition of phosphorous acid on the (benzylimine)boronic acid (Scheme 1-2-a). Dostál and coworkers described substituted 1*H*-2,1-benzazaboroles obtained by addition of RLi to activated (benzylimine)(chloro)boranes (Scheme 1-2-b). To obtain stable isolable starting imine compounds, nitrogen has to be substituted with stabilizing groups, generally alkyl, benzyl, or mesityl derivatives. A covalent dative BN bond in (benzylimine)(chloro)boranes is evidenced by X-ray diffraction on suitable monocrystals. The B–N bond length of 1.632(3) Å

(R^1 = Ph, R^2 = 2,6-^{i}Pr$_2$C$_6$H$_3$) is inferior to the sum of van der Waals radii and fall in the typical range for dative covalent BN bonds. The BN bond lengths decrease in the final 1*H*-2,1-benzazaboroles and evidence a covalent B–N interaction with a double bond character (1.401 (3) Å in **f**). We have tried to present an exhaustive list of published syntheses and one can note that very few strategies towards the preparation of 1*H*-2,1-benzazaboroles have been reported.

Aromatic 6 membered rings substituted with one BN unit constitute the 1,2-azaborine family (Figure 1-8). The first synthesis of the simplest molecule, 1,2-dihydro-1,2-azaborine, was reported by Liu and coworkers in 2009.[49] In the past decades, the development of synthetic methods to form mono and polycycles using 1,2-azaborine as building block has been fast due to their applicative potential.[50-51] The different synthetic approaches will not be detailed herein. Biomedical and photophysical properties of those new compounds have been assessed.[52] A few examples are tested for organic electronic applications even though studies are still at an early stage.[53-54] Those examples will be detailed in the next section.

Parent borazine, corresponding to the fully BN substituted benzene has been discovered by Stock and Pohland in 1926[55], and studied in 1958 for the first time.[56] Different strategies towards borazine synthesis exist starting either from preformed aminoboranes or from independent amines and boranes or ammonium and borates (Scheme 1-3).

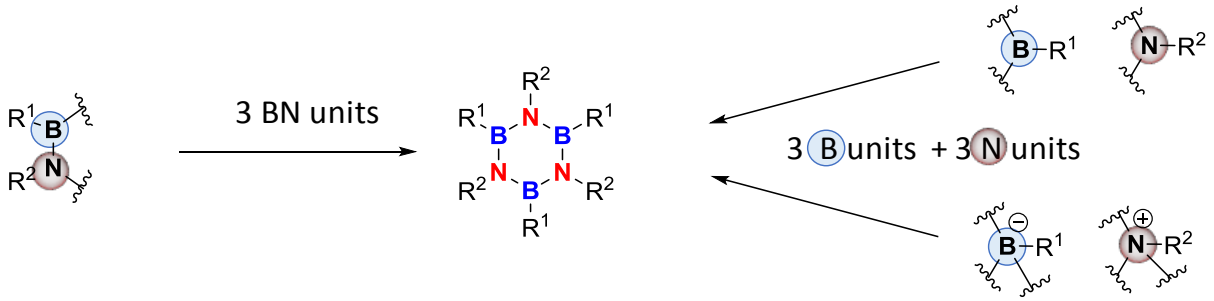

Scheme 1-3: General synthetic approach towards borazine cores

By changing the precursors and developing the synthetic methods, a variety of substituted borazines have been obtained.[6] Borazine can be post functionalized by undergoing exchange reactions at the boron sites or by electrophilic additions on aryl substituents.

I.4.2. Aromaticity

Since BN units are engaged into electron-delocalized patterns, their aromaticity appears as an important parameter. Reactivity, structure, magnetic criteria are used to evaluate aromaticity in a compound. Bond length and planarity are two structural criteria related to aromaticity. Benzene, 1,2-azaborine and borazine parent molecules **1**-**3** as well as 1*H*-2,1-benzazaborole fragment (Figure 1-10) have planar structures in agreement with electron delocalization through the whole cycles.

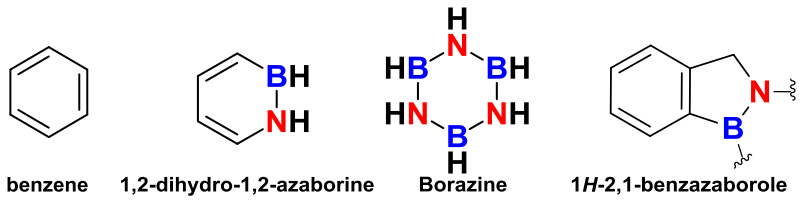

Figure 1-10: benzene, 1,2-azaborine and borazine parent molecules (1-3) as well as 1H-2,1-benzazaborole fragment (4)

C=C bond lengths in benzene are all equal and measure 1.39 Å whereas B–N bonds in the parent borazine measure 1.44 Å.[55] Substituted borazine compounds do not always show even bonds due to different BN substituents or twisted configuration induced by crowded substituents. B–N bonds distances in 1,2-azaborines and 1*H*-2,1-benzazaboroles range between 1.40 and 1.45 Å depending on boron and nitrogen substituents. Those bond lengths are in between B–N simple and double bonds supporting the reduced but existing electron delocalization in the systems. Theoretical calculations to compare benzene, 1,2-azaborine and borazine aromatic character have been realized by Champagne and coworkers.[57] Calculated magnetic criteria indicate that benzene is more aromatic that 1,2-azaborine which is more aromatic than borazine . No data is available for 5-member rings. The Nucleus-Independent Chemical Shifts (NICS) calculation is the criteria of choice to measure the aromaticity of the ring in this area.

I.4.3. Stability

Boron and nitrogen keep a Lewis acid/base character even though they take part into electron delocalization. BN embedded aromatics can suffer of decomposition by hydrolysis. Strategies to overcome degradation of BN units have been developed including the reinforcement of electron delocalization from nitrogen to boron or boron stabilization by bulky substituents. Installation of electron donating groups onr nitrogen or electron withdrawing groups on boron is one way.[58-59] Another option is to enforce planarity so the electron delocalization is improved in the whole system.[60] Bulky substituents such as mesityl on boron in borazine can enhance stability by preventing water approach.[61] With three BN units, borazine derivatives feature polarized bonds. One consequence is their reduced stability towards hydrolysis holding back the widespread development of borazine derivatives. No data are available about the relative stability of six membered rings versus five membered rings.

I.4.4. Applications

I.4.4.a. New ligands for transition metal complexes

BN/CC substitution strategy can be applied to the design of new ligands for transition metal complexes. Metallocene chemistry started with ferrocene discovery[62] and cyclopentadienyl is a key ligand in this field. It has been proven that tuning the cycle can influence the catalytic properties.[63] In this regard, installation of isoelectronic 1,2-azaborolyl ligands and subsequent study of the differences in structure and activity of the corresponding complexes is attractive. One way to achieve it, is deprotonation of 1,2-azaborole and further addition to metallic halides.[40, 64] 1,2-azaborolyl ligands are usually coordinated on iron or early transition metals widely employed in metallocene chemistry.[40, 64] In 2008, Fang and Assoud synthesized, characterized and coordinated a multisubstituted azaborolyl ligand on hafnium from 1,2-azaborolyl anions (Figure 1-11-a).[40] Wen and coworkers coordinated azaborolyl anions on ruthenium and successfully evaluated their catalytic activity in [2+2] cycloaddition of norbornene derivatives with dimethyl acetylenecarboxylate (Figure 1-11-b).[65] As surrogates of titanium cyclopentadienyl species, titanium 1,2-azaborolyl complexes exhibit high catalytic activity in olefin polymerization.[66]

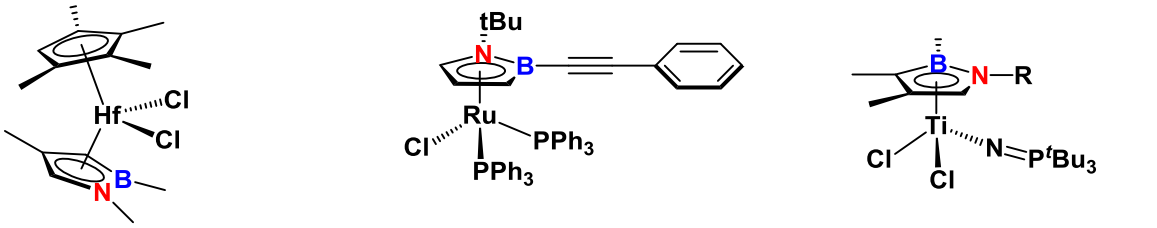

2008, coordination a

2013, cycloaddition b

2014, ethylene polymerization c

Figure 1-11: Selected hafnium (a) ruthenium (b) and titanium (c) complexes with multisubstituted 1,2-azaboryl ligand

In comparison, indene is an underexplored motif despite that, in a lot of cases, indenyl metal complexes are superior catalysts than their cyclopentadienyl counterparts.[67] A noticeable rate increase in some fundamental organometallic reactions is detected. Hart-Davis and Mawby measured this effect on ligand-induced migratory insertion and found a reaction about 10 times faster with the indenyl complex compared to the cyclopentadienyl analogue (Scheme 1-4).

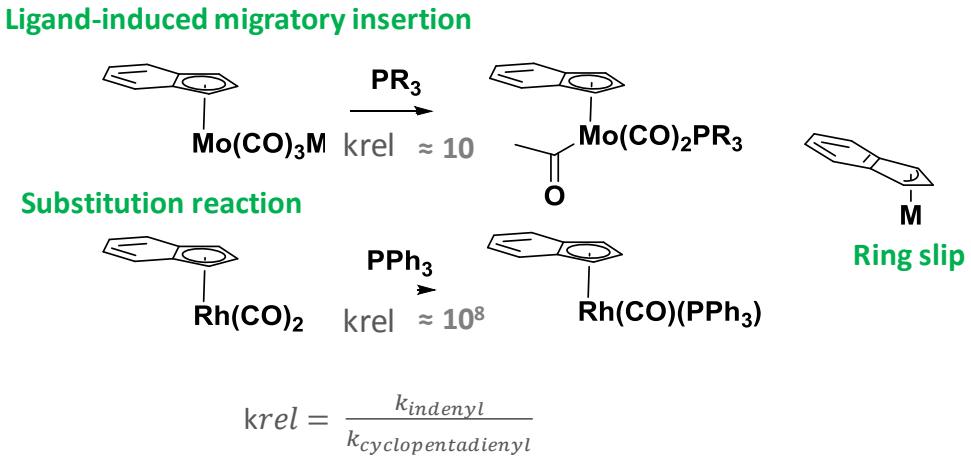

Scheme 1-4: Rate acceleration of ligand-induced migratory insertion and substitution reaction of indenyl complexes compared to the cyclopentadienyl analogues (krel = relative reaction rate constant)

An increase in rate of 10^8 was observed for the phosphine/carbonyl substitution reaction at rhodium. In both cases, the authors attributed the greater kinetic to the ring slip ability of indenyl ligands to adopt an η^3-allyl coordination mode, when room is needed for the accommodation of an additional ligand.[68-69] Also, the bulkier indenyl ligand enables asymmetric transformation with high ee.[70] Examples describing BN indenyl like ligands are

scarce. Only two studies of 1*H*-1,2-benzazaborolyl and 1*H*-3a,7a-benzazaborolyl ligands coordinated on zirconium are reported (Figure 1-12-a,b).[71] The former shows activity in ethylene polymerization affording polymers with broad molecular weight distribution.[72-73] The coordination of 1*H*-3a,7a-benzazaborolyl on zirconium shows an η^3-like coordination mode, as in the case of indenyl ligands. Recently, Dostál and coworker isolated the first example of 1*H*-2,1-benzazaborolyl anion (Figure 1-12-c).[74-75] To the best of our knowledge, no coordination of such compound on a transition metal was reported in the literature.

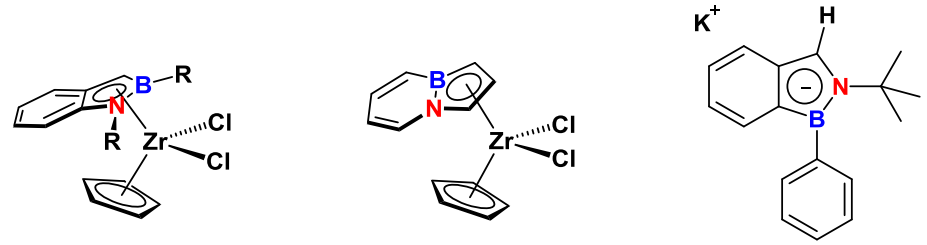

1999
ethylene polymerization

a

2002
coordination

b

c

Figure 1-12: BN indene-like ligands for zirconium complexes (a,b) and 2,1 benzazaboryl anion (c)

In 2004, an azaboratabenzene anion was prepared and coordinated on ruthenium (Figure 1-13-a).[76] The authors noted a decrease in basicity upon complexation. 1,2-azaborine and borazine derivatives have been coordinated on chromium with one example for each represented in Figure 1-13-b,c.[49, 77] While coordinated, 1,2-azaborine can undergo reaction at nitrogen, such as deprotonation. They both demonstrate a benzene like coordination, centered about the planar ring. Borazine shows weaker coordination to the metal center, which can lead to the complex decomposition.

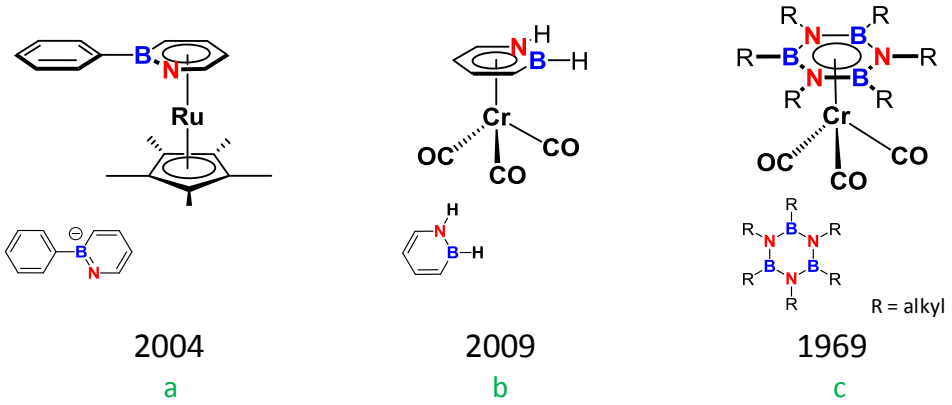

Figure 1-13: Azaborine (a,b) and borazine (c) as L_3 ligand in coordination chemistry

It is worth noting the Szymczak group achieved borazine dearomatization (Scheme 1-5). They coordinated borazine on manganese and chromium with the idea to reduce the B–N bond towards regeneration of hydrogenated AB.[78] Computational study showed that coordination of borazine dramatically changes the requirements for hydride and proton transfer to the borazine unit. They reported a hydride delivery proceeding *via* a single electron reduction mediated by anthraquinone.

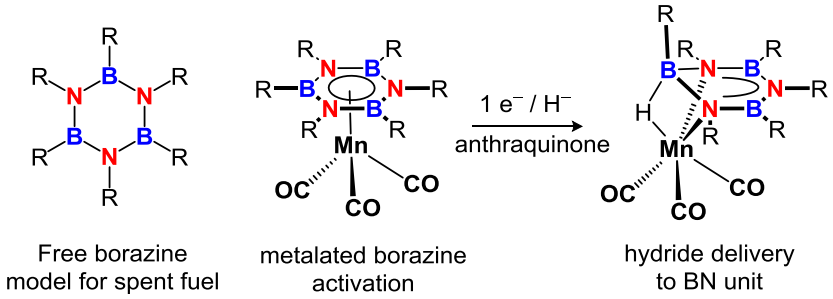

Scheme 1-5: Manganese mediated dearomatization of borazine

Nevertheless, very few is known about 1,2-azaborine and borazine as benzene like ligands in coordination chemistry and catalysis.

One emerging strategy is the incorporation of azaborine unit in the well-known aryl phosphine ligands. Liu and coworkers very recently reported two examples (Figure 1-14). The 1,4-azaborine-based phosphine Pd complex was able to remarkably enhance trans-hydroboration of enynes[79] compared to the carbon analogue which behaves more like a monodentate ligand. Hence, the interaction between the boron and the catalyst center seems to play a crucial role

in the reactivity. The azaborine based tritolylphosphine ligand appeared to be more electron donating than the carboceous counterpart with the same sterics.[80]

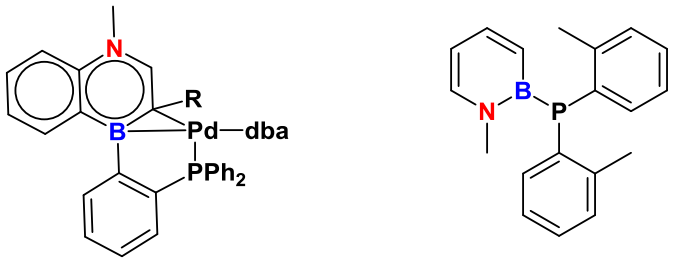

catalyst ligand

Figure 1-14: Azaborine-based catalyst for the trans-hydroboration of enynes (left) and azaborine-based tritolylphosphine ligand (right)

The encouraging results in the coordination of BN containing cyclic compounds should motivate their development in coordination and catalytic systems. Studies are still at a young stage and the door is open for new discoveries. In a context where the aromatization/dearomatization concept in metal-ligand bifunctional catalysis is at the center of attention, the introduction of BN containing ligands appears very promising. We can note that they have not been studied yet in the general field of non-innocent ligands, a very active area in organometallic chemistry and catalysis.

I.4.4.b. New compounds for optoelectronic applications

Electronic devices, capacitors, screens, Light Emitting Diodes (LEDs) are everywhere. Active components are mainly made out of metals, which are expensive and hard to recover. One emerging strategy is the replacement of metal-based active components by organic-based active ones often being polymers or polycyclic aromatics hydrocarbons. Required properties are either electronic conduction or light emission. Incorporation of boron-nitrogen unit into carbon-based active components allows tuning of those key properties. More specifically, modification of the HOMO-LUMO gap is important. This approach diversifies the stock of active molecules and materials available, increasing the chance to meet the criteria for organic based electronic devices development.

So far, only 6 membered ring BN embedded materials are studied for optoelectronic applications and it is at the infancy stage. The first electronic device based on BN-substituted aromatics appeared in 2013 with an azaborine based material incorporated as a

semiconductor in Organic Field-Effect Transistors (OFETs).[81] Azaborine based molecules were tested as semiconductor (Figure 1-15). Key parameters such as hole mobility, thermal and chemical stability and packing structures in the solid state were studied. Such a device exhibits fairly good carrier mobility in the range of 0.1 to 1.0 cm^2/Vs.[82] BN embedded aromatics are also assessed for Organic Light Emitting Diodes (OLEDs). Development of blue-light emission is challenging for OLEDs. Feng and coworkers synthesized a series of ladder-type BN heteroacenes with blue emission (Figure 1-15).[83] Those aromatics show similar geometry than the all carbon analogues but different UV-vis absorption spectra.

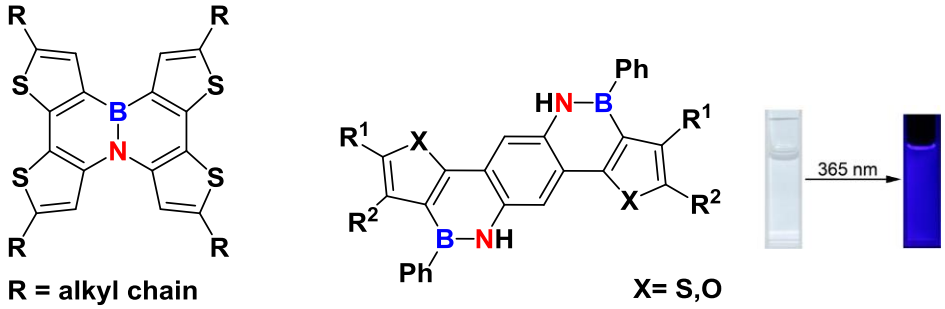

First BN-Semiconductor for OFETs

First BN blue emitters in OLEDs

Figure 1-15: Azaborine-based active compounds for optoelectronic applications

One consequence of borazine polarity is the widening of the HOMO-LUMO gap. Borazines possess a large molecular bandgap making them good UV and deep UV emitters.

In 2005, Che and coworkers synthesized and studied the decomposition temperature, the charge mobility, the absorption, the emission and the electrochemistry of five different hydrogen, alkyl and aryl substituted borazines (Figure 1-16).[84]

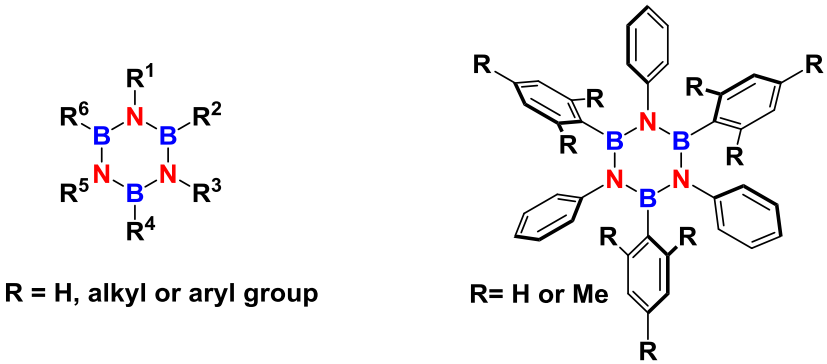

Hole transporter or host in OLEDs

Active compounds in OLEDs and OLECs

Figure 1-16: borazine-based active compounds for optoelectronic applications

The borazines show high thermal stability. The 4-t-butylphenyl–N, H–B substituted borazines revealed high charge mobility. The later one has been inserted in OLED devices as Hole Transporter Materials (HTM) or hosts. They explain that borazine can host blue emitters in contrast to previous well-studied materials and can preserve the color purity of the device since they absorb and emit in the UV region.

In 2013, Accorsi, Beljonne, Bonifazi and coworkers disclosed a chemically very stable borazine (Figure 1-16).[61] This stability has been attributed to the bulky mesityl groups (when R = Me). They report different polymorphs in the solid state leading to different luminescence profiles. Those borazines have been inserted as active materials in the emissive layer in OLEDs and OLECs. They happen to have relatively low electroluminescent quantum efficiency but are the first of their kind.

Boron and nitrogen based molecules are extended to a material scale in the form of poylaminoboranes or boron nitrides. The latest compounds are solely composed of boron and nitrogen atoms arranged in a diamond-like (c-BN), graphene-like (h-BN) or wurtzite BN (w-BN) manner. Among them h-BN is formed with sp^2 hydridized boron and nitrogen. This “white graphene” exhibits remarkable electronic properties that will not be detailed in this manuscript.[85]

II. B–H bond activation and CN bond reduction

Hydroboranes (B_xH_y) are very reactive reagents, especially with oxygen, meaning they are spontaneously flammable in air and hydrolyze very quickly. Their storage requires special conditions of inertness and temperature. For instance, BH_3 is dissolved in anhydrous THF and stored at 0°C under argon. Alkyl boranes or alkoxy boranes require more synthetic steps but are usually easier to handle. In addition, substituents tailor both sterics and the boron Lewis acid character. Those parameters influence their reactivity rendering them as exceptionally versatile reagents. A rich panel of boranes are now accessible but will not be detailed herein.

Boranes involvement in catalysis is vast due to their atypical properties and reactivity. However, they are often seen as sacrificial species enabling transformations but counting as waste products. They play a crucial role in main synthetic transformations such as C–C bond formation, selective C–H functionalization or multiple bond reduction. Electrophilic boranes (organoboranes, boronic esters, boronic acids, organotrifuoroborate salts…) are key compounds in the Suzuki-Miyaura cross-coupling reaction, first published in 1979 and rewarded in 2010 by the Nobel prize in chemistry (Scheme 1-6).[86-87] This palladium-catalyzed reaction offers distinct advantages in comparison to other methods for C–C bond formation. Indeed, this is a coupling reaction applied between a large variety of boron reagents (alkyl, alkenyl, akynyl, arylboronates) as well as halide counterparts (vinyl, aryl, alkyl chloride, bromide, iodide). Moreover, the Hartwig group developed the site-selective catalytic functionalization of C–H bonds of alkanes and aryls. Using boranes allowed first, to tailor the selectivity of the reaction and second, to establish a unique system to access a variety of C–FG bonds (Scheme 1-6).[88]

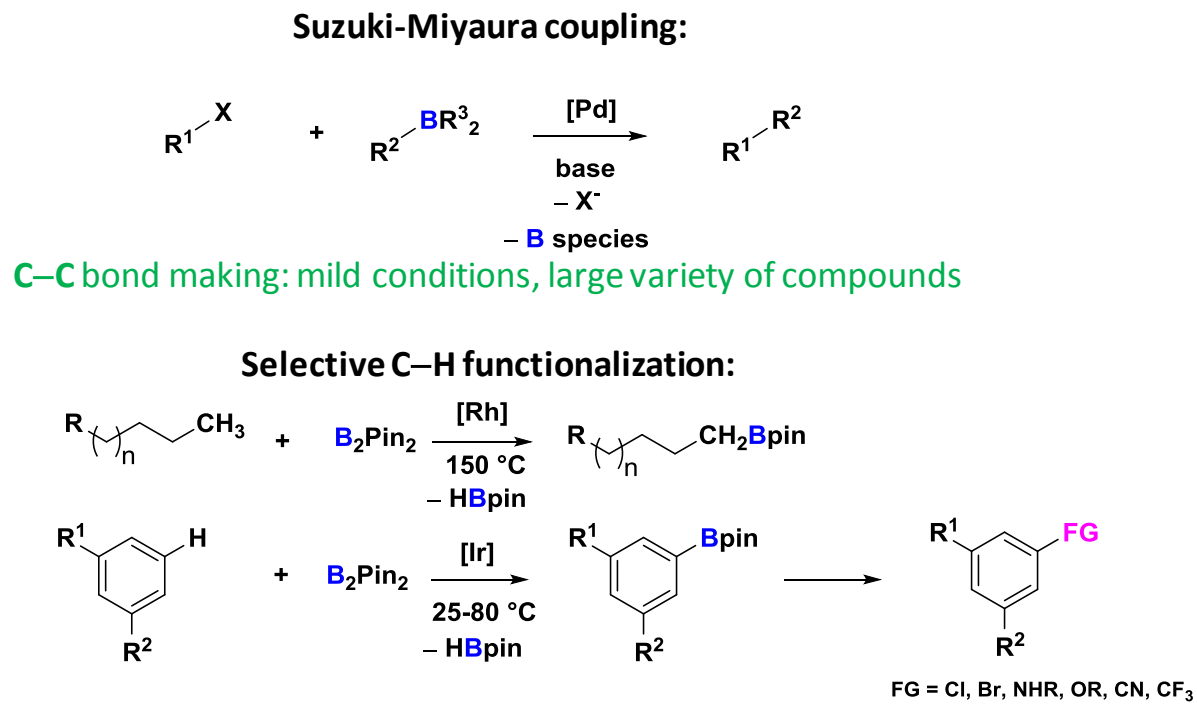

Scheme 1-6: General catalytic reactions involving boranes: (a) Suzuki-Miyaura coupling (b) selective C–H functionalization

The reduction of multiple bonds is essential for many industrial processes. Hydroboranes (R_2BH) featuring a B–H bond, are able to reduce unsaturated functions *via* hydroboration reaction. The trivalent boron is an electrophilic center while the hydridic hydrogen plays the nucleophilic role. The use of boranes notably enables to operate in mild conditions with high selectivity in the targeted product and allow a diversification of the catalytic systems. This particular reactivity will be detailed in the next sections with an emphasis on mechanistic consideration on B–H bond activation and CN multiple bond reduction. Examples of common boranes associated to further description are represented Figure 1-17. The most Lewis acidic of the series is the dialkylborane 9-borabicyclo[3.3.1]nonane (9-BBN), which dimerizes. Catecholborane (HBcat) and pinacolborane (HBpin) are two alkoxyboranes. Catecholborane reactivity towards diols is substantially greater than pinacolborane attributed to the increased Lewis acidity in HBcat.

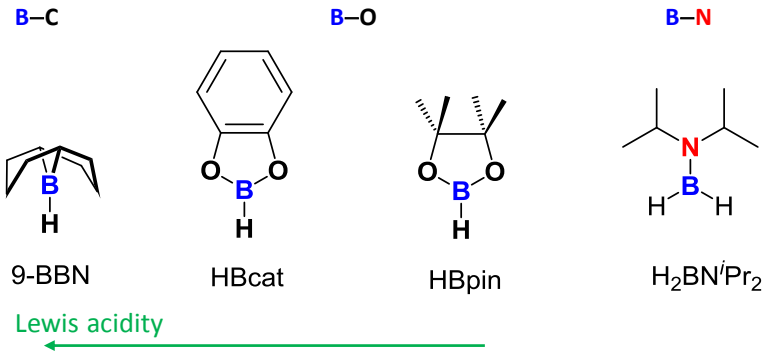

Figure 1-17: Selected commonly used hydroboranes

The rarer aminoborane $H_2BN^iPr_2$ is monomeric and features two hydrogen atoms. The Lewis acidity of the boron is decreased by nitrogen π contribution. The substituted $HRBN^iPr_2$ will be at the center of attention throughout this manuscript.

II.1. Reduction of multiple bonds with hydroboranes

Direct addition of B–H bonds to C=C bonds was first reported by H.C. Brown and coworkers with a mixture of sodium borohydride-aluminum chloride.[89] Since then, hydroboration of multiple bonds expanded to a variety of borane reagents. Reaction of the simplest borane BH_3 with alkenes proceeds spontaneously at room temperature. The transformation yields the anti-Markovnikov product as a distinction from classic electrophilic addition on alkenes. The regioselectivity of this reaction is governed by three rules. First, alkenes undergo cis-addition of the B–H bond. Second, the boron binds the less sterically hindered carbon. Third, the electrophilic boron center has a greater affinity for the more positively charged carbon. By tuning Lewis acidity and sterics of boranes this regioselectivity can be changed or improved. Sterically hindered and electrophilic 9-BBN allows selective anti-Markovnikov hydroboration of terminal alkenes.[90] Asymmetric synthesis with high enantiomeric excess is achieved with chiral alkylboranes such as $(Ipc)_2BH$ and substituted alkenes.[91]

Catalyzed B–H bond activation enables the control of the B–H bond addition to the unsaturated bond and can efficiently lead to chemoselective, regioselective and enantioselective hydroboration in mild conditions. The nature of the metal center, the ligands and the substrates control those selectivities. For instance, non-catalyzed reaction of HBcat and hex-5-en-2-one will preferentially result in hydroboration of the carbonyl with high

chemoselectivity whilst rhodium catalyzed reaction will favor hydroboration of the C=C double bond (Scheme 1-7).[92]

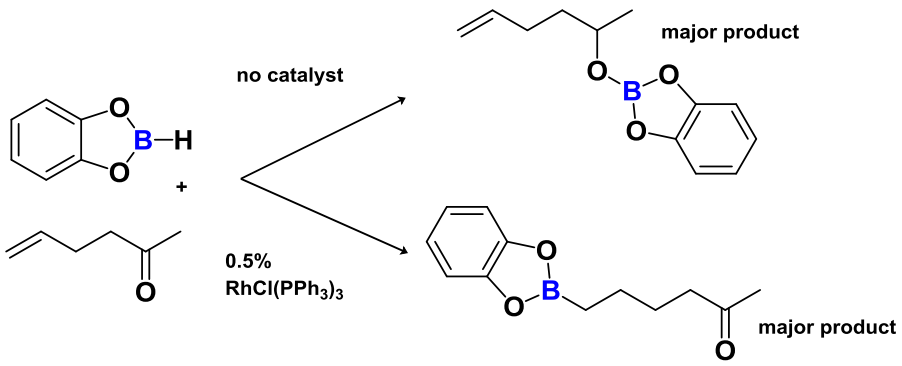

Scheme 1-7: selected example of chemoselective hydroboration with catechol borane

Anti-Markovnikov or Markonikov products can be obtained from the same substrate, depending on the pre-catalyst employed.[93-95] It should be noted that dehydrogenative borylation of alkenes can also compete with hydroboration as for example observed when using the ruthenium precursor catalyst $RuH_2(H_2)_2(PR_3)_2$ we used in our study.[96-97] At late transition metals, a parallel can be made between the mechanism for hydrosilylation/dehydrogenative silylation of alkenes, based on the modified Chalk-Harrod mechanism, and hydroboration/dehydrogenative borylation of alkenes leading to the production of the saturated silanes/boranes and/or the corresponding vinylsilanes/vinylboranes, respectively. Elementary steps such as oxidative addition of HBR_2, η^2-coordination of the alkene and hydride migratory insertion lead to reductive elimination of both Markovnikov or anti-Markovnikov products. Instead of hydride migratory insertion, boryl migratory insertion can lead to the formation of vinyl boranes *via* β-H elimination.

Latest efforts focus on environmentally benign and earth abundant metal/main group based catalysts in order to reduce the cost and complement the selectivity of existing hydroboration reactions. For example, in 2013, it has been shown that an iron pincer complex is able to catalyze chemo and regioselective hydroboration of α-olefins at room temperature with superior selectivity than precious metal based catalysts.[98]

Conventional, non-catalyzed hydroboration of alkynes is a B–H *syn* addition and yields *E*-alkenylboron. *Trans* hydroboration of alkynes can be obtained catalytically allowing the access to Z-alkenylboron. Indeed, *trans*-hydroboration of terminal alkynes has been achieved for the first time in 2000 by Miyaura and coworkers with precious metal based pre-catalysts.[99] Following reports involved ruthenium hydride pre-catalyst in 2012,[100] cobalt based precursor in 2015[101] and copper complexes in 2016.[102] All those studies present hydroboration of terminal alkynes with a mechanism systematically involving cleavage of the terminal C–H. Hydroboration of terminal alkynes was extended to aluminum-based catalysis.[103] An outer sphere mechanism was described, still involving terminal C–H cleavage and leading to the (E)-product *via syn* addition. *Trans*-hydroboration of internal alkynes is more challenging and has been described with a ruthenium based system and HBpin.[104] The data showed the importance of π coordination of the alkyne in the mechanism of the reaction. Liu and coworkers very recently published the site-selective and stereoselective *trans* hydroboration of enynes catalyzed by an azaborine-based phosphine-Pd complex with high selectivity and correct yield.[79] They illustrated the benefit brought by the BN incorporation into the catalyst ligand.

Shi and coworkers demonstrated intramolecular alkyne hydroboration from air stable amine-cyanoboranes by a triazole-gold(I) complex (Scheme 1-8).[105]

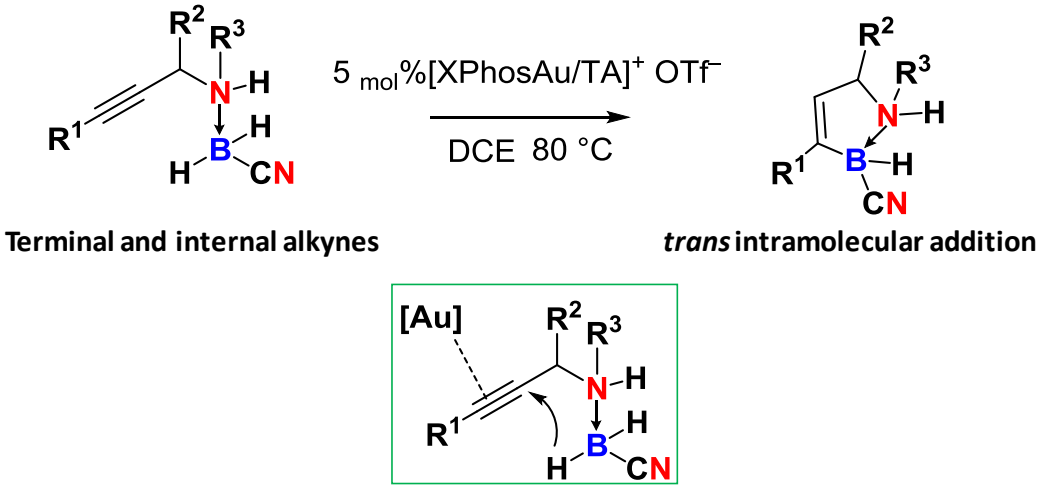

Scheme 1-8: Au-catalyzed intramolecular hydroboration of alkynes to generate cyclic amine-boranes. TA: triazole-modified

This reaction occurred in an open flask, unlike precedent strategies involving the addition of alkoxy or alkylboranes, and at high temperature (80°C). Another specificity of this report is the unprecedented intramolecular hydroboration of alkynes being a *via*ble strategy to produce BN heterocycles. The authors did not conduct in depth study on the mechanistic pathway. Yet, the produced cyclic amine boranes indicate a *trans* addition process of the internal alkyne. As a result of the π acid property of the gold-based catalyst, they postulated that the activated η^2 coordinated alkyne would react with B–H bond without B–H activation at the metal site.

Reduction of polar multiple bonds, such as CO or CN bonds, can also be mediated by hydroboranes.[106] C=O bonds hydroboration allows the production of alcohols, widely employed in the industry. This strategy is of particular interest since it allows asymmetric synthesis of alcohols with high optical purity. The use of chiral or sterically hindered ligands on titanium and zinc metal centers afforded high to moderate enantiomeric excess. Hydroboranes have also proved to reduce CO_2 in mild conditions (T < 100°C, Pco_2 < 5atm) *via* different processes including catalyzed hydroboration with metal hydrides and Lewis pairs.[107] CO bond reduction with hydroboranes constitutes an intensely studied area but our focus will now be on polar CN bonds.

II.3. Reduction of multiple CN bonds

We were very much interested in the catalytic reduction of CN bonds with boranes and dihydrogen with a focus on mechanistic consideration. Consequently, previous reports on catalyzed CN hydroboration and CN hydrogenation will be detailed, and particularly catalytic systems highlighting the discovery of elementary steps of the transformations.

Reduction of CN bonds is generally achieved with the aim to produce amines, which are of great importance in bulk chemistry, materials science, and are often encountered in molecules with biomedical applications. Nitriles are suitable precursors for the production of primary amines whereas imines and isonitriles are suitable precursors for secondary amines. (Scheme 1-9). Primary Imines are harder to synthesize and isolate, and are generally substituted with alkyl or aryl groups. Hence, imine hydroboration followed by hydrolysis give secondary amines with large substituents on nitrogen. On the contrary, isonitrile hydroboration/hydrolysis

generate methyl substituted secondary amines. Reduction of nitriles (C≡N triple bond 887 kJ mol^{-1}) is more challenging than reduction of imines (C=N double bond 615 kJ mol^{-1}).

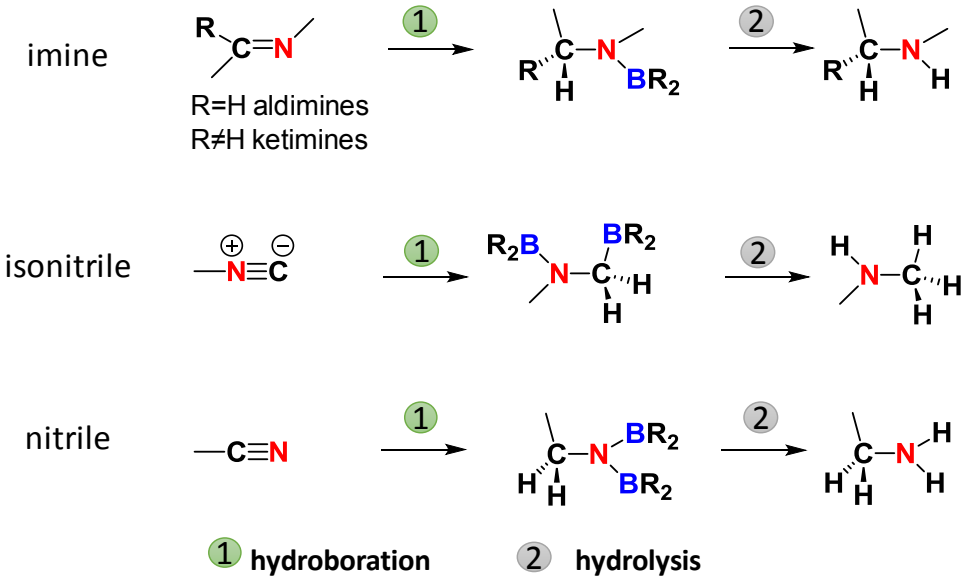

Scheme 1-9: Multiple CN bond reduction via hydroboration/hydrolysis procedures

II.3.1. imines hydroboration

The reduction of the C=N double bond of imines is often realized from the monohydrogen substituted aldimines but is also achieved with ketimines (Scheme 1-9).[106]

The first transition metal catalyzed hydroboration of imines appeared in the literature in 1995.[108] The authors describe the synthesis of coinage-based (Au, Ag, Cu) complexes with diphosphine ligands. 5 mol% of $[AuCl(L_2)]_n$ complexes in THF solution of imines and HBcat afforded borylated amines within 30 minutes. This reaction, which also occurred without any catalyst, was estimated to be over 40 times faster when using $[AuCl(L_2)]_n$. (L=1,1'-bis(diphenylphosphino)-ferrocene). Unlike conventional catalyzed alkene hydroboration mechanistic pathway going through oxidative addition of the hydroborane, they could not observe such an intermediate, even when conducting stoichiometric reactions. Hence, they proposed an alternative mechanism proceeding *via* imine-borane adduct activation (Scheme 1-10).

Imine-borane activation pathway

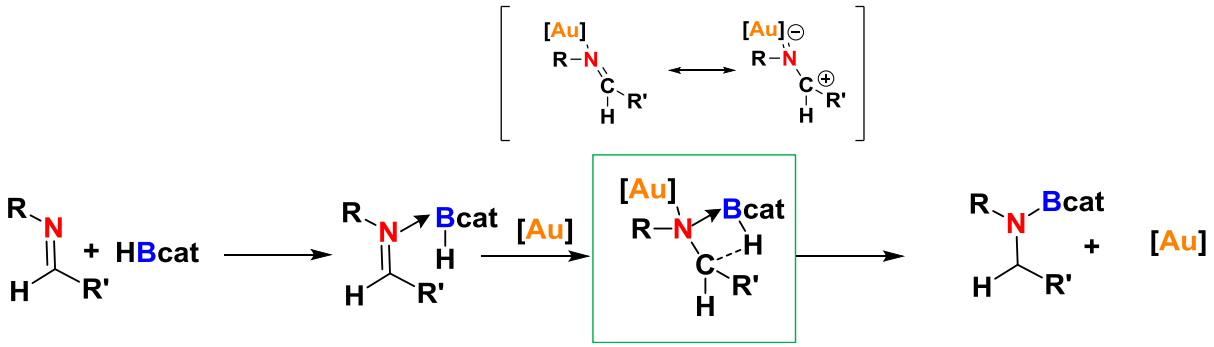

Scheme 1-10: Gold-catalyzed imine hydroboration: imine-borane activation pathway

The imine-borane adducts rapidly formed in solution. Coordination by nitrogen of the imine borane adduct increases the electrophilic character of the carbon atom, more likely to react with $B^{\delta+}$–$H^{\delta-}$ hydrogen. A few examples of imine hydroboration have been developed later on. Notably hydroboration *via* Corey-Bakshi-Shibata reduction or using the Shvo's catalyst, both well known for the reduction of carbonyl compounds.[109-110]

In 2011, Hill and coworkers proposed the hydroboration/dearomatization of pyridine by Mg compounds stabilized by a β-diketiminato ligand.[111] In 2013, they used the same complex to hydroborate aldimines and ketimines with HBpin.[112] They used 5 to 10 mol% of Mg complex precursor and heated from 25 to 70°C according to the substrates. Pre-catalyst activation was achieved by σ-bond metathesis between HBpin and (β-diketiminato)Mg(*n*Bu) (Scheme 1-11). Thanks to mechanistic investigation involving stoichiometric reactions and kinetic study, they proposed that addition of imines onto the activated catalyst afforded the imido Mg complex (Scheme 1-11). This species results from insertion of the imine into the Mg–H bond. A crystal structure of such a compound was obtained with suitable substituents. Further addition of HBpin yielded the borylated amine product. Although no intermediate in the addition of HBpin to the amido Mg complex was observed, they proposed a Mg–N/B–H metathesis to afford the product and regenerate the active species.

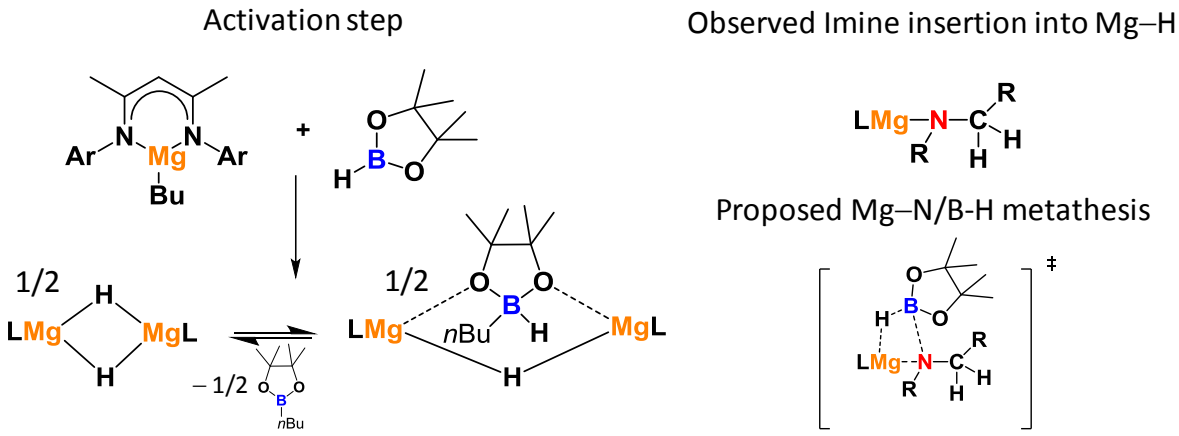

Scheme 1-11: Magnesium catalyzed imine hydroboration: catalyst activation (left) imine insertion into Mg–H and Mg–N/B–H metathesis (right)

The kinetic study indicates first order in catalyst supporting a monomolecular catalysis supposedly enabled by the β-diketiminato ligand. The rate-determining step was proposed to be the Mg–H/ C=N insertion. Excess of HBpin induced a decrease in reaction rate attributed to the inhibitor effect of the borate or borane that coordinates to the complex preventing imine coordination. A second order dependence on imine was found and attributed to the assistance of a second imine substrate for the displacement of HBpin from the Mg center during the rate-determining step.

In 2012, Crudden and coworkers reported the hydroboration of imines catalyzed by a borenium ion. They have shown that 5 mol% of the pre-formed borenium/(borohydride or borate) salt (Scheme 1-12) catalyzes bulky imine hydroboration with HBpin in 45 min to 3h at room temperature. The reaction was extended to the reduction of benzonitrile by applying a longer reaction time. They undertook kinetic experiments coupled with deuterated labelling experiment to unravel the mechanism of the reaction summarized in Scheme 1-12. The first step corresponds to the borenium transfer to the imine. It was then apparent from the high primary kinetic isotope effect (k_H/k_D = 6.7 ± 0.1) that the B–H bond cleavage took place during the rate determining step. Interestingly, the hydride comes from the HBpin substrate and the cleavage was assisted by one molecule of 1,4-diazabicyclo[2.2.2]octane (DABCO). The borylated amine was released and the borenium ion recovered. Thus, the borohydride counter ion was not found to be the hydride source and is not involved in the catalytic cycle, as a distinction to FLP-type mechanism.

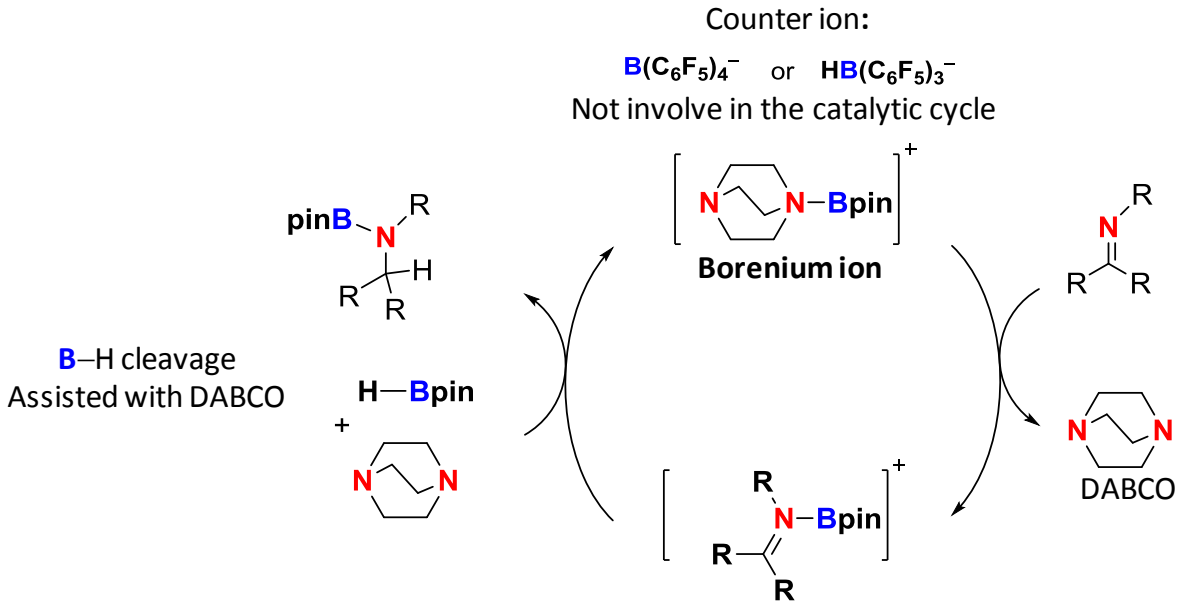

Scheme 1-12: Borenium catalyzed imine hydroboration: postulated mechanism

Reduction of imines can also be regarded as a way to afford chiral secondary amines when starting from ketimines. So far, only asymmetric hydrogenation and hydrosilylation of ketimines have been reported with transition metal based catalysts.[113-114] The two latest examples we just presented, successfully achieved the hydroboration of ketimines but no mention of any enantioselectivity.[112, 115] Formal hydroboration of ketimines with B_2Pin_2 yielded imines with correct enantiomeric excess.[116] Looking at the literature, this area seems rather unexplored.

II.3.2. Isonitrile hydroboration

Isonitriles (isocyanides) are less studied in comparison to the nitrile family. They are usually associated with a strong unpleasant smell. However, isonitriles are useful tools in organic synthesis due to their wide reactivity and ability to perform insertion, protonation or addition reaction with numerous substrates. So far, isonitriles are mainly involved in multicomponent reactions such as the Passerini or the Ugi reaction enabling bis(amide) formation. They are also used in N-containing heterocycles synthesis, and organometallic coordination. Two different electronic representations can be adopted: carbene or zwitterionic (Figure 1-18).

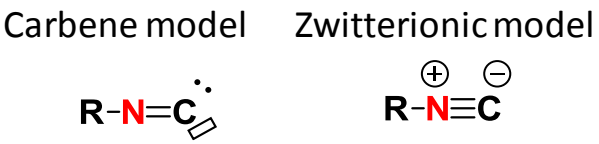

Figure 1-18: Known representations of isonitriles

The carbene model better reflects the electrophilic and nucleophilic characters consistent with the observed reactivity of isonitriles, while the zwitterionic model is more consistent regarding the linear geometry and spectroscopic data.[117] A recent theoretical study shows that isonitriles are better represented by the carbene model and the linear geometry is attributed to the N π lone pair donation. Isocyanides are considered isoelectronic to the CO ligand with strong σ-donor properties and consequently lead to very stable metal complexes. As rather stable carbenes, they have the ambiguous ability to react as a nucleophile and an electrophile (Scheme 1-13).

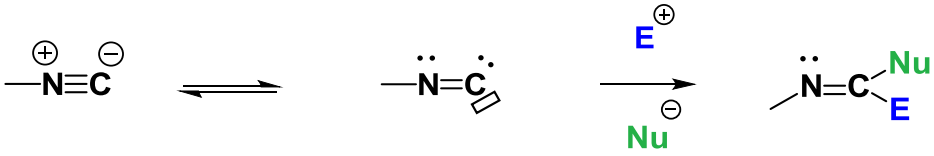

Scheme 1-13: Isonitrile general reactivity

The reactivity of isonitriles with hydroboranes illustrates well this dual character. Very few reports deal with hydroboration of isonitriles. Figueroa and coworkers showed that, in two hours at room temperature, a bulky isonitrile ($CNAr^{Dipp2}$) spontaneously undergoes hydroboration with 9-BBN (Scheme 1-14).[118]

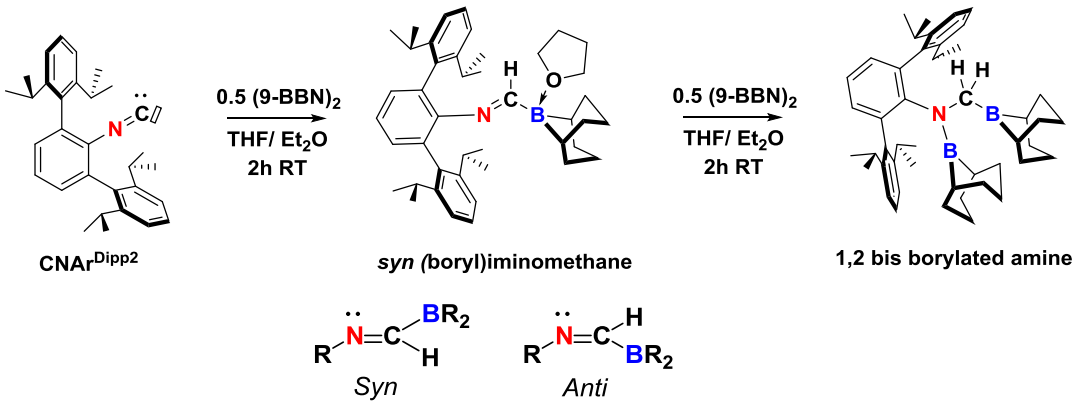

Scheme 1-14: Hydroboration of $CNAr^{Dipp2}$ isocyanide with 9-BBN

A first equivalent of hydroborane is added to the carbon atom. The (boryl)iminomethane previously formed by other methods, possessed an *anti* configuration or underwent dimerization.[119] The use of bulky substituents favored the monomer while the hydroboration strategy allowed the formation of *syn* (boryl)iminomethane. Hence, they can adopt a frustrated Lewis pair behavior and activate CO_2, organonitriles and terminal alkenes, since the frontier orbitals are correctly oriented (*syn* configuration).[118] Complete hydroboration of isonitrile (2 equiv of HBR_2) generates the 1,2-diborylated amine. Thus, the first borane addition is performed on the nucleophilic carbon and the second addition on the nucleophilic nitrogen of the (boryl)iminomethane intermediate leading to 1,2-substituted CN bond differing from nitrile hydroboration (Scheme 1-9).

First catalyzed hydroboration of isonitrile was reported in 2015 by Hill and coworkers with a magnesium precursor catalyst.[120] They also showed the exclusive formation of 1,2-diborylated amine and achieved it with less Lewis acidic HBpin. However, they evidenced a different mechanistic pathway. The first borane addition occurs at the nitrogen position while the nucleophilic carbon strongly interacts with the electropositive magnesium center.

II.3.3. Nitrile hydroboration

Reduction of C=C, C≡C and C=O bonds by hydroboranes is well documented whereas catalytic reduction of C≡N bonds is an emerging strategy. Key data concerning systems enabling catalytic nitrile hydroboration (Scheme 1-15) are summarized in Table 1-1.

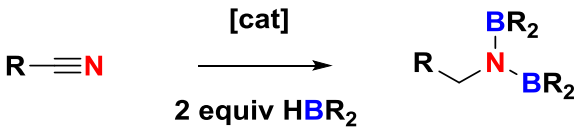

Scheme 1-15: General scheme for catalyzed nitrile hydroboration

Cat	*loading mol%*	*borane*	*Temp (°C)*	*Reaction time (h)*	*NMR Yield (%)*	*Solvent*	*ref*
[Li]	10-20	$H_2BN^iPr_2$	25 - 65	2 -24	99 – 60[a]	THF	[121]
[Mo]	5	HBcat	25	12	100	C_6D_6	[122]
[Mg]	10	HBpin	60	0.5 - 30	99 - 75	C_6D_6 toluene	[123]
[Ru]	5	HBpin	45	18	99 - 41	C_6H_6	[124]
[Ru]	1	HBpin	60	15 - 36	99 - 73	neat	[125]

Table 1-1: Key data concerning catalytic systems for nitrile hydroboration

In 2009, the reduction of aromatic and aliphatic nitriles with 2 equivalents of the aminoborane $^iPr_2NBH_2$ was described by Singaram and coworkers.[121] Mild temperatures from 25 to 65°C were applied to obtain more than 20 primary amines. The authors reported the need of catalytic amount (20 mol%) of $LiBH_4$ for the reaction to proceed. Nitriles do not convert when either $^iPr_2NBH_2$, the reducing agent, or $LiBH_4$, the catalyst, are missing. They suggest an activation of C≡N bond by lithium ion coordination to the nitrogen, promoting reduction by $^iPr_2NBH_2$. However, no comment was made on the remaining dehydrogenated BN species nor on the fate of the $LiBH_4$ salt. This method results in the reduction of nitriles with aminoboranes, but no evidence of a hydroboration process was showed.

Three years later, Nikonov and coworkers reported the first transition metal catalyzed hydroboration of nitriles.[122] Earlier in the year, they had shown the first hydrosilylation reaction mediated by the molybdenum complex (2,6-$^iPr_2C_6H_3N$)Mo(H)(Cl)$(PMe_3)_3$ **1** (Scheme 1-16). Encouraged by those results, they tested it for the hydroboration of nitriles with HBcat. Quantitative NMR conversion of nitriles to bis(borylated) amines occurred in 12 h at room temperature with 5 mol% of Mo complex **1**. Interestingly, the resulting bis(borylated) amines selectively react with aldehydes (not ketones) to yield the corresponding imines. As a result, this method allows selective formation of both primary amines and imines. Mechanistic investigation on nitrile hydroboration reduction was undertaken by stoichiometric reaction and low temperature NMR experiments.

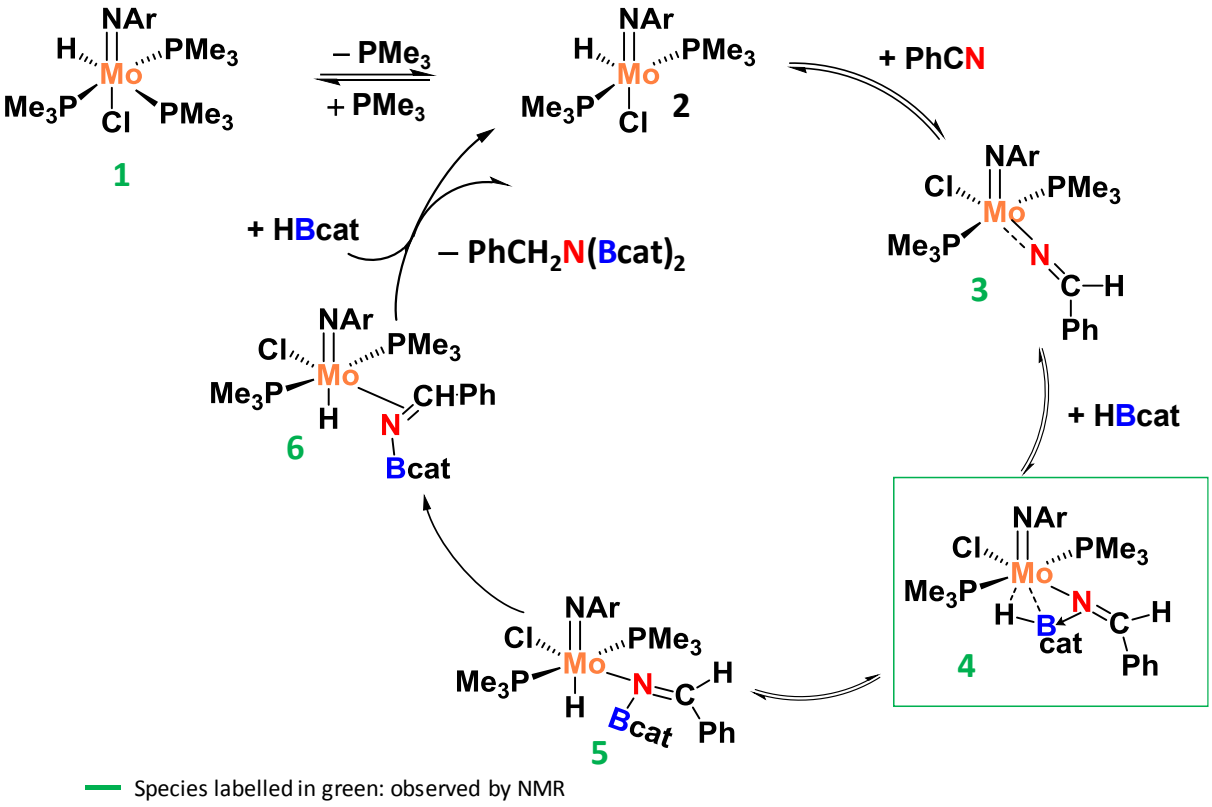

Scheme 1-16: Suggested catalytic cycle for the molybdenum catalyzed nitrile hydroboration

They observed the formation of an imido complex **3** upon addition of benzonitrile to **1**. Complex **3** results from the insertion of the C≡N bond into the metal hydride Mo–H. Interestingly, addition of one equivalent of HBcat at low temperature led to complex **4**. Spectroscopic NMR data revealed a shielded signal at 2.2 ppm by ^{11}B NMR (compared to 29 ppm for HBcat) characteristic of a tetragonal boron. The signal is a doublet meaning boron couples with one hydrogen with a reduced ^{1}J coupling constant of 50 Hz. Those data evidence a B–H agostic interaction with the metal center and a boron-nitrogen dative interaction. At slightly higher temperature (– 50°C), full activation of the B–H bond led to the M–H and B–N bond formation *via* σ-bond metathesis. Finally, the borylated imino intermediate switched to an η^2-coordination mode to afford complex **6**. Release of the bis(borylated) amino compounds occurred upon addition of a second equivalent of HBcat, this last step being not detailed.

During the study on pyridine hydroboration/dearomatization of pyridine, Hill and coworkers noticed that 4-cyanopyridine undergo hydroboration of the nitrile function instead of the pyridine ring. Hence, they carried out a study on nitrile hydroboration using the magnesium precursor catalyst.[123] They performed the reaction at 60°C with 10 mol% of the Mg precursor

catalyst. The reaction works with both alkyl nitriles and aryl nitriles but considerably faster in the first case. Also, reaction rates are lowered with bulkier substituents. They investigated on the catalytic cycle of the reaction thanks to stoichiometric reactions and in-depth kinetic studies. Pre-catalyst activation occurs in the usual fashion *via* σ-bond metathesis to generate the active Mg hydrido complex. Scheme 1-17 summarizes the intermediate species identified by NMR throughout stoichiometric study. Upon addition of one equivalent of nitrile, the imido complex **1** is formed. Once again, the complex results from insertion of the nitrile bond into Mg–H. A characteristic NMR signal at 7.84 ppm attributed to the =C–H proton raised on the spectrum. X-ray diffraction spectroscopy on a monocrystal revealed the formation of complex **2** upon further addition of one equivalent of HBpin. Similar to the previous case, boron of HBpin interacts with the imido nucleophilic nitrogen. Unlike complex **4** observed in the Mo system (Scheme 1-16), the hydride of HBpin does not interact with the Mg center but point towards the carbon atom of the imido group. The ^{11}B NMR spectrum displaying a doublet with a direct coupling constant $^{1}J_{B\text{-}H}$ of 105 Hz confirmed the B–H bond integrity.

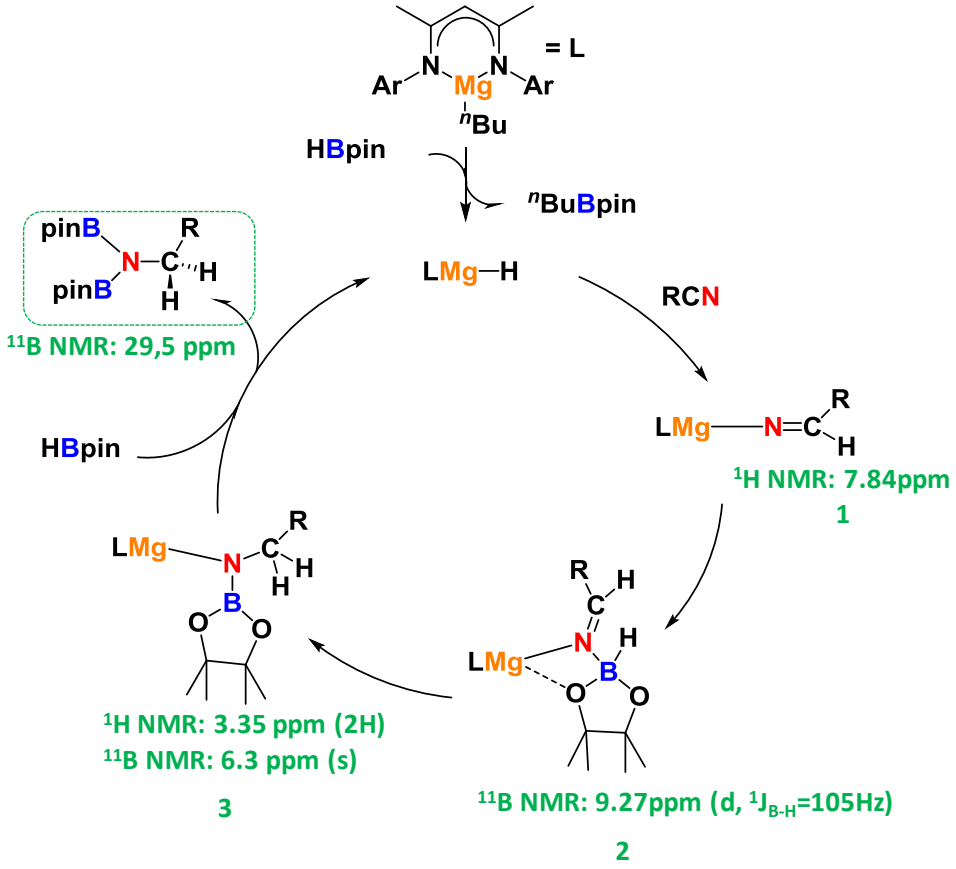

Scheme 1-17: Magnesium catalyzed nitrile hydroboration: species observed by NMR

The O–Mg interaction stabilized this configuration. After a while at room temperature, the hydridic B–H is transferred to the imido carbon atom to afford complex **3**. Final addition of a second equivalent of HBpin yielded the bis(borylated) amine and recovery of the active Mg hydride species. As in the imine hydroboration case, they do not observe any intermediate for the second addition of HBpin. A kinetic study, not detailed herein, emphasizes some alternatives in the catalytic cycle with some variant pathways depending on the nitrile substituent. The proposed mechanism goes through an outer sphere pathway where the CN bond is activated followed by addition of the B–H bond, non-interacting with the catalytic center, across the CN bond.

The Szymczak group synthesized a proton switchable bifunctional ruthenium complex (Scheme 1-18).[124] This complex was isolated in four different protonated states. It has the ability to activate H–H and H–B bonds through the Ru–O interaction. Based on this rapid bond activation they investigated the hydroboration of the polar C≡N unit. They found that 5 $_{mol}$% of the ruthenium pre-catalyst **1** promotes hydroboration of nitriles with HBpin at 45°C in 18 hours.

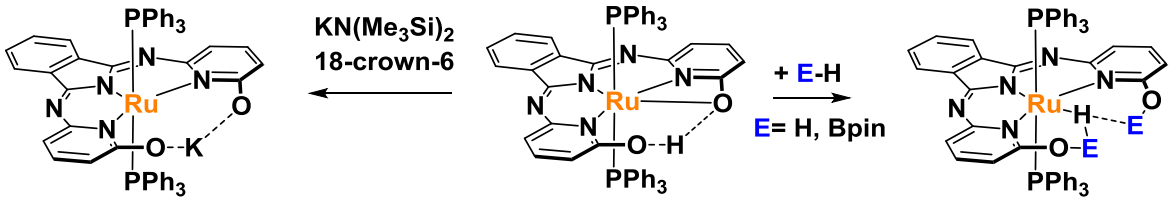

Scheme 1-18: σ-bond activation at the ruthenium center

The catalytic system involves a non-innocent ligand. Cooperation of the metal center and the ligand enables cleavage of the B–H bond and subsequent concerted addition to the nitrile bond (see transition state **4** in Scheme 1-19). *In situ* NMR observation of =C–H proton (δ 8.78) integrating 3.5 times greater than total ruthenium species supports the release of the borylated imine in the media. A second concerted step leads to the addition of another equivalent of HBpin to the imine (see transition state **6** in Scheme 1-19). Throughout the

reduction, the carbon or the nitrogen of the nitrile function do not directly interact with the Ru center. Thus, the authors reported an outer-sphere type pathway for nitrile reduction.

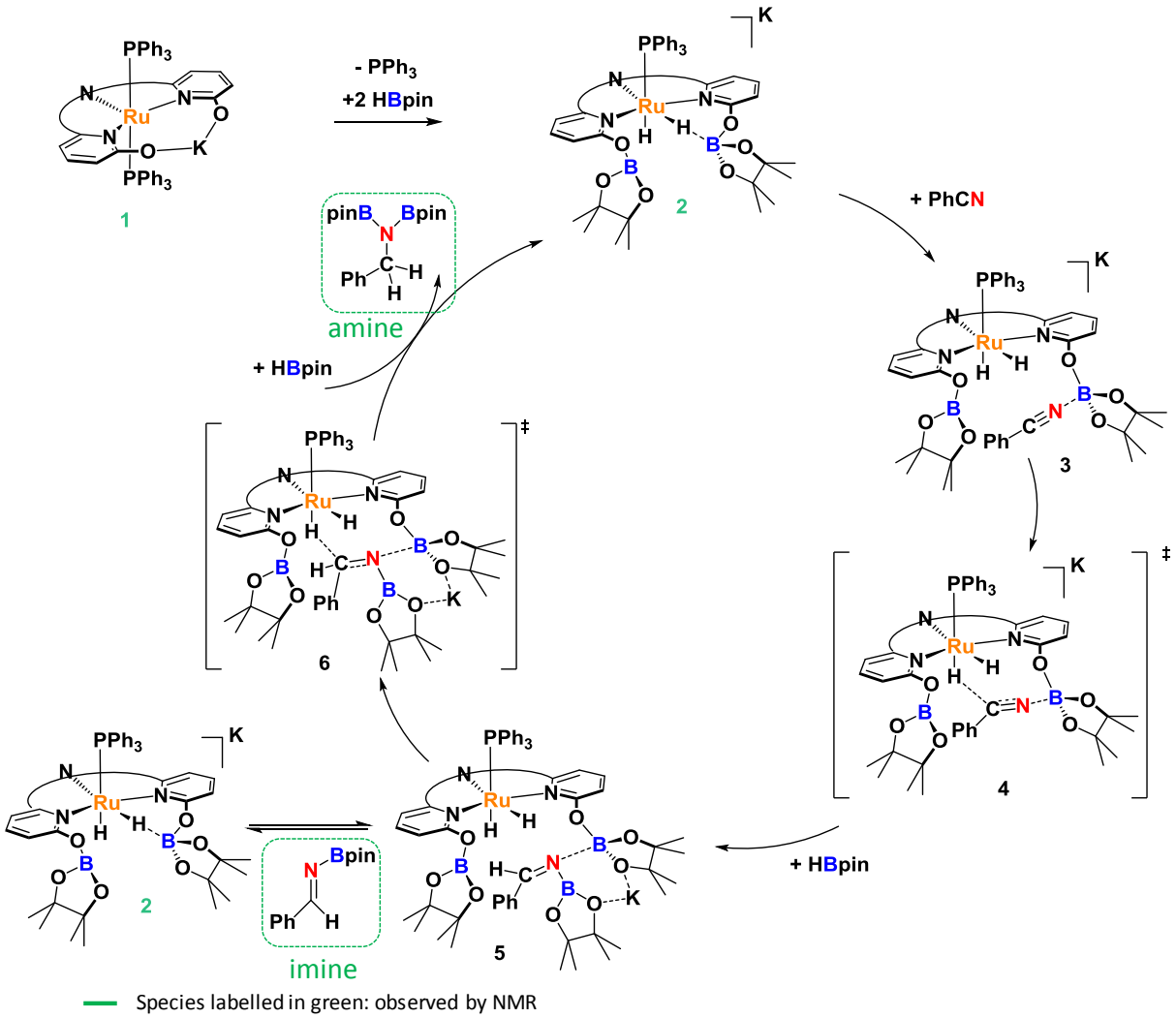

Scheme 1-19: Suggested catalytic cycle for ruthenium catalyzed hydroboration of nitrile with a proton switchable bifunctional complex

A collaboration between the boron-containing ligand and the Ru–H enabled nitrile reduction. It is reminiscent of the catalytic reduction of nitriles with $NaBH_4$ described by Williams and coworkers, where the boron of the ligand and the ruthenium center work in concert to reduce the C≡N bond.[126]

Finally, one very last example by Gunanathan and coworkers concerns both nitrile and imine hydroboration with a ruthenium precursor catalyst [Ru(p-cymene)Cl_2] **2**. [125] The authors described the reduction of nitriles and aldimines with HBpin. Under optimizing conditions, 1 mol% and 0.1 mol% of pre-catalyst, respectively, convert nitriles and imines into borylated

amines. Nitriles were fully converted after 15-36 hours at 60°C with over 73% yields for the different substituted compounds. Imines gave over 83% yields after 15 h. Insight into the mechanism of nitrile reduction was studied. The proposed mechanistic pathway is rationalized in Scheme 1-20. Activation of the dimeric ruthenium precursor with one equivalent of HBpin is necessary to form the dimeric hydro chloro complex **2**. Further activation with more HBpin was proposed to generate an unobserved monomeric borylated Ru complex **3**. Then, the nitrile function would interact with an end-on coordination mode to the metal center. In this case, both B–H and C≡N bonds are activated at the metal center. C≡N bond insertion into the Ru–H would generate the imido boryl ruthenium species **5**. NMR monitoring enabled the observation of the borylated imines released in the media. The borylated imines can coordinate to complex **3** *via* the two-electron-donor nitrogen. Repetition of insertion into the Ru–H bond and reductive elimination steps afforded B–N bond formation. This process differs from the methods described above.

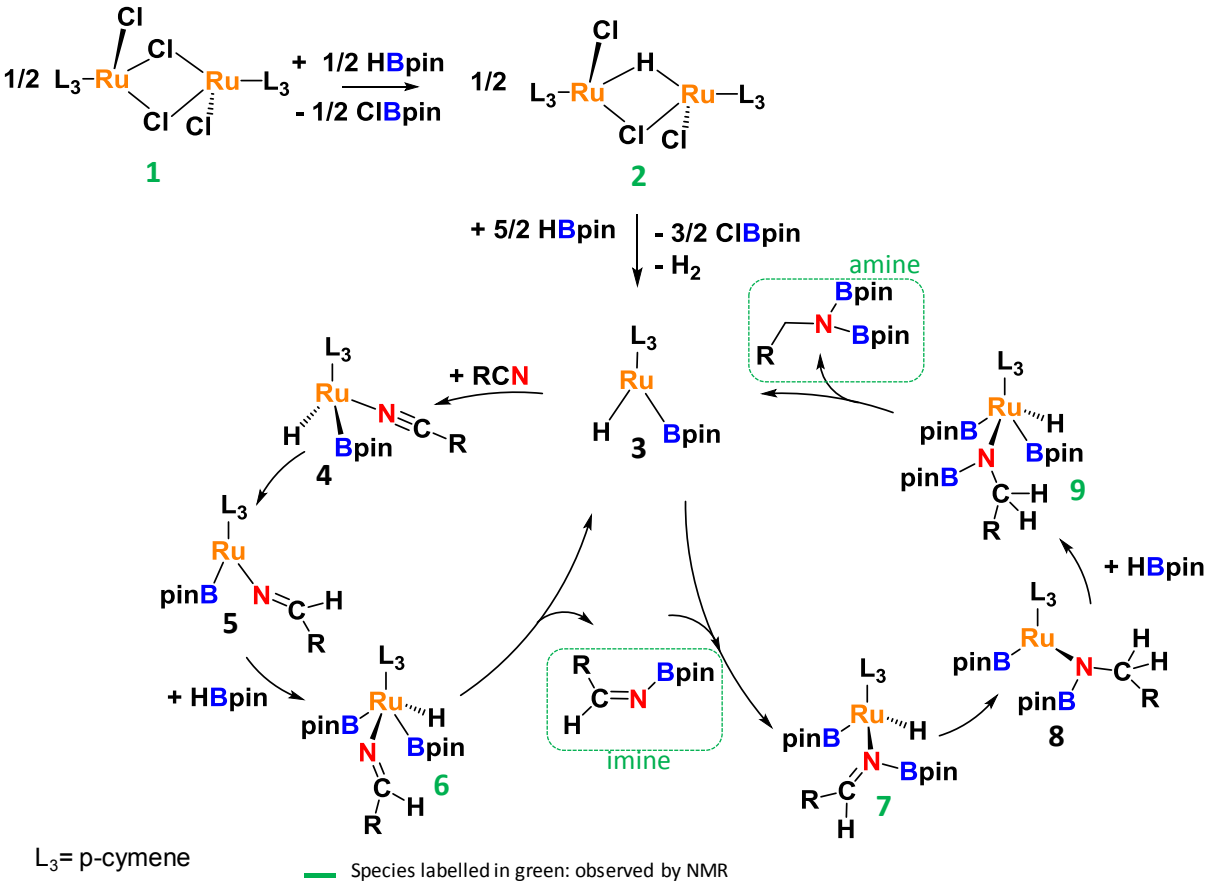

Scheme 1-20: Suggested catalytic cycle for [Ru(p-cymene)Cl₂]₂ nitrile hydroboration

In conclusion, nitrile hydroboration offers an alternative way to reduce nitrile. The reduction occurs in mild conditions and allow control of the selectivity of the product. Aminoborane, $^{i}Pr_2NBH_2$, reduces nitriles with catalytic amount of lithium compounds, even though no borylated product was reported. Hydroboration is achieved with more or less electropositive centers namely magnesium, molybdenum and ruthenium based catalysts. The borane source for those systems is either HBpin or HBcat. All the processes involved mononuclear species in the catalytic cycle. The authors commonly described a metal hydride complex as an active species in the catalysis. Some general considerations on the hydroboration of nitriles catalyzed by metal hydride complexes are proposed in Scheme 1-21.

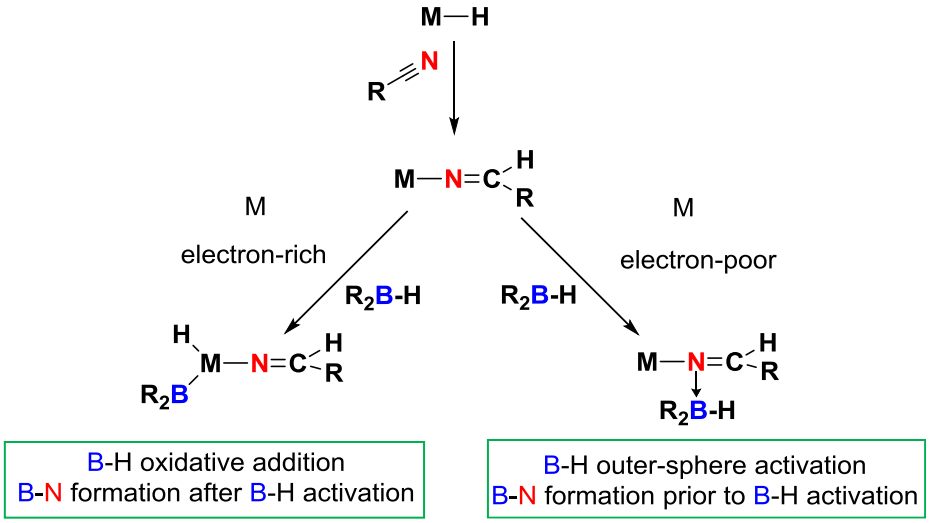

Scheme 1-21: General considerations for the hydroboration of nitriles with metal hydride complexes

Except in the specific case of ruthenium catalysis with non-innocent ligands,[124] the nitrile function is inserted into the M–H bond to afford an imido complex. However, the processes of B–H bond activation differ with the catalyst employed. In ruthenium-based catalysis, the B–H bond was fully cleaved by the catalyst prior to B–N bond formation. Electron-rich and high-valent ruthenium species are more likely to accommodate and cleave σ-bonds. Molybdenum and magnesium based catalysts involved an outer-sphere B–H bond activation *via* B–N interaction. The M–N bond is more polarized in low valent and electron poor catalysts favoring B–H activation at the nitrogen of the imido complex rather than oxidative addition of the B–H bond at the metal center. It is interesting to note that in the case of electron-rich ruthenium species, the iminoborane is released in the medium. Despite those general considerations, all those systems show a specific pathway. Rationalization in one unequivocal

route, as done for alkene hydroboration, seems not applicable for catalytic nitrile hydroboration.

II.3.4. Nitrile hydrogenation

Catalyzed nitrile hydrogenation with molecular H_2 is an atom-economic way to get primary amines. One important related industrial process is the hydrogenation of adiponitrile for the synthesis of Nylon-6,6. Nowadays, industrial processes work with cobalt or nickel heterogeneous catalysts. They usually operate in harsh conditions of pressure and temperature and are poorly selective. The control of the selectivity in nitrile hydrogenation is challenging. The intermediary imines are highly reactive and can combine with primary amines to generate secondary and even tertiary amines. Homogeneous catalytic systems have been studied to overcome this lack of selectivity. The first ones were based on platinum group metals. Ruthenium, rhodium, palladium, iridium and platinum based catalysts show great activity and selectivity toward nitrile hydrogenation into primary amines. Ruthenium based systems are the most exemplified.[127] The example of nitrile hydrogenation with $RuH_2(H_2)_2(PR_3)_2$ will be detailed in the next section.

With the idea to lower the price and "toxicity" of such systems, very recent reports propose non-precious metal based catalytic nitrile hydrogenation. The first example appeared in the literature in 2014 and was published by Beller and cowokers.[128] They disclosed an iron PNP pincer precursor catalyst able to reduce selectively numerous alkyl, aryl and heterocyclic nitriles to primary amines. The reaction occurred between 70 and 100°C under 30 bar of H_2 loaded with 1 mol% of the iron precursor catalyst. The last 2 years, more examples appeared in the literature with iron[129-130] manganese[131] and cobalt[132] pincer pre-catalysts. They operate in similar conditions and sometimes require additives such as bases. Mechanistic considerations show the implication of the non-innocent ligand in the hydrogenation of the polar CN bond with pincer complexes.[133]

In conclusion, the reduction of CN bonds under dihydrogen is atom economic and starts to be be extended to non-precious metal-based catalysts, affording good selectivity in primary amines. The required hydrogen pressures are still high. The reduction of multiple CN bonds with hydroboranes can be performed in mild conditions in comparison, and do not suffer from poor selectivity. The control of imine generation can also be achieved. This emerging strategy

also allows a diversification of the efficient catalytic systems. Beyond the control of the selectivity, the hydroboration of CN bonds can be used to produced valuable BN containing molecules as demonstrated by Figueroa and coworkers.[118]

II.4. Nitrile reduction and B–H bond activation with $RuH_2(H_2)_2(PR_3)_2$

Hydrogen is the simplest element, core component of many molecules and a source of energy. Hydrogenation/dehydrogenation are essential chemical transformations. In nature, iron and nickel-based hydrogenaze enzymes activate molecular dihydrogen. In this respect, chemists invented organometallic systems able to split and transfer dihydrogen to various substrates. Until 1984, scientists believed dihydrogen had to go through oxidative addition to bind the metal center. Yet, Kubas and coworkers isolated and characterized the first stable σ-H–H complex.[134] M-(η^2-H–H) is a three-center-two-electron interaction, intermediate in the oxidative-addition and reductive-elimination of H_2. In this configuration, H–H σ-bond is activated but not cleaved. This coordination mode requires a subtle balance between H–H σ-donation and the metal d-back donation, influenced by the nature of the ligands around the metal, and the metal itself (Figure 1-19). σ-ligands are a new kind of L ligands with a coordination mode reminiscent of the Chatt-Dewar-Duncanson model for olefin coordination. Since their discovery, this class of ligands has been extended to various σ-E–H bonds including B–H bonds.

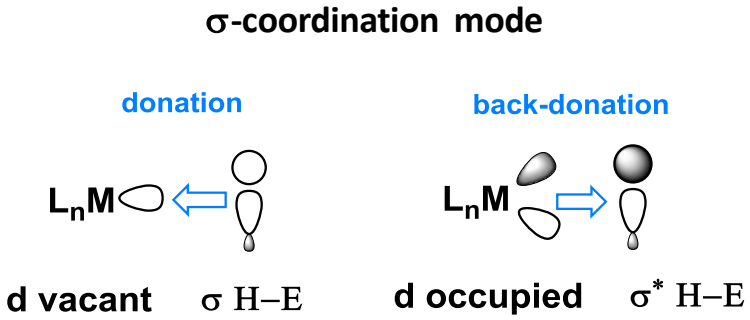

Figure 1-19: Description of σ-bond coordination mode

Hundreds of σ-dihydrogen complexes have been characterized whereas very few examples of bis(dihydrogen) complexes exist. Among them, the most studied one is the ruthenium dihydride bis(dihydrogen) bis(phosphine) complex $[RuH_2(H_2)_2(PR_3)_2]$ that we use in the team (Figure 1-20). Synthesis with tricyclohexylphosphine affords complex **I** while complex **II** is obtained starting from tricyclopentylphosphine.[135-136] The complex displays two types of hydrogen ligands: two hydride X ligands and two η^2-H–H dihydrogen L ligands. Hydrides and dihydrogen ligands fast exchange around the metal center. As a result, ^{1}H NMR spectra of **I** and **II** show only one signal around – 8 ppm being a pseudo triplet.

Hydrides/σ-dihydrogen ligands fast exchange

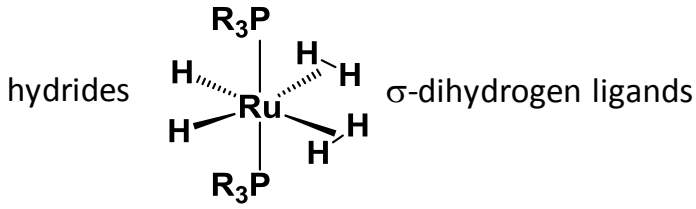

| PR_3= PCy_3 = tricyclohexylphophine, || PR_3= $PCyp_3$ = tricyclopentylphophine

Figure 1-20: $RuH_2(H_2)_2(PR_3)_2$ complexes

The two σ-dihydrogen ligands are labile, offering the possibility to coordinate other σ-bonds such as Si–H bonds and, more relevant to our study, B–H bonds.[137] Formally, a very reactive 14-electrons species is generated upon H_2 decoordination endowing the complex with great catalytic ability. Hence, σ-bond coordination onto **I** and **II** have been studied and subsequent catalytic activity have been demonstrated. The use of complexes **I** and **II** in nitrile hydrogenation reaction and B–H bond activation will be more particularly detailed.

II.4.1. $RuH_2(H_2)_2(PR_3)_2$: nitrile hydrogenation

With its great ability to coordinate/decoordinate H_2, complexes **I** and **II** seemed to be suitable precursors for hydrogenation reactions. In 1996, the use of **I** as a catalyst precursor for nitrile hydrogenation was disclosed by Beatty and Paciello in a series of patents.[138] In 2010, our team presented an efficient nitrile hydrogenation process employing $RuH_2(H_2)_2(PCyp_3)_2$ as pre-catalyst.[139] The conversion is selective to primary amine and performed in mild conditions (P_{H2} = 3 bar, RT). The addition of 0.5 mol% of **II** in pentane led in two hours to the recovery of 88

% of primary amine. Ruthenium loading can be lowered to 0.2 % when performed in THF but requires a longer reaction time (24h).

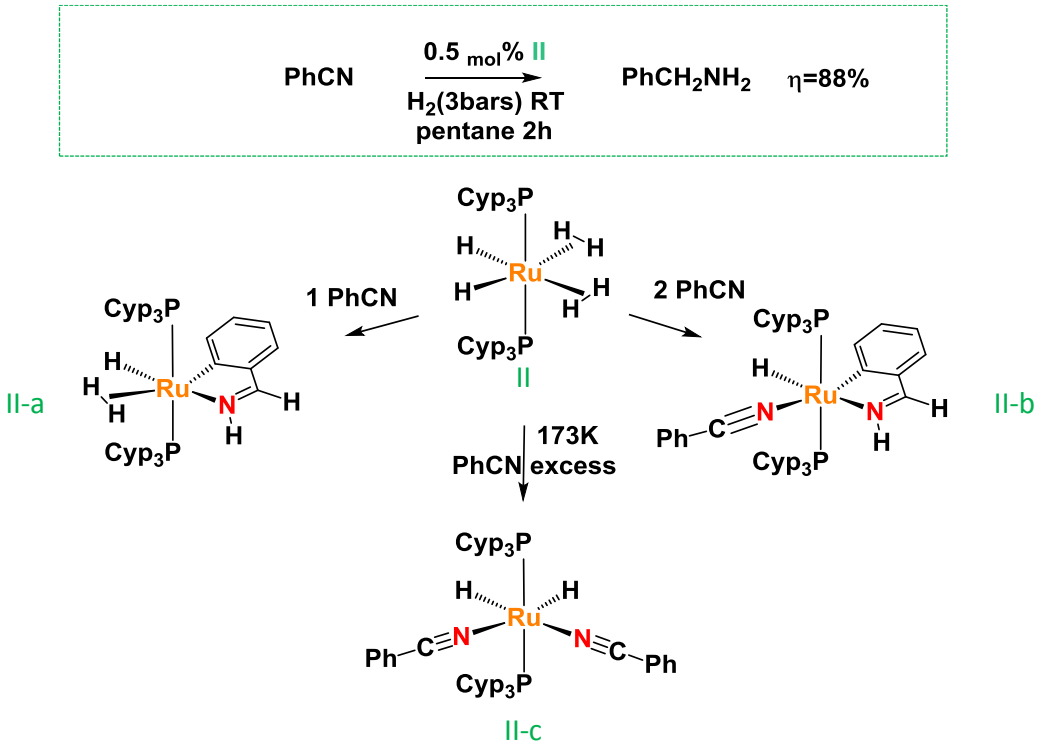

Scheme 1-22: Nitrile hydrogenation with $RuH_2(H_2)_2(PCyp_3)_2$

A series of catalytic and stoichiometric experiments have been conducted to gain information on the transformation pathway. Isolated and/or characterized species are represented in Scheme 1-22. Catalytic reaction monitoring by NMR at low temperatures allowed the observation of three intermediate complexes **II-a**, **II-b** and **II-c** (Scheme 1-22). The bis(nitrile) complex **II-c** resulted from σ-H–H substitution by two benzonitriles with an end-on coordination mode. **II-c** was observed throughout the catalysis but could not be isolated. Yet, **II-a** and **II-b** were successfully isolated at a stoichiometric level. One equivalent of PhCN was added to complex **II** and gave complex **II-a**. An ortho-metalated benzylimine is formed. It is the result of one equivalent of H_2 added across the C≡N bond and C–H bond activation at the phenyl ring. The ortho-directed C–H activation is reminiscent of Murai's reaction[140] and seems to be a key step in cyclometallation and subsequent trapping of **II-a**. When two equivalents of PhCN were added to **II**, complex **II-b** was observed. It differs from **II-a** in substitution of one H_2 ligand by an end-on coordinated nitrile. **II-b** contains two different activation stages of benzonitrile: an early-stage end-on nitrile and the monohydrogenated imine. Complexes **II-a**

and **II-b** have both been characterized by X-ray diffraction, IR and NMR spectroscopy. They have proven to catalyze the selective benzonitrile hydrogenation into benzylamine in standard conditions established with complex **II**.

II.4.2. B–H bond activation and related reactivity with $RuH_2(H_2)_2(PCy_3)_2$

II.4.2.a. σ-borane complexes and hydroboration

Hartwig and coworkers isolated the first σ-borane on titanium in 1996.[141] They further discovered that σ-borane could be an intermediate species involved in catalytic hydroboration. In 2002, our team isolated a Ru borohydride σ-borane complex when an excess of HBpin was mixed with complex **I** (Scheme 1-23). It is remarkable that the boranes can coordinate with two different modes on the same metal center: one σ-borane and one borohydride. This complex happened to be an efficient catalyst for hydroboration of linear and cyclic alkenes.[96-97] Alkylboranes, or more interestingly, vinylboranes are favored according to the operating conditions.

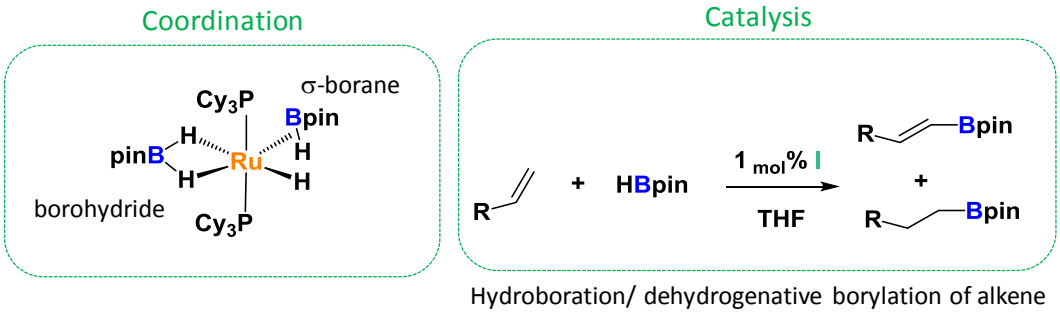

Scheme 1-23: HBpin coordination on $RuH_2(H_2)_2(PCy_3)_2$ (left) and related reactivity (right)

II.4.2.b. Bis σ(B–H)-aminoborane complexes and amine-boranes dehydrogenation

The first bis σ-borane was characterized in 2007. It is the result of a stoichiometric mixture of mesitylborane and **I**.[142] This unusual coordination mode engages two geminal B–H in a σ-bond interaction fashion with ruthenium. Analogueous bis σ(B–H)-aminoborane complexes have been trapped on the way to amine-borane dehydrogenation. In particular, stoichiometric reaction of **I** with AB generates the dihydride bis σ(B–H)-aminoborane ruthenium complex as depicted in Scheme 1-24.[7]

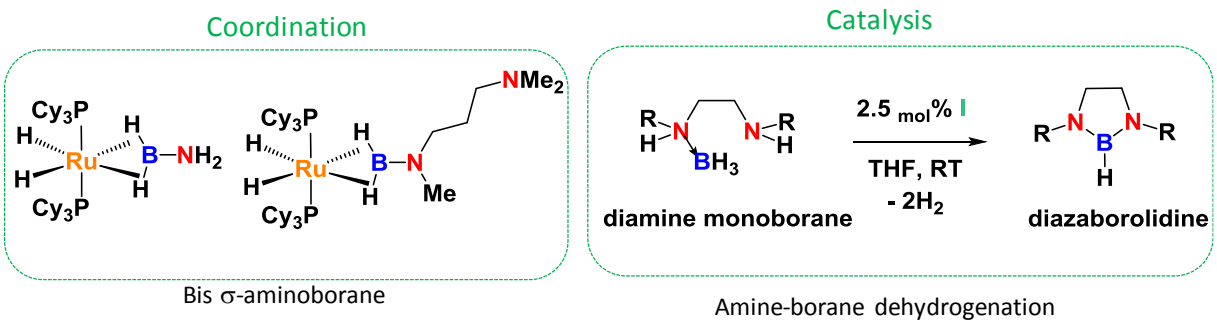

Scheme 1-24: Amine-borane coordination to $RuH_2(H_2)_2(PR_3)_2$ (left) and related catalysis (right)

Observing the aminoborane coordination mode on **I**, encouraged the search for catalytic systems. Our team disclosed the catalytic dehydrogenation of diamine monoborane using 2.5 mol% of **I** in THF at room temperature to form cyclic diazaborolidines (Scheme 1-24). [143] This reaction is a clean process extended to a range of diamine monoboranes and one amineborane alcohol. The mechanism of the catalytic dehydrogenation goes through the formation of an intermediate bis σ(B–H) -aminoborane. The representative bis σ(B–H) -aminoborane intermediate with a hydrogen-free nitrogen did not led to BN intramolecular interaction. Sequential B–H and N–H bond activation was postulated, and formation of a six membered ring featuring a dihydrogen bond led finally to the release of the cyclic product.[144]

II.4.2.c Agostic σ-B–H interaction

Green and Brookhart used the agostic terminology for the first time in 1983 to describe a 3-center-2-electron interaction between a metallic fragment and a C–H bond of a ligand.[145] They believed this type of interaction was more common than expected. Agostic interactions are described as weak and often fluxional,[146] thus difficult to detect. They often stabilize electron-poor species. Agostic complexes appeared to be key intermediates in numerous chemical transformations such as ethylene polymerization.[147] They play a role in lowering energetic barriers in certain steps of the transformation or induce specific selectivity. Nowadays, the term of agostic interaction has been extended to various σ-bonds such as σ-C–H, σ-C–C, σ-C–B, σ-C–Si, σ-Si–H and σ-B–H.

Braunschweig and coworkers isolated the first agostic σ-B–H in 2008 on the way to alkene borylation.[148] The chromium center interacts with both π-C=C bond and σ-B–H bond in an η^2-coordination mode (Figure 1-21). One can note that boron is tricoordinated and substituted

with a stabilizing $N(SiMe_3)_2$ moiety. This configuration favors the 3-center-2-electron interaction.

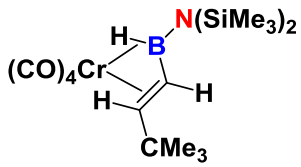

2008
First agostic σ-B–H complex

Figure 1-21: First isolated agostic σ-B–H (alkene) complex

Around the same time, our team developed a new class of borane-attached ligands in an attempt to isolate new B–H agostic complexes. The synthesis of such species was challenging, as this class of L-BHR compounds remained rather unexplored. The borane needs a stabilizing group such as nitrogen to remain tricoordinated. It must also feature a B–H moiety excluding all common bidentate alkoxy substituents. In this respect, bifunctional versatile phosphino~boranes ligands including a B–H moiety were successfully synthesized from $^{i}Pr_2NBHCl$ (Figure 1-22). Four phosphino~aminoborane ligands with different spacer groups have been created.

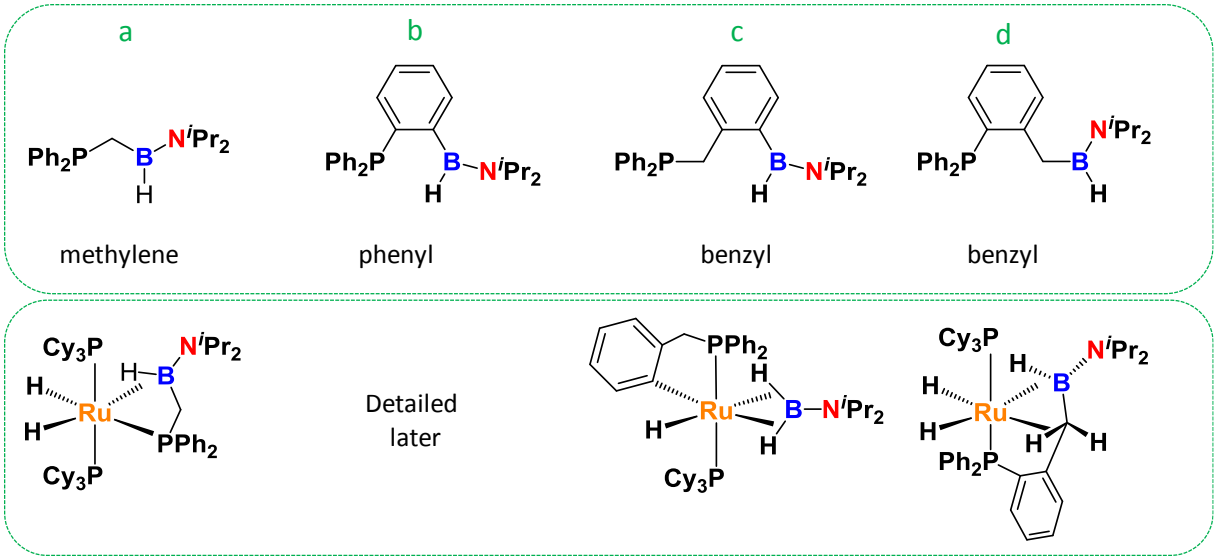

Figure 1-22: Series of bifunctional phosphino~aminoborane ligands recently developed in the team (top) and subsequent coordination on $RuH_2(H_2)_2(PCy_3)_2$ (bottom)

The team chose $RuH_2(H_2)_2(PCy_3)_2$ as a precursor for the coordination study. The ligands would react with the 14 electrons species obtained by decoordination of the σ-H_2 ligands. Upon coordination, the phosphino~aminoborane with the methylene spacer replaced the σ-H_2 ligands in the equatorial plane to generate a new complex (Figure 1-22-a).[149] The phosphorus and B–H bond both interacts with the ruthenium center to form a σ-B–H agostic complex. Modifying the spacer drastically changed the coordination. The ruthenium complex cleaved the B–C bond of the phosphino~aminoborane with a benzyl spacer upon coordination (Figure 1-22-c).[150] Yet, the phosphino~aminoborane with a reverse benzyl spacer displayed a surprising coordination on ruthenium with both B–H and C–H agostic interactions (Figure 1-22-d).[151] Finally, coordination of the phosphino~aminoborane with a phenyl spacer on complex **I** provided an equilibrium of σ-B–H agostic complexes (Scheme 1-25).[152]

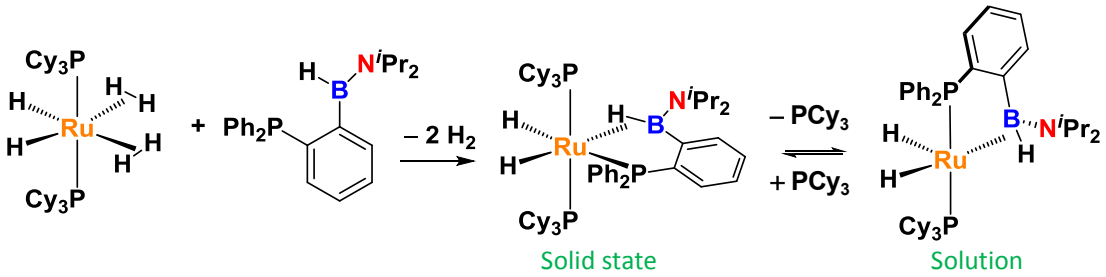

Scheme 1-25: Coordination of aryl(phosphino)(aminoborane) ligand onto $RuH_2(H_2)_2(PCy_3)_2$ both in solution and in the solid state

Upon stoichiometric reaction of the ligand and **I**, a new complex was observed in solution. Complex **I** lost one phosphine and two dihydrogen ligands to accommodate the aryl(phosphino)(aminoborane). The PPh_2 moiety is in the apical position while the B–H bond interacts in the equatorial plane *via* an agostic interaction. Surprisingly, in the solid state (after evaporation), they identified a different complex reminiscent of the coordination of the aryl(phosphino)(aminoborane) with a methylene spacer where the phosphorus and the B–H moiety substituted the σ-H_2 ligands in the equatorial plane. In both cases, the B–H bond interacts in a 3-center-2-electron fashion with the metal center (Scheme 1-25).

II.4.2.d Project description:

The systematic study carried out with phosphino~borane compounds always resulted in the activation of the B–H bond *via* σ-B–H interaction. We had in mind to transpose this

coordination study to a catalytic system. The idea was to bring the activation of the B–H bond to a further stage. To do so, we designed a substrate bearing a reactive function in the vicinity of the B–H bond. The model molecule is depicted in Figure 1-23. In place of the coordinative phosphine, the nitrile group was incorporated since we knew that complex **I** catalytically reduces this function under H_2. To start with, we decided to transpose the phosphino~borane structure depicted in Figure 1-22-b to the corresponding aryl(cyano)(aminoborane) as shown in Figure 1-23. The borane part of the molecule remains unchanged featuring a B–H bond, a stabilizing N^iPr_2 group and a phenyl spacer. The synthesis and characterization of a series of aryl(cyano)aminoboranes will now be described in chapter 2 together with their catalytic transformation in presence of complex **I** under H_2 pressure.

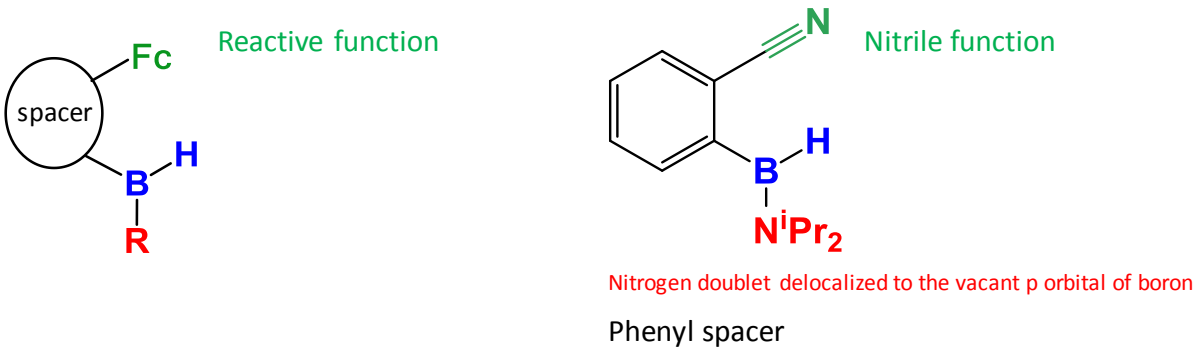

Figure 1-23: Ligand design for a catalytic transformation with $RuH_2(H_2)_2(PR_3)_2$

CHAPTER 2:

RUTHENIUM CATALYZED B–H AND C≡N BOND ACTIVATION UNDER H_2

CHAPTER 2: RUTHENIUM CATALYZED B–H AND C≡N BOND ACTIVATION UNDER H_2

I. Synthesis of aryl(cyano)(aminoborane) derivatives

I.1. Synthetic approach

Inspired by the synthesis of bifunctional aryl(phosphino)(aminoborane) ligands, we prepared a series of new aryl(cyano)(aminoborane) substrates. The synthetic approach was first assessed for a representative aryl(cyano)(aminoborane) possessing a nitrile group ortho to the B(sp^2)–H aminoborane. A few cyanoarylboranes or cyanoarylborates were reported in the literature but all feature alkoxy or halogen substituents.[153-154] Those cyanoaryl borate and boronates can be obtained *via* aromatic borylation and are often engaged in coupling reaction generating boron-based waste. However, no B(sp^2)–H ortho to a nitrile function had been described prior to our work. We proposed a synthetic strategy in two steps one pot, involving lithiation/ borylation sequences from 2-bromobenzonitrile (Scheme 2-1).

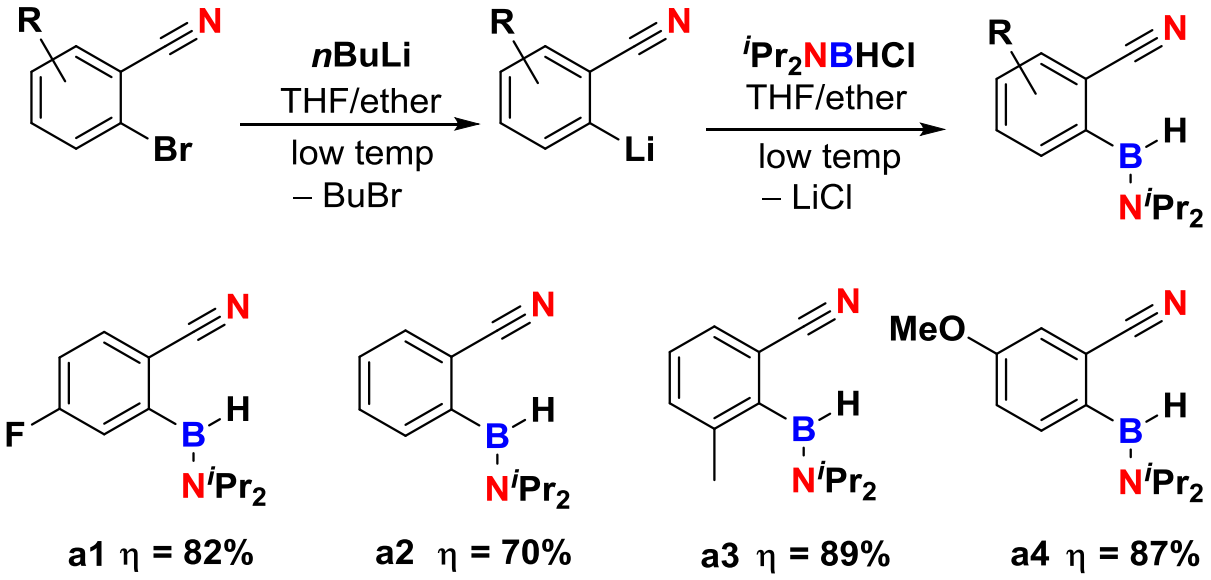

Scheme 2-1: Synthetic procedure towards aryl(cyano)(aminoborane) derivatives

This procedure is in accordance with the one previously reported for the synthesis of phosphino~boranes[152] and has been successfully transposed to the synthesis of the representative aryl(cyano)(aminoborane) **a2**. The lithiation/borylation steps occur through slow addition of *n*BuLi at −78°C in THF followed by quick addition of $^{i}Pr_2NBHCl$ onto the lithiated benzonitrile intermediate. Compound **a2** was obtained in a reproducible manner in 70% isolated yield. Temperature is a key parameter and has to be monitored accurately throughout the procedure. Otherwise, NMR spectra showed broad signals, probably corresponding to polymers. Indeed, the lithiated benzonitrile tends to self-condense owing to the presence of the nucleophilic carbon C−Li and electrophilic carbon of the nitrile function.[155]

We were then willing to extend the reaction to several aryl-substituted derivatives. Our motivation was to study both the influence of electronics and sterics. We selected a fluorine as an electron withdrawing group in **a1**, a methyl substituent positioned ortho to the borane in **a3** and an electron donating group para to the borane in **a4**. As the selected substituents do not stand in the same position of the aryl, the comparison is not straightforward but one can study the influence of the substituent by comparing to the parent **a2**. Extending the lithiation/borylation sequence to the aryl-substituted derivatives **a1**, **a3** and **a4** was successfully achieved. Yet, when 4-fluoro-2-bromo benzonitrile and 5-methoxy-2-bromo benzonitrile were treated in the same conditions, numerous unexpected NMR signals were observed along with low yields in the desired products **a1** and **a4**. Fluorine and methoxy are directing metalation groups for aromatic lithiation and might favor the generation of lithiated products in unwanted positions.[156] As a result, the lithiation/borylation sequence to obtain **a1** and **a4** was realized with adjusted conditions. The reaction occurred in 1:1 volume mixture of THF/diethylether at − 100°C to afford **a1** and **a4** in 82% and 87% isolated yields, respectively. On the contrary, 3-methyl substituted aryl(cyano)(aminoborane) was recovered with a high isolated yield (89%) in slightly milder conditions (− 78°C, THF). Hypothetically, the methyl group could disfavor self-condensation for steric reason and not to be recognized as a directing metalation group.

I.2. Characterization of the aryl(cyano)(aminoborane) series and comparison

I.2.1. Spectroscopic characterization of the parent compound a2

Compound **a2** was isolated as a colorless oil, stable at room temperature. The compound was fully characterized by HRMS, IR and multinuclear NMR spectroscopies. Specifically, ^{11}B NMR is a powerful tool for the characterization of boranes. The singlet at 37.5 ppm in ^{11}B{^{1}H}c NMR becomes a doublet in ^{11}B NMR with a coupling constant of 115 Hz (Figure 2-1). The downfield chemical shift is characteristic of a trigonal boron while the large coupling constant is in the typical range for a direct B–H coupling. The related ^{1}H NMR spectrum shows a broad quartet at δ 5.5 attributed to the B–*H* resonance (Figure 2-1).[47, 149-150] The ^{11}B isotope has a spin 3/2 so the B–*H* proton must be a quartet according to the multiplicity rule. The signal is broad owing to the large quadrupolar moment of the ^{11}B nuclei. In the ^{1}H{^{11}B} NMR spectrum, the B–*H* resonance is associated to a define singlet.

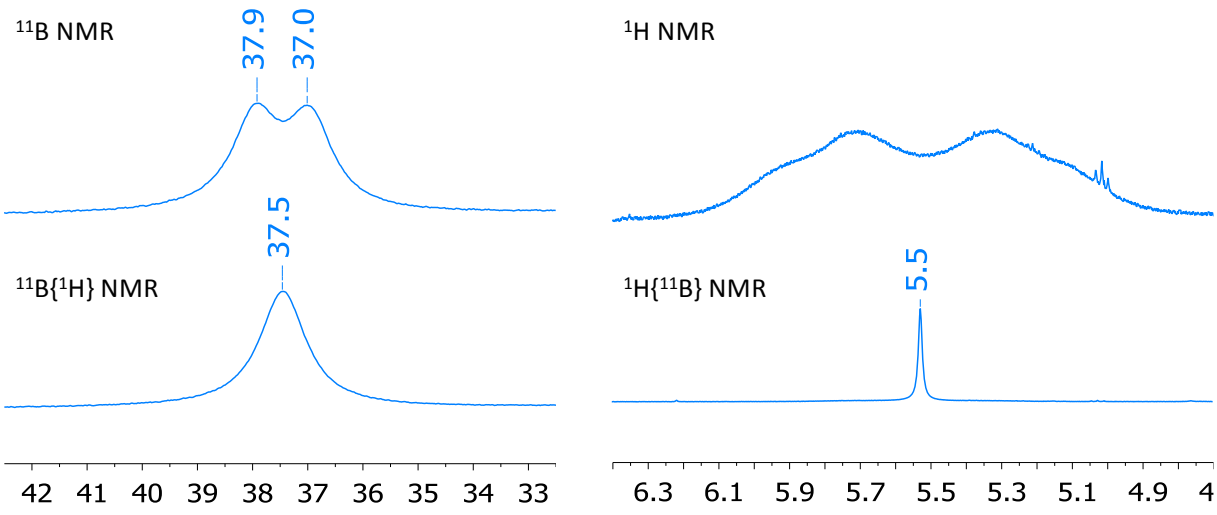

*Figure 2-1: ^{11}B NMR, ^{11}B{^{1}H} NMR (left) and ^{1}H NMR, ^{1}H{^{11}B} NMR (right) spectra of **a2***

The ^{1}H NMR spectrum reveals two distinct signals for C*H* ^{i}Pr each integrating for 1H and two peaks for C*H*$_3$ ^{i}Pr, each integrating for 6H. The two isopropyl groups are inequivalent supporting hindered rotation around the B–N bond due to its double bond character. Yet, the two CH_3 within the isopropyl group are equivalent indicating free rotation around the N–C

bond. Altogether, those data reflect the presence of a B(sp^2)HN^{i}Pr$_2$ group in **a2**. The ^{13}C NMR spectrum displays in particular a quaternary carbon at 119.8 ppm attributed to the nitrile carbon (see experimental section and appendices for full characterization).

The infrared spectrum of the oil revealed the presence of the key functions in the molecule. The characteristic B–H bond stretching frequency is detected at 2491 cm^{-1} with a shoulder at 2460 cm^{-1} within the typical range for B–H vibration bands.[157] The integrity of the cyano group is evidenced by a strong IR stretching frequency observed at 2219 cm^{-1}.

Compound **a2** is soluble in most common organic solvents, including pentane. However, crystals were successfully grown, by slow evaporation at room temperature, of a saturated solution of **a2** in pentane. X-ray diffraction analysis on a monocrystal of suitable size confirmed the identity of **a2** as well as **a1** and **a3** (see below).

I.2.2. Characterization of the substituted compounds and comparison

Compounds **a1**, **a3** and **a4** were isolated and characterized in a similar manner. A comparison of their main characteristics is provided below with a selection of spectroscopic data reported in Table 2-1. Substituents on the aryl do not greatly influence the spectroscopic data. Very small differences in ^{11}B {^{1}H} chemical shifts are observed.

Compounds	*IR (cm^{-1})*		*NMR (ppm)*			
	ν_{B-H}	$\nu_{C\equiv N}$	^{11}B {^{1}H}	$^1J_{B-H}$ (Hz)	^{1}H (B–H)	^{13}C (CN)
a1	2495 (s) 2482 (sh)	2219	37.1	110	5.35	118.75
a2	2491 (s) 2460 (sh)	2219	37.5	115	5.52	119.55
a3	2470 (s) 2450 (sh)	2220	37.8	120	5.49	119.84
a4	2488 (s) 2454 (sh)	2222	37.7	115	5.51	119.54

*Table 2-1: Selected spectroscopic data related to **a1-4***

The ^{1}H NMR spectra all evidence non-equivalent isopropyl groups with 2 signals for the C*H$_3$* ^{i}Pr and two signals for the C*H* ^{i}Pr except in the case of **a3** displaying four C*H$_3$* ^{i}Pr resonances. We attribute this singular behavior to the restricted rotation around the N–C bond induced by the proximity of the methyl substituent on the phenyl ring. The carbons of the nitrile

functions were found around 119 ppm in the $^{13}C\{^{1}H\}$ NMR spectrum within the series. Substituents have thus a small impact on the chemical shift.

The four compounds show very similar C≡N vibration bands. Yet, the B–H elongation slightly varies according to the substituents in the following manner: ν **a1** > ν **a2** > ν **a4** > ν **a3**. The fluorine derivative exhibits the highest B–H vibration band of the series indicative of a stronger bond. Comparatively, the methyl-substituted derivative is shifted of 25 cm^{-1} towards lower values informing of a weaker B–H bond. Giving a closer look to the infrared spectra of the compounds, in addition to the strong B–H stretching band, we see two or more shoulders (see appendices section and Figure 2-7). In contrast, the B–H resonances in the $^{1}H\{^{11}B\}$ NMR spectra appeared as a unique singlet for each compound. The infrared spectrum of **a2** in solution was identical to that of the oil. As only a few examples of related $R(NR'_2)BH$ are known, we decided to investigate on this phenomenon using computational methods (see experimental section for DFT details). We assumed the additional B–H frequencies were due to limited rotation around the B–N bond. The compounds were modeled accordingly to the crystal structure. It appeared impossible to find another minimum by rotation around the B–N bond. In order to mimic the phenomenon, we positioned the ^{i}Pr moieties in different directions. The calculated B–H and C≡N vibrations are reported in Table 2-2. The model compounds of **a1-3** are labeled **A1-3.**

	A B–H	*A C≡N*	$A_{180°}$ *B–H*	$A_{180°}$ *C≡N*
A1	2495	2229	2470	2228
A2	2492	2229	2468	2228
A3	2466	2224	2441	2226

*Table 2-2: B–H and C≡N vibration bands (cm^{-1}) generated from the simulated crystal structure (**A1-3**) and the simulated structure after a turn of 180° around the B–N bonds ($\mathbf{A_{180°}}$). A correction factor of 0.95 was applied.*

The model structure $\mathbf{A_{180°}}$ was generated by rotating the ^{i}Pr moieties of 180 °around the C–N bonds (equivalent to a 180° rotation around the B–N bond). **A2** and $\mathbf{A2_{180°}}$ are depicted in Figure 2-2.

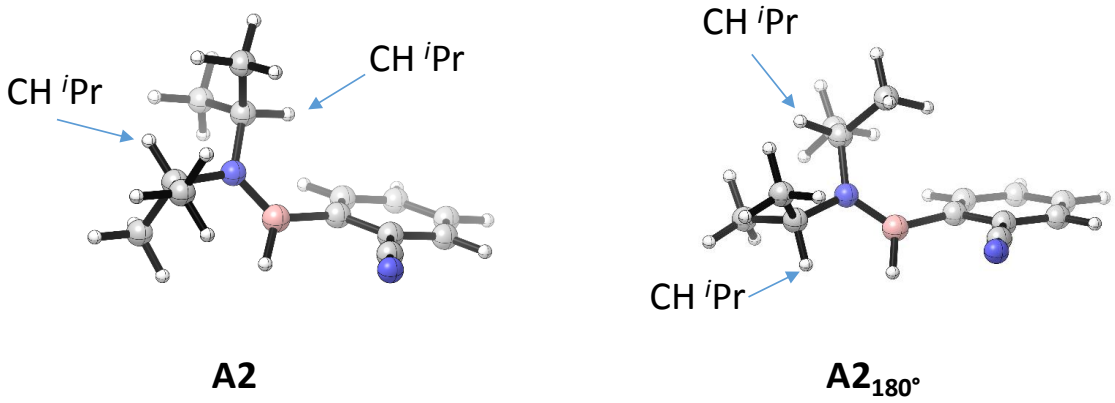

*Figure 2-2: Model structure of **a2** (**A2**) and the related structure after 180° rotation of the ^{i}Pr groups (**A2**$_{180°}$)*

In all cases, **A** and **A**$_{180°}$ display a shift of about 25 cm^{-1} regarding the B–H bond vibrations. The experimental IR spectrum of compound **a2** shows a major stretching band at 2491 cm^{-1} and a second one around 2460 cm^{-1} (≈ 30 cm^{-1} of difference), in agreement with the theoretical calculations. The phenomenon is recurrent within the series. However, the band shift fluctuates from 13 (**a1**) to 34 (**a4**) cm^{-1} experimentally for the different compounds. Thus, we calculated other possible isomeric structures involving different angles for the rotation of the ^{i}Pr moieties. We observed that the values shift depended on the angle of rotation we had chosen. Notably, the calculated C≡N vibration bands were not influenced in accordance with the experimental spectra displaying a sharp and unique vibration for each derivative.

In summary, the double bond character of the B–N bond induces a hindered rotation, which influences the B–H bond regardless of the C≡N function. The phenomenon is not observable at the NMR timescale (ms) but becomes clear at the infrared timescale (ps). R(NR'$_2$)BH compounds possess multiple vibration bands corresponding to the B–H bond.

The structures obtained by X-ray diffraction on monocrystals of **a1**, **a2** and **a3** are depicted in Figure 2-3 along with the related aryl(phosphino)(aminoborane) compound for comparison.

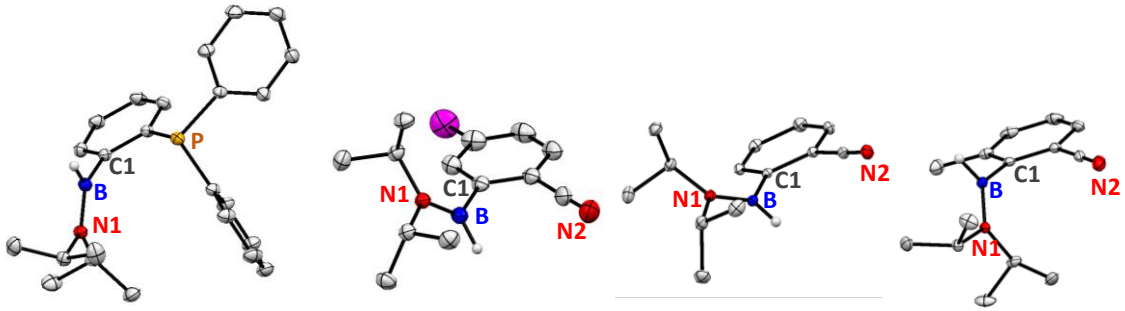

	Aryl(phosphino)(aminoborane)	a1 (F)	a2 (H)	a3 (Me)
d B-N1 (Å)	1.3921 (8)	1.376 (2)	1.383 (2)	1.382 (2)
d B-C1 (Å)	1.5877 (9)	1.586 (2)	1.580 (2)	1.588 (2)
d C≡N (Å)		1.144 (3)	1.143 (2)	1.148 (2)

*Figure 2-3: Crystal structures of the aryl(phosphino)(aminoborane), **a1**, **a2** and **a3** compounds with selected bond distances. Hydrogen atoms are omitted for clarity except for the B–H hydrogen atoms, which were located by Fourier differences.*

In 2011, X-ray data were reported for the aryl(phosphino)(aminoborane) with a B···P distance over 3 Å excluding any interaction between those two atoms.[152] Similarly, in the aryl(cyano)(aminoboranes), B···CN2 distance is over 2.887 Å in all cases and particularly B···N2 is even longer exceeding 3 Å indicating no interaction between the boron Lewis acid and the nitrogen of the rigid nitrile function. Substituents have no significant influence regarding the C≡N bond distances, which are in the typical range for a CN triple bond. In **a2**, the B–N1 bond length falls within simple and double BN bonds, evidencing π overlapping. B–N1 distances in **a1**, **a2**, and **a3** are slightly shorten compare to that of aryl(phosphino)(aminoborane) but it is only significant in the case of **a1**. This observation is consistent with the electron withdrawing character of the nitrile function that increases the boron Lewis acidity. This effect is reinforced in the case of **a1** with the electronegative fluorine substituent strengthening the boron acidity. The hydrogen of the B–H moiety points towards the C≡N in **a1** and **a2** while it is pushed away in **a3**. This different arrangement can be attributed to the steric hindrance between the isopropyl and the methyl substituents, in the solid state.

II. Catalytic transformation of aryl(cyano)(aminoboranes) with $RuH_2(H_2)_2(PCy_3)_2$

II.1. Catalytic protocol

The coordination study carried out with a series of phosphino~borane ligands and $RuH_2(H_2)_2(PCy_3)_2$ (**I**) always resulted in the B–H bond activation *via* 3-center-2-electron interaction with the metal center.[149, 152]Precisely, the aryl(phosphino)(aminoborane), led to the formation of an agostic σ-B–H complex. With the aim to push this coordination study to a catalytic system, in place of the coordinative phosphine ligand, we incorporated a nitrile function that could be reduced by complex **I** under H_2, as previously described in the group.[139] We thus prepared a series of aryl(cyano)(aminoborane) and decided to look at the reactivity under conditions where both the C≡N and the B–H bond could be activated, in a catalytic manner.

The representative aryl(cyano)(aminoborane) **a2** was selected to conduct this study. **a2** was reacted in pentane, at room temperature, with a catalytic amount of **I** (5 mol%) under dihydrogen (1 bar(g)). The first experiment led to the complete disappearance of **a2** after 5h as monitored by ^{1}H and ^{11}B NMR. NMR spectra of the crude mixture indicated the clean formation of a new compound that we attributed to the 1*H*-2,1-benzazaborole as represented in Scheme 2-2.

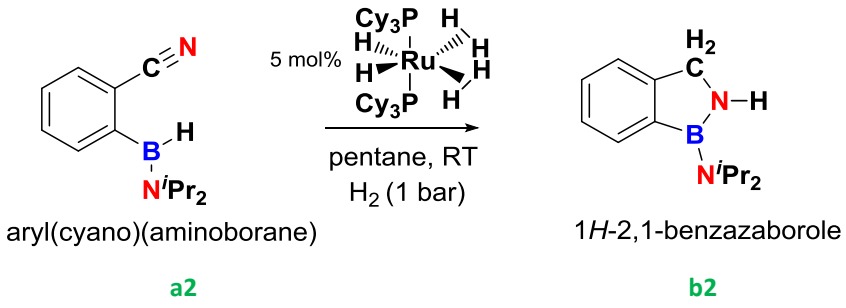

*Scheme 2-2: Catalytic conversion of aryl(cyano)(aminoborane) into 1H-2,1-benzazaborole with **I***

Products resulting from an intermolecular reaction have not been detected, excluding intermolecular hydroboration. When using anisole as internal standard, a NMR yield of 85% was determined. The remaining 15% were attributed to the formation of insoluble borazine resulting from cyclotrimerization of the 1*H*-2,1-benzazaborole (see chapter V). The 1*H*-2,1-benzazaborole can be further isolated by Kügelrohr distillation and recovered as a white solid in 82% yield.

The reaction time was first approximately determined starting from 600 mg of **a2**. It appeared to be dependent on the scale of the reaction when using a Fisher-Porter set up. We established standard conditions for the reaction, using 2.5 mL of pentane as solvent and performing the reaction at room temperature, under 1 bar (g) of H_2. Reactions were run in a Fisher-Porter bottle (20 mL), starting with 100 mg of **a2** and 5 mol% of **I.** To monitor the reaction, the reactive media was sampled under argon and placed into a NMR tube containing deuterated benzene. Under such conditions, full conversion of **a2** was observed after 25 min and recovery of the precursor catalyst occurred within one hour (as shown by ^{31}P and ^{1}H NMR).

Once mastered with the parent aryl(cyano)(aminoborane) **a2**, the catalytic reaction was extended to the aryl-substituted derivatives namely fluorine **a1**, methyl **a3** and methoxy **a4.** The reaction occurred using the standard conditions established with **a2**. The four 1*H*-2,1-benzazaborole **b1-4** have been isolated by Kügelrohr distillation as white solids in good yields (Figure 2-4).

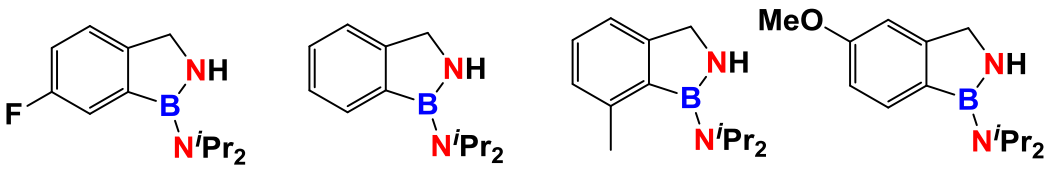

b1 b2 b3 b4

NMR yield (borazine)	**7**	**7**	**24**	**ND**
NMR Yield (b)	**84**	**85**	**73**	**ND**
Isolated yield (b)	**50**	**82**	**57**	**54**

Figure 2-4: NMR yields of 1H-2,1-benzazaboroles and borazine side products as well as Isolated yields of 1H-2,1-benzazaborole derivatives in % (ND: not determined)

NMR yields were determined using the methyl group of anisole as internal reference. Yields in **b1-3** were determined from the methylene signal. The formation of borazines as side-

products results in concomitant release of HN^iPr_2. Thus, yields in borazine were indirectly calculated integrating the C*H* ^{i}Pr of the soluble diisopropylamine. Samples of the crude mixtures gave similar NMR yields in the case of **b1** and **b2**. The fluorinated version shows a poor stability to high temperature, ending in loss of product during the distillation step. In the case of the methyl and methoxy derivatives, we observed the formation of a white precipitate in the reaction mixture. The higher NMR yield in borazine for **b3** is in agreement with this finding. The precipitate can be filtered off and recovered as pure borazine after washing with toluene. As higher temperatures were required for the purification of the substituted benzazaboroles, this is associated with a loss in isolated products.

Mechanistic investigation of this catalytic reaction will be detailed in the next chapter.

II.2. Characterization and comparison of the 1*H*-2,1-benzazaborole series

*II.2.1. Spectroscopic characterization of 1*H*-2,1-benzazaborole b2*

Compound **b2** was isolated as a white solid, stable at room temperature. The compound was fully characterized by HRMS, IR and multinuclear NMR spectroscopies.

When monitoring the catalytic reaction, the doublet at 37.5 ppm for **a2** in the ^{11}B NMR spectrum disappeared and the new species showed a singlet shifted upfield at 30.6 ppm. NMR spectra of the isolated compounds **a2** and **b2** are depicted in Figure 2-5. The chemical shift indicates an electron-richer boron center while the change in multiplicity evidences a cleavage of the B–H bond.

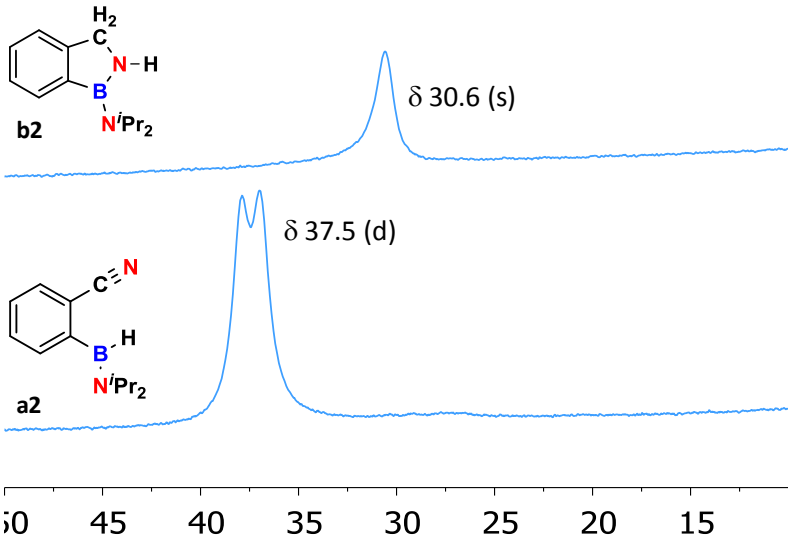

*Figure 2-5: Stacked ^{11}B NMR spectra of **a2** and **b2** (128.39 MHz, 298 K, C_6D_6)*

The ^{1}H NMR spectra of aryl(cyano)(aminoborane) **a2** and 1*H*-2,1-benzazaborole **b2** are represented in Figure 2-6. The ^{1}H NMR spectrum gives confirmation of B–H bond cleavage with no B–H signal around 5.5 ppm for **b2**. A methylene singlet, as evidenced by the correlation found with the carbon at 50.8 ppm in 2D HMQC $^{13}C\{^{1}H\}$/ ^{1}H NMR, appeared at 4 ppm with an integration of 2H. The methylene carbon was detected as a secondary carbon by ^{13}C DEPT NMR. A broad proton signal at 2.86 ppm was attributed to the N–H moiety. The corresponding nitrogen signal was found at – 312 ppm in 2D ^{15}N-DEPT$\{^{1}H\}$/^{1}H. The nitrogen resonance is clearly shifted compared to nitrogen substituted 1*H*-2,1-benzazaborole reported by Dostál[158] with ^{15}N resonances around – 230 ppm.

In contrast with **a2**, the isopropyl groups in **b2** are magnetically equivalent with only one signal for $CH_3{}^{i}Pr_2$ integrating for 12H. A cross peak in 2D ^{1}H COSY NMR spectrum reveals correlation between the doublet at 1.15 ppm and the broad peak at 3.78 ppm attributed to C*H* ^{i}Pr. The latest one is not well-defined because of hindered rotation around the B–N bond. The aromatic hydrogens shifted downfield. The $^{13}C\{^{1}H\}$ NMR spectrum no longer shows a resonance for the quaternary carbon of the nitrile.

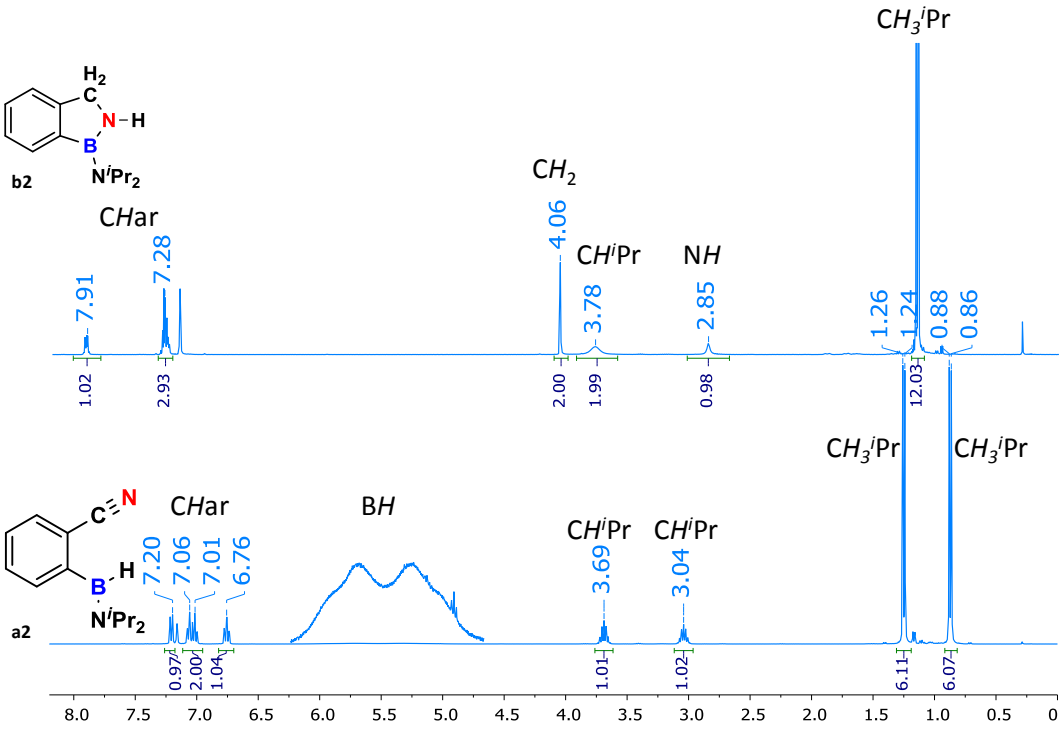

*Figure 2-6: ^{1}H NMR spectra of **a2** and **b2** in C_6D_6 solution (400.18 MHz, 298K)*

A comparison of the infrared spectra of **a2** and **b2** is displayed in Figure 2-7. **b2** infrared spectrum no longer shows B–H and C≡N vibration bands but exhibits a medium N–H stretching band at 3480 cm^{-1}. There is thus evidence for B–H bond cleavage and C≡N bond reduction.

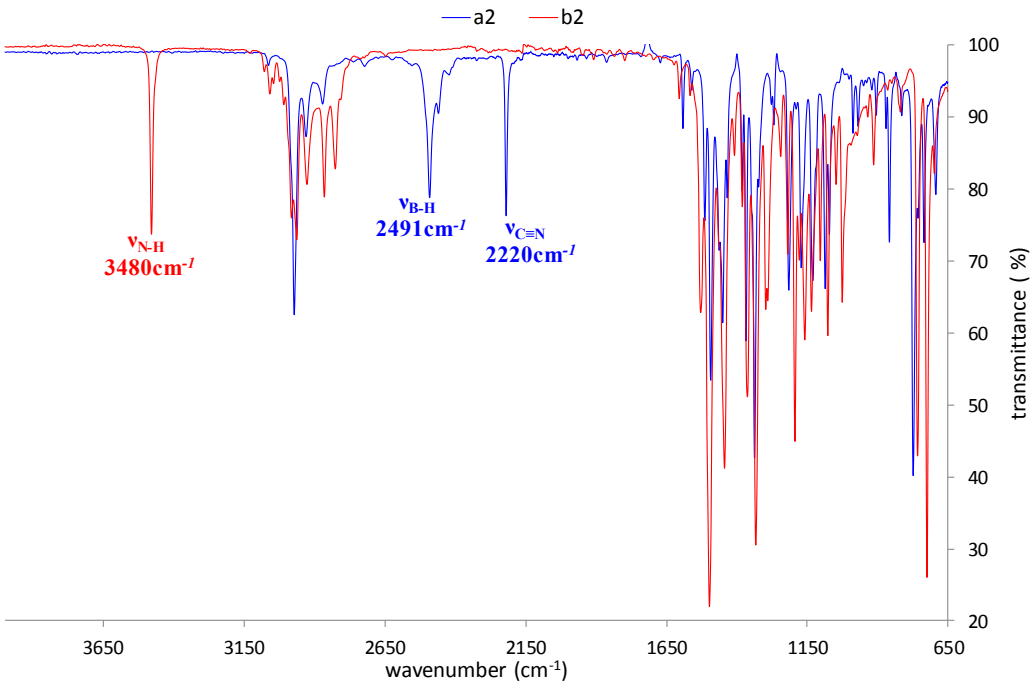

*Figure 2-7: Superimposed infrared spectra of **a2** and **b2***

The identity of **b2** was unambiguously confirmed by X-ray diffraction on a monocrystal that will be commented in the next section.

II.2.2. Characterization of the substituted compounds and comparison

Substituted 1*H*-2,1-benzazaboroles were characterized in a similar manner. The UV spectra of the series **b1-4** will be presented together with the corresponding borazines in chapter V.

A selection of spectroscopic data for compounds **b1-4** is reported in Table 2-3.

Compounds	*IR (cm^{-1})*		*NMR (ppm)*		
	ν_{N-H} (solid)	ν_{N-H} (toluene)	$^{11}B\{^1H\}$	^1H CH_2	^1H (N–H)
b1	3496	3482	30.1	3.91	2.84
b2	3480	3486	30.6	4.06	2.86
b3	3481	3496	32.3	4.08	3.18
b4	3472	3486	30.5	4.07	2.80

*Table 2-3: Selected spectroscopic data related to 1H-2,1-benzazaboroles **b1-4***

Again, aryl substituents do not greatly influence the corresponding spectroscopic data. N–H vibration bands of compounds **b** fall in the normal range of N–H stretching frequencies for secondary amines. The infrared analyses were first performed in the solid state. The wavenumber associated to this vibration is the greater for **b1** and decreases for **b3**, **b2** and **b4**, in this order. In this regard, the N–H bond appears to be stronger in **b1** and weaker in **b4**, in the solid state. In contrast, in toluene solution, the N–H vibration bands are very similar for **b1**, **b2** and **b4** around 3485 cm^{-1}. The band is shifted to higher frequency for **b3**. This distinct behavior is in accordance with the singular behavior of the N–H proton by NMR analysis.

The acidic N–H proton displays very similar chemical shifts for **b1**, **b2** and **b4** but in comparison, **b3** shows a downfield value. The chemical shift of the methylene protons is the same for **b2**, **b3** and **b4** and is about 0.2 ppm lower for **b1**. ^{11}B NMR spectra show a singlet close to 30 ppm except for **b3** deshielded to 32.3 ppm accounting for a less electron rich boron. Dostál and coworkers reported comparable chemical shifts for the amino-B substituted benzazaboroles and relatively downfield values for the alkyl-B substituted ones.[158] One can note that for **b1**, **b2** and **b4**, the isopropyl groups are equivalent and are represented by a

broad C*H* ^{i}Pr resonance in the ^{1}H NMR spectra. In contrast, the ^{1}H NMR spectrum of **b3** shows C*H* ^{i}Pr as a well-defined septet.

Compounds **b1-4** were isolated as white solids at room temperature. They are soluble in a large variety of common organic solvents just as their precursors **a1-4**. In the same manner, we were able to grow suitable crystals for X-ray analysis by slow evaporation from a saturated solution of pentane. All the structures obtained by X-ray diffraction on monocrystals are represented in Figure 2-8.

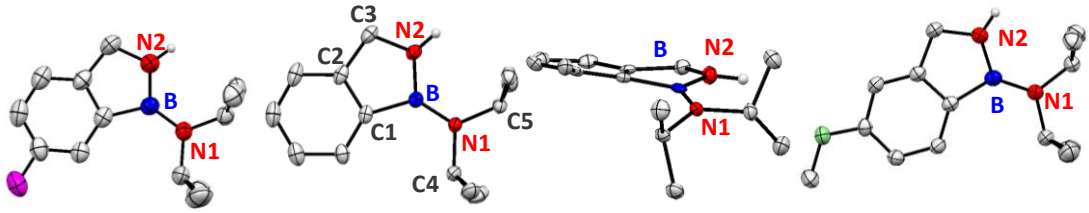

	b1 (F)	b2 (H)	b3 (Me)	b4 (OMe)
d B-N_1 (Å)	1.408 (3)	1.412 (2)	1.418 (4)	1.412 (3)
d B-N_2 (Å)	1.407 (3)	1.432 (2)	1.421 (4)	1.419 (3)

*Figure 2-8: Crystal structures of **b1-4** with selected bond distances. Hydrogen atoms are omitted for clarity, ellipsoids are given at the 50 % probability level. The N–H hydrogen atoms were located by Fourier differences. Crystal of **b4** contains 2 molecules per asymmetric unit, only one is presented.*

The parent **b2** presents an ortho-fused bicyclic planar structure. The exocyclic nitrogen atom N1 and B atoms both adopt a trigonal planar geometry as evidenced by the sum of the surrounding angles (ΣN1 = 360.01° and ΣB = 360°). The N2–B (1.432 (2) Å) and N1–B (1.412 (2) Å) bond distances are indicative of significant conjugation between the nitrogen atoms and the boron. The intracyclic N2–B bond is slightly elongated by comparison to alkyl-B 1*H*-2,1-benzazaborole and very similar to amino-B 1*H*-2,1-benzazaborole, as reported by Dostál.[47, 158] In the first ones, B–N bond lengths lie in the interval 1.403 (4)-1.419 (2) Å whilst the second kind shows intracyclic B–N bond lengths between 1.431 (3) and 1.422 (4) Å. The exocyclic N1–B (1.412 (2) Å) is significantly elongated by comparison to **a2** (N2–B (1.383 (2) Å). The exocyclic N1–B bond in **b2** is noticeably shorter than the intracyclic N2–B indicating a greater electron donation from N1 than N2 to boron. The B–C1 bond length (1.591 (2) Å) is comparable to the one in compound **a2** and falls in the range of single B–C bond as compared with the sum of the covalent radii (1.6 Å). C3 adopts a tetrahedral geometry. The C2–C3

distance is significantly elongated in **b2** (1.495 (2) Å) compared to **a2** (1.446 (2) Å) and the C3–N distance (1.452 (2) Å) lies in the range of C–N single bond.

For the other structures **b1**, **b3** and **b4**, all the B–N bonds exhibit also a double bond character. It is worth noting that intracyclic N2–B (1.407 (3) Å) in **b1** is shorter compared to that of **b2.** This indicates a stronger double bond character so a greater delocalization through the cycles. The N1–B and N2–B distances in **b1** are equal, indicative of a π delocalization evenly distributed. Like **b2**, **b1** and **b4** present a bicyclic planar structure. In contrast, **b3** shows some distortion probably as a result of steric hindrance between the isopropyl groups and the methyl. This is illustrated in Figure 2-8. This configuration suggests a lower degree of π-π interaction between boron and nitrogen atoms. The sum of the angles formed around the central B or N2 atoms only slightly divert from the ideal 360° (ΣN2 = 357.82, ΣB = 359.84). The methyl group, N2, C3 and N1 came out of the plane formed by the benzene ring. As a result, a relatively downfield ^{11}B NMR signal was detected for this compound showing a lower degree of electron donation from the nitrogen atoms to the boron. This structural arrangement may also account for the stronger N–H bond.

In summary, a series of aryl(cyano)(aminoborane) have been synthesized *via* an efficient lithiation, borylation strategy. Their reactivity with $RuH_2(H_2)_2(PCy_3)_2$ has been assessed. The starting borane undergoes catalytic intramolecular hydrogenation/cyclization involving both nitrile reduction and B–H bond activation, under dihydrogen. The reaction occurs in mild conditions (RT, P_{H2} = 1 bar). The resulting products, 1*H*-2,1-benzazaboroles, are BN analogues of indene with a B–N double bond character. For the first time, the synthesis is achieved directly from a nitrile function as well as in a catalyzed manner. The compounds feature a N–H bond moiety as a result of the new synthetic method. The reaction has been successfully extended to three substrates featuring more or less electron-withdrawing groups on the aryl. Little impact of the substituents on the spectroscopic data is found. However, the methyl substitution ortho to the borane, induced a change in the selectivity of the reaction. Both precursors and products are fully characterized by NMR, infrared and mass spectrometry as well as X-ray diffraction (except for **a4**). In the next chapter, we will study the mechanism of the described catalytic reaction.

CHAPTER 3:

MECHANISTIC INVESTIGATION ON 1*H*-2,1-BENZAZABOROLE SYNTHESIS

CHAPTER 3: MECHANISTIC INVESTIGATION ON 1*H*-2,1-BENZAZABOROLE SYNTHESIS

I. First assumptions

As a starting point, we made a few assumptions on the mechanism on the basis of previous works. Our first hypothesis laid on two main studies both conducted with $RuH_2(H_2)_2(PR_3)_2$ (Scheme 3-1).

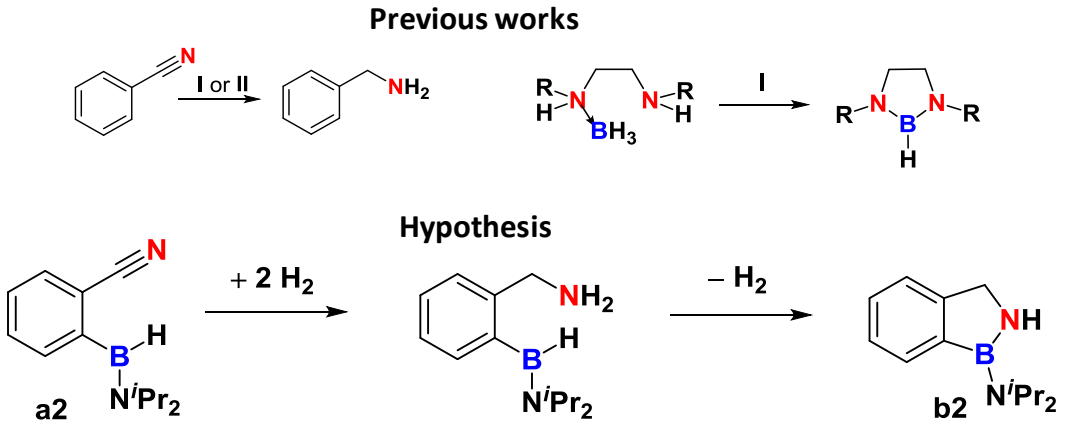

*Scheme 3-1: Proposition 1: hydrogenation/dehydrogenation sequences towards the formation of **b2***

We knew that complexes **I** and **II** can catalyze the hydrogenation of benzonitrile into benzylamine.[139] Thus, we could envisage a first step in which the nitrile function of the aryl(cyano)(aminoborane) **a2** would be fully hydrogenated, regardless of the borane moiety. The team also reported the dehydrogenation of diaminemonoborane compounds using **I** as catalyst. They disclosed a sequential activation of both B–H and N–H bonds to release H_2 and form the B–N bond.[143-144] We could imagine the same process happening with the benzylamine borane to form **b2**. Overall, the reaction would still require one dihydrogen equivalent but the process would involve a dehydrogenation step.

It was also established that complex **I** can catalyze intermolecular hydroboration of alkenes.[96] In addition, aminoboranes have proven to hydroborate benzonitrile with a lithium based catalyst.[121] As a result, a second hypothesis would be to consider the intramolecular

hydroboration of the nitrile function (Scheme 3-2). Once the B–N bond is formed the 2,1-benzazaborole would undergo hydrogenation of the imine moiety.

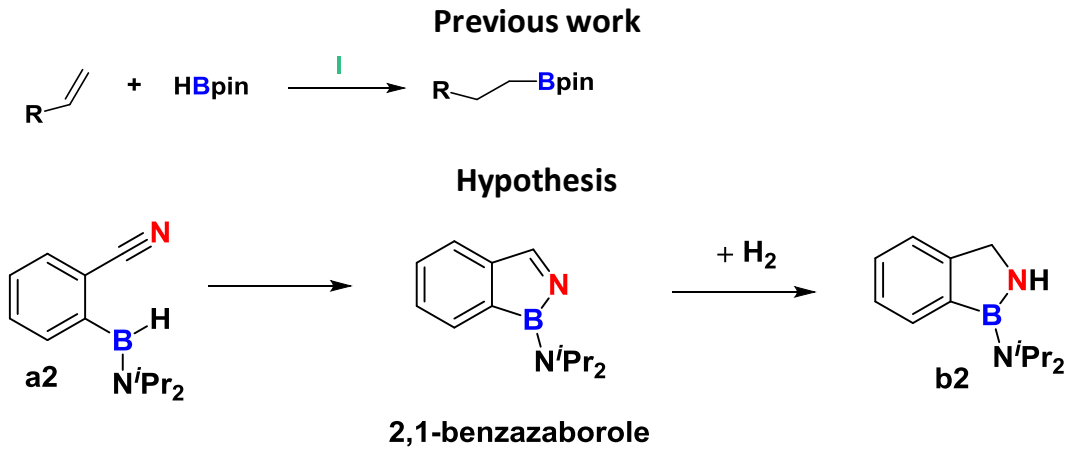

*Scheme 3-2: Proposition 2: hydroboration/hydrogenation sequence towards the formation of **b2***

The last option we considered was the reverse hydrogenation/hydroboration sequence as depicted in Scheme 3-3. In this case, partial hydrogenation of the nitrile function would occur generating an imine function, more likely to undergo an intramolecular hydroboration than an intermolecular hydrogenation.

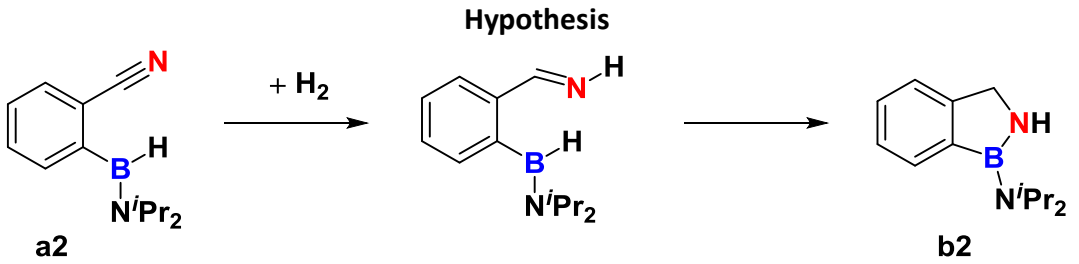

*Scheme 3-3: Proposition 3: hydrogenation/hydroboration sequences towards the formation of **b2***

In summary, we can propose three transformation pathways. We suggest that **a2** either go formally through:

- a hydrogenation/dehydrogenation sequence (1)
- a hydroboration/hydrogenation sequence (2)
- a hydrogenation/hydroboration sequence (3)

We assume that the proposed intermediates in those sequences are not necessarily released in the media due to their possible instability or reactivity.

Beyond the selection of a sequence pathway, we would like to comment on the coordination of the substrate on the catalyst as well as on the activation processes of both C≡N and B–H bonds. Based on previous studies concerning the synthesis of ruthenium agostic aryl(phosphino)(aminoborane), we can propose a η^2-C≡N, σ-B–H agostic coordination mode on the ruthenium (Figure 3-1).[152]

Reminiscent of aryl(phosphino)(aminoborane) coordination

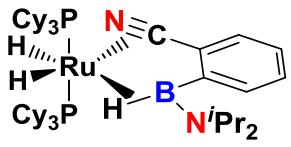

η^2-C≡N, agostic σ-B–H

Reminiscent of benzonitrile hydrogenation

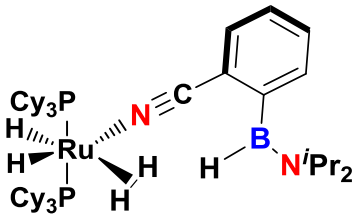

η^1-C≡N, dangling σ-B–H

Figure 3-1: Proposition describing the coordination mode of the substrate on the ruthenium complex

This proposition refers to a simultaneous C≡N and B–H bond activation. Further activation of the B–H bond could possibly lead to B–N bond formation. Another perspective, reminiscent of benzonitrile hydrogenation, would engage the nitrile in an η^1 coordination mode with the metal center. In that case, the C≡N bond would be activated together with dihydrogen at the metal center and would be more likely to react regardless of the non-activated B–H moiety.

Those propositions constitute a starting base for our work. An in depth study combining experimental and computational results will now be exposed.

II. Reaction monitoring

In order to gain information on the process and mechanism of the catalysis, we monitored the reaction by multinuclear NMR. For practical reason, we first conducted the reaction at the NMR scale. A NMR tube for high pressure was charged with 40 mg of **a2** in deuterated toluene. 5 mol% of **I** was added at once. Instantly, the reaction mixture turned red and simultaneously gas bubbles were observed. In a first assumption, the precedent findings certainly account for

dihydrogen release coming from decoordination of the σ-dihydrogen ligands. At this point, a NMR spectrum was recorded and represented in entry 3 of Figure 3-2. The ^{1}H NMR spectra of the isolated complex **I** (entry 1), substrate **a2** (entry 2) and product **b2** (entry 5) are associated for comparison. Spectra were sliced off for clarity but all the resonances are shown apart from the cyclohexyl region.

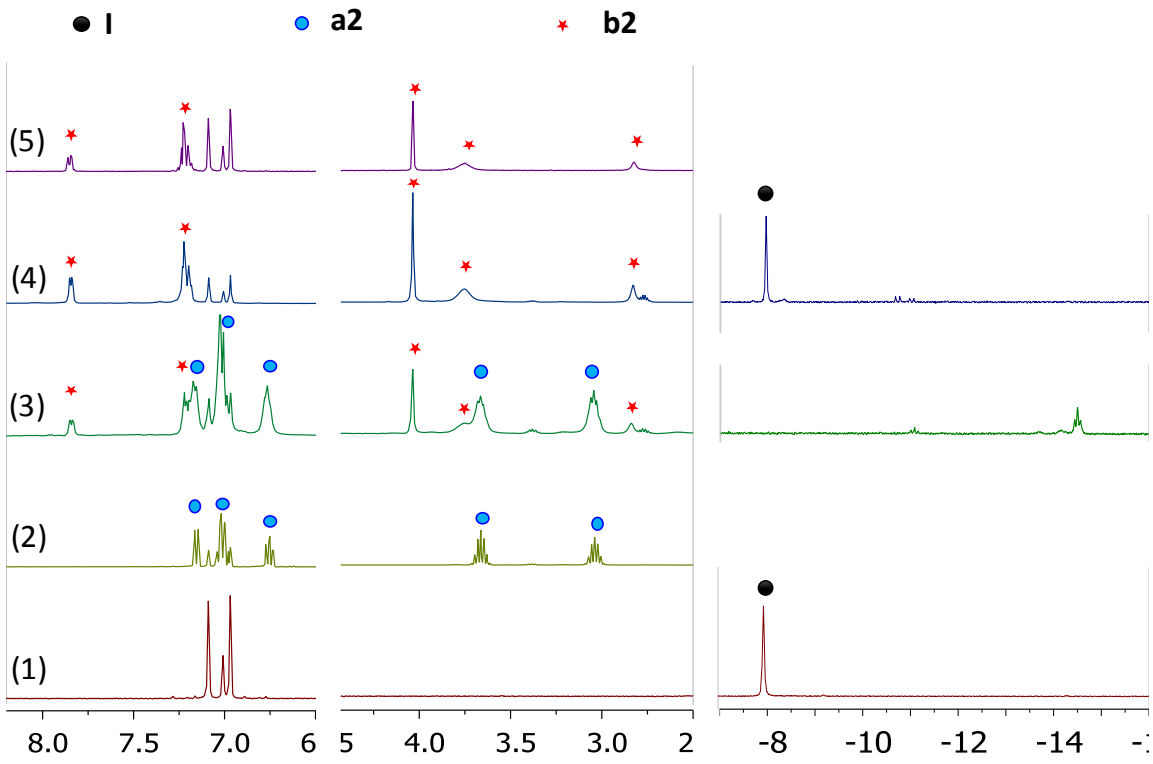

*Figure 3-2: ^{1}H NMR spectra in deuterated toluene of the catalytic reaction at different points and isolated compounds for comparison: (1) isolated complex **I**, (2) isolated **a2**, (3) 15 min after mixing **I** and **a2**, (4) end of the catalytic reaction after pressurizing with H_2 and (5) isolated **b2***

As we can see in entry 3, complex **I** was no longer present in the media. A new hydridic signal was detected as a triplet around – 14 ppm in the ^{1}H NMR spectrum. The hydride signal correlates with that of the major product in the corresponding $^{31}P\{^{1}H\}$ NMR spectrum at 64 ppm. In the positive chemical shift region, we already observed formation of **b2** even though we did not pressurize with H_2 yet. Considering the reaction needs at least one equivalent of H_2 to proceed, an internal compound, likely to be complex **I**, must provide and transfer hydrogen to the substrate. In the next step, the tube was pressurized with 2 bar(g) of H_2. At this stage, it is important to note that no ruthenium species was detected by ^{31}P NMR, at room temperature. The spectrum showed solely a resonance for the free phosphine at 9.8 ppm.

Spectrum 4 in Figure 3-2 was recorded at the end of the reaction. We see that the spectrum of the crude mixture is comparable to that of the isolated products **b2** and **I** except for minor signals attributed to some diisopropylamine (δ 2.86) and borazine **d2** (see Chapter 5) resulting from cyclotrimerization of **b2**. Remarkably, the negative chemical shift area now indicates the regeneration of complex **I**: the pseudotriplet at $-$ 7.8 ppm correlates with the phosphorus signal at 76 ppm, characteristic of $RuH_2(H_2)_2(PCy_3)_2$ observed in the reaction mixture. The latest is the major signal observed in the $^{31}P\{^1H\}$ NMR spectrum, together with a non-assigned signal at 54 ppm and a weak peak for free phosphine PCy_3. Importantly, monitoring the reaction in standard catalytic conditions gave the same information.

One can note that the **b2**/diisopropylamine ratio remained the same throughout the monitoring. Besides, no reaction was observed between the final product **b2** and $RuH_2(H_2)_2(PCy_3)_2$ as checked in an independent experiment. Consequently, the formation of borazine seems to be part of the catalytic process.

This first study proved to be as productive in gaining information as in arising questions. We need to identify the ruthenium complex seen in entry 3 to understand the transformation of **a2** in **b2** without exogenous hydrogen. In addition, we want to find a way to observe ruthenium species during the reaction. With the aim to answer those questions towards mechanistic understanding of the reaction, we performed stoichiometric reactions and NMR variable temperature experiments.

III. Stoichiometric reactions and variable temperature experiments

III.1. Stoichiometric reactions: a hydrogen transfer study

Stoichiometric reactions were performed in deuterated THF. When one equivalent of **a2** was mixed with one equivalent of **I**, full conversion of **a2** was observed by ^1H NMR along with formation of **b2** and a residual amount of diisopropylamine. The **b2**/diisopropylamine ratio was comparable to the one calculated from the catalytic reaction. Complex **I** provided and transferred hydrogen atoms to **a2** allowing the formation of **b2**. Complex **I** proved to be able to convert up to five equivalents of **a2** in a stoichiometric manner. Upon addition of six then

eight equivalents, we see some remaining **a2** in the media, even after a prolonged time. We were then willing to understand how one molecule of **I** could transform up to five equivalents of **a2**. We paid a close attention to the dehydrogenated stages of the ruthenium complex. With this goal, we performed independent stoichiometric reactions as described in Scheme 3-4.

General equation	**a2** + Complex **I**	$\xrightarrow[45\ min]{THF\ d_8}$	**b2** + Dehydrogenated Ru species
equiv	1 to 5 : 1		1 to 5

Scheme 3-4: General equation related to the stoichiometric reactions

In light of our previous observations, we recorded both ^{1}H and $^{31}P\{^{1}H\}$ NMR spectra for each experiment after 45 minutes, assuming the reaction would be over and the system would not have time to evolve. The ^{31}P NMR spectra recorded after mixing one, two, three, four or five equivalents of **a2** with one equivalent of **I** are represented in Figure 3-3.

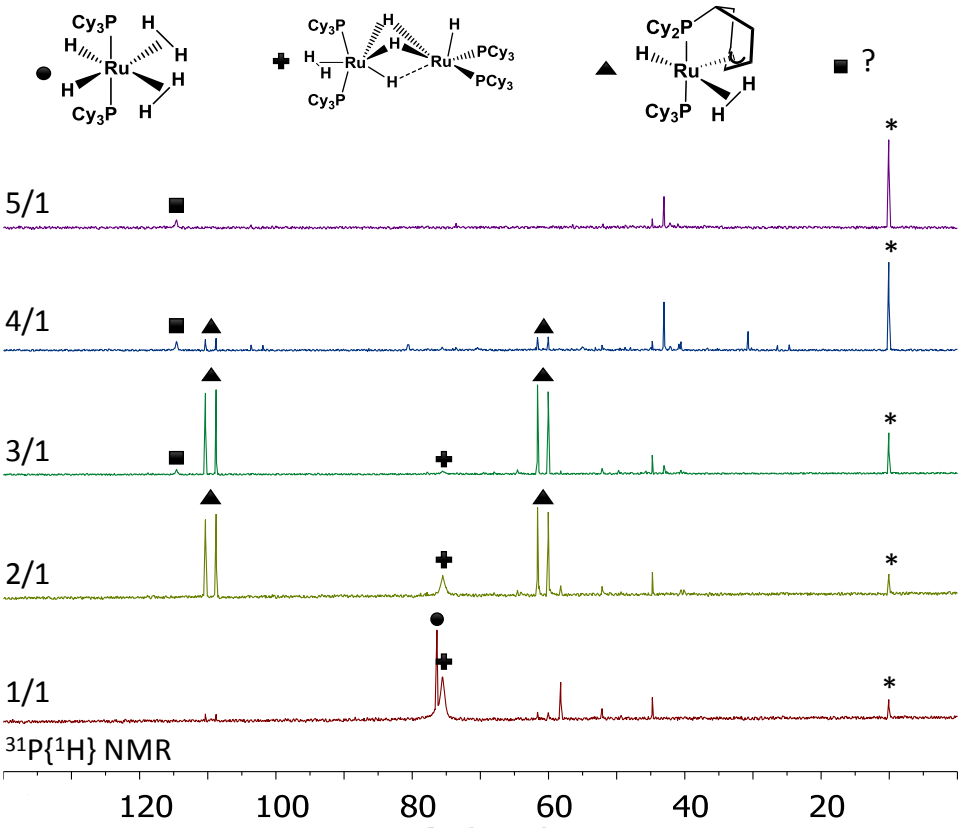

*Figure 3-3: $^{31}P\{^{1}H\}$ NMR spectra recorded after 45 min of stoichiometric reactions using various (**a2/I**) molar ratio. The five reactions are independent.* free phosphine*

III.1.1. Stoichiometric reaction of a2 and I in a 1/1 molar ratio

When **I** and **a2** were reacted in a 1/1 molar ratio, we detected the characteristic resonance at 76.4 ppm of complex **I** as well as an adjacent broad signal at 75.5 ppm correlating with a very broad resonance in the hydride region of the ^{1}H NMR spectrum around – 12 ppm. We attributed these signals to a dehydrogenated stage of **I** being a dimeric ruthenium complex. In 1988, Chaudret and coworkers reported that complex **I** loses hydrogens thermally (85°C) or photochemically in toluene to give the dehydrogenated ruthenium dimer $[Ru_2(H_2)(H)_4(PCy_3)_4]$.[135] The dehydrogenation occurred as in the equation depicted in Scheme 3-5.

known dehydrogenation process for **I**

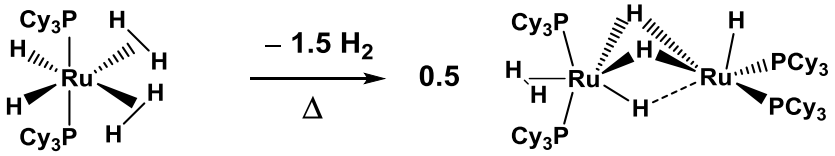

I **I-a**

*Scheme 3-5: Dehydrogenation of complex **I** under thermal treatment into complex **I-a***

Complex **I-a** results from the loss of 1.5 equivalents of H_2. We know that the formation of **b2** only requires 1 equivalent of H_2. Hence, the observed ^{31}P NMR pattern seems in agreement with a partial consumption of complex **I** for the formation of **b2** (**I-a** being the major species). In this manner, the provided hydrogens came from the σ-H_2 ligands. We can assume that, after release of the newly formed 1*H*-2,1-benzazaborole **b2**, unsaturated ruthenium fragments of 14 or 16 electrons are formed and rearrange into the more stable dimeric ruthenium complex **I-a**.

III.1.2. Stoichiometric reaction of a2 and I in a 2/1 molar ratio

The combination of **a2** and **I** in a (2/1) molar ratio led to their total conversion, as also seen by ^{1}H NMR. The corresponding $^{31}P\{^{1}H\}$ NMR spectrum still shows the signature of complex **I-a** and an AB system at 109.5 and 60.8 ppm (Figure 3-3). We recognized the dehydrogenated ruthenium complex $RuH_3\{(\eta^3\text{-}C_6H_8)PCy_2\}(PCy_3)$ (**I-b** in Scheme 3-6) which was previously

isolated in the team, when employing complex **I** as hydrogenation catalyst of functionalized olefins.[159] Indeed, complex **I** undergoes stepwise dehydrogenation of the phosphine ligands, *via* C–H activation, upon addition of olefins bearing donor substituents such as CH_2=CH($SiEt_3$) or CH_2=CH^{t}Bu. Two dehydrogenated stages were isolated with complexes **I-b** and **I-c** resulting from the addition of 3 or 5 equivalents of olefin, respectively (Scheme 3-6).

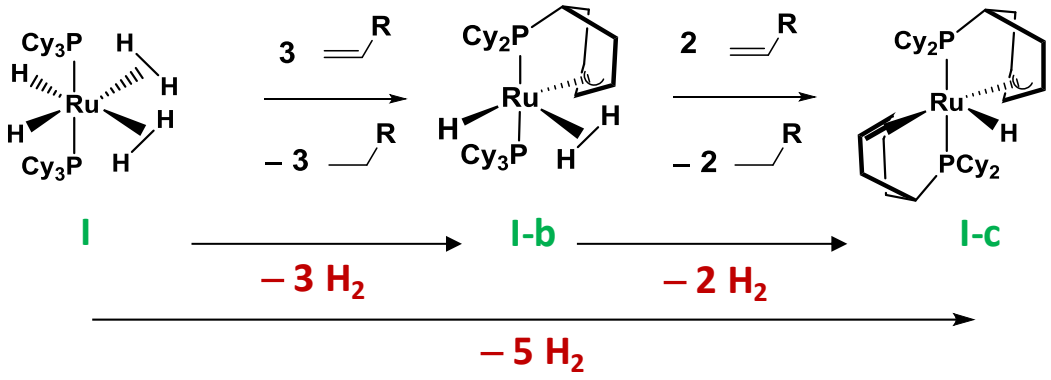

*Scheme 3-6: Dehydrogenated stages of complex **I** observed upon reaction with functionalized olefins*

Complex **I-b** displays an allylic cyclohexenyl phosphine η^3 bonded to ruthenium, one hydride, and a σ-H_2 ligand. Complex **I-c** results from further dehydrogenation and features an additional η^2 coordinated cyclohexenyl and a unique hydride. Overall, complex **I** can provide up to 5 equivalents of dihydrogen: two equivalents from the σ-H_2 ligands and 3 equivalents from the C–H activation of the cyclohexyl ligands. Noteworthy, the reactions are fully reversible under dihydrogen atmosphere. Theoretically, in our case, it could allow the formation of 5 molecules of **b2** from **a2**.

In light of the previous considerations, the chemical reaction engaging **a2** and **I** in a 2/1 molar ratio mainly generated two stages of dehydrogenated ruthenium species, namely **I-a** and **I-b**. Both σ-H_2 ligands and C–H activation of the cyclohexyl of the phosphine ligand contribute for hydrogen transfer from **I** to **a2**.

III.1.3. Stoichiometric reaction of a2 and I in a 3/1 molar ratio

Reaction of **a2** and **I** in a 3/1 ratio led, after 45 minutes, to the recorded ^{31}P NMR spectrum depicted in Figure 3-3. The set of doublets of complex **I-b** correspond to the major product. We can assume that two molecules of **b2** were produced with hydrogens provided from the

σ-H_2 ligands while the third molecule of **b2** needed hydrogens furnished by one cyclohexyl ligand leading to the dehydrogenated ruthenium species **I-b**. In order to support the hypothesis, we generated the bis(dinitrogen) ruthenium complex $RuH_2(N_2)_2(PCy_3)_2$ and made it react with **a2**. We bubbled a pentane solution of complex **I** with 1 bar of high purity dinitrogen gas during 10 minutes following the procedure previously described in the group.[160] The ^1H and ^{31}P NMR spectra (^1H: – 12.5 ppm; ^{31}P: 60.0 ppm) confirmed the formation of complex **I-d** as represented in Scheme 3-7.

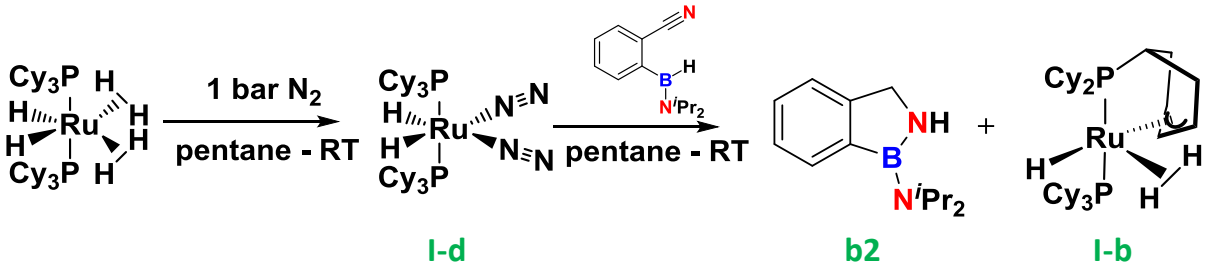

*Scheme 3-7: Generation of the bis(dinitrogen) ruthenium complex $RuH_2(N_2)_2(PCy_3)_2$ and its reactivity with **a2***

The reactive σ-H_2 ligands are replaced by inert dinitrogen ligands binding the ruthenium center in an η^1 coordination mode. Reaction of such a complex with **a2** would assess the ability of the cyclohexyl of the phosphine ligand to enable **b2** formation by providing hydrogens. Indeed, upon mixing **a2** and **I-d** in a 1/1 molar ratio, we observed stoichiometric formation of the final product **b2** and of the dehydrogenated ruthenium complex **I-b**. Generation of **I-b** from **I-d** requires the loss of one equivalent of H_2 which has been transferred and used in the formation of **b2**.

III.1.3. Stoichiometric reaction of a2 and I in a 4/1 and 5/1 molar ratio

We wondered whether the addition of more than 3 equivalents of **a2** would lead to the **b2** product along with the third dehydrogenated stage of the ruthenium complex, namely **I-c** (Scheme 3-6). Unexpectedly, addition of a greater amount of **a2** to **I** did not generate complex **I-c**. Instead, we observed a broad signal at 114.5 ppm together with an increased intensity of the peak corresponding to the free phosphine at 10 ppm in the $^{31}P\{^1H\}$ NMR spectrum (Figure 3-3). We were able to attribute this new species to complex **I-e**, represented in Figure 3-4, by

preparing it independently. **I-e** has been fully characterized by X-ray diffraction and multinuclear NMR (see next section).

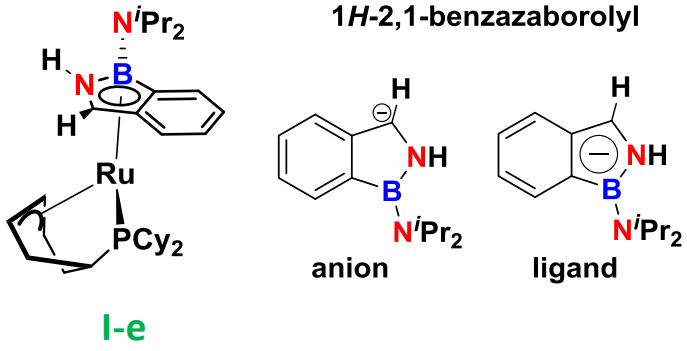

*Figure 3-4: Last dehydrogenated stage of the ruthenium complex into complex **I-e** bearing a 1H-2,1-benzazaborolyl ligand*

One can assume that complex **I-b** could convert **a2** but was not able to provide enough hydrogen to complete the formation of **b2**. When four equivalents were used complex **I-b** was still visible but disappeared with 5 equivalents: complex **I-e** accompanied with free phosphine, became preponderant. The absence of signals in the hydride region of the corresponding ^{1}H NMR spectrum was in accordance with the identity of complex **I-e**. Remarkably, **I-e** is a picture of the substrate in transformation captured onto the ruthenium center. The B–N bond has been formed but the cycle comprises a methine carbon instead of the final methylene. The 1*H*-2,1-benzazaborolyl binds the ruthenium center in an η^5 coordination mode. At this stage, no hydrogen remained available for further **a2** conversion. Consequently, we supposed this new species corresponded to the last dehydrogenated stage. Indeed, the addition of 6 equivalents of **a2** did not lead to total conversion, confirming that 5 equivalents of **a2** are the maximum that one molecule of complex **I** can convert.

III.1.4. Additional experiments

We conducted further studies with a view to learn about the formation of **I-e** and complete the understanding of the hydrogen transfer from complex **I** to **a2**. We synthesized complex **I-b** according to the previously reported protocol.[159] Complex **I-b** was first reacted with **a2** in a 1/1 molar ratio as depicted in Scheme 3-8.

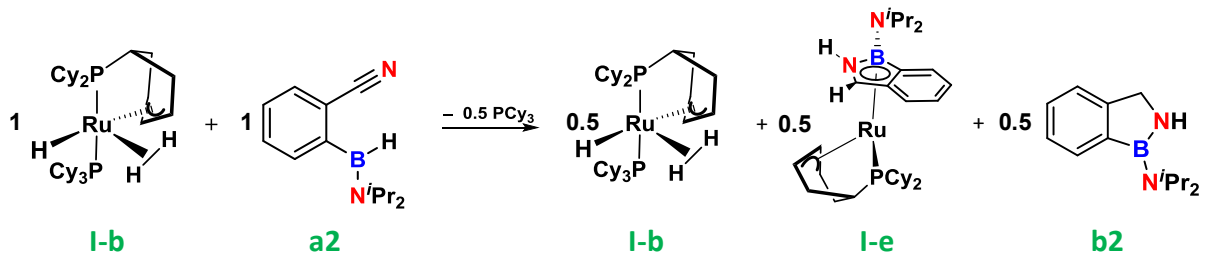

*Scheme 3-8: Stoichiometric reaction of **a2** with complex **I-b** in a 1/1 molar ratio, in THF or toluene*

We observed full conversion of **a2** within one hour and the reaction was very clean as observed by ^{31}P NMR (Figure 3-5).

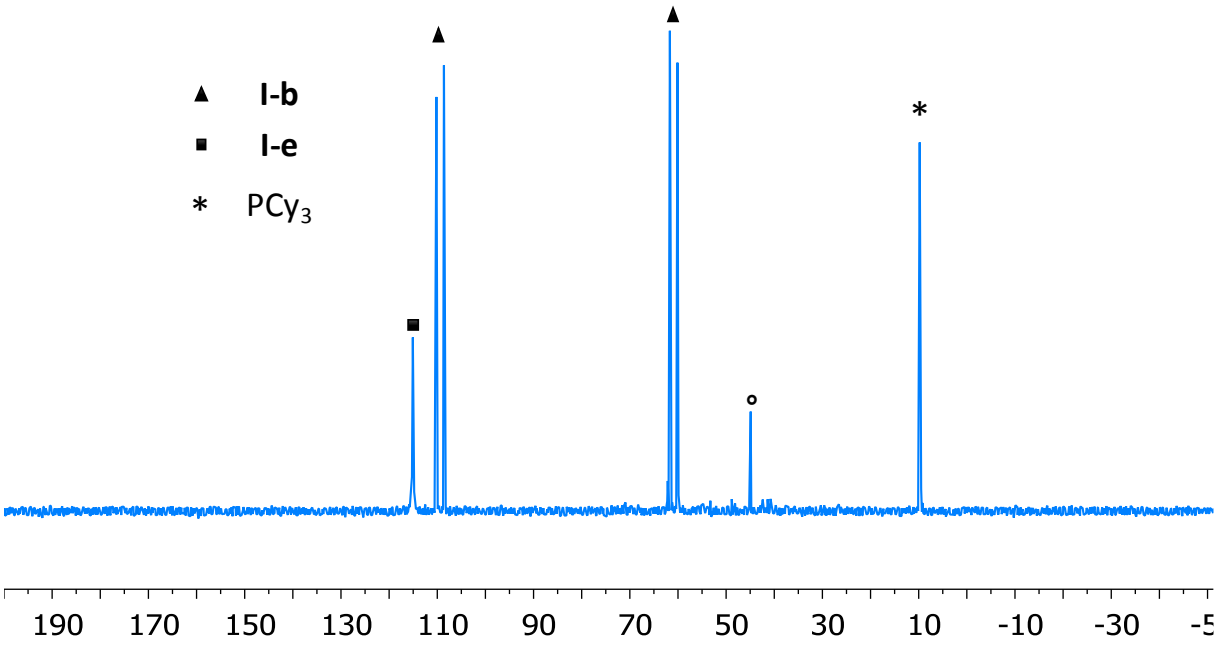

Figure 3-5: $^{31}P\{^{1}H\}$ NMR spectrum of the crude mixture corresponding to the reaction depicted in Scheme 3-8 (C_7D_8, 400 MHz, 298K) °($OPCy_3$)

Noticeably, the equivalent of **a2** only consumed half of complex **I-b** and yielded complex **I-e** and product **b2** in the same ratio. Therefore, **I-b**, **I-e** and **b2** all integrate in the same ratio in the ^{1}H NMR spectrum of the crude mixture (Figure 3-6).

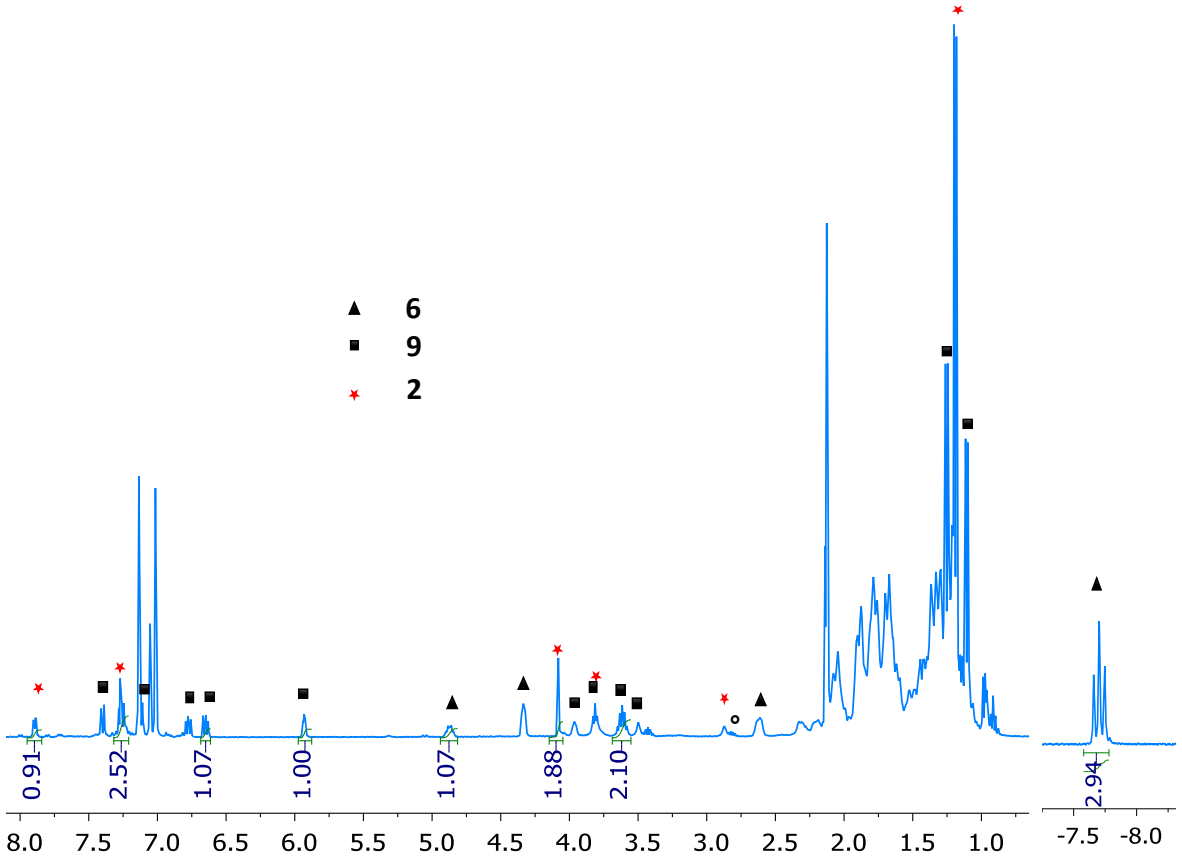

Figure 3-6: ^{1}H NMR spectrum of the crude mixture corresponding to the reaction depicted in Scheme 3-8 (C_7D_8, 400 MHz, 298K) °(diisopropylamine)

Complex **I-b** is a ruthenium II complex counting 18 electrons. It is reasonable to imagine that **a2** would react with **I-b** by substitution of H_2. The formation of **b2** requires transfer of two hydrogen atoms leaving the ruthenium complex with a unique hydride after release of the product. We propose the 16 electron intermediate species represented in Scheme 3-9. The later would react faster than **I-b** with **a2**, leading to complex **I-e**. Thus, only half of complex **I-b** was consumed.

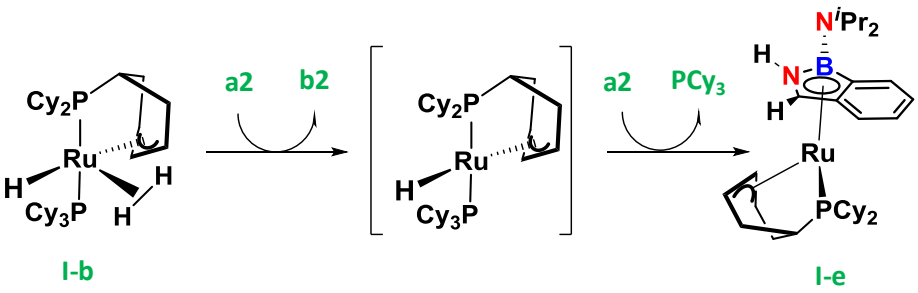

*Scheme 3-9: Hypothetic intermediate in the formation of **I-e***

Since we learned that the cyclohexyl of the second phosphine ligand does not participate in the hydrogen transfer *via* the formation of **I-c**, only one hydride remains available for the conversion of **a2**. To form the benzazaborolyl moiety, the boron-attached hydrogen must be transferred to the carbon or the nitrogen atom. Either the B–H bond undergoes oxidative addition at the metal center and is further redistributed to the carbon or the nitrogen atom, or a boron-nitrogen interaction enables the hydrogen transfer. In any case, only one equivalent of H_2 is available for the formation of **b2** dismissing the first proposition we made (section I). Indeed, we proposed a first step of hydrogenation of the nitrile unit into amine requiring two equivalents of H_2 which would have been synonym of full conversion of **I-b**, at least at the beginning of the reaction. In addition, this intermediate demonstrates the feasibility of B–N bond making prior to full nitrile hydrogenation featuring a CH_2.

In a second experiment, complex **I-b** and **a2** were reacted in a 1/2 molar ratio as shown in Scheme 3-10.

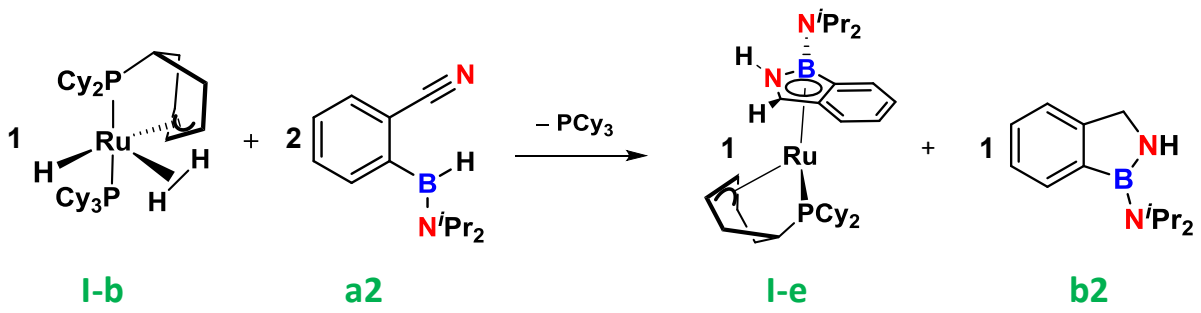

*Scheme 3-10: Stoichiometric reaction of **a2** with complex **I-b** in a 2/1 molar ratio, in THF or toluene*

In this case, complex **I-b** was utterly converted yielding complex **I-e** and product **b2** with the same integration ratio as the only products of the reaction together with PCy_3 and traces of diisopropyl amine. We monitored the reaction by ^{1}H and $^{31}P\_INVGATED\_^{1}H$ NMR. Products **I-e** and **b2** integrate the same throughout the reaction. As the benzazaborolyl complex seems to be an intermediate in the transformation of **a2** into **b2**, we were willing to isolate it and study its reactivity.

III.2. Synthesis, characterization and reactivity of the benzazaborolyl ruthenium complex I-e

The crude solution obtained after the reaction depicted in Scheme 3-10 was dried under vacuum. We succeeded in isolating the complex by precipitation in a mixture of diethylether and acetonitrile at – 40°C. Owing to the similar solubility of the three products of the reaction, we isolated complex **I-e** in a modest 40% yield. Crystals of the complex were grown in the same solvent mixture by slow evaporation at room temperature. A monocrystal of suitable size was analyzed by X-ray diffraction techniques.

III.2.1. NMR characterization of complex I-e

The crystals were solubilized in deuterated toluene. The recorded ^{1}H NMR spectrum is shown in Figure 3-7.

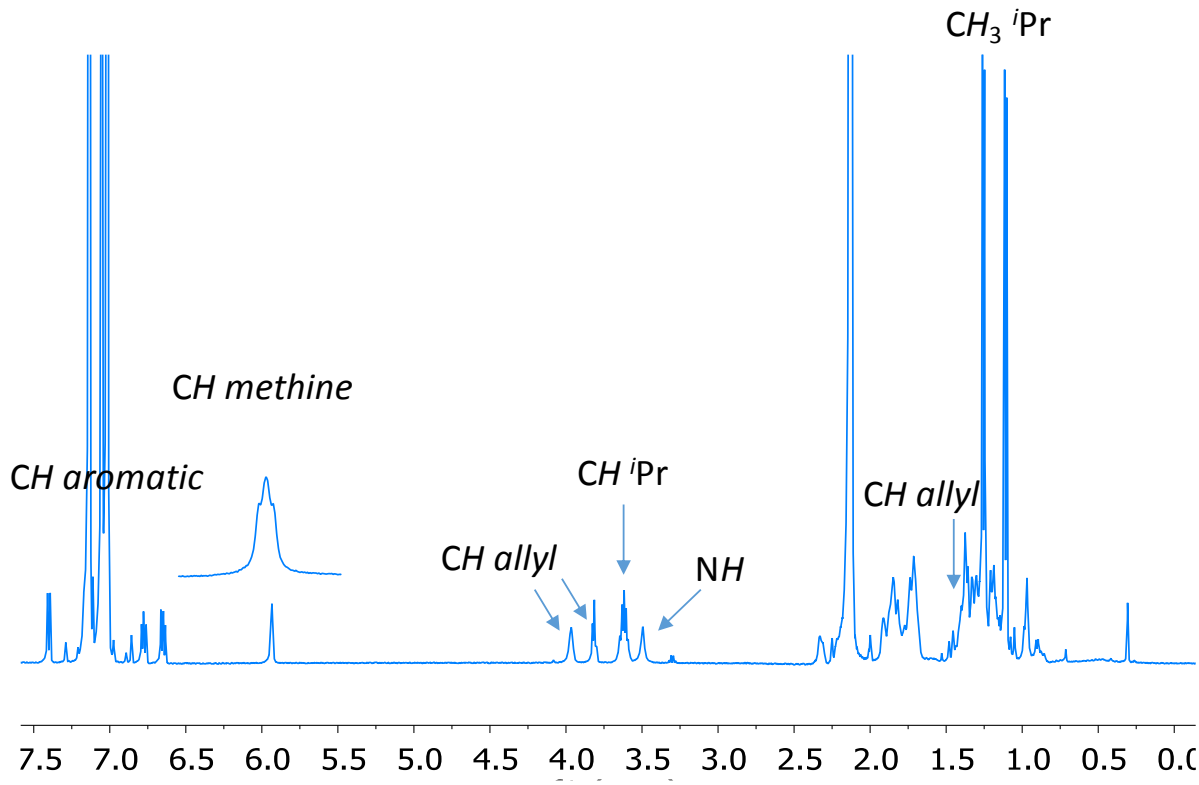

*Figure 3-7: ^{1}H NMR spectrum of complex **I-e** in deuterated toluene*

The isopropyl groups of the benzazaborolyl moiety are magnetically inequivalent and resonate as two doublets at 1.05 and 1.21 ppm. In ^{1}H COSY experiment, a cross peak indicates their direct coupling with a well-defined septet at 3.58 ppm assigned to the C*H* ^{i}Pr (2H) which, surprisingly, are equivalent. The N–*H* proton (δ 3.46) was found downfield compared to the 1*H*-2,1-benzazaborole **b2** (δ 2.86). The two-dimensional ^{15}N-DEPT{^{1}H}/^{1}H experiment revealed the nitrogen chemical shift at – 337 ppm, also shifted downfield compared to the 1*H*-2,1-benzazaborole (δ – 312). The ^{31}P{^{1}H} NMR spectrum displays a large peak at 115 ppm. The broadness might be due to the presence of the boron atom engaged in the η^5 coordination of the benzazaborolyl, approaching *trans* configuration to the phosphine. The two-dimensional HMQC ^{31}P{^{1}H}/ ^{1}H and ^{13}C{^{1}H}/ ^{1}H NMR experiments enabled the detection of the allylic protons of the cyclohexenyl. Notably, the hydrogen bonded to the central carbon of the allyl resonates at 3.87 ppm as a triplet and correlates with a downfield carbon at 66.9 ppm. The methine signal in the heterocycle is detected at 5.90 ppm as a pseudo triplet in the ^{1}H NMR spectrum. Two-dimensional experiments evidenced its coupling with the phosphorus atom and with the hydrogen of the N–*H* moiety ($^{3}J_{H\text{-}H}$ = 2.7 Hz). The ^{13}C NMR spectrum also revealed interesting patterns. The quaternary carbon ipso to the boron and the one ipso to the methine resonate at 85.4 ppm (δ 139.3 in **b2**) and 104.6 ppm (δ 152.3 in **b2**), respectively. These shifts result from the coordination to the ruthenium center. Finally, the ^{11}B{^{1}H} NMR spectrum shows a broad signal at 16 ppm (δ 30.6 in **b2**) clearly evidencing a boron center richer in electrons due to the coordination with the ruthenium. The boron chemical shift of one relevant example, the 1*H*-2,1-benzazaborolyl potassium salt, was reported at 23.4 ppm.[74] The comparison is limited since it is the first time that the 1*H*-2,1-benzazaborolyl fragment is coordinated to a transition metal center.

III.2.2. X-ray structure of complex I-e

Complex **I-e** crystalized in a triclinic space group P-1 with Z = 2. The asymmetric unit contains two isomeric complexes. The molecular structure determined by X-ray diffraction technique is depicted in Figure 3-8. For clarity, only the complex containing the asymmetric carbon in the R configuration is represented.

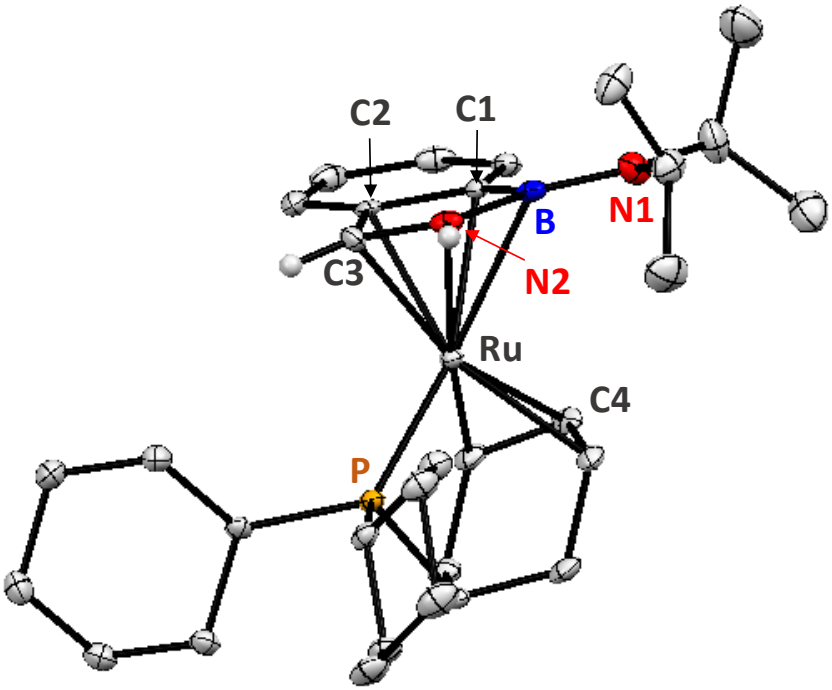

Ru–B	2.456 (3)	Ru–C1	2.369 (2)
Ru–N2	2.273 (2)	Ru–P	2.246 (1)
Ru–C3	2.127 (2)	Ru–C4	2.093 (2)
Ru–C2	2.295 (2)	B–N1 B–N2	1.425 (4) 1.469 (4)

*Figure 3-8: Molecular structure of complex **I-e** and selected bond distances (Å). Ellipsoids are given at the 50 % probability level and hydrogen atoms are omitted for clarity except for C3H and N2H*

The ruthenium complex exhibits a distorted geometry. The phosphorus and the boron are closer to a *trans* than a cis position (∑ B-Ru-P = 145°) in agreement with the observed pattern in NMR. One cyclohexyl of the phosphine underwent C–H activation and the allylic fragment coordinates the ruthenium in an η^3 mode. The 1*H*-2,1-benzazaborolyl ligand might be considered as η^5 bound to ruthenium. The benzene and the BN rings in complex **I-e** are not coplanar, in contrast to the 1*H*-2,1-benzazaborole **b2**. The bonding situation within the 5 member-ring is also different compared to that of **b2**. The B–C1, C2–C3 and C3–N bonds are significantly shorter (**I-e**: 1.559 (4), 1.402 (4), 1.422 (3), **b2**: 1.5907 (19), 1.495 (2), 1.4523 (18) Å) confirming the presence of a methine group and electron delocalization around the C1, C2, C3 atoms. The B–N2 bond is elongated (**I-e**: 1.469 (4), **b2**: 1.4317 (18) Å) suggesting less double bond character of the intracyclic B–N bond as a result of bonding to ruthenium.

It is important to note that the five atoms are unsymmetrically bonded to the metal. Indeed, the methine carbon C3 is strongly bonded to ruthenium with a Ru–C3 distance of 2.127 (2) Å. The coordination leans towards the N2, C3, C2 atoms slipping away from boron and C1. Indenyl ligands show similar features approaching an η^3 coordination mode.[67, 161] There, the coordination engages the three carbons of the five –member ring while the two quaternary carbons are slipped away.[67] The same behavior is observed for 1*H*-3a,7a-benzazaborole on zirconium where the boron and the nitrogen at the 3a and 7a positions are moved away from the metal center (Figure 1-12, Chapter 1).[71] Wen and coworkers crystallized an 1,2-azaborolyl ligand on ruthenium that showed tighter coordination towards the three carbon atoms of the five member ring (Figure 3-9).[65]

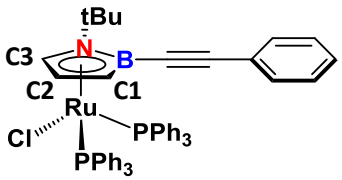

Ru–N = 2.280 (2) Å; Ru–B = 2.357 (3) Å;
Ru–C1 = 2.244 (2) Å; Ru–C2 = 2.202 (2) Å;
Ru–C3 = 2.157 (3) Å

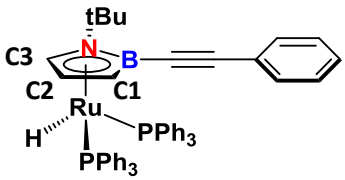

Ru–N = 2.384 (2) Å; Ru–B = 2.402 (3) Å;
Ru–C1 = 2.256 (2) Å; Ru–C2 = 2.217 (2) Å;
Ru–C3 = 2.194 (3) Å

Figure 3-9: Crystal structure data reported for ruthenium complexes bearing a 1,2-azaborolyl ligand

The authors report shorter Ru–B distances (2.357 (3) Å for X = Cl, 2.402 (3) Å for X = H) but similar or longer Ru–N distances (2.280 (2) Å for X = Cl, 2.384 (2) Å for X = H) by comparison to **I-e**. Fang and coworkers explained that the ring orientation of their azaborolyl ligand on titanium depends on the substituents on nitrogen.[66] When the nitrogen was methyl substituted, the coordination leaned towards the B–N bond whilst it leaned towards the intra-ring carbons when the nitrogen was ^{t}Bu substituted. Altogether, the bonding situation between the BN ring and the metal center is highly influenced by the nature of the metal, the other ligands, and the BN substituents.

Thus, in our case, the coordination of the BN heterocycle to the ruthenium center could be considered as approaching an η^3 instead of a true η^5 mode, providing a total 16-electron versus 18-electron configuration.

III.2.3. Reactivity of complex I-e with H_2

With a view to assess the formation of **b2** from the 1*H*-2,1-benzazaborolyl complex, we exposed **I-e** to H_2. A NMR tube for high pressure was charged with 15 mg of complex **I-e** in deuterated toluene and pressurized with 2 bar(g) of H_2. The reaction was monitored by ^{1}H and ^{31}P NMR experiments. Within 30 minutes, complex **I-e** was fully converted. One major product in the ^{31}P NMR spectrum was first detected as a singlet at 96.7 ppm that we attributed to complex **I-f**, depicted in Figure 3-10, on the basis of multinuclear NMR data.

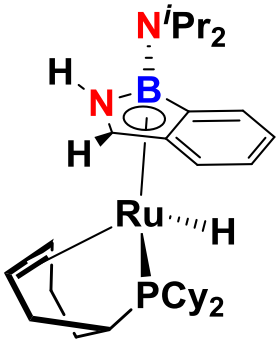

*Figure 3-10: Proposed structure for complex **I-f***

Complex **I-f** results from partial rehydrogenation of the phosphine ligand. With a hydride ligand, the complex remains at the oxidation state II. Characterization of a monohydride came from a ^{31}P NMR experiment with selective decoupling of the ^{1}H of the cyclohexyl groups. The phosphorus resonates as a doublet at 96.7 ppm as seen in Figure 3-11 with the same J_{P-H} value found for the hydride signal at – 17.2 ppm.

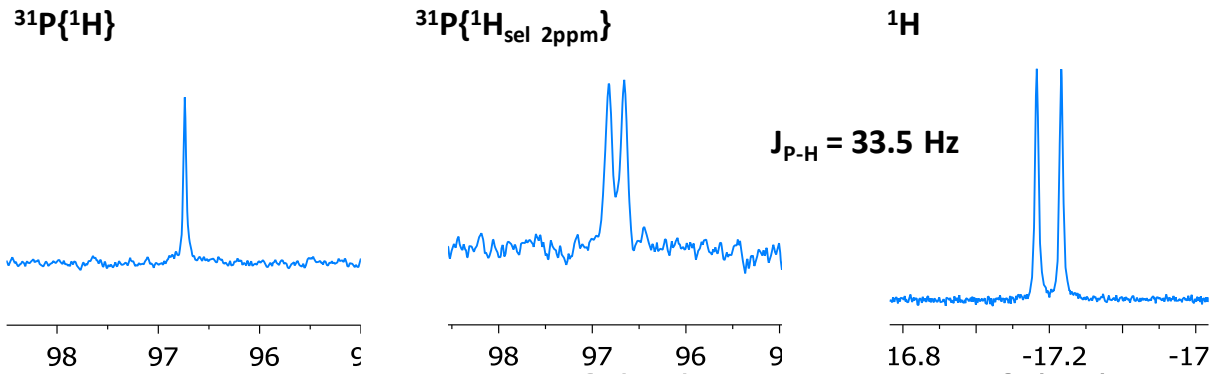

*Figure 3-11: $^{31}P\{^{1}H\}$, $^{31}P\{^{1}H$ sel 2ppm$\}$ and ^{1}H NMR spectra of complex **I-f***

Correlation was confirmed by a two-dimensional HMQC $^{31}P\{^{1}H\}/^{1}H$ experiment. The multiplicity of the hydridic signal indicates that the hydrogen is coupled with only one phosphorus atom. The phosphorus and the hydride couples with a J_{P-H} value of 33.5 Hz, which is in the typical range for ligands arranged in a piano-stool configuration (J_{P-H} = 36.8 ppm for (η^5-pyrrole)RuH(PCy_3)$_2$).[162] The N–*H* proton (δ 3.65) resonates slightly downfield compared to that of **I-e** (δ 3.46). The methine signal compares well with that of **I-e** (5.84 ppm vs 5.90 ppm). Two signals attributed to the protons of the η^2-C_6H_9 coordination resonate downfield (δ 4.43 and 3.43) compared to the cyclohexyl protons of the free phosphine.

After a while under H_2, a new species appeared in the $^{31}P\{^{1}H\}$ NMR spectrum at 78.2 ppm coexisting with the previous one. The signal was attributed to the next hydrogenated stage complex **I-g**, depicted in Figure 3-12, on the basis of multinuclear NMR data.

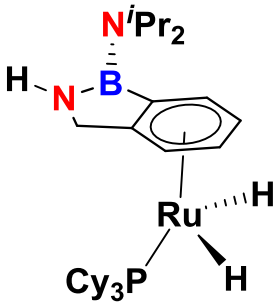

*Figure 3-12: Proposed structure for complex **I-g***

Complex **I-g** results formally from the addition of two molecules of dihydrogen to **I-f**. The cyclohexyl group of the phosphine ligand is now fully hydrogenated. We are now in presence of a dihydride complex. More importantly, the BN bicyclic ligand which was coordinated to ruthenium *via* the BN cycle is now coordinated through the C_6H_4 ring. Precedents for haptotropic rearrangement exist as reported for example during the protonation of η^5-indenyl ruthenium complexes.[161] Presumably, the ring slip occurred after the formation of the methylene group from the former methine. The hydrogen transfer from the ruthenium to the methine carbon occurred while engaged in the η^5 coordination. In **I-g**, the 1*H*-2,1-benzazaborole fragment is complete. It was previously shown in the team that catalytic hydrogenation of indole into indoline with complex **I** occurred at 80°C under 3 bar of H_2 with only 25% of conversion.[162] Herein, the asymmetric coordination of the 5-member ring with a tighter bonding of the methine carbon might facilitate the hydrogen transfer.

The phosphorus resonates as a singlet at 78.2 ppm in the $^{31}P\{^{1}H\}$ NMR experiment and became a well-defined triplet when properly decoupled from the cyclohexyl in the $^{31}P\{^{1}H$ sel 2ppm$\}$ spectrum (Figure 3-13). The multiplicity of the phosphorus signal accounts for a coupling with two hydrides.

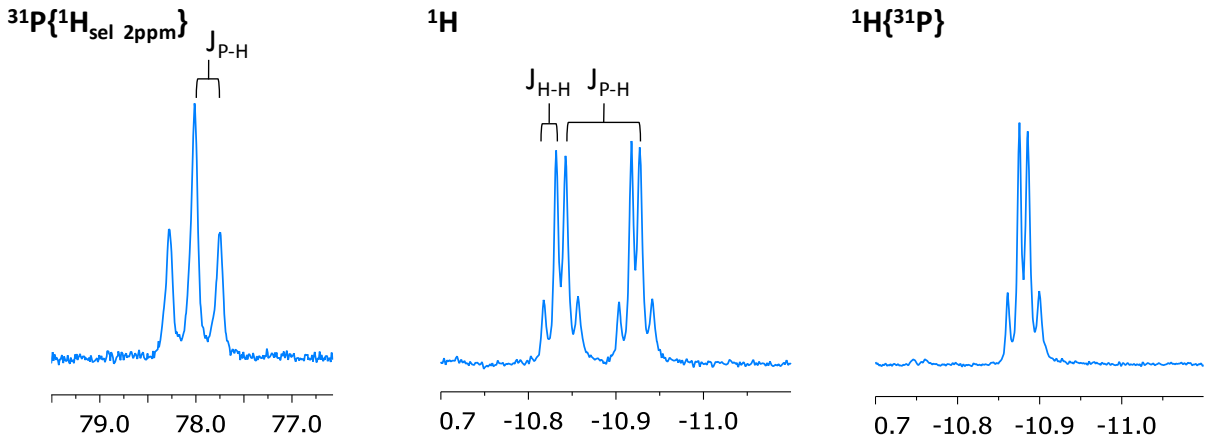

*Figure 3-13: $^{31}P\{^{1}H$ sel 2ppm$\}$, ^{1}H and $^{1}H\{^{31}P\}$ NMR spectra of complex **I-g***

The triplet correlates with the hydridic signal at – 10.9 ppm according to the cross peak found in the two-dimensional HMQC $^{31}P\{^{1}H\}/^{1}H$ spectrum. The hydrides show a well-defined pattern (Figure 3-13). The $^{1}H\{^{31}P\}$ NMR spectrum shows an AB system where the two atoms are slightly magnetically inequivalent and couple with a coupling constant of 7 Hz. The ^{1}H NMR experiment illustrates the coupling between the hydrides and the phosphorus atom with a doublet of two ABs (J_{P-H} = 43 Hz). This value falls in the typical range for η^6-arene substituted Ru species.[150, 163] In light with the non-equivalence of the hydrides, the rotation of the 1*H*-2,1-benzazaborole ligand must be slowed down either due to an unsymmetrical benzene bonding to ruthenium or to some steric hindrance between the isopropyl and cyclohexyl groups. The absence of a methine signal along with a new methylene resonance confirmed the hydrogen transfer at this position. The two hydrogen atoms of the CH_2 group resonate as an AB system (δ 3.98 and 4.07). A special sequence of two-dimensional HSQC $^{13}C\{^{1}H\}/^{1}H$ evidenced the direct coupling between the hydrogen atoms and a secondary carbon. One unambiguous proof of the η^6 coordination of the benzene ring was the upfield shifts of the aromatic protons in the 5.1 to 5.9 ppm ^{1}H NMR spectral region. In addition, the N–*H* chemical shift resonates at 2.5 ppm being more in the range of non-coordinated nitrogen for our class of 1*H*-2,1-benzazaboroles (**b2**: δ 2.86; **I-e**: δ 3.46).

It is worth noting that throughout the monitoring of the reaction, we observed the release of **b2** which became the major product at the end of the reaction. In order to see if complex **I** could be regenerated together with the release of **b2**, we repeated the experiment starting from complex **I-e** and one equivalent of free phosphine. The major product at the end of the reaction in the $^{31}P\{^{1}H\}$ NMR spectrum corresponded to the precursor catalyst **I**. However, in these conditions complex **I-g** was not totally converted.

III.3. Summary of the stoichiometric study

This stoichiometric study highlighted the ability of the $RuH_2(H_2)_2(PCy_3)_2$ complex (**I**) to provide and transfer dihydrogen to the benzonitrile borane (**a2**) and to enable the formation of the 1*H*-2,1-benzazaborole (**b2**). Ruthenium species have been characterized in different stages of dehydrogenation depending on the amount of **a2** we added. The different dehydrogenated ruthenium species are depicted in Scheme 3-11.

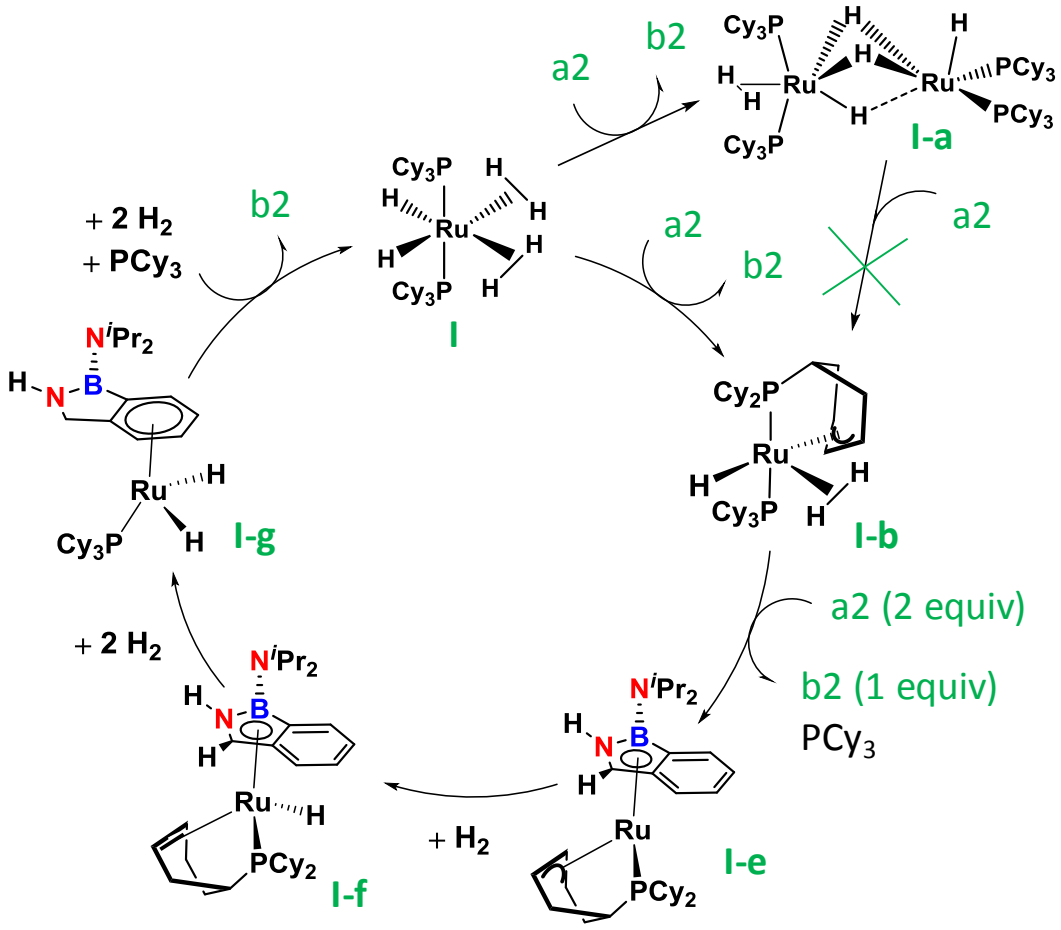

Scheme 3-11: Summary of our mechanistic investigation based on stoichiometric reactions

The provided hydrogen atoms can come from the σ-H_2 ligands yielding the dimeric complex **I-a**. Once the σ-H_2 are consumed, the cyclohexyl of the phosphine can also furnish hydrogen *via* C–H activation to yield the further dehydrogenated complex **I-b**. However, we noticed that complex **I-a** do not lead to **I-b** upon addition of **a2**. The 2/1 mixture of **a2** and the isolated complex **I-b** led to the release of one equivalent of **b2** and the generation of the last dehydrogenated stage, complex **I-e**, together with release of PCy_3. The substrate was thus captured during its chemical transformation on the ruthenium center. It was captured in the form of the 1*H*-2,1-benzazaborolyl ligand, coordinated through the BN cycle to the ruthenium center. **I-e** underwent a stepwise hydrogenation of first, the cyclohexenyl of the phosphine producing the monohydride **1-f** and second, transforming the methine carbon of the substrate to complete the formation of the 1*H*-2,1-benzazaborole **b2** as seen in **I-g**. The product can then be released along with the recovery of the hydrogenated precursor catalyst complex **I** when free phosphine and H_2 are present in the mixture.

The overall material balance for the stoichiometric reactions can be summarized by the following equation:

$$\boldsymbol{I} + n\ a2 + n\ H_2 = n\ b2 + \boldsymbol{I}$$

Overall, nine hydrogen atoms of complex **I** were available for the hydrogenation of **a2** (Figure 3-14). The precedent statement is in agreement with the capacity of **I** to transform up to 5 equivalents of **a2**.

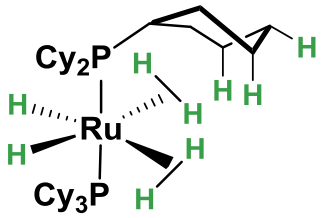

*Figure 3-14: Available hydrogen atoms in complex **I** for the hydrogenation of **a2***

This first study emphasized hydrogen transfer phenomena from the Ru complex to the substrate that can occur *via* the σ-H_2 ligands, C–H activation of the cyclohexyl of one phosphine ligand and η^5 coordination of the 1*H*-2,1-benzazaborolyl fragment. Noteworthy, the full hydrogenation of the nitrile function prior to the B-N bond formation does not appear as a necessary step, disfavoring proposition 1. The investigation also highlighted the possibility

to recover the catalyst at the end of the reaction. In light of the reactivity of complex **I-e** with dihydrogen, the 1*H*-2,1- benzazaborolyl formation and coordination seems to be a *via*ble intermediate to consider in the catalytic hydrogenation of **a2** to form **b2**. We will now investigate further details considering the coordination of the benzonitrile borane on the ruthenium center. Specifically, we will look at the C≡N and/or B–H bond activation process. According to the ^{31}P NMR spectra, no intermediate was observed during the catalytic reaction at room temperature. Consequently, we conducted an investigation at low temperatures in catalytic conditions, with the aim to characterize *in-situ* intermediate species.

III.4. Variable temperature experiments

III.4.1. Beginning of the reaction

We performed a first experiment in catalytic conditions. The ruthenium precursor (10 mg, 10 mol%) and the benzonitrile borane **a2** were mixed at room temperature, in deuterated toluene in a NMR tube for high pressure. Argon was rapidly removed under vacuum and the tube was pressurized with 2 bar(g) of H_2. The mixture was immediately frozen in liquid nitrogen. The first NMR spectrum was recorded at – 80°C. The $^{31}P\{^1H\}$ NMR spectrum shows a unique signal at 64 ppm correlating with a ^1H NMR hydride signal at – 14.1 ppm. We already observed this species during the monitoring of the reaction (see section II.1.) but we were not in the position to characterize it properly due to its rapid evolution into other species. At low temperature, we have been able to attribute those resonances to a species formulated as the bis(nitrile) dihydride ruthenium complex **I-h** (Figure 3-15).

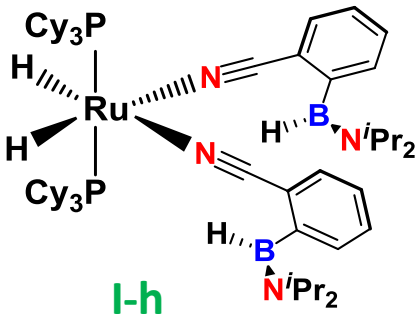

*Figure 3-15: Proposed bis(nitrile) dihydride ruthenium complex **I-h** observed when complex **I** is in presence of an excess of **a2***

In presence of an excess of **a2** (catalytic conditions), the ruthenium complex **I** loses the two σ-H_2 and coordinates two molecules of **a2** by the nitrile function. This explains gas evolution upon mixing of the catalyst and the substrate. The substrate **a2** preferentially binds the metal by the nitrogen of the nitrile function in a η^1 fashion. Direct activation of the nitrile function seems to be favored compared to B–H activation or oxidative addition. Complex **I-h** is an analogue of complex **II-c** ($RuH_2(NCPh)_2(PCyp_3)_2$, (Scheme 1-22, Chapter 1) observed during the hydrogenation of benzonitrile with complex **II** as previously reported in the group.[139] An X-ray structure of the corresponding bis(acetonitrile) complex had also been obtained. In our case, we were not able to isolate **I-h** due to its high reactivity.

Hence, complex **I-h** was observed in different conditions. The complex was present in the mixture directly after mixing **a2** and **I** in catalytic conditions, either before pressurizing with H_2 at room temperature or after pressurizing with H_2 at − 80°C. In other words, complex **I-h** is the result of the coordination of **a2** to **I** before exogeneous hydrogen gets involve. With a view to characterize **I-h**, we conducted a reaction in stoichiometric conditions with **a2** and **I** in a 2/1 molar ratio. Complex **I** was charged in a NMR tube for high pressure containing deuterated toluene and maintained at – 80°C. A cold solution of **a2** was added at once. The tube was directly inserted in the NMR spectrometer and the complex was characterized by NMR at − 40°C where the maximum concentration of **I-h** was detected.

A cross peak in the two-dimensional HMBC (long range) $^{13}C\{^{31}P\}/^{1}H$ NMR spectrum indicates a correlation between the hydrides and the quaternary carbon of the nitrile function at 120.3 ppm. The chemical shift of the carbon is slightly shifted downfield compared to free **b2** (δ 119.3 at − 40°C). For comparison, the nitrile carbon of acetonitrile resonates at 116.4 ppm ($CDCl_3$) and that of $RuH_2(\eta^1\text{-}NCCH_3)_2(PCyp_3)_2$ at 116.3 (THF d_8). The small difference discards an η^2 coordination mode of the C≡N bond.[164] The same two-dimensional experiment shows an interaction between the carbon of the nitrile and the aromatic hydrogen atom, confirming the presence of the aryl. The B–H resonance in the ^{1}H NMR spectrum was found at 5.70 ppm (**b2**: δ 5.5 at 40°C) dismissing any agostic B–H bond that are usually characterized by an upfield shift.[149] The signal appeared as a broad singlet slightly sharpening upon ^{11}B decoupling. Although the NMR pattern matches with a dangling B–H moiety, the behavior under ^{11}B decoupling of the signal in the coordinated aryl(cyano)(aminoborane) clearly differ from that of free **a2** (appendices section). It is apparent that the Δ(ω ½) is greater in the case of **a2** than

in **I-h**. One explanation could be the large molecular radii that should severely influence the ^{11}B quadrupolar relaxation and result in a B–H decoupling.[165-166]

III.4.2. Middle of the reaction

A new tube was prepared following the catalytic procedure. The tube was frozen and introduced in the NMR instrument set at – 30°C. This temperature was determined optimal since we can observe the ruthenium intermediate species while the reaction still proceeds.

A series of $^{31}P\{^1H\}$ and ^1H NMR experiments were recorded over a period of 24 hours. One representative $^{31}P\{^1H\}$ NMR spectrum and the corresponding ^1H NMR spectrum in the hydride region are depicted in Figure 3-16.

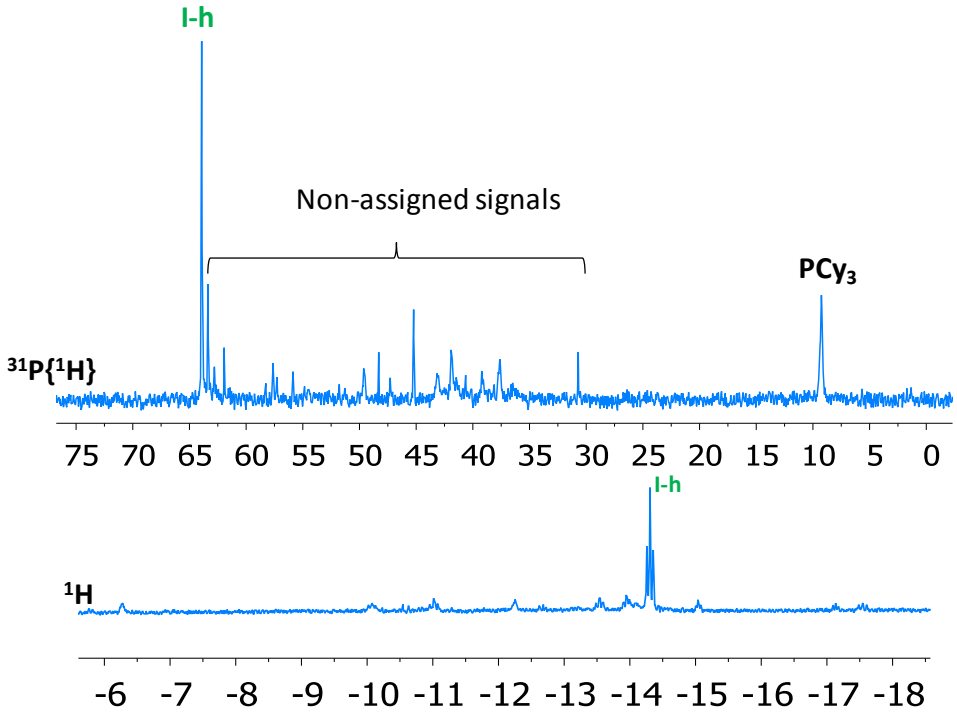

Figure 3-16: $^{31}P\{^1H\}$ NMR spectrum recorded at – 30°C while the reaction proceeds and the corresponding ^1H NMR spectrum in the hydride region

We noted that the concentration of complex **I-h** in the reaction mixture decreased when the temperature increased. At – 30°C, complex **I-h** was detected in both spectra. Free phosphine was also observed in the media and could account for the need to decoordinate one phosphine ligand to perform the catalysis. A multitude of new signals (about 20) appeared in the $^{31}P\{^1H\}$ NMR spectrum spanning from 30 to 63 ppm. We encountered the same

phenomenon in the related ^{1}H NMR spectrum where we found numerous hydride signals. As a result, the different species were in very low concentration rendering them impossible to identify. However, the downfield region (8-10 ppm) of the spectrum showed a certain number of resonances that we could attribute to imine moieties coordinated onto the metal. For instance, a doublet of low intensity (δ 8.25, $^{3}J_{H-H}$ = 7.2 Hz) was associated to a downfield carbon (δ 161) in two-dimensional experiment. This association of data is reminiscent of the imine intermediate complexes (**II-a, II-b**, Scheme 1-22**,** chapter 1) observed during the hydrogenation of benzonitrile.[139] In such complexes, the doublet multiplicity reflects the coupling between the C–H and the N–H protons of the imine unit. In our case, both chemical shifts and coupling constants fall in the range of the previously described complexes.

The same signals were roughly detected throughout the monitoring, except that the intensity for complex **I-h** decreased as long as the reaction proceeded and the temperature rose. The conversion of **a2** was complete after about 15 hours.

III.4.3. End of the reaction

The end of the reaction corresponds to the time for which the substrate **a2** was fully converted. In order to observe it, we performed another experiment, at room temperature, keeping the same conditions (NMR scale, toluene d_8). The substrate and complex **I** (5 mol%) were mixed, and the argon atmosphere replaced by dihydrogen. The first NMR spectrum was recorded after 25 minutes. The ^{1}H NMR spectrum shows the characteristic pseudotriplet of complex **I** as the major hydridic complex. The related $^{31}P\{^{1}H\}$ NMR spectrum is represented in Figure 3-17.

We observe complex **I** as the major complex along with free phosphine. A peak of low intensity was assigned to complex **I-g**. We decided to assess the ability to recover the pre-catalyst by adding a new batch of substrate. We reloaded the tube with the same starting amount of **a2**. The signal corresponding to complex **I** disappeared of the $^{31}P\{^{1}H\}$ NMR spectrum while free phosphine remained in the media (Figure 3-17-middle).

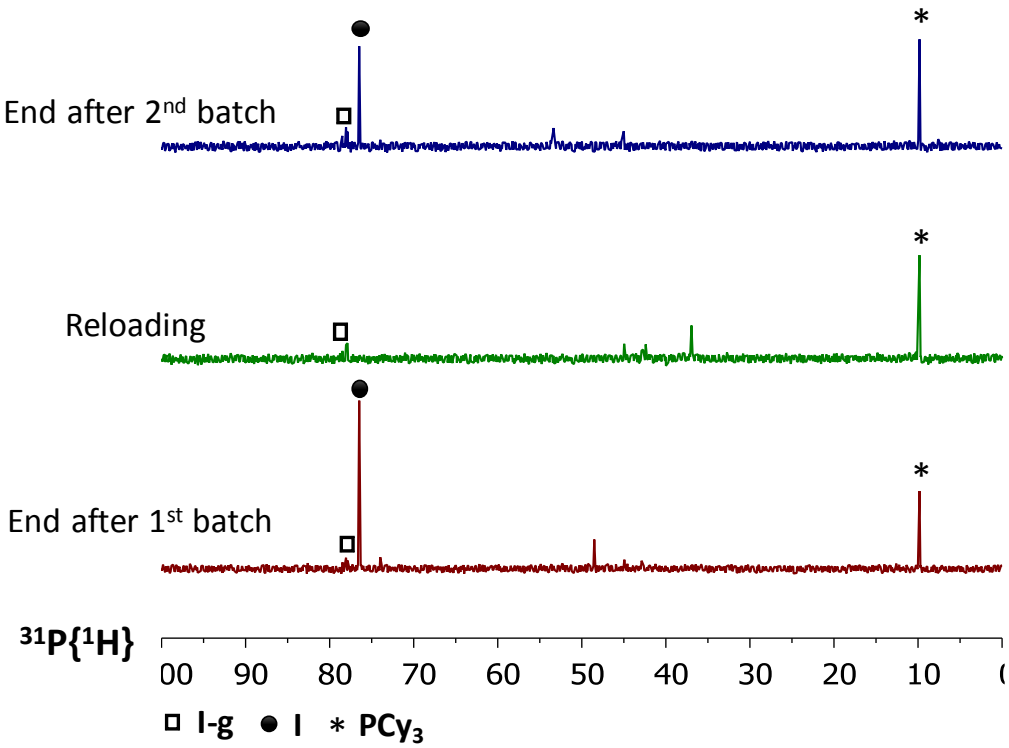

*Figure 3-17: $^{31}P\{^{1}H\}$ NMR spectra recorded at the end of the reaction (bottom), after reloading with **a2** (middle), at the end of the reloaded reaction (top)*

The catalyst utterly converted **a2** into **b2** and borazine with the same ratio than in the first catalytic reaction. The $^{31}P\{^{1}H\}$ NMR spectrum recorded at the end of the second batch is similar to the first one, another time indicating the recovery of the pre-catalyst. However, we observed relatively more of complex **I-g** and free phosphine in comparison to complex **I**. In addition, some toluene complex (η^6-C_7H_8)$RuH_2(PCy_3)$ was formed as characterized by the same ^{31}P chemical shift as **I-g**. With the aim to obtain a spotless view of the end of the reaction, we repeated the experiment in a Fisher-Porter bottle, in the standard conditions earlier established (see experimental section). The reaction mixture was sampled after one hour and the NMR analysis was done adding a closed capillary tube containing C_6D_6 for reference. The pseudotriplet for **I** was the unique signal in the hydride region of the ^{1}H NMR spectrum. It should be noted that the $^{31}P\{^{1}H\}$ NMR spectrum revealed a non-assigned minor signal at 54 ppm at the end of the reaction.

IV. Parameters influencing the catalysis

IV.1. Catalytic behavior of the dehydrogenated ruthenium species

The following section is dedicated to assess the influence of the starting catalyst precursor on the catalytic reaction. A table gathering the results of the performed experiments is presented below:

catalyst	*a2 conversion*	*I recovery*	*Time*
I	total	yes	1 hour
I-a	partial	no	1 day
I-b	total	yes	1 hour
I-e	partial	no	3 day
I-e + PCy_3	total	yes	2-4 hours

*Table 3-1: Comments on **a2** conversion and **I** recovery using **I, I-a, I-b, I-e** and **I-e+PCy_3** as pre-catalysts*

We conducted several reactions starting from the dehydrogenated ruthenium species isolated during the stoichiometric study. We were willing to see if they would bring the reaction to completion. When the dimeric complex **I-a** was used as precursor catalyst in standard conditions, the reaction did not reach full conversion of **a2** after 24 hours. We also noticed a different selectivity with a **b2**/diisopropylamine ratio inferior to 1, meaning the major product formed was actually the borazine. The reason for this poor activity could be assigned to the possible non-rehydrogenation of complex **I-a** into **I** under 1 bar of dihydrogen. On the contrary, complex **I-b** shows the same catalytic activity than complex **I** for the conversion of **a2**. Indeed, it was reported a reversible dehydrogenation/hydrogenation of complexes **I-b** and **I-c**. We can then imagine that under an atmosphere of H_2, complex **I-b** rapidly hydrogenates into **I** that we detect as the only hydridic complex at the end of the reaction.

When using complex **I-e** as precursor catalyst, the reaction occurs at low rate (about 30 % conversion after 3 days). However, when starting the catalytic reaction with a mixture of **I-e** and PCy_3, the reaction was complete within 2 - 4 hours. The coordination of the previously lost

phosphine plays a crucial role in the catalytic formation of **b2** through this pathway. However, the time of the reaction is longer compare to that with **I**. Indeed, in light of the study conducted with the hydrogenation of complex **I-e** (section III.2.3.), the thermodynamically stable complex needs some time to rehydrogenate.

IV.2. Influence of the pressure and the phosphine ligand on the catalysis

In order to gain more information on the catalytic process, we decided to look at the influence of the pressure, the addition of an excess of PCy_3 and the change of phosphine ligand to $PCyp_3$.

We created experimental conditions which enable to measure the conversion of **a2**, the formation of **b2** and the selectivity. All the reactions were performed in a Fisher-Porter bottle, in standard conditions. We applied vacuum in the bottle prior to pressurize with H_2. A solution of anisole was prepared and used as internal standard. The reaction was sampled after 5 minutes of reaction which corresponds to the time for which **a2** is still present in the media and can be integrated. The standard reaction was first performed (P_{H2} = 1 bar(g), RT, 5 mol% of **I**) and is reported in Table 3-2, entry 2.

entry	*catalyst*	*H_2 Pressure Bar(g)*	*PCy_3 Cat: PCy_3*	*Conversion (%)*	*b2 (%)*	*Borazine (%)*	*b2 : d2 mol ratio*
1	**I**	< 1	no	51	49	5	9.8 : 1
2	**I**	1	no	83	74	8.5	8.7 : 1
3	**I**	3	no	full	87	10.5	8.2 : 1
4	**I**	5	no	full	85	13	6.5 : 1
5	**I**	1	1: 5	82	73	8	9.1 : 1
6	**I**	1	1: 10	71	57	10	5.7 : 1
7	**II**	1	no	full	94	6	15.6 : 1

Table 3-2: Catalytic reactions in 2.5 mL of pentane, RT, and different operating conditions with the conversion and selectivity associated. All the data were collected after 5 minutes of reaction. Around 5 % of uncertainty are associated to a quantification using NMR spectroscopy.

We then looked at the influence of the H_2 pressure on the catalytic reaction. The sequence involving hydrogenation/dehydrogenation (proposition 1) could imply a lower rate of the reaction when increasing the pressure if the dehydrogenation process takes part in the rate determining step of the reaction. We know that in the dehydrogenation-cyclization of diamine monoborane,[144] N–H activation, involved in the dehydrogenation step, is the rate determining step. We performed one test at lower pressure (< 1 bar) and two tests at higher pressure (3 bar(g) and 5 bar(g)). The results are given entries 1 to 4 in Table 3-2. The conversion after 5 minutes of reaction is clearly increased when increasing the pressure. 51% of conversion are observed under a pressure of < 1 bar while full conversion of **a2** is obtained under 3 bar(g) after 5 minutes of reaction. This finding is not in favor of a hydrogenation/dehydrogenation pathway for the formation of **b2**. We also noticed a decrease in **b2** selectivity when increasing the pressure. For instance, when working under 1 bar(g) and 5 bar(g) the **b2**: **d2** ratio goes from 8.7: 1 to 6.5 : 1.

Throughout the catalytic reaction we see some free phosphine even though we have not been able to quantify it. We also know that complex **I-e**, formed in the absence of added H_2 gas, is the result of one phosphine dissociation and coordination of the 1*H*-2,1-benzazaborolyl fragment. We have demonstrated that the 1*H*-2,1-benzazaborolyl coordination mode might be involved in an intermediate of the reaction. Thus, we wondered whether the addition of free phosphine at the beginning of the catalytic reaction would slow down or even quench the reaction by precluding phosphine dissociation. We performed a first experiment adding 5 equivalents of phosphine compared to the catalyst. This reaction did not lead to a significant change. We then doubled the amount of phosphine. This time, we observed a lower conversion (71 compared to 83% for the standard reaction). However, the reaction still proceeds. Thus, if phosphine dissociation occurs it should not be the rate determining step. We could attribute the loss of conversion to the competitive coordination of a third phosphine ligand towards the formation of $RuH_2(H_2)(PCy_3)_3$.

We then performed the catalytic reaction starting from complex **II**. As seen in entry 7, this version of the ruthenium catalyst precursor with tricyclopentyl phosphines converts the substrate more efficiently with higher selectivity. Indeed, complex **II** usually favors hydrogen transfer processes.

V. Theoretical calculations and general discussion on the mechanism

With the view to complement our experimental findings, we undertook DFT calculations in collaboration with Chiara Dinoi and Iker del Rosal at LPCNO, Toulouse. DFT details are reported in the experimental section.

First, we looked at the thermodynamics of the general reaction (Scheme 3-12). The studied reaction is a thermodynamically favored process. The substituents on the aryl have a small influence on the ΔG indicating the reaction tolerates the different substituents.

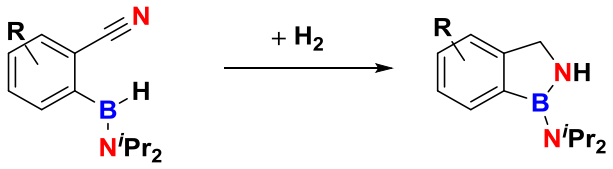

Δ G (ΔH) kcal mol^{-1}

b1: – 40.8 (– 50.3)
b2: – 39.4 (– 50.3)
b3: – 33.0 (– 44.1)
b4: – 40.3 (– 50.7)

Scheme 3-12: Thermodynamics of the general reaction

We were then interested in the coordination of the substrate with the catalyst precursor. The different species represented in Scheme 3-13 have been optimized by DFT/B3PW91. It is worth to point that several isomeric structures can exist due to many conformations resulting from the inherent dynamics associated to the cyclohexyl and isopropyl groups.

The coordination by the nitrile function is greatly favored compared to the B–H σ-bond interaction (9.4 vs 32.1 kcal mol^{-1}). Formation of a η^2-CN, σ-B–H agostic complex is also more energetically demanding (19.6 kcal mol^{-1}). As demonstrated experimentally in complex **I-h**, the calculations support an early stage coordination by the nitrile function in a η^1 fashion with dangling B–H bond. The activated nitrile and dihydrogen at the ruthenium center seem more likely to react than the non-coordinated B–H bond, favoring a hydrogenation process prior to hydroboration. Furthermore, it should be noted that prolonged heating of **a2** at 130°C in toluene did not lead to any hydroborated product.

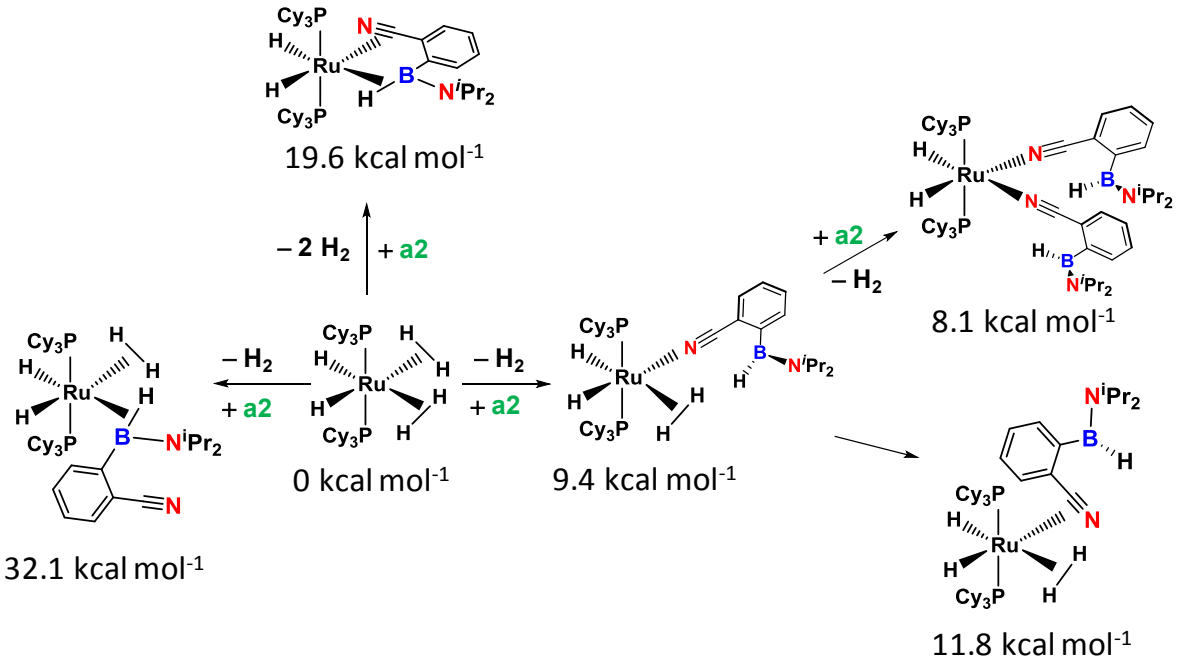

*Scheme 3-13: Energetic pathways of different possible coordination modes of **a2** on **I** involving substitution of one or two dihydrogen ligands*

Different competitive pathways were calculated but here we will present solely the most favorable one (Scheme 3-14). Key calculated complex minima are represented. Transition states were located between every minimum.

The relative energies for the coordination of two substrates versus the monosubstituted dihydrogen species are very close (Scheme 3-13). Under a pressure of H_2, one can assume the reaction should be displaced towards the monosubstituted dihydrogen species (**I-A**). No transition state could be located for the hydride transfer when the nitrile was η^1- coordinated. The switch to η^2-CN coordination (**I-B**) has proven to be necessary for the following hydride transfer. Leitner and coworkers also reported an η^2-CN coordination enabling hydride transfer while nitrile hydrogenation in metal-ligand bifunctional catalysis requires simultaneous carbon and nitrogen interaction with the catalyst.[133, 167]

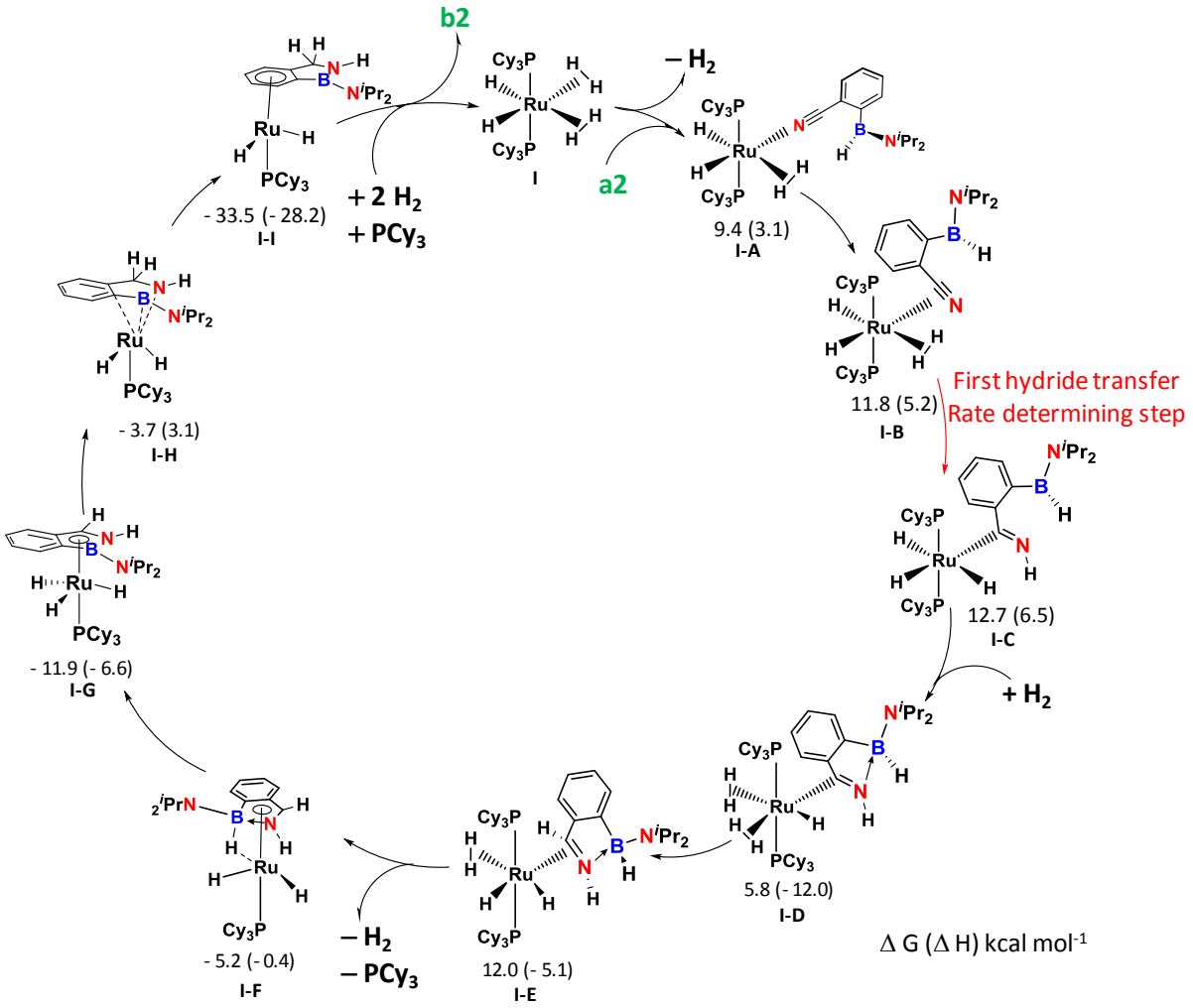

*Scheme 3-14: Key calculated intermediates for the hydrogenation/cyclization of **a2** with **I***

Hydrogen transfer can occur either to C or N of the nitrile function. We will only discuss H transfer to N to form the iminoacyl species (**I-C**), as it was found the most energetically favorable. This finding is in contradiction with previously described cycles for the hydroboration of nitriles with a first hydride transfer generally occurring at the carbon with metal hydride complexes (see chapter 1). It is probably the result, in our case, of the presence of polarized σ-H_2 ligands. A DFT investigation on nitrile hydrogenation carried out by Leitner and coworkers showed that the barrier corresponding to the first hydride transfer on nitrogen or carbon is rather close, even if transfer on the carbon was the most favorable one.[167] In the same way, hydride transfer on the C occurred first in metal-ligand bifunctional systems but hydride and proton transfers occurred in a nearly concerted manner.[133] In our case, the first

hydride transfer was calculated as the rate-determining step of the reaction with a barrier of 25.1 kcal mol^{-1}. The associated transition state is represented in Figure 3-18.

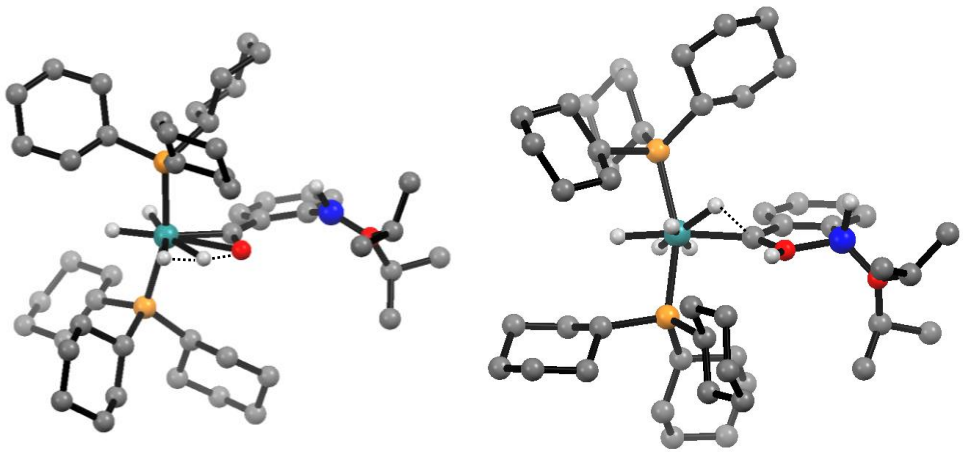

TS I-B····I-C
25.1 (17.9)
First H transfer

TS I-D····I-E
18.7 (2.6)
second H transfer

Figure 3-18: Calculated transition states for the first (left) and second (right) hydrogen transfer (N in red and B in blue)

The H_2 ligand is greatly elongated (**I-B** (H-H): 0.85 Å; **TS I-B-I-C** (H-H): 1.23 Å) with one hydrogen interacting with the nitrogen towards N–H bond formation (**TS I-B-I-C** (N-H): 1.39 Å; **I-C** (N-H): 1.05 Å). As a result, the minimum **I-C** features an aminoacyl coordinated to ruthenium by the carbon atom and three hydrides. Boron-nitrogen interaction within the trihydride aminoacyl species (**I-C**) was barrier less to form the corresponding hydrido dihydrogen species ready to coordinate an additional H_2 ligand to form (**I-D**). Then, the second hydrogen transfer can occur at carbon producing the minimum **I-E**, in which the cyclic imineborane binds ruthenium through the C=N bond. The transition state associated to the second hydride transfer is depicted in Figure 3-18. **TS I-D-I-E** features only one σ-H_2 ligand while the other split into two hydrides. A third hydride interacts with the aminoacyl carbon but the C–H bond is far from being formed (**TS I-D-I-E** (C-H): 1.69 Å; **I-E** (C-H): 1.09 Å). From intermediate **I-E**, no hydrogen transfer of the B–H hydrogen was found possible. The full hydrogenation of the CN bond was energetically disfavored due to the B–N interaction, one more time discarding proposition 1. Instead, the loss of one phosphine ligand and H_2 led to the B–H agostic intermediate **I-F** in which the ruthenium center interacts with the 5-member BN ring. Then, B–H bond cleavage

can occur to generate the hydrogenated version **I-G** of the experimentally isolated complex **I-e**. The transition state associated to the B–H bond cleavage is represented in Figure 3-19.

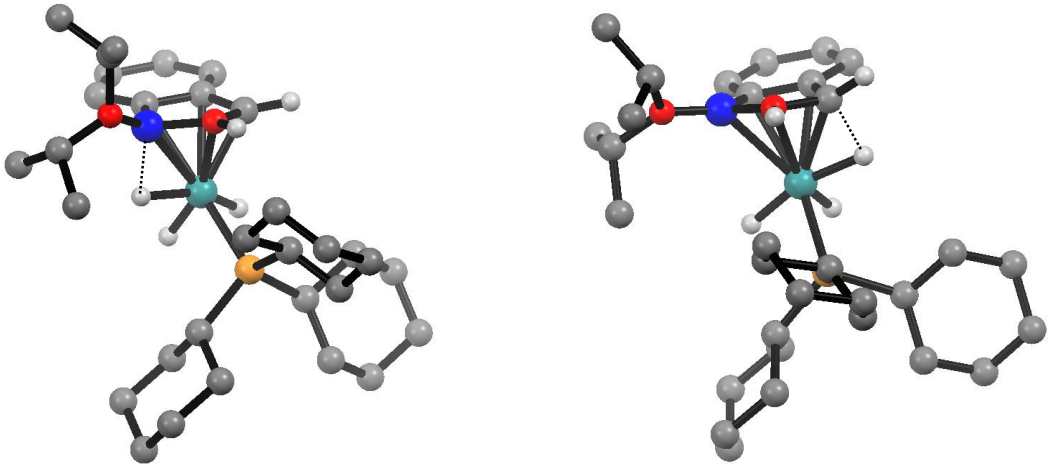

TS I-F····I-G
– 5.9 (– 1.5)
B–H bond cleavage

TS I-G····I-H
3.6 (– 6.6)
Third H transfer

Figure 3-19: Calculated transition states for the B-H cleavage (left) and third hydrogen transfer (right)

The B–H bond is close to the cleavage (**TS I-F-I-G** (B-H): 1.63 Å) and the Ru–H bond nearly formed (**TS I-F-I-G** (Ru-H): 1.71 Å; **I-G**: 1.60 Å). In **I-G**, the 1*H*-2,1-benzazaborolyl ligand approaches an η^5 coordination to the ruthenium trihydride species (Table 3-3).

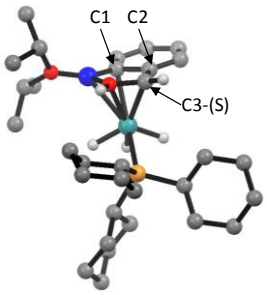

	I-G *DFT (C3-S)*	***I-e*** *Xray structure (C3-S)*
Ru–N	2.23	2.270 (2)
Ru–B	2.47	2.500 (3)
Ru–C1	2.42	2.371 (2)
Ru–C2	2.35	2.290 (2)
Ru–C3	2.16	2.122 (2)

*Table 3-3: Bond distances in **I-e** crystals and **I-G** calculated species for C3 in the (S) configuration*

The Ru–C distances are slightly elongated in **I-G** compared to **I-e** but the bonding situation is similar, slipping away from boron and leaning towards N, C3, and C2 (the modeled species was calculated in the S configuration, and the corresponding X-ray data are given for comparison). **I-G** undergoes the third hydride transfer to the C3 atom with a barrier of 15.5 kcal mol^{-1}. The transition state associated to this step is depicted in Figure 3-19. The Ru-H is elongated (**I-G** (Ru-H): 1.58 Å**; TS I-G-I-H** (Ru-H): 1.69 Å) and the hydride interacts with C3 (C3-H: 1.58 Å). The haptotropic rearrangement, as observed experimentally, occurs through η^3 coordination of the B, N, C1 moiety in **I-H**. Upon addition of PCy_3 and $2H_2$, the release of the substrate **b2** together with regeneration of complex **I** is a thermodynamically favored process ($\Delta G = -39.4$, $\Delta H = -50.3$ kcal.mol^{-1}). It is reasonable to assume that σ-CAM sequences could lower the barriers all along the catalytic cycle.[168]

Hence, the combination of experimental and theoretical works enabled a better understanding of the mechanism of the reaction. The interaction between the substrate **a2** and complex **I** is dominated by the influence of the nitrile function. Therefore, **a2** interacts differently than the related aryl(phosphino)(aminoborane) with **I**.[169] The aryl(cyano)(aminoborane) binds the ruthenium center by the nitrile function leaving at first the B–H bond inactivated, as observed experimentally and confirmed by calculation. The nitrile first reacts with dihydrogen discarding a hydroboration process as postulated in proposition 2. The mechanism start with partial hydrogenation of the nitrile function. In comparison to classical hydrogenation mechanism, when boron is present, a stabilizing B-N interaction is preferred as soon as the nitrile bond starts to be reduced. Hence, the C≡N bond cannot be fully hydrogenated discarding proposition 1. Once the imine moiety is formed, the B–H bond is activated *via* uncommon η^5 coordination of the BN cycle to the metal center, together with the loss of a phosphine ligand. A dehydrogenated version of the intermediate after B–H cleavage (complex **I-e**) was captured and fully characterized as the first 1*H*-2,1-benzazaborolyl ligand isolated on a transition metal. We demonstrated that such an intermediate can afford the targeted product and regenerate complex **I** under H_2 *via* stepwise hydrogenation. The theoretical calculations support our experimental findings with the presence of the modeled hydrogenated version (**I-G**). Keeping in mind that PCy_3 release was always observed when monitoring the catalytic reaction, it is important to note that competitive pathways could also be calculated in particular with no phosphine dissociation.

In conclusion, the proposed mechanistic pathway is a variant of proposition 3 where the nitrile function is partially reduced prior B–N interaction to finally observe B–H bond activation *via* an unprecedented intermediate. We may now wonder whether this strategy could be extended to (cyano)(aminoborane) with different spacers or to different reactive functions.

VI. Comparison with the corresponding aryl(isocyano)(aminoborane)

One perspective of our work is to change the reactive function ortho to the B–H bond and study the related reactivity. With this in mind, we decided to incorporate the reverse function of the nitrile group by forming the aryl(isocyanide)(aminoborane) analogue (Figure 3-20).

Nitrile Isonitrile

Figure 3-20: Two isomers: aryl(cyano)(aminoborane) and aryl(isocyano)(aminoborane)

VI.1. Synthetic strategy towards the formation of aryl(isocyano)(aminoborane)

A few isonitrile molecules can be prepared from alcohols. Yet, the main synthetic route towards isonitrile compounds is a two-step synthesis from primary amines. The approach consists in formylation, dehydration sequences. In our case, we were willing to prepare the 2-bromoaryl isocyanide whose experimental procedure was described in the literature.[170] We used ethyl formate and $POCl_3$ as formylation and dehydration agents, respectively (Scheme 3-15). The two products were isolated in excellent yields.

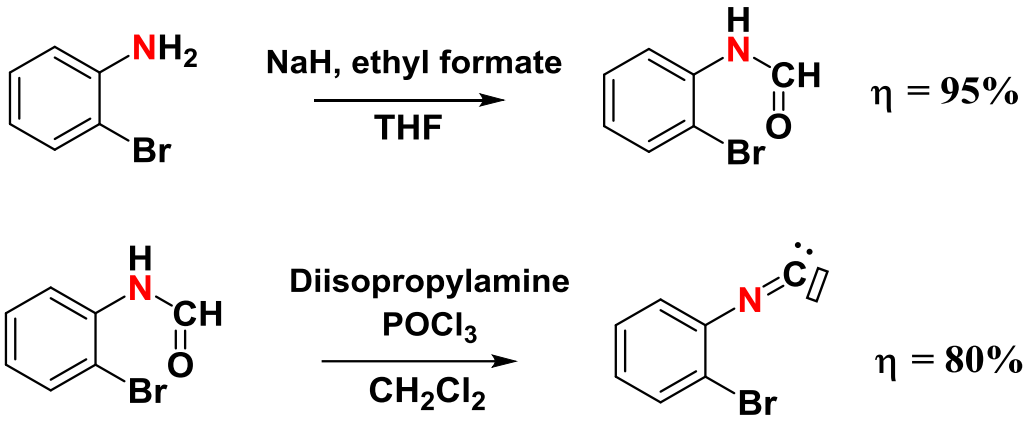

Scheme 3-15: Formylation/dehydration sequences from o-bromoaniline towards 2-bromoaryl isocyanide

Meijere and coworkers employed the o-bromoaryl isocyanide towards the synthesis of 2-substituted phenyl isocyanide by lithiation and addition of an electrophile at low temperature.[170] Encouraged by their results, we intended to transpose the lithiation/borylation strategy developed in chapter II towards the synthesis of the aryl(isocyanide)(aminoborane) **c** (Scheme 3-16).

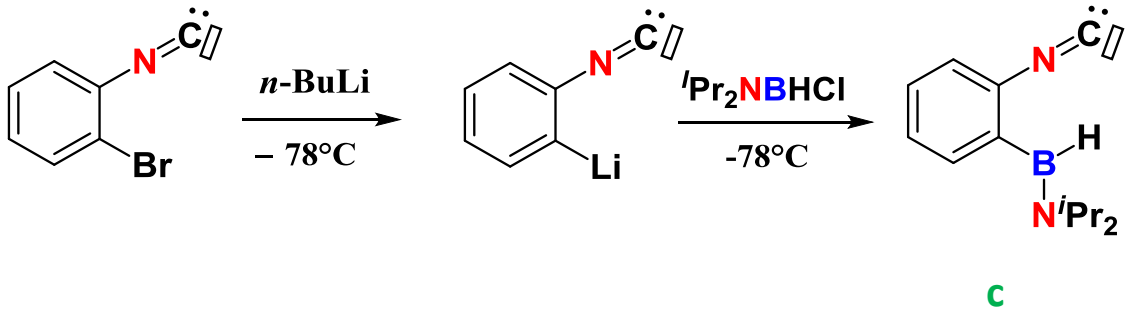

*Scheme 3-16: Synthesis of aryl(isocyano)(aminoborane) **c***

We performed the lithiation and borylation steps at low temperature. At first, the reaction was maintained at –78°C during 3 hours before reaching room temperature, as described by Meijere and coworkers. The procedure was then realized leaving the mixture warming up right after the addition of the borane and led to similar results. We were able to observe compound

c in solution by sampling the reaction mixture for NMR characterization. Compound **c** shows very similar NMR resonances with the nitrile analogue **a2** as seen in Table 3-4.

	^{1}H (CH_3 ^{i}Pr)	^{1}H (CH ^{i}Pr)	^{1}H (B-H)	^{1}H (Har)	^{11}B	$^{11}B\{^{1}H\}$
a2	0.87, 1.25	3.04, 3.69	5.5	6.75, 7.02,	37.5	37.5
C_6D_6	(d)	(sept)	(br)	7.06, 7.21	(d, J_{B-H} = 115Hz)	s
c	0.87, 1.24	3.06, 3.69	5.5	6.79, 6.94,	37.4	37.4
THF/ C_6D_6	(d)	(sept)	(br)	6.98, 7.04	(d, J_{B-H} = 115Hz)	s

*Table 3-4: ^{1}H, ^{11}B and $^{11}B\{^{1}H\}$ NMR data of compound **a2** (isolated) and **c** (in situ)*

However, all our attempts to isolate compound **c** failed. The product degraded under reduced pressure when trying to remove the solvent. Broad signals appeared in the ^{1}H NMR spectrum as well as numerous signals in the 2, –10 ppm region of the ^{11}B NMR spectrum. We assumed that intermolecular reactions occurred upon concentration of the mixture leading to various species (oligomers, polymers) including tetragonal boron. After washing with cold pentane and filtration, we obtained the postulated compound **c** together with a new set of signals. The new species was characterized by a singlet at 8.9 ppm in the ^{1}H NMR spectrum along with a septet at 3.92 ppm and a doublet at 1.18 ppm. The downfield singlet is characteristic of C–H carbaldimine compounds.[171] The two other resonances are comparable to that of the CH ^{i}Pr and CH_3 ^{i}Pr of the 1*H*-2,1-benzazaborole **b2**. This association of data led us to propose an intramolecular reaction generating the cyclic borane carbaldimine compound represented in Scheme 3-17.

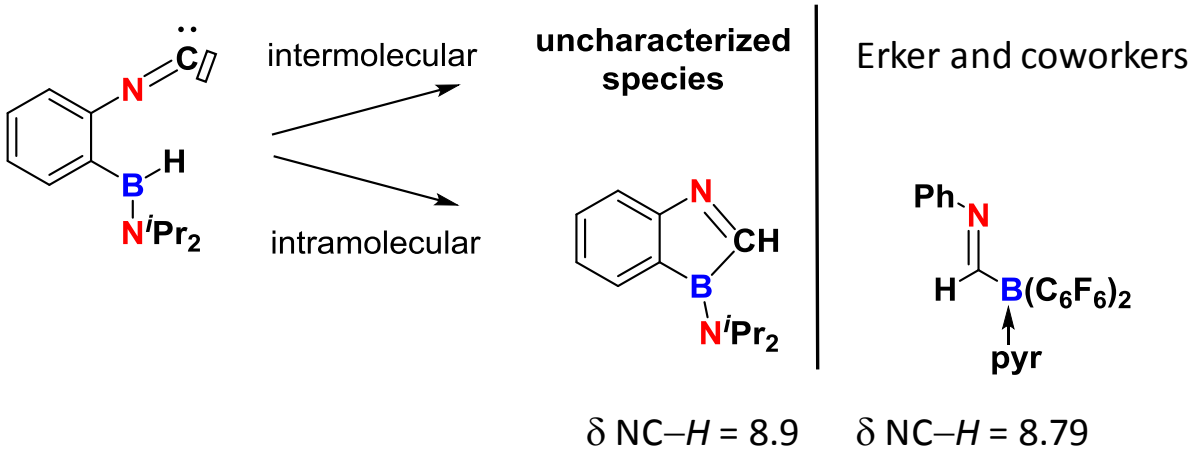

*Scheme 3-17: Behavior of compound **c** under reduced pressure*

Such species are scarcely found in the literature. Erker and coworkers reported this year the synthesis of the borane carbaldimine represented in Scheme 3-17.[171] They evidenced a quaternarized boron in the molecule due to the interaction with a pyridine Lewis base. They described this interaction as a key stabilizing element of the borane carbaldimine compound. In our case, the B–N double bond character inducing electron delocalization through the cycles could be responsible for the stabilization of such molecules.

In conclusion, the aryl(isocyanide)(aminoborane) **c** can be prepared *in situ* but displays a very different stability than the nitrile analogue. Those preliminary results show that the borane seems more likely to react with the isonitrile function than with the nitrile one. Theoretical works suggest that the carbenic electronic structure of the isonitrile is predominant while the zwitterionic character is secondary.[117] Although isonitriles possess a rigid geometry, the triple bond character is attributed to the stabilizing nitrogen π lone pair donation and consequently can be more easily perturbed than that of the nitrile function. Thus, the carbenic character of the isonitrile group seems to allow more accessible intra and intermolecular reactions in our case.

Yet, the uncontrolled generation of the different products made impossible the isolation of such compounds.

VI.2. Reactivity of aryl(isocyano)(aminoborane) with $RuH_2(H_2)_2(PCy_3)_2$

As we were unable to isolate compound **c**, we directly added one equivalent of the ruthenium precursor **I** to a freshly prepared THF reaction mixture containing **c**. Due to the presence of Br^- in the media as a result of the starting compound, we observed as a side product the formation of $RuHBr(H_2)(PCy_3)_2$ **I-j** (Scheme 3-18)**.** The bromo complex **I-j** was identified *in situ* and its structure was confirmed by X-ray diffraction techniques. Complex **I** also reacted with two equivalents of the isocyanide compound **c** to form complex **I-i** (Scheme 3-18) as postulated from multinuclear NMR data.

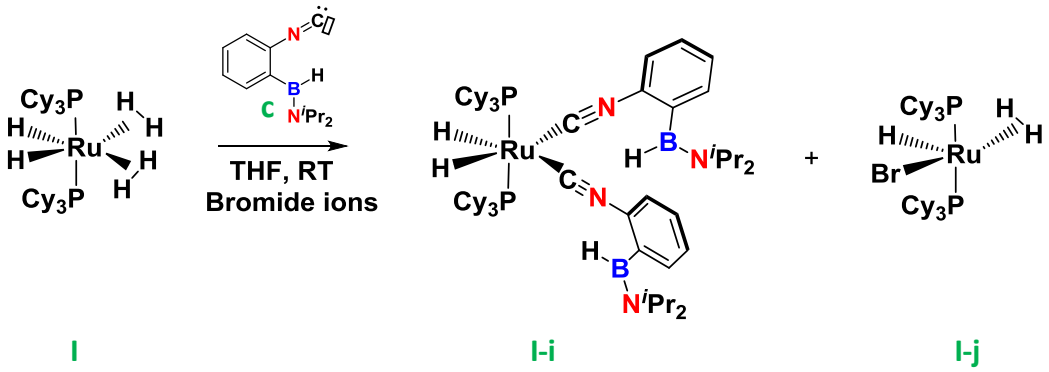

*Scheme 3-18: Products from the addition of $RuH_2(H_2)_2(PCy_3)_2$ in the crude mixture containing **c***

The reaction does not readily proceed, complex **I** being utterly consumed after 4 hours. Complex **I-i** is an isomer of complex **I-h** in the isonitrile version. In contrast, complex **I-i** is stable at room temperature and can be isolated after purification with traces of complex **I-j**. Complex **I-i** was characterized by multinuclear NMR analysis. The ^1H NMR spectrum shows an upfield triplet at – 8.48 ppm correlating with a phosphorus signal detected at 72.35 ppm with a coupling constant of 24 Hz. The related bis(^{t}BuNC)Ru complex was previously isolated in the group and showed comparable characteristic peaks in the ^{31}P and ^1H NMR spectra (^{31}P: δ 71.3, ^1H: δ – 9.5, t, J_{H-H} = 24 Hz).[172] In 2013, they isolated the bis(isocyano) complex, $RuH(CN)(CNBHN^iPr_2)_2(PCy_3)_2$, during the reactivity study of the cyanoaminoborane $N^iPr_2BH(CN)$ with **I**. The starting cyano compound isomerizes to lead to the bis(isocyano) complex with dangling B–H bonds. ^{31}P NMR data are hardly comparable due to the presence

of the CN ligand in place of a hydride in our case, but the ^{1}H NMR data match well (^{31}P: δ 56.40, ^{1}H: δ – 7.55, t, J_{H-H} = 22.5 Hz).[173] The resonances of the coordinated aryl(isocyano)(aminoborane) in the ^{1}H NMR spectrum are all slightly shifted downfield compared to the free compound **c**. We have seen that compound **c** had similar overall NMR pattern than the related nitrile compound **a2**. In the same manner, the NMR of the coordinated aryl(isocyano)(aminoborane) in **I-i** is close to that of the coordinated aryl(isocyano)(aminoborane) in **I-h**. The slight downfield shift of the B–H resonance (δ 5.5 in **c**, δ 5.7 in **I-i**) discards any B–H agostic interaction. No boron resonance was observed at this stage of our investigation.

Hence, the replacement of the nitrile by the isonitrile function also led to the formation of a bis(aryl(isocyano)(aminoborane)) complex with dangling B–H bond and η^1 coordination of the isocyanide carbon. Although, the overall NMR pattern of the boron containing ligand is not influence by the change of function, the electron donation/back donation within the complex is slightly modified as evidenced by the shift of the hydrides and phosphorus signals. The isonitrile ligand **c** behaves as a better π acceptor compared to the nitrile ligand **a2**.

Most importantly, combination of $RuH_2(H_2)_2(PCy_3)_2$ (**I**) and two equivalents of **a2** led to spontaneous formation of **b2**. In contrast, combination of **I** with **c** did not enable any hydrogen transfer from the ruthenium complex to the isonitrile substrate. Instead, we observe the formation of complex **I-i** which is stable at room temperature. Isonitriles are known to be strong σ-donors. This property might preclude easy association/dissociation of the ligand to coordinate H_2 or perform C–H activation.

In summary, the nitrile compound **a2** and the isonitrile compound **c** possess very similar spectroscopic data. However, the isonitrile function reacts more easily with the B–H bond either in an intra or intermolecular manner. Thus, we were unable to isolate it at room temperature. Compound **c** exhibits a different behavior than compound **a2** towards $RuH_2(H_2)_2(PCy_3)_2$ (**I**). One acts as a reactive substrate (**a2**) while the other acts as a stable ligand (**c**).

CHAPTER 4:

SYNTHETIC POTENTIAL OF 1H-2,1-BENZAZABOROLE

CHAPTER 4: SYNTHETIC POTENTIAL OF 1*H*-2,1-BENZAZABOROLE

We now enter into the second part of this work aiming at studying the newly formed BN-molecules. As no other 1*H*-2,1-benzazaborole derivatives feature a N–H moiety, we decided to take advantage of the function and look at the reactivity it may offer. In this chapter, we disclose the functionalization at nitrogen as well as a dehydrogenation study that would involve N–H and C–H bond activation of the 1*H*-2,1-benzazaborole **b2**.

I. Functionalization at nitrogen

If no report was found concerning functionalization at the nitrogen of 1*H*-2,1-benzazaborole derivatives, a few examples were reported regarding the related 6-member ring 1,2-azaborine derivatives.[51, 174] Liu and coworkers carried out the first reactivity study on the 1,2-dihydro-1,2-azaborine that they recently successfully synthesized (Scheme 4-1).[174]

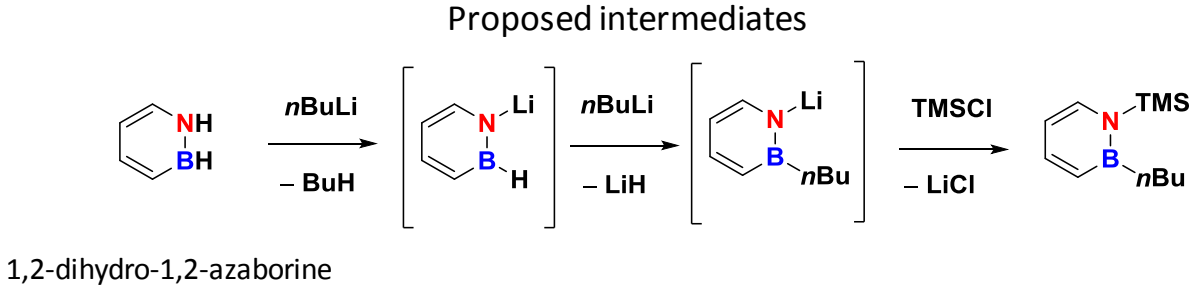

Scheme 4-1: Reactivity of 1,2-dihydro-1,2-azaborine with nucleophiles and electrophiles

They showed that the BN compound could react with nucleophiles, first with *n*BuLi and then with various nucleophiles. Supported by theoretical calculations, they showed that the 1,2-dihydro-1,2-azaborine undergo deprotonation of the N–H bond prior to nucleophilic substitution at the boron center with the second equivalent of *n*BuLi. They added various electrophiles to obtain the disubstituted products. The authors also recently published a Negishi coupling variant compatible with BN heterocycles to lead to late-stage functionalization of 1,2-azaborines.[175]

I.1. Formation of the lithium amide salt

The 1*H*-2,1-benzazaborole compounds comprise various reaction sites: a Brønsted acid N–H hydrogen, a Lewis acid trigonal boron, and a CH_2 methylene group that, in specific conditions, can be deprotonated. The boron atom shows a reduced acidity owing to nitrogen stabilization. Hence, with the aim to selectively deprotonate the N–H moiety, we examined the reactivity of the B-NH-CH_2 moiety in basic conditions. We selected *n*BuLi as a base. When a solution of **a2** was treated with 1.1 equiv of the base at – 20°C a white precipitate appeared within a few minutes. The insoluble solid was identified as the product resulting from selective N–H deprotonation. We conducted the reaction in pentane or in diethylether, yielding in both cases the lithium amide salt in around 75 % yield. The equation of the reaction is depicted in Scheme 4-2.

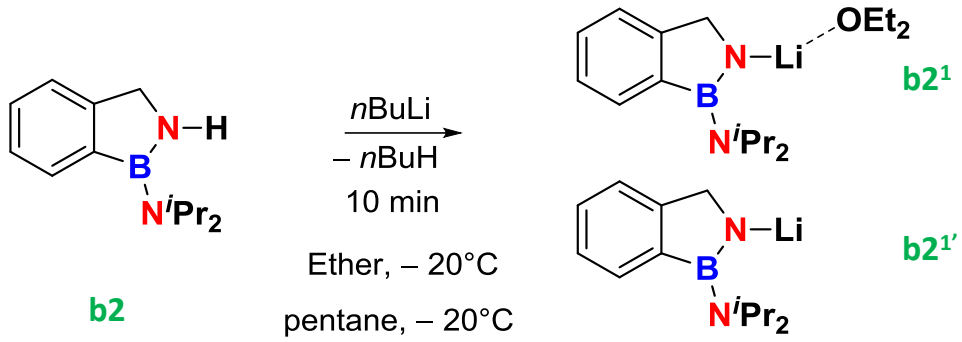

Scheme 4-2: Reaction of 1H-2,1-benzazaborole b2 with nBuLi to yield the lithium amide salts

When conducting the reaction in the coordinating ether solvent, the reaction generated the etherate amide salt (**b2^1**) while the experiment conducted in pentane generated the ligand free amide salt (**b2$^{1'}$**). Compound **b2^1** and **b2$^{1'}$** were characterized by multinuclear NMR spectroscopy, with further characterization by infrared and elemental analysis in the case of **b2^1**. The N–H footprint disappeared from both ^{1}H NMR and infrared spectra. It was apparent from the ^{1}H NMR spectrum of **b2^1** that one equivalent of ether remained coordinated to the lithium atom when conducting the reaction in this solvent. A noticeable broadening of the resonances was observed for both salts (see the appendices section). The methylene was shifted downfield (δ **b2**: 4.06; δ **b2^1**: 4.5) as well as the boron signals (δ **b2**: 30.6; δ **b2^1**: 38).

Thus, the boron center is electron deficient compared to that of **b2**, in accordance with a fewer π contribution from nitrogen atom to the boron.

The X-ray structures of both **b2^{1}** and **b2$^{1'}$** were determined at 110 K confirming their identity. Despite the easy formation of **b2^{1}** crystals, none enabled a structure refinement with sufficient quality (R indices ≈ 0.17). Nevertheless, **b2$^{1'}$** monocrystal was suitable for accurate characterization by X-ray diffraction. Both structures are illustrated in Figure 4-1. Structural parameters and specifically bond distances in **b2^{1}** crystal will not be discussed.

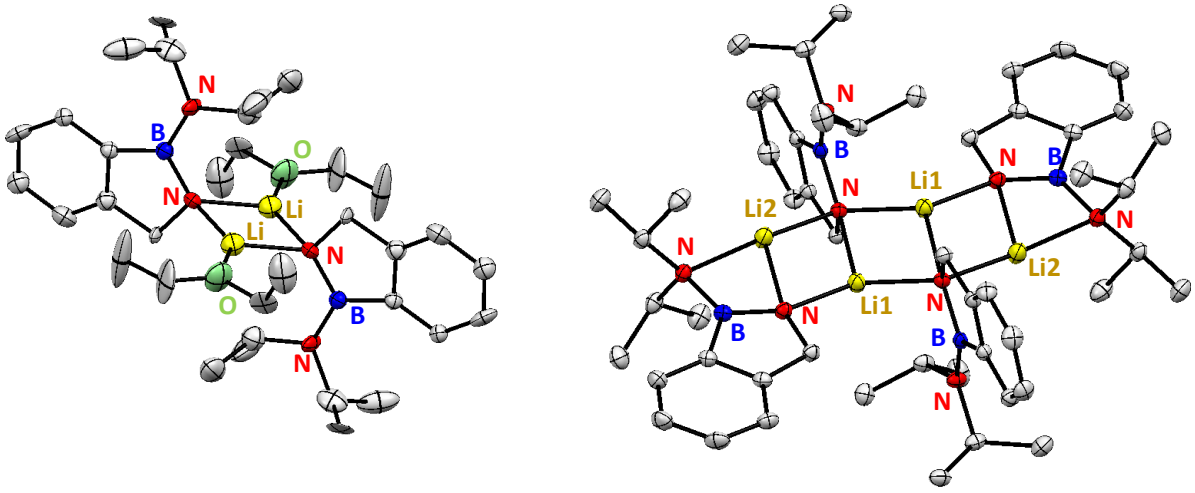

Crystallized in diethylether (b2^{1}) **Crystallized in pentane (b2$^{1'}$)**

Figure 4-1: Asymmetric unit of b2^{1} and b2$^{1'}$ crystals

Lithium amides are often schematically depicted as monomers. In reality, they organize as clusters (aggregates) that help stabilizing the electropositive lithium. They aggregate both in the solid state and in solution, although they might adopt a different arrangement in the two media.[176] Hence, we were not surprised to observe aggregates in the asymmetric units of **b2^{1}** and **b2$^{1'}$**. Crystal of **b2^{1}** arranged as a dimer while that of **b2$^{1'}$** arranged as a tetramer. In both cases, the lithium centers were tricoordinated, as commonly encountered in the case of lithium amide. When crystallized in ether, the electron donating solvent acts as a ligand, stabilizing the alkali-metal and decreasing the degree of aggregation of the salt. This strategy is usually employed to enhance the reactivity of lithium species by rendering the nucleophilic center more accessible, hence improving the kinetic of the reaction. On the contrary, crystal

b2$^{1'}$ generated and crystallized in pentane, arranged as a tetramer in which the two different nitrogen atoms stabilize the lithium centers. In this structure, two independent lithium boramidinates are associated, with the 1*H*-2,1-benzazaborole backbones in two nearly perpendicular planes (ca 82°). This pattern adopts a head-to-tail arrangement forming a centrosymmetric ladder-type structure. Each lithium is tri-amide coordinated, having a close contact with three 1*H*-2,1-benzazaborole endocyclic nitrogens for Li1, and only two in the case of Li2 that is also connected to one N^{i}Pr$_2$ nitrogen atom. The averaged B–N bond distances very much support those observations. The π electrons are well distributed between the endocyclic and exocyclic B–N bonds in the 1*H*-benzazaborole with non-coordinated N^{i}Pr$_2$ (exo: 1.437 (2) Å, endo: 1.443 (2) Å). In contrast, the 1*H*-benzazaborole unit, in which the N^{i}Pr$_2$ interacts with lithium, possesses an exocyclic B–N bond distance typical of single bond (1.520 (2) Å), and an endocyclic bond exhibiting a very strong double bond character (1.397 (2) Å).

I.2. Reaction of b2^1 with electrophiles

Because of their strongly polarized N–Li bond, lithium amides are excellent nucleophiles. Thus, in a second stage, we investigated the reactivity of **b2^1** with various halogenated electrophiles. The objective of this study was to make new N–E bonds. The different N-substituted 1*H*-2,1-benzazaboroles generated *via* this route are represented in Scheme 4-3. The four compounds were obtained *via* the same overall synthetic path involving lithiation in ether and further silylation, methylation, phosphorylation or borylation to form the corresponding N–E (Si, C, P, B) bonds.

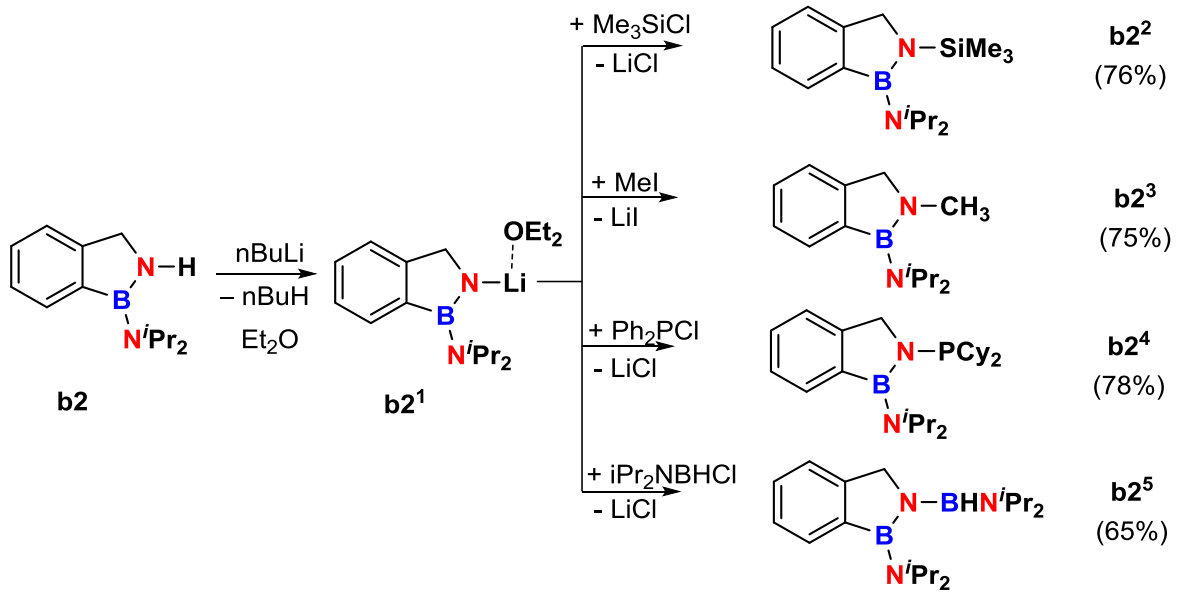

Scheme 4-3: Synthesis of N-substituted 1H-2,1-benzazaboroles b2[1-5]

Conditions were optimal when the lithium amide was freshly generated. The reaction mixture containing the salt was filtered off and the recovered solid was dissolved in fresh ether before the addition of the electrophilic halide. Products **b2[1-5]** were recovered in very good overall isolated yields more or less corresponding with that of the lithiation step indicating that the transmetallation is quantitative. The four compounds were fully characterized by multinuclear NMR spectroscopy, IR spectroscopy, high-resolution mass spectrometry and X-ray diffraction (in the case of **b2[3]** and **b2[5]**, appendices section).

The infrared spectra confirm the cleavage of the N–H bond. A selection of NMR data are listed in Table 4-1 for compound **b2[1-5]** as well as compound **b2** for comparison.

	^{11}B NMR	*CH_3 ^{i}Pr*	*CH ^{i}Pr*	*CH_2*
b2	30.6	1.15	3.78	4.06
b2[2]	34.7	1.31	4.01	4.19
b2[3]	31.0	1.28	3.82	3.92
b2[4]	34.6	1.39	4.36	4.13
b2[5]	36.2	1.37	3.88	4.36
b2[6]	31.3	1.20	3.72	4.34
b2[7]	31.7	1.27	3.81	4.40

Table 4-1: Selected NMR data for compounds b2 and b2[1-7]

The ^{11}B NMR chemical shifts of **b2$^{1-5}$** all support a trigonal boron atom within the molecules. The N-substitution caused a general downfield shift of the signals in ^{11}B NMR spectra. Borane substitution has the greater influence on the electronic density of the intracyclic boron (δ 36.2). Silicon and phosphorus N-substituted products display a 4-ppm shift while the methyl substituent has no meaningful influence on the ^{11}B chemical shift. Substitution induced some deshielding of the signals in the ^{1}H NMR spectra. Particularly, the resonances corresponding to the ^{i}Pr groups are shifted around δ 1.35 (CH_3 ^{i}Pr) with the same trend for the CH ^{i}Pr. Magnetic coupling through the N-B-N unit is well illustrated in compound **b2^{4}** where the phosphorus couples with the carbon of the ^{i}Pr groups ($^{4}J_{P\text{-}C}$ = 13 Hz, $^{5}J_{P\text{-}C}$ = 2 Hz). Coupling is also observed with the CH_2 group ($^{2}J_{P\text{-}C}$ = 7 Hz). It should be noted that the isopropyl groups are magnetically equivalent. Commonly to all substituted products, the CH ^{i}Pr signal is a well-defined septet, as in the case of **b3** and unlike that of **b1**, **b2** and **b4.** A common feature with **b3** is the slight distortion induced by sterics and pushing the N$^{i}Pr_2$ groups out of the benzofused plane (Figure 4-2).

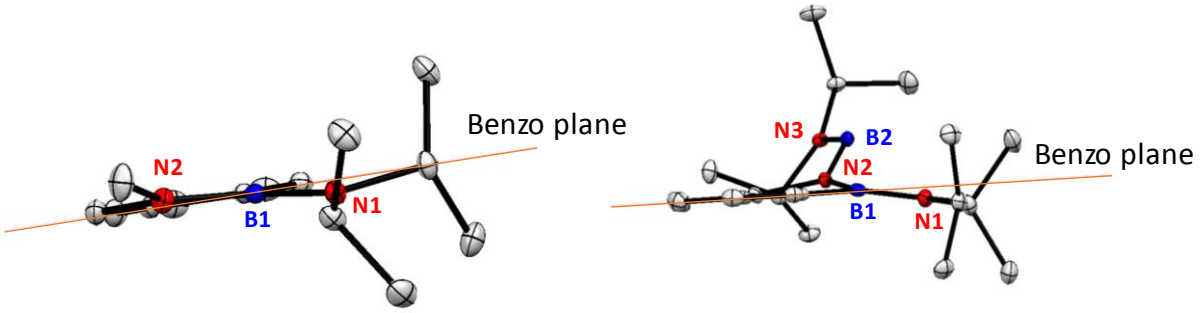

B1-N1 = 1.426 (2), B1-N2 = 1.434 (2)

b2^{3}

B1-N1 = 1.414 (2), B1-N2 = 1.463 (2)

b2^{5}

Figure 4-2: Crystal structure of b2^{3} and b2^{5} view along the benzo plane with selected bond distances. Hydrogen atoms are omitted for clarity. Ellipsoids are given at the 50 % probability level.

I.3. Buckwald-Hartwig amination of 1*H*-2,1-benzazaborole

Going one step further, we envisioned to extend this synthetic methodology for the efficient introduction of aryl groups onto the 1*H*-2,1-benzazaborole core by using **b2^{1}** in a Buchwald-Hartwig amination.[177] The catalytic amination is commonly performed using palladium

catalyst supported by dialkylbiaryl phosphine ligand or NHC ligands.[178-179] Key parameters in the catalytic aminations are the pre-catalyst, the base and the solvent. We selected the PEPPSI™-IPr (Pyridine-Enhanced Pre-catalyst Preparation, Stabilization and Initiation) pre-catalyst which shows remarkable activity in the amination of secondary amines.[179] The catalytic amination requires a base to deprotonate the amine.[180] In our case, the organolithium fulfilled this role prior to the catalytic reaction. The experiment was performed in dry toluene, at room temperature, with a stoichiometric amount of salt **b2¹** and aryl halides in the presence of PEPPSI™-IPr (2 or 4 mol%) as the palladium pre-catalyst as depicted in Scheme 4-4.

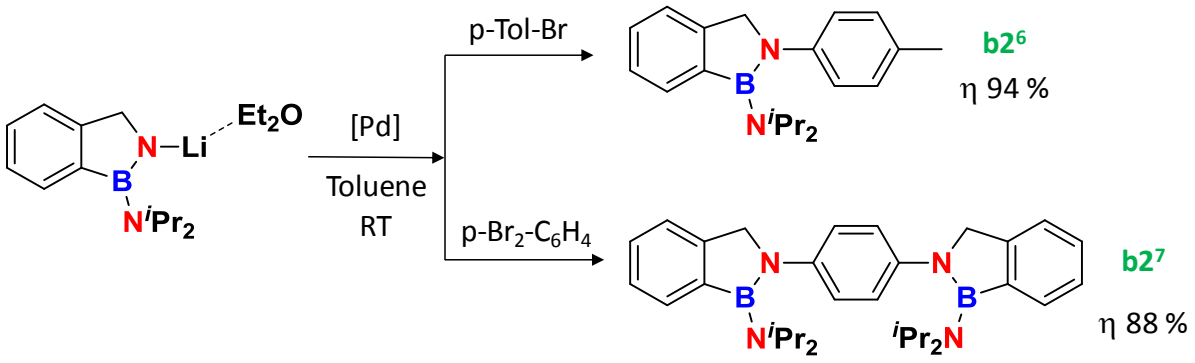

Scheme 4-4: Buchwald-Hartwig amination of the lithiated 1H-2,1-benzazaborole salt

These conditions were amenable for Pd-catalyzed N–C bond formation and the corresponding N-aryl functionalized 1*H*-2,1-benzazaboroles were successfully obtained. Neither ^{1}H nor ^{11}B NMR data were significantly influenced by the substitution.

This study highlights the possibility to adapt powerful coupling reactions to boron containing heterocycles. It is noteworthy that compound **b2⁷** is a closed analogue to the boronic acid compounds described in chapter 1, section I-3. We could imagine grafting larger fluorophore on nitrogen to obtain new sugar sensors.

II. Catalytic testing on dehydrogenation of 1*H*-2,1-benzazaborole

II.1. introduction

As we highlighted in chapter 1 (section I.2.), the dehydrogenation of amine boranes is of great importance along with the fundamental understanding of the N–H and B–H activation processes. The dehydrogenation of cyclic amine boranes such as BN cyclohexane has been demonstrated several times and led to the formation of well-defined borazines *via* thermal or catalytic routes (Scheme 4-5-a).[25]

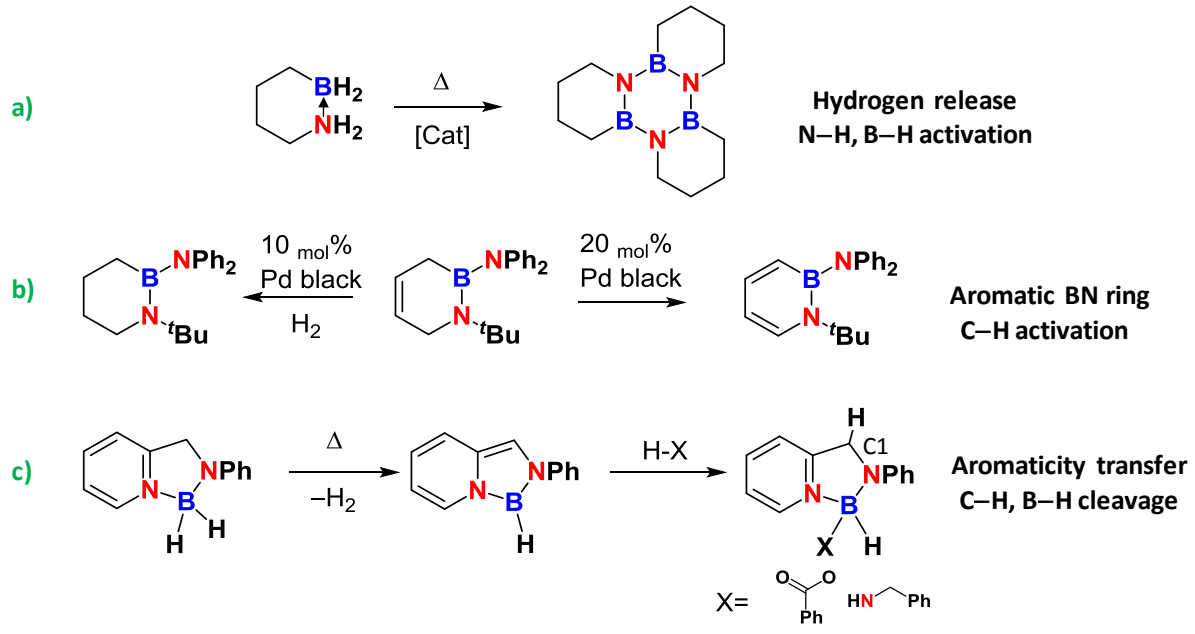

Scheme 4-5: Previous reports from the literature concerning dehydrogenation of BN heterocycles

The dehydrogenation of BN heterocycles is also regarded when incorporating BN bond in electron-delocalized systems. Liu and coworkers conducted a crystallographic analysis of different dehydrogenated stages of 6 membered BN rings, on the road to aromatic 1,2-azaborines. The authors proved that the BN unit takes part in the π delocalization when the carbon part is dehydrogenated (Scheme 4-5-b).[181] Very recently, Milstein and coworkers were interested in the concept of bond activation *via* dearomatization/rearomatization in a metal-

free system.[182] The authors documented the aromaticity shift at a bora-cycle upon thermal dehydrogenation (Scheme 4-5-c). They managed the stabilization of the dearomatized compound *via* nitrogen-stabilization and consequently, transfer of the aromaticity from the pyridine ring to the 5 membered ring. The later compound was able to activate σ-bonds such as OH and NH bonds. The electron donor interacts with the tricoordinated boron that subsequently disturbs the aromaticity within the 5-membered ring. The carbon C1 becomes nucleophilic allowing the OH or NH bond cleavage together with the rearomatization of the pyridine ring.

Aromaticity is a central concept in chemistry. Incorporation of BN atoms into aromatic systems should offer new opportunities in aromatized/dearomatized systems and more generally in systems involving the aromatic notion. We were thus willing to dehydrogenate the 1*H*-2,1-benzazaborole into 2,1-benzazaborole (**e2**) as a result of C–H, N–H activation at the 5-membered ring (Scheme 4-6).

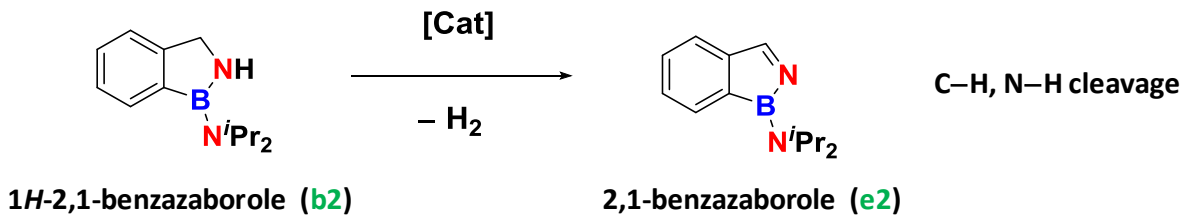

Scheme 4-6: Catalyzed-dehydrogenation of b2 into e2

Jones and coworkers recently reported the first acceptorless dehydrogenation of N-containing heterocycles (1,2,3,4-tetrahydroquinaldine or indole derivatives for example) using the iron pincer precursor catalyst **III-a** (Scheme 4-7).[183] Evaluation of the feasibility of the proposed dehydrogenation reaction was carry out during my internship at the University of Rochester, in the Jones' group, using their dehydrogenation system. The aim of this study was to assess the compatibility of homogeneous dehydrogenation catalytic systems with BN-heterocycles and to evaluate the stability of the dehydrogenated compound possibly formed.

II.2. Dehydrogenation study on the 1*H*-2,1-benzazaborole b2

Complex **III-a** is a precursor catalyst of choice in the acceptorless and reversible dehydrogenation of N-heterocycles (Scheme 4-7).[183] Mechanistic investigation demonstrated that complex **III-b** is the active species in the catalysis. Theoretical calculations suggested a concerted N–H and C–H bond activation process in the case of unpolarized C–N bonds. On the contrary, substrates with polarized C–N bonds entail a stepwise dehydrogation.[184] The cobalt based pincer complex also exhibits activity for the reversible dehydrogenation of N-heterocycles while the pincer iridium compound shows activity in C–H activation and particularly alkane dehydrogenation.[185]

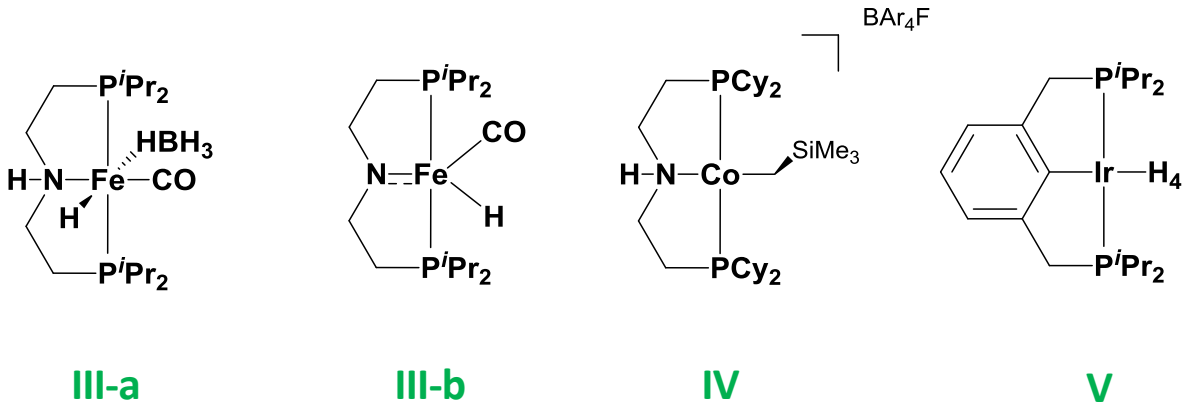

Scheme 4-7: Precursor catalysts used in the Jones' group in dehydrogenation reaction

To start, the iron complex **III-a** was selected to conduct the dehydrogenation regarding its ability to readily loose BH_3 and H_2 under thermal treatment (no need of base) and generate the active species complex **III-b**. The iron complex **III-a** was produced in two steps summarized in Scheme 4-8.

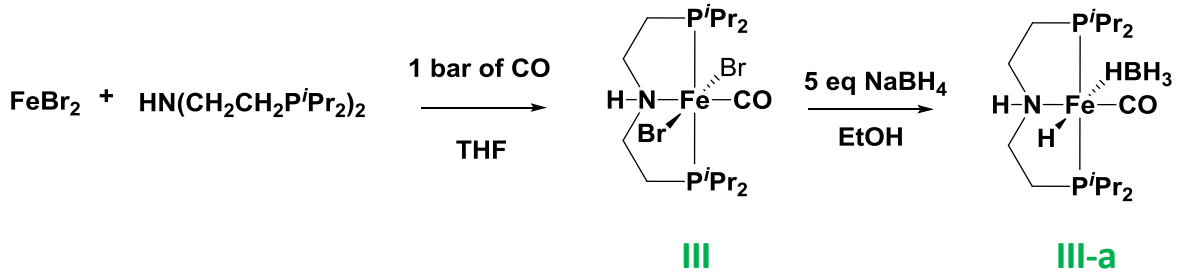

Scheme 4-8: Iron-based precursor catalyst synthesis

$HN((CH_2CH_2)P(^iPr))_2$ ligand was coordinated on iron(II) bromide in THF under 1 bar of CO to afford the iron based PNP pincer complex **III**. The ^{31}P NMR spectrum exhibits a singlet at 67.7 ppm. Compound **III** was treated in ethanol with 5 equiv of $NaBH_4$ to obtain the desired **III-a** precursor catalyst. The ^1H NMR spectrum shows the hydridic resonance (Fe-H) as a triplet at −19.5 ppm. The HBH_3 group was detected as a broad singlet around − 2.8 ppm as a result of the dynamic B–H interaction with the iron center. The ^{31}P NMR spectrum shows the expected doublet at δ 99.6 ($J_{P\text{-}H}$ = 40Hz).

Standard dehydrogenation catalytic tests were performed using 3 mol% of **III-a** in 1 mL of deuterated xylene at 140°C following the described procedure for N-heterocycles.[183]

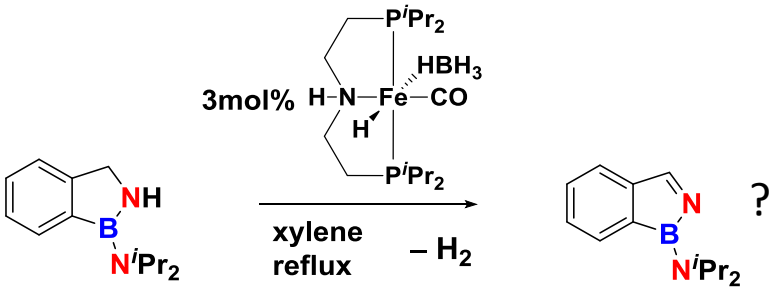

*Scheme 4-9: Hypothetical dehydrogenation of **b2** into **e2** with **III-a** as a catalyst precursor*

	condition	*catalyst*	*loading*	*Temp(°C)*	*C (g/L)*	*Time(h)*	*products*
1	standard	III-a	3	140	90	24	b2/d2
2	Lower concentration	III-a	3	140	45	30	b2/d2
3	Active species	III-b	5	140	90	2-3days	b2/d2
4	Hydrogen scavenger	III-a	5	140	90	24	b2/d2
5	Cobalt catalyst	IV	5	140	35	24	d2
6	Iridium catalyst Hydrogen scavenger	V	2	140		24	b2/d2
7	No catalyst			140	45	3	d2

Table 4-2: Catalytic testing on the dehydrogenation of 1H-2,1-benzazaborole (deuterated xylene, 140°C)

A 500 mL reaction flask was used in order to leave room for the dihydrogen to escape. In those conditions, no dehydrogenated product **(e2)** was detected by NMR (Table 4-2, entry1). Several strategies have been envisaged to favor the dehydrogenation reaction. First, the iron complex **III-b**, identified as the active species in dehydrogenation of N-heterocycles, was used directly to catalyze the reaction. The modified procedure did not lead to the 2,1-benzazaborole **e2**. The addition of *tert*-butylethylene as hydrogen scavenger in the reaction mixture did not improve the reaction (Table 4-2, entry 4).

In all cases, 1*H*-2,1-benzazaborole (**b2**) was partially self-condensed into borazine, probably as a result of the thermal activation. The same outcome was reached when lowering the 1*H*-2,1-benzazaborole concentration as an attempt to disfavor intermolecular reactions (Table 4-2, entry 2). Interestingly, cyclotrimerization of **b2** into borazine occurred, without catalyst, in only 3 hours at 140°C (Table 4-2, entry 7) whereas cyclotrimerization remained incomplete after 24 h when the iron catalyst was in the media. We first wondered whether the iron complex was able to catalyze the reverse reaction (decyclotrimerization by addition of HN^iPr_2). Yet, when heating borazine in presence of HN^iPr_2 (3 equiv) and 5 mol% of iron pre-catalyst, no

reaction was detected. The presumed active species in dehydrogenation reactions, **III-b**, was reacted in a stoichiometric manner with **b2** as represented below:

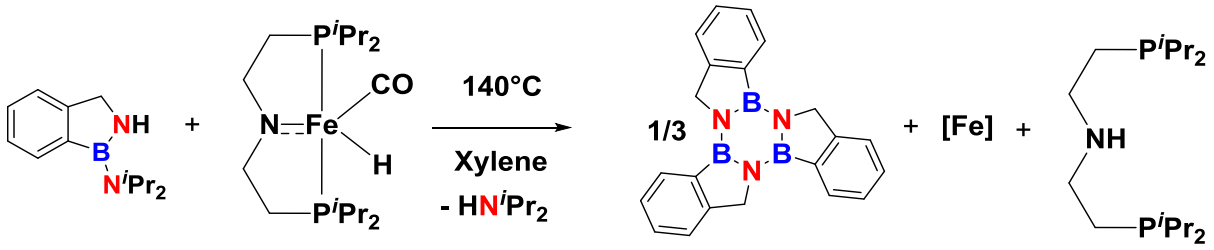

*Scheme 4-10: Stoichiometric reaction of **b2** and **III-b** in xylene at 140°C during 3 days*

Compound **b2** trimerized into borazine together with degradation of **III-b** as evidenced by only one ^{31}P NMR signal in the mixture corresponding to the PNP free ligand. The degradation was slow indicating that the complex influenced the competing trimerization reaction. Yet, no complex-substrate interaction was observed.

With the view to generate the desired dehydrogenation product, other metal-based precursor catalysts have been used. We tested the related cobalt pre-catalyst **IV**, which has also proved to reversibly dehydrogenate N-heterocycles.[185] However, **IV** did not enable the dehydrogenation of **b2**. Moreover, 1*H*-2,1-benzazaborole was fully converted into borazine after 24 h of reaction unlike when using the iron-based catalyst. Finally, iridium based pre-catalyst **V**, was tested in presence of *tert*-butylethylene as hydrogen scavenger. Employing precious metal-based catalyst and a hydrogen scavenger did not lead to **e2** after 1 day of reaction at 140°C (Table 4-2, entry 7). However, only a few amount of 1*H*-2,1-benzazaborole was converted into borazine also demonstrating the influence of the iridium complex on the trimerization reaction.

In conclusion, the iron complex Fe(H)(HBH$_3$)(CO)[HN((CH$_2$CH$_2$)P^{i}Pr$_2$] was synthesized in two steps. It was used as a pre-catalyst for the 1*H*-2,1-benzazaborole catalytic dehydrogenation in an attempt to obtain 2,1-benzazaborole **e2**. No dehydrogenated product was detected by NMR. It is however interesting to note that the competing thermally activated cyclotrimerization reaction, which occurs within 3 hours at 140°C without any catalyst, is disfavored when iron and iridium hydride complexes are used. The hydride complexes induced a noticeable slowing down of this reaction. One possible explanation is the interaction of the boron atom with the hydride or the metal center.

The tests remained very preliminary but according to our study, the dehydrogenation of nitrogen containing heterocycles could not be extended to BN containing heterocycles. As a perspective, we may need to synthesize 1*H*-2,1-benzazaboroles with a non-leaving group to disfavor the cyclotrimerization through release of HN^iPr_2. A deeper understanding of the interaction between the complexes and the substrate might help selecting or designing appropriate systems for the dehydrogenation of this type of compounds.

In conclusion, we defined the objective of the chapter as the assessment of the synthetic potential of the newly formed 1*H*-2,1-benzazaborole. To start with, in basic conditions (*n*BuLi), we demonstrated that we can selectively deprotonate N–H to form the corresponding lithium amide in etherated or non-etherated versions. In such conditions, the trigonal borane is stable enough and does not undergo any nucleophilic attack, demonstrating the role of the N^{i}Pr stabilizing group. The reaction of the etherated lithium amide with various halogenated electrophiles led to N–Si, N–C, N–P and N–B bond formation suggesting that a wide variety of BN-compounds could be generated. We then established the compatibility of trigonal boron containing molecule with powerful catalytic amine transformations. We successfully adapted the Buchwald-Hartwig amination strategy starting from the etherated lithium salt. Double amination was also achieved and the compounds were isolated in excellent yields. Hence, we developed an efficient route for BN-incorporation into electron-delocalized systems paving the road for late-stage functionalized BN heterocycles. The dehydrogenation of 1*H*-2,1-benzazaborole **b2** that would involve N–H, C–H cleavage was also tested at the university of Rochester. At that stage of the study, the catalytic testing was unsuccessful using iron, cobalt or iridium pincer precursor catalysts, presumably owing to both the thermally activated competing trimerization and the boron influence on the substrate/complex interaction. Following Liu and coworkers' reactivity study on 1,2-dihydro-1,2-azaborine, we demonstrated that stoichiometric and catalytic powerful synthetic tools are compatible with BN 5-member rings and can lead to the preparation of previously inaccessible materials.

CHAPTER 5:

BORAZINES

CHAPTER 5: BORAZINES 139

CHAPTER 5: BORAZINES

As explained in chapter 1, borazines are BN analogue of benzene. They have very similar structures but very different optoelectronic properties and stability. The strong polarity of the moiety induces a widening of the HOMO-LUMO gap. Insertion of such a BN unit in electron-delocalized systems modifies the absorption/emission profiles and endows the molecule with electronic insulator properties. The design and functionalization of sophisticated borazines led to the first examples of borazine-based materials for optoelectronic devices. Applications are still at a very early stage and the synthesis of innovative compounds is required for the development of the field.

I. Introduction

Borazine compounds can be synthesized from amonium/borohydride salts, amine-boranes or aminoboranes.[6] Initially, the borazine core was obtained *via* dehydrogenation of AB upon thermal treatment (200°C).[55] In spite of the rather harsh conditions required, this first protocol inspired further synthetic development. Different precursors including ammonium/borohydride couples or substituted amine-boranes were used enabling the modification of the operating conditions as well as the generation of N or B substituted borazines.[186-188] The temperature of the dehydrogenation reaction can also be lowered when using a catalyst. For instance, Manners and coworkers prepared borazine compounds from the dehydrocoupling of AB or MeH_2NBH_3 in presence of $[Rh(1,5\text{-cod})(\mu\text{-Cl})]_2$ at 45°C.[14] The reaction goes through the formation of borazane and a lowering of product yield is observed due to intermolecular coupling. In order to obtained B-substituted borazines, other strategies were developed. Condensation reactions from BCl_3 or BBr_3 led to trihaloborazines that can be further functionalized.[61] Boron and nitrogen phenyl substituted borazines result from this strategy as seen in Scheme 5-2.

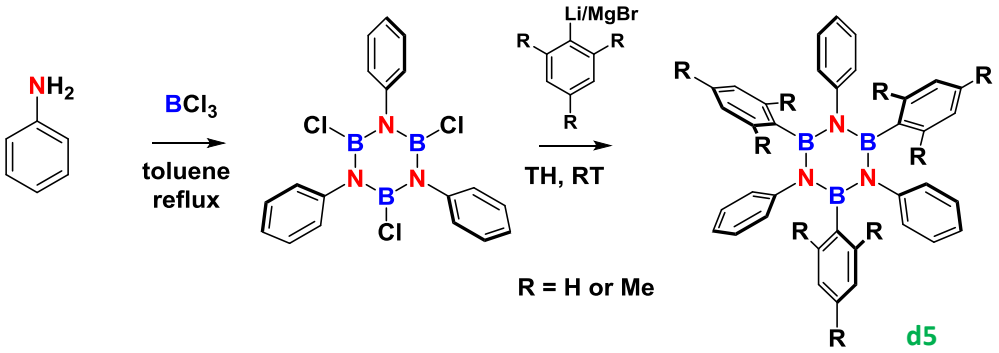

Scheme 5-1: Synthesis of boron and nitrogen aryl substituted borazines

The described borazines are examples of BN core insertion into electron delocalized frameworks examined for their distinct optoelectronic properties. In this case, X-ray diffraction techniques revealed that the phenyl rings are quasi-orthogonal to the borazine core (Figure 5-1).[61]

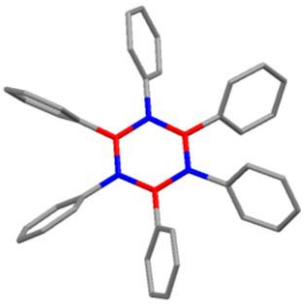

d5

*Figure 5-1: Previously reported X-ray diffraction structure of **d5***

Compound **d5** shows a planar BN ring with quasi-orthogonal phenyl ring substituents. The B–N bond distances are equal with an average of 1.440 (4) Å. Hence, the B–N bond exhibits a double bond character and electrons are evenly distributed over the BN ring as in aromatic cycles. However, borazine core and phenyl rings do not belong to the same plane predicting a reduced electron delocalization through the whole molecule.

The method consisting in trimerization of aminoborane offers a direct access to B and N substituted borazines. Liu and coworkers reported the efficient synthesis of alkyl borazines from 1,2-BN cyclopentane or 1,2-BN cyclohexane as depicted in Scheme 5-2.[28]

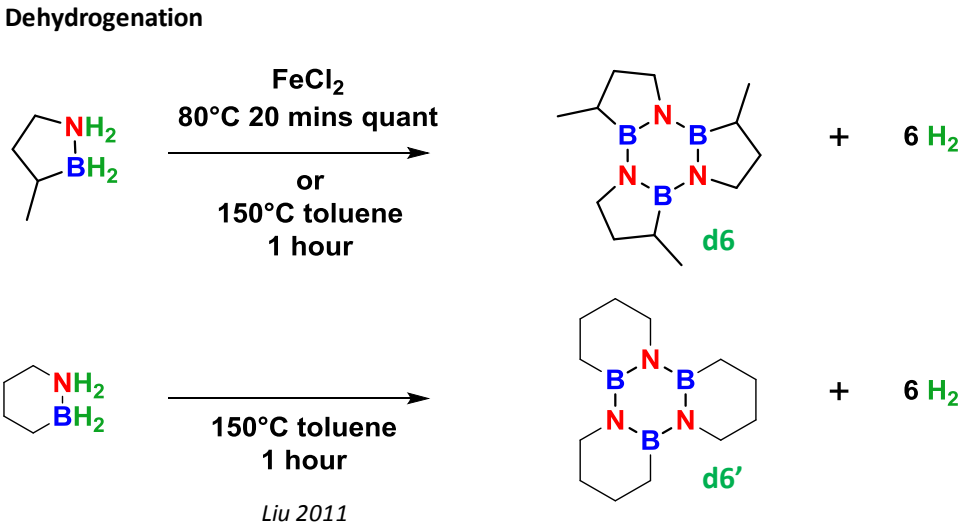

Scheme 5-2: Borazine synthesis from cyclic aminoboranes reported by Liu and coworkers

The reaction can either be performed with a catalytic amount of cheap and easily available $FeCl_2$ at 80°C in 20 minutes (1,2-BN cyclopentane) or by thermal activation (150°C, 1 hour). In this case, the BN compounds were synthesized with the view to generate a *via*ble material for liquid hydrogen storage. X-ray structure of **d6'** was described. The borazine shows a planar BN ring with B(π)–N(π) interaction. The bridged BN bonds are significantly shorter (1.418 (3) Å) than the non-bridged ones (1.444 (3) Å). In parallel, Bettinger and coworkers reused Koster work[189] to incorporate the borazine core into an electron delocalized scaffold as represented in Scheme 5-3.[190]

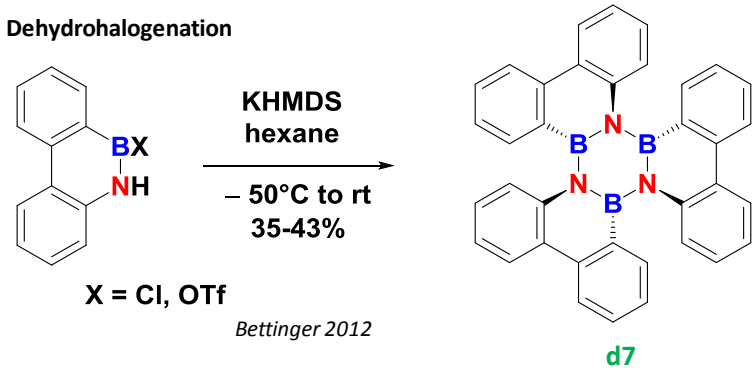

Scheme 5-3: Borazine synthesis from cyclic aryl aminoboranes

The overcrowded borazine was generated *via* dehydrohalogenation, enhancing the yield in **d7** (η = 35%). This protocol requires the use of a base and low temperature to generate the trimer

in moderate yield. They suggest that the base-induced dehydrohalogenation allows the formation of reactive BN-arynes that trimerize. The authors were able to obtain a X-ray structure of **d7** (Figure 5-2).[191]

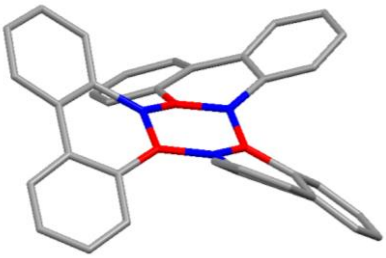

d7

Figure 5-2: Previously reported X-ray diffraction structure of d7 obtained from the CCDC

In this case, the phenyl rings are linked together forcing the biphenyl cycles to remain in a similar plane and reducing the distortion from the BN core compared to the previously described hexaphenyl borazine.[61] However, compound **d7** shows a distorted BN ring induced by the rigid and crowded substituents and permitted by the rather flexible 6-member ring bridge. The torsion angles lie between 23.2 and 26.3°. The bridged BN bonds exhibit a double bond character (1.429 (3) while the others are significantly elongated (1.490 (3) Å). In this case also, we can assume the electrons are not equally distributed over the whole framework.

Finally, an emerging research field is devoted to the synthesis of BN-doped coronene derivatives in which a central borazine core is incorporated in place of the benzene ring. The goal is to widen the HOMO-LUMO gap of well-defined polycyclic aromatic hydrocarbons (PAH) in order to broaden their application scope to semiconductors. By extension, the strategy aims at introducing an optical gap in graphene. A bottom-up synthetic strategy is necessary to obtain controlled BN-doping. Two synthetic methods describe the synthesis of well-defined BN-doped coronene. Bettinger and coworkers published the first article in 2015, where they demonstrate the pyrolysis of N,N',N''-tris(2-biphenyl)borazine to yield the desired product in about 5% yield.[192]

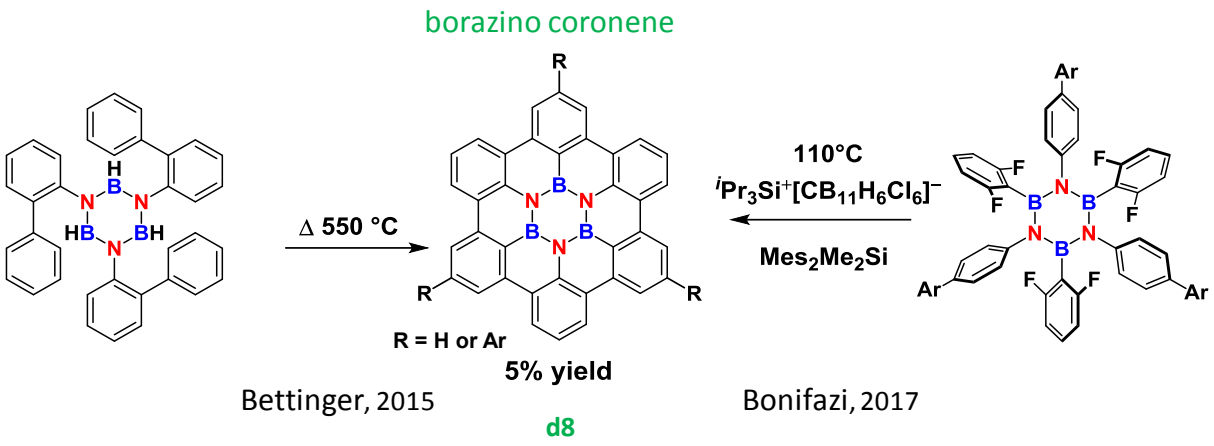

Scheme 5-4: Synthetic methods to access BN-doped coronene reported in the literature

Two years later, Bonifazi and coworkers used the Friedel-Craft ring-closing reaction of fluoroarenes from fluorinated phenyl substituted borazine to access the BN-doped coronene (**d8**).[193] They also achieved the synthesis in 5% yield. In this case, the borazine core comprised in the aromatic scaffold is expected to be planar.

Very few reports deal with trimerization of aminoborane compounds leading to sophisticated borazines. This synthetic approach is held back by the lack of precursors available underlying the necessity of developing efficient routes to generate uncommon aminoboranes. During the catalytic formation of the 1*H*-2,1-benzazaboroles described in chapter II, and the dehydrogenation study presented in chapter IV, we observed the trimers corresponding to the 1*H*-2,1-benzazaboroles, as side-product of the reactions. These borazines were so far unknown and correspond to BN-benzene insertion into electron delocalized systems. Thus, we decided to synthesize them and study their properties.

II. Synthesis of borazines from 1*H*-2,1-benzazaborole derivatives

II.1. Synthesis of the parent d2

In light of previous observations, we studied the trimerization of 1*H*-2,1-benzazaboroles under thermal activation. We first started from the parent 1*H*-2,1-benzazaborole **b2**. The

corresponding borazine compound **d2** was obtained along with the released HN^iPr_2 in a clean and reproducible manner. The equation of the reaction is depicted in Scheme 5-5.

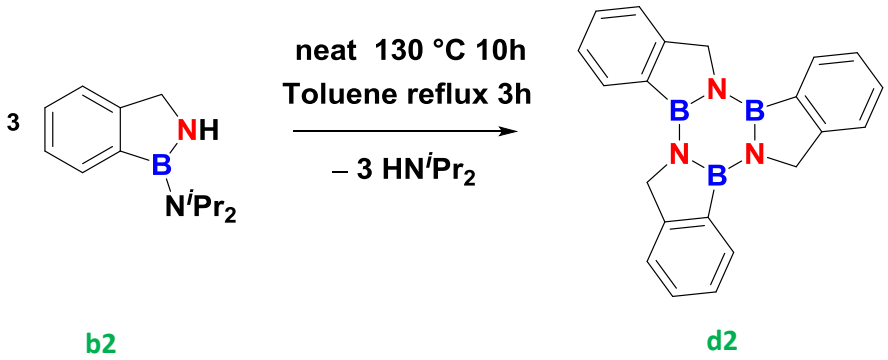

*Scheme 5-5: Thermal trimerization of **b2** towards borazine synthesis*

A first experiment was performed neat in a sealed flask. The full conversion of **b2** was observed after 10 hours. The reaction was then conducted in refluxing toluene. In this condition, the reaction was complete within 3 hours. The insoluble borazine was observed as a white precipitate at the end of the reaction. The trimer **d2** was readily recovered after filtration and washing of the solid with pentane. To compare to the previously described dehydrogenation and dehydrohalogenation, we herein propose a net dehydroamination process occurring under thermal activation.

Borazine **d2** is the BN analogue of truxene. The later one exists in two different isomeric forms (truxene and isotruxene), but the symmetric truxene often corresponds to the targeted product (Figure 5-3).

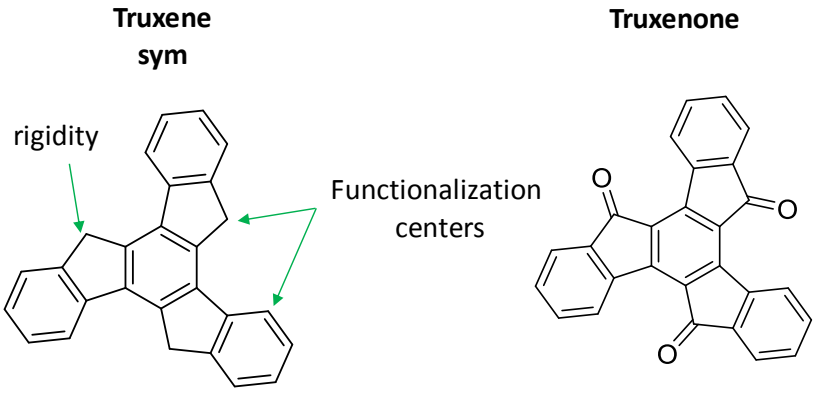

Figure 5-3: symmetric truxene and truxenone

As a reference for our work, the cyclotrimerization of 1*H*-indene gave 9% and 5% of truxene and isotruxene at 300°C.[194] To overcome the lack of efficiency, a strategy starting from 1,3 indandione treated in acidic conditions at 100°C gave truxenone without contamination in 90% yield. The produced truxenone can be reduced efficiently using a modified Wolff-Kishner reduction.[195] Recent reviews appeared in the literature[196-197] expressing the promising role of truxene in future materials. The star-shaped, planar, thermally stable polyaromatic hydrocarbon (PAH) is described as a building block for many extended aromatic structures. Research devoted to truxene exploded with the breakthrough in its synthesis and peripheral functionalization. We are also aware of the possible functionalization strategies compatible with borazines in general. For instance, borazines do not degrade under basic conditions (*t*BuLi) and can undergo bromination of aryl substituents just as truxene.[6] This building block found a place in various fields such as non-linear optic (NLO), transistors, organic photovoltaıcs (OPVs), organic light-emitting diodes (OLEDs), fluorescent probes or self-assembly, to name a few.

II.2. Extension to substituted borazine derivatives

Once optimized with the parent **b2** the synthetic protocol was transposed to the substituted 1*H*-2,1-benzazaboroles **b1**, **b3** and **b4**. Reaction time together with the isolated yields corresponding to the formation of the borazine compounds are reported in Table 5-1.

Borazines	*d1 (F)*	*d2 (H)*	*d3 (Me)*	*d4 (OMe)*
Reaction time (h) *neat*	5	10	x	10
Reaction time (h) *toluene*	3	3	24	3
Isolated yield (%)	82	66	53	85

*Table 5-1: Reaction time for the formation of compound **d** from **b** derivatives with the corresponding isolated yields*

We see that the reaction time to generate compound **d1**, **d2** and **d4** are comparable when refluxing in toluene. The 3 hours of reaction correspond to a maximum since the reaction has not been monitored. Under neat conditions, a shorter reaction time is observed for the

formation of **d1** by comparison to **d2** and **d4**. Indeed, the reaction is complete after 5 hours of heating indicating a favorable trimerization of the fluorinated compound. We also remember that a considerable loss of 1*H*-2,1-benzazaborole **b1** was observed after purification by distillation at 130°C (see chapter 2) which can now be related to the formation of borazine. Compounds **d1**, **d2** and **d4** were isolated in good yields.

An important change in reaction time, both in toluene or neat, was noticed for the conversion of **b3** into **d3**. Indeed, full conversion of **b3** needed 24 hours to be complete. As the methoxy substituted borazine is not kinetically disfavored, we associated the slow conversion of **b3** to steric effect. Throughout the reaction, we could observe intermediate species that, for some of them, persist at the end of the 24 hours. We were able to characterize one intermediate species observed in the media. This species was much more soluble than the borazine allowing its separation. We attribute the recorded spectroscopic data to the dimeric species resulting from the condensation of two molecules of **b3** along with the release of diisopropylamine. The postulated intermediate is represented in Figure 5-4.

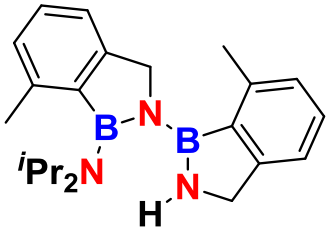

Intermediate in the formation of d3

*Figure 5-4: intermediate observed during the thermal trimerization of **b3** into **d3***

The ^{11}B NMR spectrum shows two upfield resonances (δ 37.7; 34.1) evidencing trigonal boron in the molecule. As expected, the ^{1}H NMR spectrum manifests magnetically inequivalent 1H-2,1-benzazaborole units. Both methylene groups present a distinct AB system. A cross peak in the ^{1}H 2D COSY NMR spectrum reveals magnetic coupling between one CH_2 moiety (δ 3.58; 4.32) and N–H hydrogen (δ 3.8) (Figure 5-5).

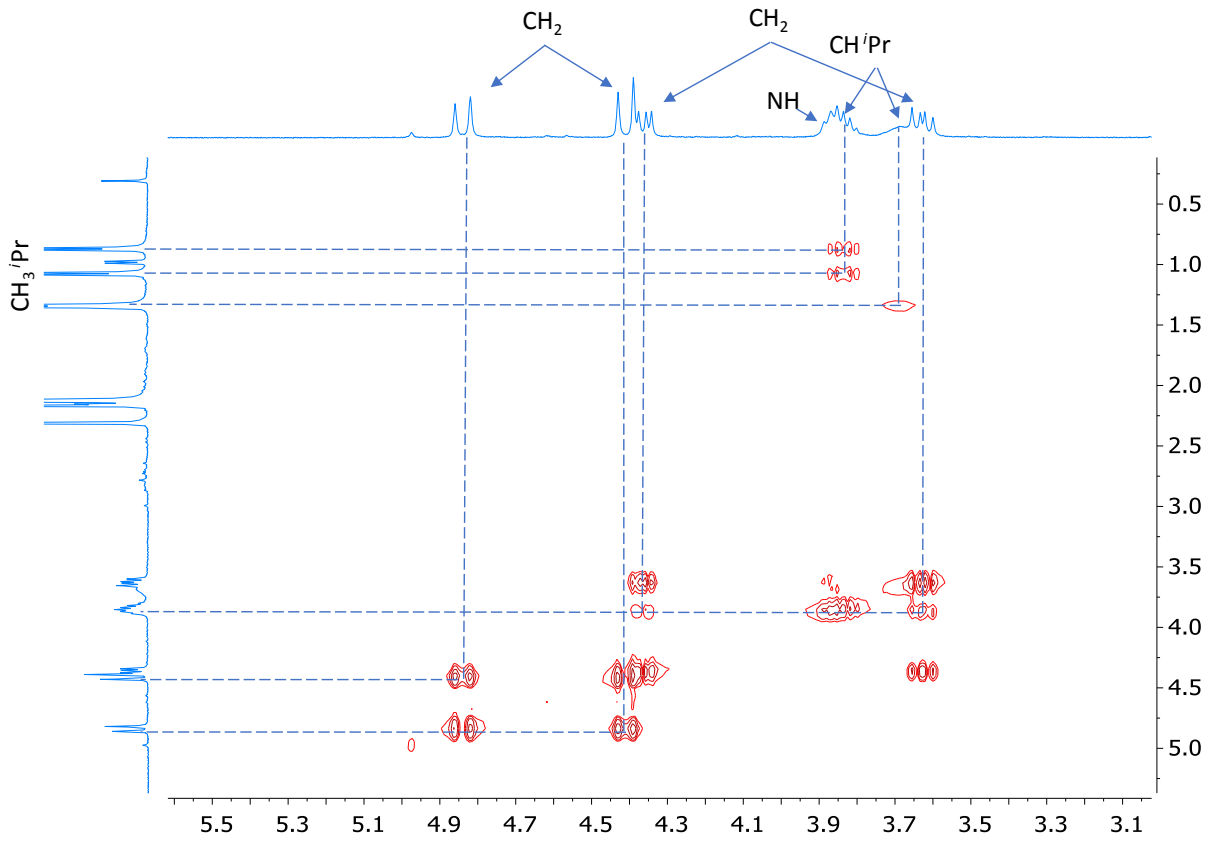

*Figure 5-5: 2D ^{1}H COSY NMR spectrum of the intermediate compound during **d3** formation (toluene d_8, 400.18 MHz, 298K)*

One CH_3 ^{i}Pr group shows equivalent CH_3 coupling with a CH ^{i}Pr resonating as a broad signal. The other CH_3 ^{i}Pr group shows inequivalent CH_3 coupling with a CH ^{i}Pr resonating as a septet. The methyl groups on the aryl also resonate as two independent signals.

Hence, on the road to the trimer, we could characterize the dimer due to a slower transformation in the methylated version. It seems that the formation of the trimer occurs through a stepwise condensation of the 1*H*-2,1-benzazaborole molecules rather than a trimerization followed by elimination of $HN^{i}Pr_2$.

III. Characterization of borazine derivatives

III.1. Spectroscopic characterization

The borazine was poorly soluble in common organic solvents. Toluene and THF were the most solubilizing ones. The parent trimer **d2** was found to be more soluble in such solvents than the others. The ^{1}H NMR spectra of the starting 1*H*-2,1-benzazaborole **b2** and the produced borazine **d2** are depicted in Figure 5-6.

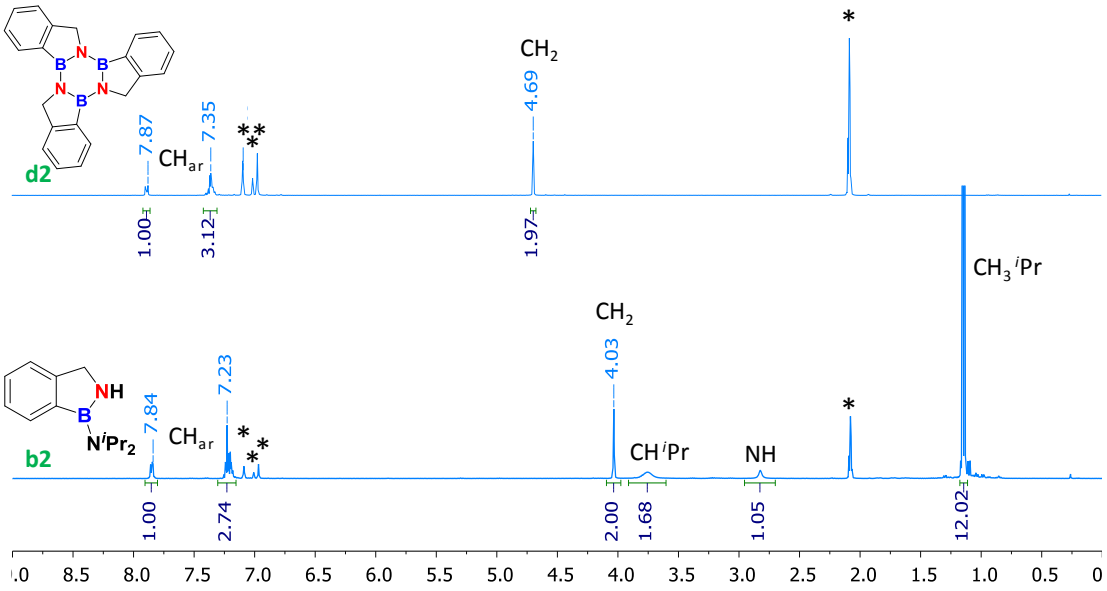

*Figure 5-6: ^{1}H NMR spectra of the starting 1H-2,1-benzazaborole **b2** and the produced borazine **d2** in toluene d_8 (400 MHz) *(C_7D_8)*

The aromatic pattern corresponding to the newly formed **d2** remains unchanged compared to the precursor molecule. The methylene signal shifted downfield from 4.0 to 4.7 ppm. The resonances related to the isopropyl group as well as the N–H signature are no longer present in the spectrum in agreement with the loss of diisopropylamine during the process.

A selection of spectroscopic data found for compounds **d1-4** are reported in Table 5-2.

Borazines	*d1 (F)*	*d2 (H)*	*d3 (Me)*	*d4 (OMe)*
^{1}H CH_2 (ppm)	4.38	4.69	4.93	4.74
^{11}B solution (ppm)	35	35	N/A	N/A

Table 5-2: Selected NMR data for the borazine derivatives in toluene d_8 (400 MHz) N/A: not applicable

The methylene singlet is deshielded compare to that of **b1-4** and ranges from δ 4.38 (**d1**) to δ 4.93 (**d3**). The ^{11}B NMR spectra of **d1** and **d2** were alike showing a broad resonance around 35 ppm. This value is in line with previously reported ^{11}B NMR shift for borazine compounds. For instance, a chemical shift of 36 ppm was reported for borazine **d7**.[190] Compounds **d1** and **d2** were soluble enough to be characterized by ^{13}C {^{1}H} NMR technique as well. Due to the poor solubility of **d3** and **d4** combined with the broad signals characteristic of trigonal boron no signal was detected by ^{11}B NMR.

The infrared spectrum of **d2** (red) no longer shows the N–H vibration as observed for **b2** (blue)(Figure 5-7).

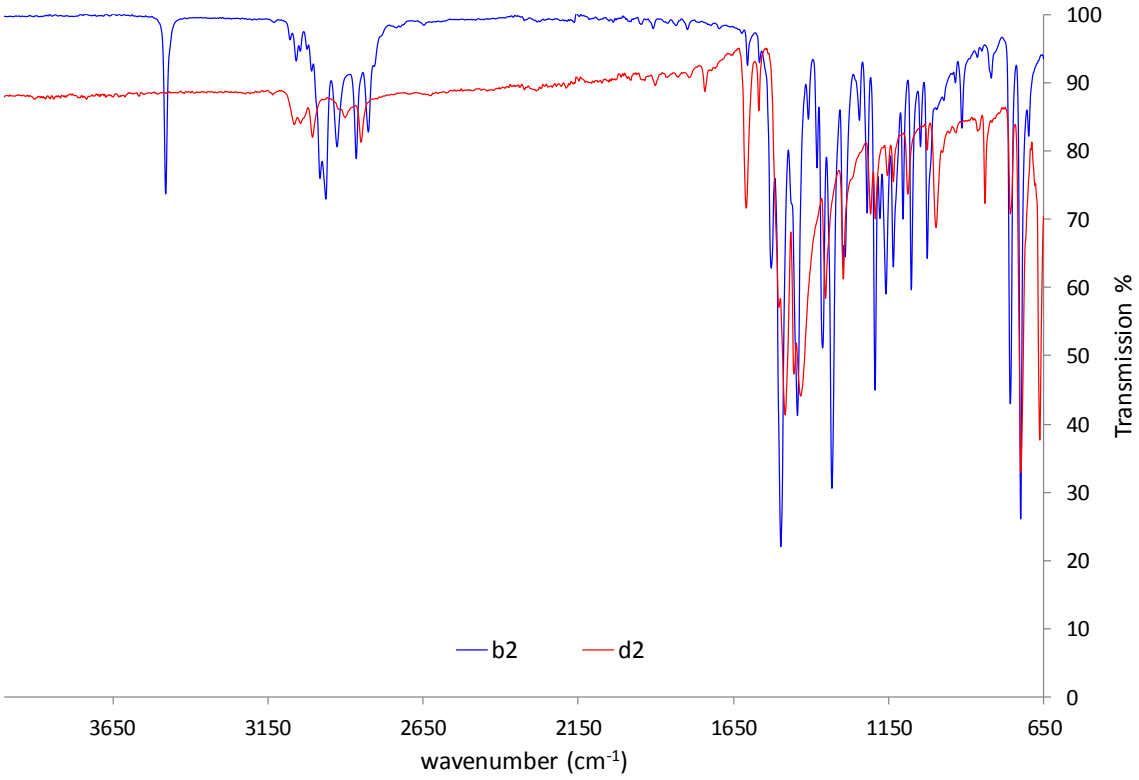

*Figure 5-7: Superimposed infrared spectra of **b2** and **d2***

The disappearance of intense asymmetric (≈ 2960 cm^{-1}) and symmetric (≈ 2870 cm^{-1}) CH_3 elongation bands is also noted. A vibration band around 1350 cm^{-1} appears in borazine spectra, possibly associated to the BN stretching vibration.

The four borazine compounds are characterized by mass spectroscopy confirming their identity with the presence of the monoisotopic peaks.

III.2. X-ray diffraction of borazine derivatives

X-ray diffraction on suitable monocrystals of **d2** gave the structure represented in Figure 5-8.

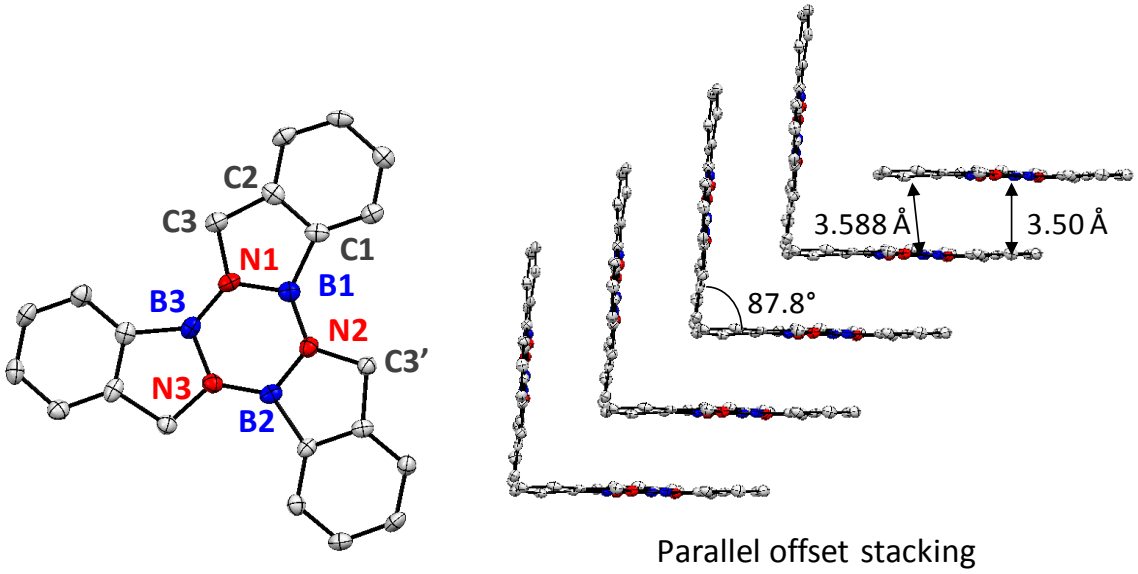

Bridged N–B (average)	1.442 (3)	N1–C3	1.472 (3)
Non-Bridged N–B (average)	1.419 (3)	B1–C1	1.564 (3)
Average N–B	1.431 (3)		
C2–C3	1.512 (3)		

*Figure 5-8: Crystal structure of **d2**, view orthogonal to the N1, B1, N1, B2, N3, B3 plane (left) packing structure (right)*

Although the molecule exhibits a C3 symmetry, the crystal shows three 1*H*-2,1-benzazaborole fragments per asymmetric unit. Unlike previously reported borazines, such as **d5** and **d7,** displaying a borazine core incorporated into an electron-delocalized system, the trimer is planar. The de*via*tions from the BN ring range from 0.1 to 7.6°. Hence, the borazine is a BN-benzene insertion into a planar electron delocalized system. The B–N bond shows a double bond character and the average B–N bond distance (1.431 (3) Å) is close to the classical 1.44 Å encountered in borazine compounds. We have seen that trimer **d6'** and **d7** display shorter bridged B–N bonds compared to the others. In contrast, **d2** possesses significantly longer bridged B–N bond distances. The bridged B–N bond is not significantly changed compared to

the intracyclic B–N bond in **b2** (1.432 (2) Å). We noticed a shorter C1–B1 bond (1.564 (3) Å) compared to the related bond in **b2** (1.591 (2) Å) while N1–C3 is slightly elongated. The molecular packing of the crystal is represented in Figure 5-8. Molecules arranged in two defined layers quasi-orthogonal (Σ = 87.8°). Within the same layer, molecules packed in a parallel manner with an angle of 0.6° between the two planes including two consecutive molecules. The distance separating two molecules of the same layer was found to be 3.50 Å. The borazine cores are displaced and closely interact with one benzene ring of the consecutive molecule. In addition, the distance between the BN ring and the phenyl ring centroids is 3.588 Å which is characteristic of π stacking interaction between the molecules.[198] The BN ring seems to take part in the π–π interaction. The rings are in a parallel-offset arrangement with a displacement angle of 12.6° in the case of the BN ring with the phenyl cycle[199].

Crystal structures of **d3** and **d4** were also determined by X-ray diffraction techniques. Their view along the borazine plane is shown in Figure 5-9.

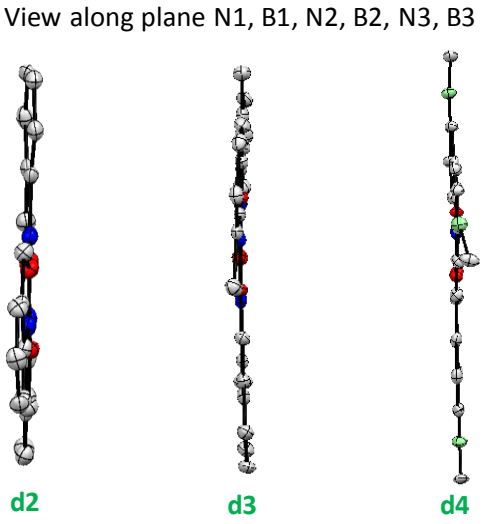

	d2	d3	d4
Average B–N distances (Å)	1.431 (3)	1.435 (3)	1.429 (10)
Deviation to BN plane (°)	2.1, 4.2 and 4.8 (0.2)	1.8, 2.3 and 2.6 (0.1)	1.1, 1.6 and 3.3 (0.5)

*Figure 5-9: Crystal structures of compounds **d2**, **d3** and **d4** viewed along the borazine plane and their corresponding B-N bond length average*

Compound **d3** and **d4** also exhibit a planar structure with maximum de*via*tion of 2.6 and 3.3°, respectively. They possess comparable B–N average bond distances to that of **d2** with significant shortening of the fused BN bonds.

The molecular packing structure of **d3** also evidences an organization in two differently oriented layers each pilling up parallel molecules separated by 3.535 Å. In contrast, molecules in **d4** arranged in four differently oriented layers. Such singular packing seems to result from secondary interactions of the oxygen of the methoxy group either with CH_2 or CH_3 hydrogens. Yet, layers comprise a pile of parallel borazines separated by 3.508 Å, just as for the other compounds of the series.

IV. Stability of borazine derivatives

Most targeted applications for borazine compounds are found in the field of materials science where, for instance, the BN compounds are used as emissive or host layers in OLEDs. Such uses expect the material to possess a certain stability regarding temperature as well as air and more particularly dioxygen and water.

IV.1. Thermal stability

The thermal properties of the borazine derivatives **d1-4** were assessed by thermogravimetric analyses (TGA). With the aim to compare our data to the literature, we performed the measurements under a nitrogen atmosphere starting from powders of compounds **d1-4.** The curves weight (%) versus temperature (°C) are plotted in Figure 5-10.

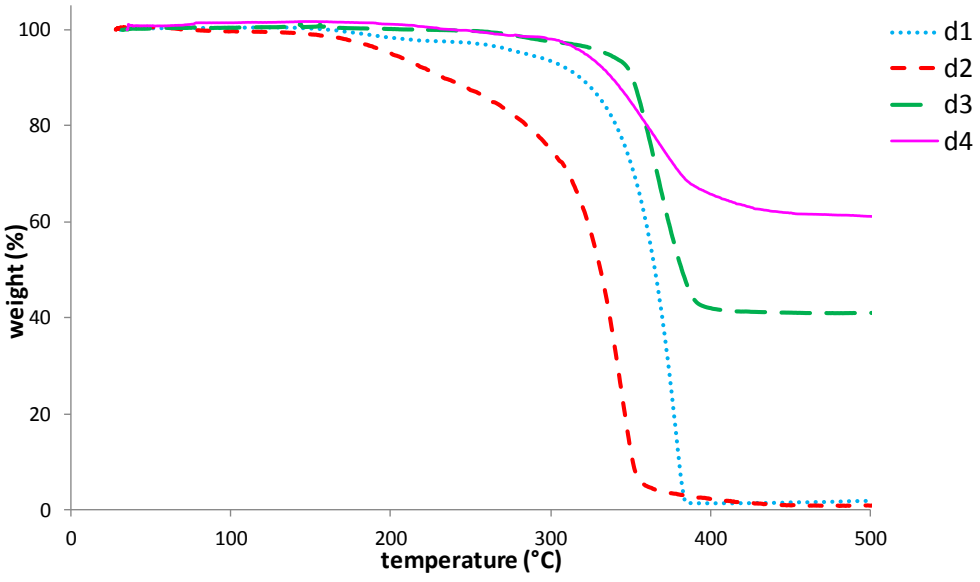

Figure 5-10: Thermograms of borazine derivatives under nitrogen atmosphere heated at 10°C/min

The decomposition temperatures with a 5% weight loss for compounds **d1-4** are 284, 200, 335 and 321°C, respectively. Those values fall in the expected range for aryl substituted borazine compounds[61] and are acceptable for many optoelectronic applications. For instance, Che and coworkers reported decomposition temperatures spanning from 230 to 340°C for phenyl, biphenyl or naphthyl substituted borazines heated in similar conditions.[84] Notably the parent borazine **d2** shows a lower decomposition temperature. The methyl substituted borazine **d3** is the most thermally stable of the series with 5% weight loss at 335°C. The simple methyl substitution resulted in a shift of 135°C of the decomposition temperature. Compounds **d1** and **d2** are fully decomposed above 400°C. In contrast, **d3** and **d4** derivatives did not reach full decomposition, presumably due to remaining boron nitride species. When heating **d3** until 1100°C, a slower decomposition was observed which remained incomplete at the highest temperature.

IV.2. Stability versus H_2O and O_2

Borazines are known to undergo hydrolysis in a 10 : 90 w% ratio in homogeneous conditions.[58] In the context of materials science, this property can appear as a drawback. More recently, borazine **d5** featuring methyl substituents was reported to show extraordinary stability towards hydrolysis due to the steric hindrance generated around the boron center.[61]

We decided to look at the stability of our planar borazines versus water in solution. We performed the test starting with the parent molecule **d2**. The borazine was solubilized in deuterated THF by sonication technique. A solution of dioxane was prepared and used as internal reference. The first ^{1}H NMR spectrum was recorded after about 20 equivalents of water were added to the borazine solution. The reaction was monitored by ^{1}H and ^{11}B NMR spectroscopy until full conversion of **d2** was detected (Figure 5-11). 9% of **d2** were converted after 2.5 hours, 31% after 7 hours and full conversion was observed after 5 days. Borazine **d2** degrades in THF solution, at room temperature.

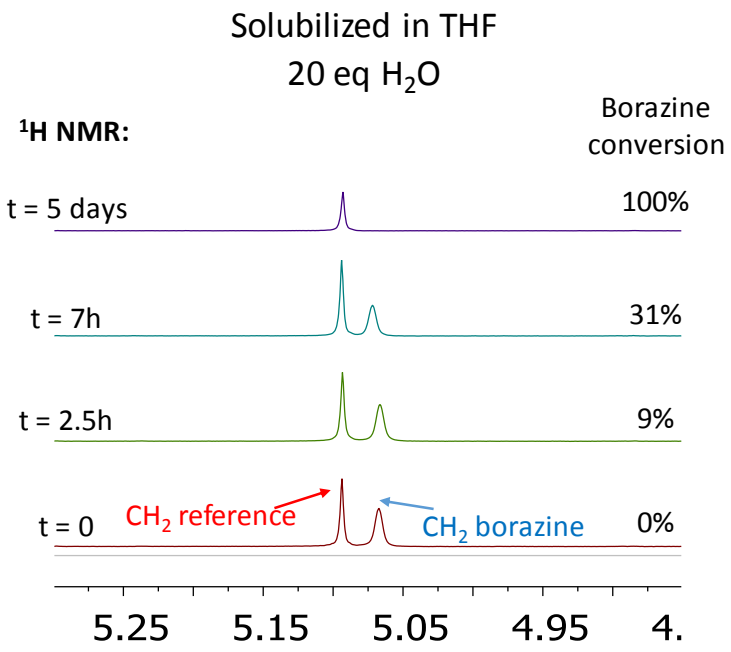

*Figure 5-11: Stacked ^{1}H NMR spectra recorded at various times of the reaction between **d2** and water with dioxane as internal reference*

Most applications require the material to be in the solid state. Hence, we decided to assess the reactivity of borazine **d2** with air in the solid state as a mean to comment on its stability. We exposed a powder of **d2** to the ambient media for 6 months. We used different techniques to assess the possible reactivity of the compound. Because of its poor solubility, we analyzed **d2** in the solid state. Infrared analysis of the air-exposed powder, gave the same spectrum than the air-free sample (see appendices section). Especially, no OH stretching frequency corresponding to the addition of water was observed. The NMR in solution of the product gave a clean ^{1}H NMR spectrum fully consistent with the expected signals for **d2**.

In conclusion, borazine **d2** undergoes hydrolysis in solution, however the compound exhibits a good stability in the solid state (at least 6 months). Hence, its stability is acceptable regarding an application as material.

V. Optoelectronic properties of borazine derivatives

Optoelectronic properties of such compounds are key properties when considering their study in organic electronics or sensing chemistry. It is relevant to compare the present properties to

that of the carbon analogues to assess the influence of the incorporation of the BN units in place of the CC ones. Measurements were performed at ISCR – CNRS, Rennes. Electrochemical measurements were conducted in collaboration with Corinne Lagrost.

V.1. Absorption measurements

We recorded UV-vis spectra of the 1*H*-2,1-benzazaborole series in CH_2Cl_2. The spectra of the four compounds are represented in Figure 5-12 along with the maximum of absorption listed in Table 5-3.

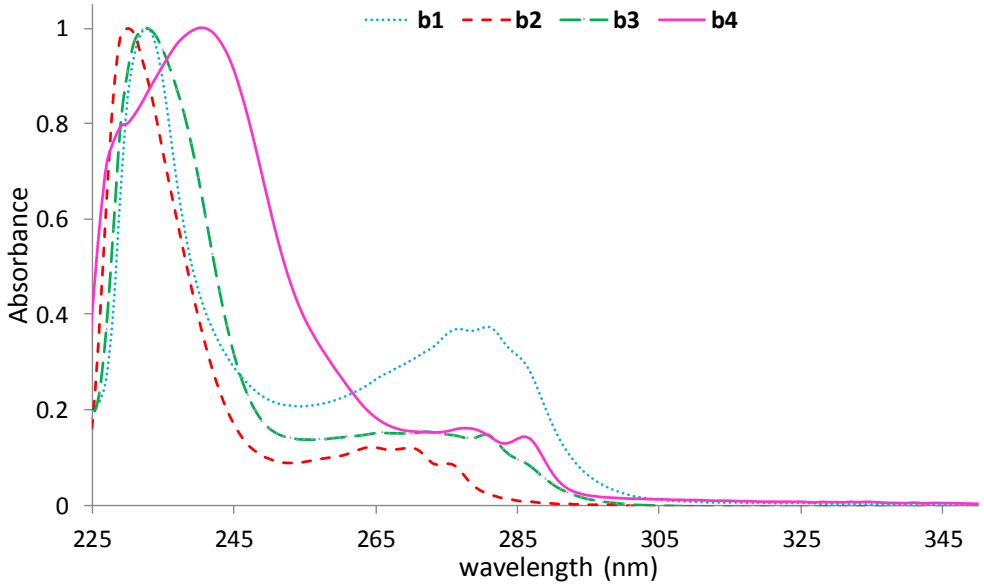

*Figure 5-12: normalized UV spectra of compounds **b1-4** in CH_2Cl_2 at 298K*

	b1 (F)	*b2 (H)*	*b3 (Me)*	*b4 (OMe)*
λmax (nm)	233	230	233	240

*Table 5-3: Maximum of absorption of compounds **b1-4***

All the derivatives absorb in the UV region. A recurrent pattern is found for the series with a high absorption band at high energy and a set of lower absorption bands after 250 nm. Maximum absorptions (λmax) were found at 233, 230, 233 and 240 nm for **b1**, **b2**, **b3** and **b4** respectively. The molar extinction coefficient was approximated between 5000 and 10000

L.mol^{-1}.cm^{-1} for the series. We observe a slight bathochromic shift when the 1*H*-2,1-benzazaborole is substituted with electron-donor groups, as expected. Dostál and coworkers reported λmax for alkyl and/or aryl B,N substituted 1*H*-2,1-benzazaboroles ranging between 207 and 215 nm in hexane.[158] Comparatively, compounds **b1-4** are shifted of about 20 nm. A second set of absorption bands is detected at lower energy including two or three bands for each derivative. The band of lower energy was detected around 290 nm for **b1**, **b3** and **b4** whereas the one for **b2** is revealed at 276 nm.

We then recorded UV-vis spectra of the borazine derivatives in the same solvent (Figure 5-13). Compounds **d1-4** absorb in the UV region. The maximum absorption bands were seen at 240 nm for **d1** and **d2** and red-shifted to 249 and 257 nm for **d3** and **d4**, respectively. The methyl and methoxy electron-donating groups are responsible of the noticeable bathochromic shift.

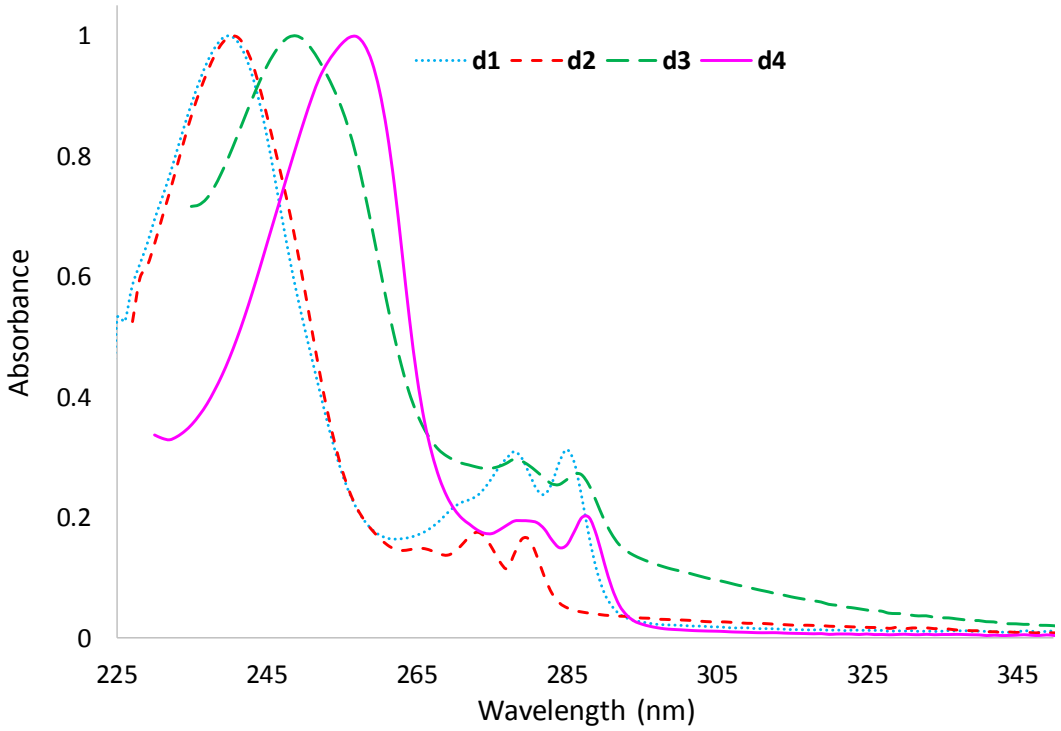

*Figure 5-13: Normalized UV spectra of compounds **d1-4** in CH_2Cl_2 at 298K*

Overall, the λmax of the borazine derivatives shifted to lower energy when compared to that of the precursor series. This behavior is consistent with the red-shift usually observed when increasing the number of aromatic rings and suggests a high degree of conjugation consistent with the planar structure of the borazines. We still detected a set of two or three absorption

bands for each compound at lower energy. The wavelengths associated are similar to that of 1*H*-2,1-benzazaboroles being around 290 nm for **d1**, **d3** and **d4** and 280 nm for **d2.**

ε of the borazine derivatives were accurately determined in solution (Table 3) by plotting the absorbance versus the concentration. The linear relationship between them rules out the presence of borazine aggregates ascertaining their full solubility in CH_2Cl_2 in our experimental conditions (see experimental part).

	d1 (F)	*d2 (H)*	*d3 (Me)*	*d4 (OMe)*	*Truxene*
λmax (nm)	240	240	249	257	273[a,b]
ε (L.mol^{-1}.cm^{-1})	80000	68000	33000	63000	58000[a],70000[b]

*Table 5-4: Maximum of absorptions (λmax) and molar extinction coefficient (ε) of compounds **d1-4** in CH_2Cl_2 as well as Truxene [a]($CHCl_3$) and [b](THF)*

The substituents on the aryl groups of borazine derivatives exert a moderate influence on the intrinsic absorption properties of the compounds. Similar ε were calculated for all the compounds except **d3** which exhibits a ε twice lower than the others.

Truxene absorption spectra were measured either in THF[200] or $CHCl_3$[201] solutions with a maximum of absorption at 273 nm and two less intense bands of lower energy at 290 and 297 nm. The associated ε at λmax were found to be 70000 and 58000 L. mol^{-1}. cm^{-1} in THF and $CHCl_3$, respectively. Hence, the substitution of the central benzene ring by a BN core induced a hypsochromic shift. This phenomenon was previously observed in the case of borazine **d5**, **d7** as well as **d8** compared to the all-carbon analogues.[61, 190, 193] Such behavior is usually indicative of a lower degree of conjugation within the molecule, consistent with the reduced aromatic character of the borazine core compared to a benzene ring and in agreement with a widening of the HOMO-LUMO gap in these molecules.

The general UV-vis pattern of borazine **d5** in CH_2Cl_2 resembles that of our borazine compounds but shows an overall hypsochromic shift (λmax: 232 nm; λlower energy: 273 nm). Although **d5** features more aromatic rings, those values suggest a lower degree of conjugation. One can assume the planarity of our compounds allows a greater electron delocalization throughout the molecule and consequently favors the conjugation. UV-vis spectrum of borazine **d7** in CH_2Cl_2 spans from 235 to 360 nm and shows a higher molar extinction coefficient at the

maximum of absorption (ε = 140000 L. mol^{-1}. cm^{-1}). Indeed, the coefficient usually increases with the number of aromatic rings included in the molecule. Similarly, the UV-vis spectrum of the BN coronene covers approximately the 230–385 (nm) region.[193] In the two latest cases, the lowest-energy electronic transition appeared at higher wavelength than for borazines **d1-4**. As a result, borazines **d7** and **d8** should feature a narrower HOMO-LUMO gap in accordance with a larger aromatic system. The ε corresponding to **d8** was found of approximately 65000 L.mol^{-1}.cm^{-1} at the highest point of the curve.[193]

V.2. Emission measurements

The photoluminescence is a phenomenon resulting from the radiative relaxation of a photon previously excited to a higher level of energy. The relaxation can occur either by fluorescence from an excited singlet state (S1) or by phosphorescence from an excited triplet state (T1) resulting from a S→T intersystem crossing (Figure 5-14).

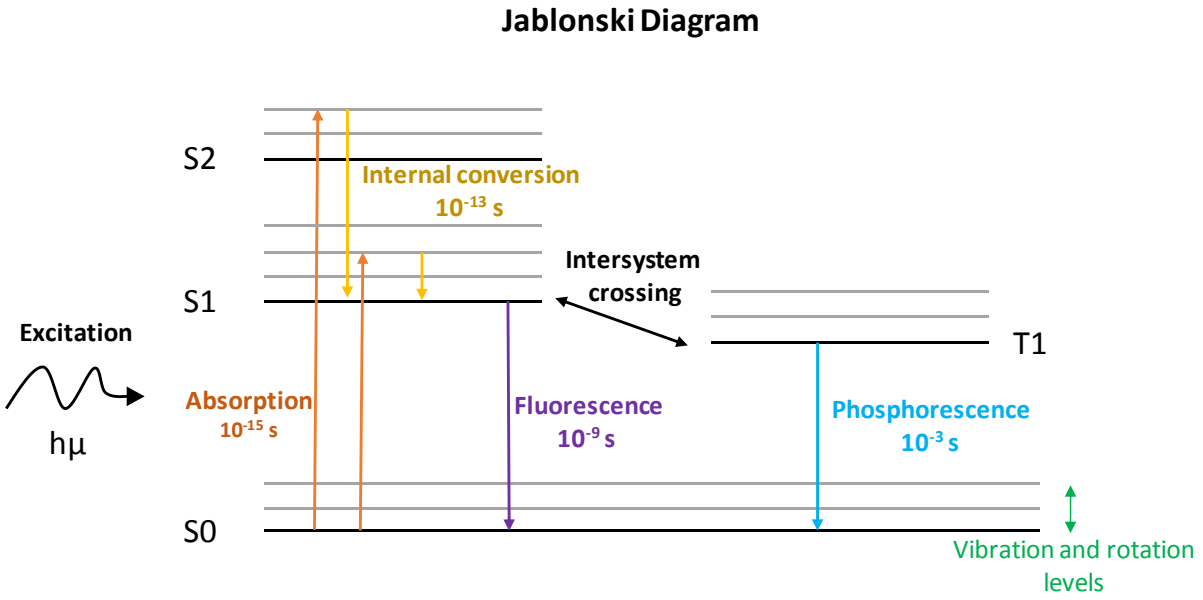

Figure 5-14: Simplified version of the Jablonski diagram

UV/Vis emission spectra have been recorded in the same conditions, in air equilibrated CH_2Cl_2, at room temperature, upon excitation at 250 nm for **d1-2** and 260 nm for **d3-4**. The solutions were prepared in dried CH_2Cl_2 to limit hydrolysis of borazine derivatives but under an air atmosphere. The dioxygen quenches the phosphorescence phenomenon. Thereby, the

recorded emission spectra should reflect solely the fluorescence of the borazine compounds. The emission data of **d1-4** and truxene are listed in Table 5-5. The spectrodistribution in the 250 – 350 nm region of compounds **d1-4** are depicted in Figure 5-15, Figure 5-16, Figure 5-17 and Figure 5-18.

	d1 (F)	*d2 (H)*	*d3 (Me)*	*d4 (OMe)*	*Truxene*
λmax (cm^{-1})	297	280	300	300	361
ΔE (eV)	4.37	4.42	4.33	4.33	
Stokes' shift (cm^{-1})	478	255	478	357	

*Table 5-5: maximum of emission, optical bandgaps and Stokes shift for compounds **d1-4***

The four compounds show similar emission profiles being the mirror image of their respective UV-vis absorption spectra. They feature two overlapping emission bands more or less shouldered. Borazines **d1-4** all emit in the near-UV region with no emission in the visible region. Hence, the compounds can be seen as selective UV-emitters without any colored pollution. The emission spectra of the obtained substituted borazines are red-shifted compared to **d2** with a maximum of emission at 300 nm for **d3** and **d4**, 297 nm for **d1** and 280 nm for **d2**, respectively.

An hypsochromic shift of 60-80 nm is observed on the maximum of emission of borazines **d1-4** compared to truxene (361 nm) (Table 5-6).

	d2	*d5*	*d7*	*d8*
Δ λmax (nm)	80	30	100	80
Δ λmax (eV)	1	0.3	0.7	0.3

*Table 5-6: Difference in emission between the borazines and the all carbon analogues in nm and eV (CH_2Cl_2 except for the emission of the all carbon analogue of **d7** (cyclohexane))*

This finding supports the general trend observed in the emission spectra when incorporating a borazine core in place of a benzene in a polyaromatic scaffold. Borazines **d5**, **d7** and **d8** are blue-shifted of about 30, 100 and 80 nm, respectively. Speaking of energy, the replacement of benzene by the BN core in truxene led to a large difference. The BN part is greatly involved in the emission process, presumably due to the planarity of the molecule that could involve

electron distribution all-over the molecule. **d8** also demonstrated a remarkable increase in the quantum yield when comparing to the all carbon analogue (coronene: 3%, BN coronene: 43%).

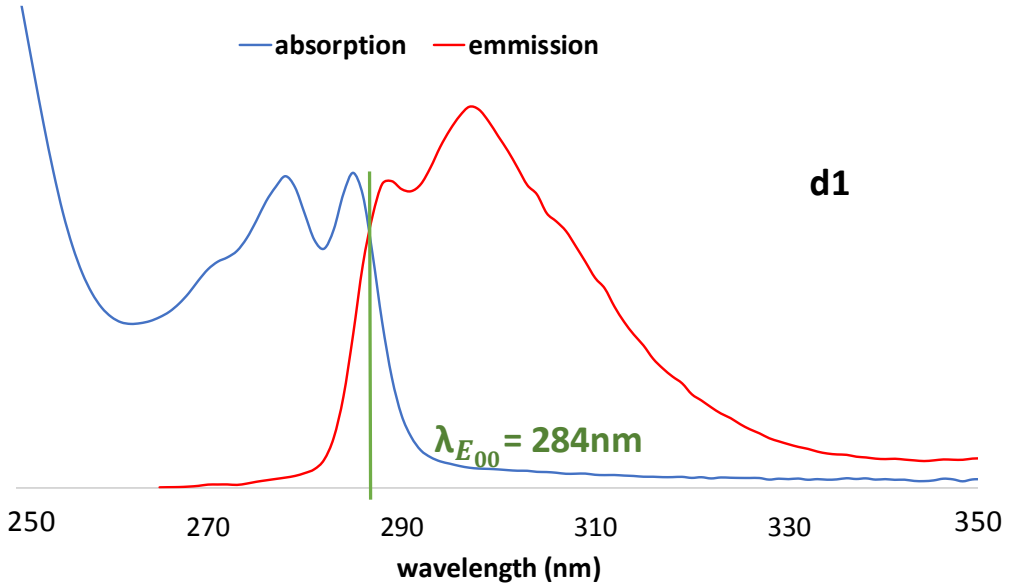

*Figure 5-15: Spectrodistribution in the 250-350 nm region of **d1** in air equilibrated CH_2Cl_2 at RT*

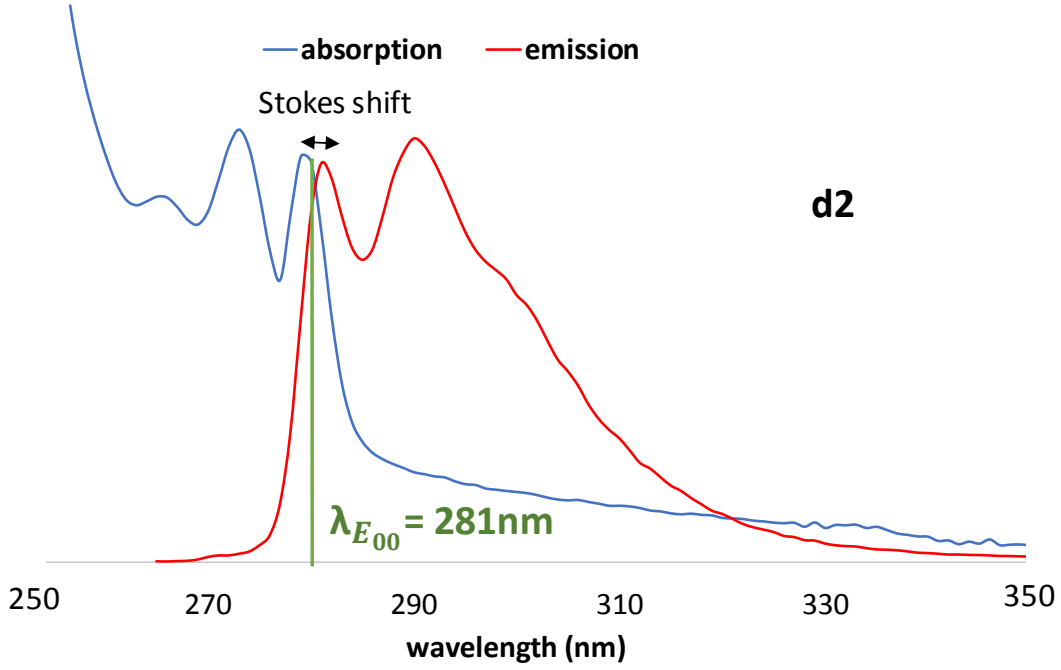

*Figure 5-16: Spectrodistribution in the 250-350 nm region of **d2** in air equilibrated CH_2Cl_2 at RT*

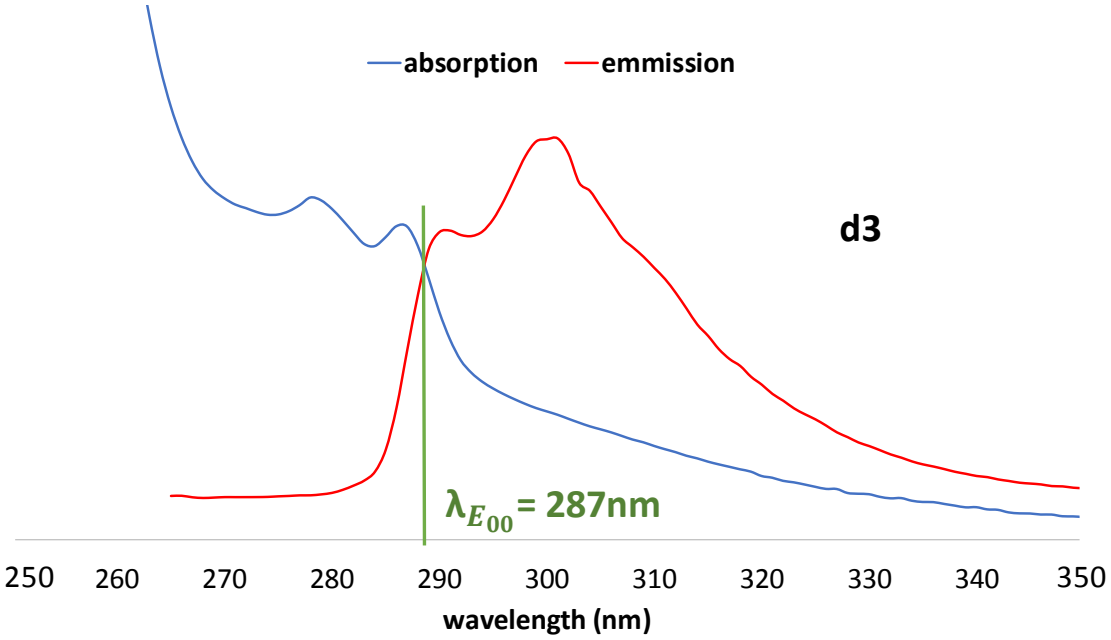

*Figure 5-17: Spectrodistribution in the 250-350 nm region of **d3** in air equilibrated CH_2Cl_2 at RT*

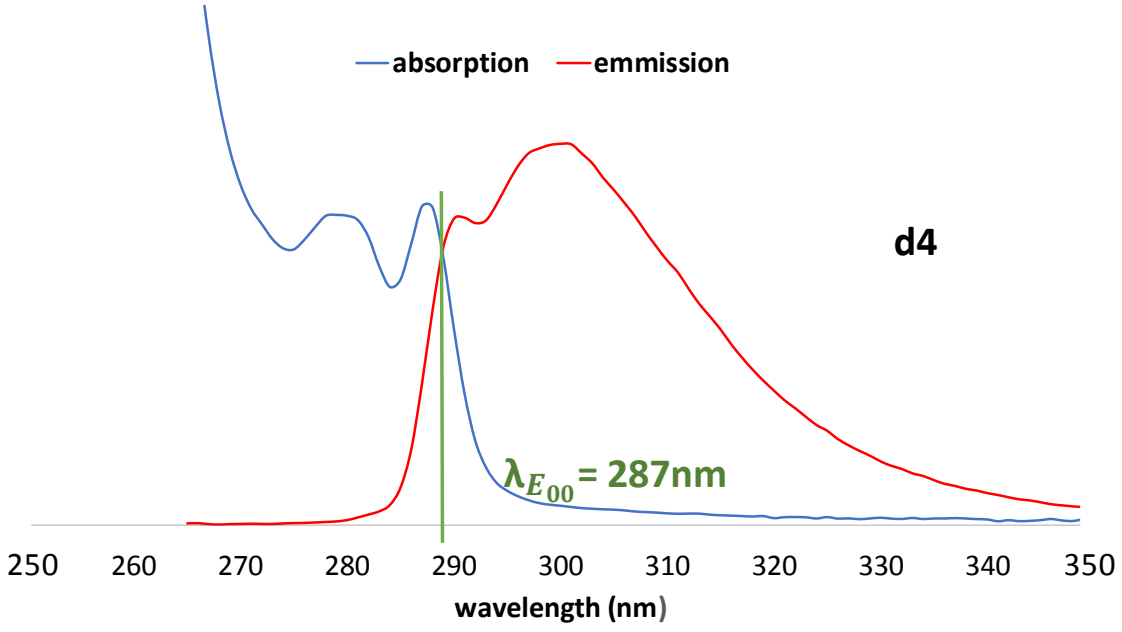

*Figure 5-18: Spectrodistribution in the 250-350 nm region of **d4** in air equilibrated CH_2Cl_2 at RT*

The cross section of the absorption and emission spectra corresponds to the S0→S1 electronic transition (Figure 5-14) and enables the measurement of the HOMO-LUMO energy gap referred as the optical bandgap. It can be calculated from the following equation:

$$\Delta E = \frac{h \times c}{\lambda_{E_{00}}}$$

h = Planck constant $6.63.10^{-34}$ J.s, c = 3.10^{8} m.s^{-1} 1eV = 1,6022e-19 J

The optical bandgaps were calculated for the four compounds following the same procedure and are listed in Table 5-5. Comparable ΔE were obtained for the four compounds. Those large bandgaps are typical for borazine compounds. For instance, Che and coworkers reported the synthesis of various H–N, R–B or R–N, H–B borazines with R = aryls, featuring optical bandgaps ranging from 3.3 to 4.5 eV (Figure 5-18).[84] More recently, Bonifazi and coworkers calculated the optical gap of the BN coronene (3.29 eV) being wider than the coronene itself (2.76 eV).[193]

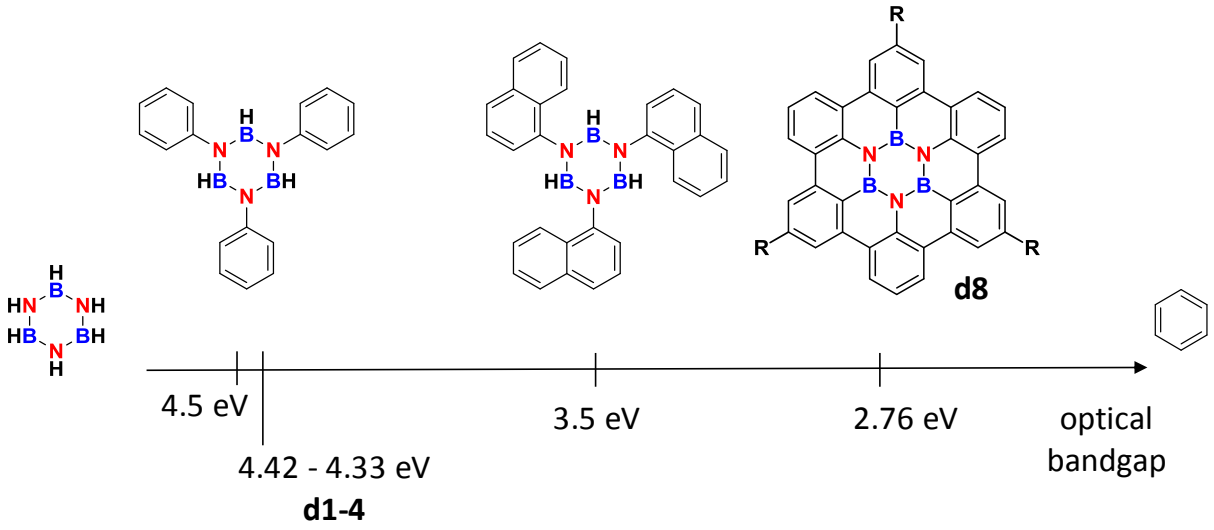

Figure 5-19: Experimentally determined optical bandgaps in the literature and in this work

We also extracted the stokes shift from the spectrodistribution of our compounds. This factor correspond to the difference in wavelength between the maxima of the absorption and emission spectra corresponding to a same electronic transition.[202] It has to be converted to an energy difference to be properly compared. Compounds **d1-4** show a Stokes shift between 2 and 4 nm leading to an energy loss between 255 and 478 cm^{-1} (Table 5-5). The Stokes shifts associated to **d1-4** can be considered small. As a result, few energy is lost during the emission process. The stokes shifts show a tendency to decrease upon incorporation of a borazine core in a polyaromatic scaffold, as seen for borazine **d5** and **d8**. One can assume that the same trend would be observed with borazines **d1-4** versus truxene**.**

V.3. Electrochemical measurements

The electrochemical behavior of the borazine derivatives were studied by cyclic voltammetry (CV) in N,N-dimethylformamide (DMF) containing $TBAPF_6$ as supporting salt. Provided that it is thoroughly dried and degassed, this electrolyte allows reaching potential window with highly negative potentials. Then, it was found much more suitable than CH_2Cl_2 (+ $TBAPF_6$) since in the latter, the electrolyte decomposition overlaps the observation of the reduction peak of our borazine compounds. The measurements allow a clean determination of the related electrochemical bandgaps.

The electrochemical behavior was first investigated for **d2.** A chemically irreversible oxidation process is clearly observed in the range of studied scan rates (0.02 – 1 V s^{-1}) when the potential is swept between – 0.5 and 1.5 V (Figure 5-20).

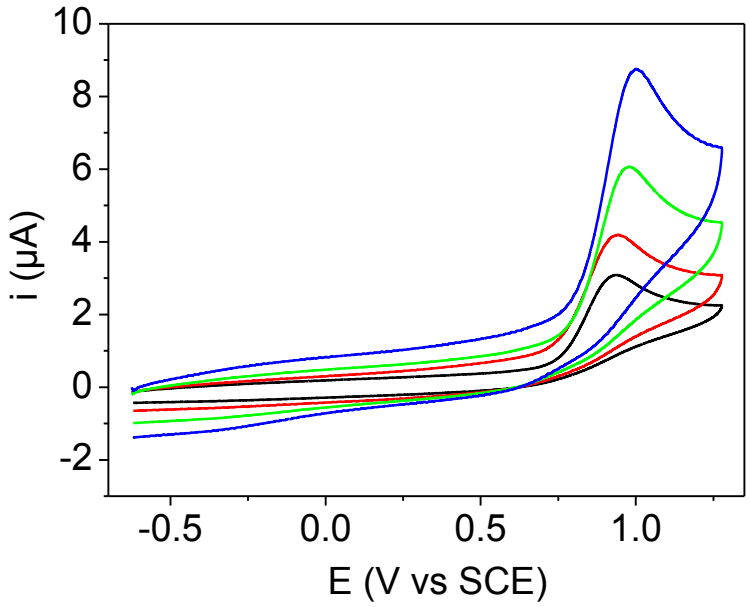

Figure 5-20: Cyclic voltammograms of d2 in DMF + 0.1 M $TBAPF_6$ at 1 mm glassy carbon electrode showing the oxidation at different scan rates (0.1 (black), 0.2 (red), 0.5(green) and 1 (blue) V s^{-1}.

The oxidation peak potential of **d2** was found at 0.93 V vs SCE or 0.525 V vs (Fc/Fc^+) with $E°_{Fc/Fc+}$ = 0.405 V vs SCE. Such an irreversible process is in line with previous examples. 4-*t*-butylphenyl–N, H–B as well as **d7** borazines undergo chemically irreversible oxidation at Epa = 0.76 V vs (Fc/ Fc^+) in DMF and at Epa = 0.6 V vs (Fc/Fc^+) in CH_2Cl_2 respectively.[84, 190] However, CV associated to borazine **d8** shows a reversible oxidation for scan rates above 0.5 V s^{-1} at $E_{1/2}$

= 1.46 V vs SCE (1 V vs (Fc/Fc^+)) in CH_2Cl_2.[193] Note that the peak potential Epa was located at 1.53 V vs SCE or 1.07 V vs (Fc/Fc^+). Borazine **d2** is easier to oxidize than previously described borazines. The all carbon analogue always show a reversible oxidation process whereas the borazine derivatives undergo an irreversible process (except for **d8**).

The CVs display a reduction peak at approximately –2.8 V vs SCE (or -2.37 V vs (Fc/Fc^+) under our experimental conditions) as displayed in Figure 5-21. At low and moderate scan rates (0.02 – 0.2 V/s), the reduction process is found chemically irreversible but becomes reversible upon increasing the scan rates, being fully reversible at 5 V s^{-1} (see insert). This behavior is probably associated to slow chemical processes triggered by the electron transfer such as structural reorganization. For the first time, reduction peak of a borazine compound can be observed by cyclic voltammetry.

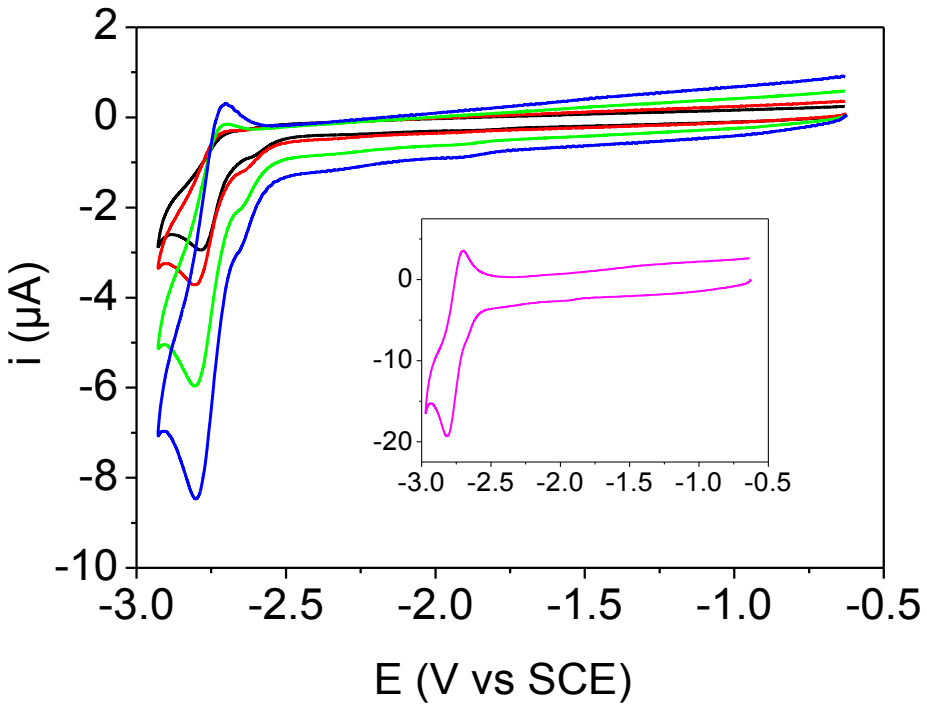

*Figure 5-21: Cyclic voltammograms of **d2** in DMF + 0.1 M $TBAPF_6$ at 1 mm glassy carbon electrode showing the reduction at different scan rates (0.1 (black), 0.2 (red), 0.5(green) and 1 (blue) V s^{-1}. Insert CV at 5 V s^{-1} showing the fully reversible reduction of **d2**.*

The substituted borazines **d1**, **d2** and **d3** exhibit close electrochemical behaviors to that of **d2**, except that their reduction processes are always found irreversible in the scan rate ranges (0.02 – 5 V s^{-1}), suggesting that the kinetics of the associated chemical processes is probably larger. Moreover, the reduction process for the most-donating substituents (**d3** and **d4**) is

much less defined than for **d1** and **d2**, being partially hidden by the electrolyte decomposition, since it occurs at much more negative potentials. Reduction and oxidation peak potentials are listed in Table 5-7.

	d1 (F)	*d2 (H)*	*d3 (Me)*	*d4 (OMe)*
Reduction	– 2.52	– 2.78	– 2.82	– 2.81
oxidation	0.86	0.93	0.83	0.82

*Table 5-7: Reduction and oxidation peak potentials vs SCE determined from CV of compounds **d1-4** at 0.05 V/s*

The reduction process is more favorable in the case of fluorine-substituted borazine in agreement with less electron rich species. The electron donating-substituted borazines show higher reduction onset potential. Slight variations on the oxidation onset potentials of **d1-4** are observed with **d2** compound being the harder to be reduced.

Relationship between peak current (ip) and the square root of the scan rate was linear indicating a diffusional system with the reduced or oxidized species in solution (see appendices section).

The oxidation process corresponds to the removal of an electron from the highest occupied molecular orbital (HOMO) energy level, whereas the reduction corresponds to the electron injection into the lowest unoccupied molecular orbital (LUMO). The HOMO-LUMO gap could be estimated from the difference in onset potentials between reduction and oxidation. The values of the electrochemical bandgaps of compounds **d1-4** are gathered in Table 5-8.

	d1 (F)	*d2 (H)*	*d3 (Me)*	*d4 (OMe)*
ΔE_{EC} *(eV)*	3.1 ± 0.1	3.3 ± 0.1	3.5 ± 0.1	3.1 ± 0.1

*Table 5-8: Electrochemical bandgaps calculated from the onset potentials of **d1-4***

The calculated electrochemical bandgaps range from 3.1 (**d1, d4**) to 3.3 (**d2**) and 3.5 (**d3**) eV. If measured in the same experimental conditions, ΔE_{EC} should be slightly wider than the optical bandgaps owing to the electron-hole columbic interaction.[203] In our case, $\Delta E_{EC} < \Delta E_{Op}$ evidencing an unexpected outcome. Conditions might have influenced the HOMO-LUMO levels. Although the absorption spectra of **d2** are the same in CH_2Cl_2 and DMF, the salt is not

present in optical measurement. In addition, the concentration is significantly higher during the electrochemical experiments than during the optical measurements. The electrochemical gap calculated directly from experimental reduction and oxidation waves of borazine compounds is calculated here for the first time.

In conclusion, unprecedented borazines were synthesized starting from the uncommon 1*H*-2,1-benzazaborole precursors. The thermally induced dehydroamination/trimerization of the parent 1*H*-2,1-benzazaborole and aryl-substituted derivatives, cleanly led to the formation of the corresponding borazines. The compounds were isolated in very good yields except for the methylated version, which also showed a slower kinetic attributed to steric effect. Borazine formation seems to occur *via* stepwise condensation reactions of the 1*H*-2,1-benzazaborole units, as indicated by the characterization of the intermediate dimer. The four compounds were characterized by HRMS, NMR and IR spectroscopy as well as X-ray diffraction (except **d1**). Borazines possess remarkable planar structures and are consequently model molecules of choice to study the incorporation of BN core into electron-delocalized systems. The planar character suggests a large degree of conjugation throughout the molecule that should involve the BN unit. The four compounds exhibit a high stability to temperature and ambient conditions in the solid state, acceptable for application as materials. The optoelectronic properties of the four derivatives were assessed in solution. Borazines absorbed in the UV region with a noted increase of ε compared to the 1*H*-2,1-benzazaboroles. The compounds are emissive with a maximum of absorption around 300 nm. They emit exclusively in the UV region with no contamination in the visible. The emission is greatly blue shifted compared to the all-carbon analogue truxene indicating the strong influence of the BN incorporation and suggesting a widening of the HOMO-LUMO gap. The optical bandgap was determined to be large in the scale of previously reported gap for borazine compounds, one more time underlying the great contribution of the BN unit in optical processes. Finally, the experimental electrochemical gap was determined by cyclic voltammetry for the first time for this class of compound, being smaller than the optical bandgap. In any cases, the gap is characteristic of semiconductor compounds. Theoretical calculations to come, should clarify the nature of the HOMO-LUMO orbitals and help to illustrate the contribution of the BN unit.

GENERAL CONCLUSION

It is important to underline that the chemistry of cyclic BN compounds is emerging but is still at an early stage, both in coordination chemistry and in materials science. The different BN containing molecules synthesized and described in this manuscript are rare examples of their class. We have demonstrated that the coordination of $RN^{i}Pr_2B–H$ with the bis(dihydrogen) ruthenium complexes could be extended to a catalytic system when incorporating a reactive nitrile function in place of a coordinative phosphine. Firstly, we successfully transposed the synthetic strategy towards aryl(phosphino)(aminoborane) to the synthesis of a series of aryl(cyano)(aminoborane). The lithiation/borylation sequences led to sophisticated substrates bearing a $RN^{i}Pr_2B–H$ sp^2 borane and a nitrile function separated by a phenyl spacer. In the presence of a catalytic amount of $RuH_2(H_2)_2(PCy_3)_2$, under a pressure of dihydrogen, B–N bond is created from the reduction of both C≡N and B–H bonds. The reaction proceeds in mild conditions (P_{H2} = 1 bar(g), RT) and leads to BN 5-membered rings. The reaction tolerates different groups on the aryl and the catalyst is regenerated at the end of the reaction.

We investigated the mechanism of this new catalytic transformation. The study was carried out by combining stoichiometric reactions, multinuclear variable temperature NMR experiments, *in situ* monitoring of the catalytic reaction, and completed by theoretical calculations. Stoichiometric reactions evidenced various hydrogen transfer processes from the resourceful $RuH_2(H_2)_2(PCy_3)_2$ pre-catalyst to the substrate. Notably, we could capture the substrate in transformation in the form of the 1*H*-2,1-benzazaborolyl ligand, coordinated by the BN cycle to the metal center as also evidenced by X-ray diffraction. We showed that the isolated complex undergoes stepwise hydrogenation, followed by haptotropic rearrangement before release of the final product and regeneration of the pre-catalyst. We demonstrated its possible implication in the catalytic cycle. We were then able to comment on activation modes for both C≡N and B–H bonds by *in situ* monitoring and theoretical calculations. It is apparent that the coordination of the substrate on $RuH_2(H_2)_2(PCy_3)_2$ is dominated by the nitrile function which first interacts with the complex and is partially hydrogenated. The role of boron in the catalysis is revealed during the hydrogenation process. The boron-nitrogen interaction appears as a key event stabilizing the imine *via* an intermediate imine-borane species, and being the driving force for B–H bond cleavage which occurred afterward at the metal center.

We then assessed the synthetic potential of the generated BN heterocycles. We were particularly interested in the boron tolerance with well-established synthetic tools. The 1*H*-

2,1-benzazaboroles feature, for the first time, an N–H moiety, as a result of the synthetic method, and a stabilized sp^2 borane due to the BN π interaction. We demonstrated that we can selectively deprotonate the amine and make a variety of N–E bonds (E = Si, C, P or B) by adding halogenated electrophiles. More importantly, we adapted the Buckwald-Hartwig amination to attach, catalytically, aryl substituents on nitrogen. Yet, the catalytic dehydrogenation of 1*H*-2,1-benzazaborole did not proceed in our experimental conditions, on one part owing to competitive reactions at elevated temperatures. Finally, cyclotrimerization of the 1*H*-2,1-benzazaboroles led to the formation of remarkably planar borazines being model molecules to study the incorporation of BN-benzene into electron delocalized systems. The borazines possess acceptable stability for materials application. We showed that the BN incorporation has a great influence on the optoelectronic properties of the molecules. The borazines are fluorescent molecules, emitting in the UV region and featuring a wide HOMO-LUMO gap making them semi-conductors.

First assessment of the synthetic potential of the 1*H*-2,1-benzazaborole is promising. We could imagine developing the Buckwald-Hartwig amination strategy to incorporate relevant fluorophores for sensing applications. The ligand ability of the generated phosphino 1*H*-2,1-benzazaborole could be assessed. Borazine functionalization with solubilizing groups could allow a deeper characterization in solution and extension to different optoelectronic properties. The properties of borazines in the solid state could also be evaluated along with their electron-hole mobility in view to incorporate them in model devices.

As additional perspectives, the catalytic reaction could be extended to substrates bearing:

- A different spacer
- A different reactive function
- A different group on the borane replacing N^iPr_2
- A silane instead of a borane.

We wish that this work illustrates how an in-depth study of new bond activation systems can drive the discovery of original catalytic intermediates and lead to the synthesis of uncommon compounds.

EXPERIMENTAL SECTION

General considerations

All experiments were performed under an atmosphere of dry argon using standard Schlenk and glove box techniques. Unless stated, all chemicals were purchased from Aldrich and used without further purification. Solvents (Et_2O, pentane and toluene) were purified and dried through an activated alumina purification system (MBraun SPS-800). NMR solvents were dried using appropriate methods and degassed prior to use. NMR samples of sensitive compounds were prepared in the glovebox under an argon atmosphere. Nuclear magnetic resonance spectra were recorded on Bruker Avance 300, 400 or 500 spectrometers operating at 300.13, 400.13 or 500.33 MHz, respectively for ^{1}H, 121.5, 162 or 202.5 MHz, respectively for ^{31}P, 75.48, 100.62 or 125.72 MHz, respectively for ^{13}C, 75.47, 128.38 or 160.42 MHz respectively for ^{11}B and 282.23, 376.31 or 470.39 MHz for ^{19}F. ^{1}H and ^{13}C chemical shifts are reported in ppm referenced internally to the residual solvent peak, while ^{31}P are relative to 85% H_3PO_4, and ^{11}B are relative to $BF_3.OEt_2$ external references. Chemical shifts are quoted in ppm (δ) and coupling constants in Hz. The following abbreviations and their combination are used: br, broad; s, singlet; d, doublet; t, triplet; m, multiplet; p, pseudo; sept, septet. Infrared spectra were recorded on a Perkin Elmer Spectrum 100 FT-IR spectrometer fitted with ATR accessories. The crystal in the ATR module is Ge. HR–MS spectra were recorded by the mass spectroscopy service at the Université Paul Sabatier, Institut de Chimie de Toulouse (ICT) or by the corresponding facilities at the CRMPO (Centre Régional de Mesure Physiques de l'Ouest), University Rennes 1.

X-ray data were collected at low temperature on a Gemini Agilent diffractometer using a graphite-monochromated Cu-Kα enhanced radiation (λ = 1.54184 Å) or Mo- Kα radiation (λ = 0.71073 Å), and equipped with an Oxford Cryosystems Cryostream Cooler Device.

Throughout the manuscript, relative pressures are used and will be noted (bar(g)) for gauge pressure.

Computational details

Calculations were carried out using the Gaussian09 package[1] at the DFT level by means of the hybrid density functional B3PW91.[2] For the Ru atom, the Stuttgart-Dresden pseudopotentials[3] were used in combination with their associated basis sets[4] augmented by

a set of polarization functions (f-orbital polarization exponents of 1.235)[5]. For the C, H, N, P and B atoms, a double-zeta 6-31G basis set[6] augmented by a polarization and diffuse function were used. The nature of the optimized stationary point, minimum or transition state, has been verified by means of analytical frequency calculations at 298.15 K and 1 atm. The geometry optimizations have been achieved without any geometrical constraints. IRC calculations were carried out in order to confirm the connectivity between reactant(s), transition state and product(s). Energy data are reported in the gas phase. The energy data presented correspond to the free enthalpy of the computed compounds in which thermal, vibrational electrostatic and non-electrostatic contributions have been included.

References:

[1] Gaussian09, revision D.01. Frisch, M. J.; Trucks, G. W.; Schlegel, H. B.; Scuseria, G. E.; Robb, M. A.; Cheeseman, J. R.; Scalmani, G.; Barone, V.; Mennucci, B.; Petersson, G. A.; Nakatsuji, H.; Caricato, M.; Li, X.; Hratchian, H. P.; Izmaylov, A. F.; Bloino, J.; Zheng, G.; Sonnenberg, J. L.; Hada, M.; Ehara, M.; Toyota, K.; Fukuda, R.; Hasegawa, J.; Ishida, M.; Nakajima, T.; Honda, Y.; Kitao, O.; Nakai, H.; Vreven, T.; Montgomery, Jr., J. A.; Peralta, J. E.; Ogliaro, F.; Bearpark, M.; Heyd, J. J.; Brothers, E.; Kudin, K. N.; Staroverov, V. N.; Keith, T.; Kobayashi, R.; Normand, J.; Raghavachari, K.; Rendell, A.; Burant, J. C.; Iyengar, S. S.; Tomasi, J.; Cossi, M.; Rega, N.; Millam, J. M.; Klene, M.; Knox, J. E.; Cross, J. B.; Bakken, V.; Adamo, C.; Jaramillo, J.; Gomperts, R.; Stratmann, R. E.; Yazyev, O.; Austin, A. J.; Cammi, R.; Pomelli, C.; Ochterski, J. W.; Martin, R. L.; Morokuma, K.; Zakrzewski, V. G.; Voth, G. A.; Salvador, P.; Dannenberg, J. J.; Dapprich, S.; Daniels, A. D.; Farkas, O.; Foresman, J. B.; Ortiz, J. V.; Cioslowski, J.; Fox, D. J.; Gaussian, Inc., Wallingford CT, **2013**.
[2] a) J. P. Perdew, J. A. Chevary, S. H. Vosko, K. A. Jackson, M. R. Pederson, D. J. Singh, C. Fiolhais, *Phys. Rev. B* **1992**, *46*, 6671; **b)** A. D. Becke, *J. Chem. Phys.* **1993**, *98*, 5648.
[3] D. Andrae, U. Haeussermann, M. Dolg, H. Stoll, H. Preuss, *Theor. Chim. Acta* **1990**, *77*, 123.
[4] J. M. L. Martin, A. Sundermann, *J. Chem. Phys.* **2001**, *114*, 3408.
[5] A. W. Ehlers, M. Böhme, S. Dapprich, A. Gobbi, A. Hollwarth, V. Jonas, K. F. Köhler, R. Stegmann, A. Veldkamp, G. Frenking, *Chem. Phys. Lett.* **1993**, *208*, 111.
[6] a) R. Ditchfield, W. J. Hehre, and J. A. Pople, *J. Chem. Phys.* **1971**, *54*, 724; b) W. J. Hehre, R. Ditchfield, J. A. Pople, *J. Chem. Phys.* **1972**, *56*, 2257; c) P. C. Hariharan, J. A. Pople, *Theor. Chem. Acc.* **1973**, *28*, 213; d) P. C. Hariharan, J. A. Pople, *Mol. Phys.* **1974**, *27*, 209; e) M. M. Francl, W. J. Pietro, W. J. Hehre, J. S. Binkley, D. J. DeFrees, J. A. Pople, M. S. Gordon, *J. Chem. Phys.* **1982**, 77, 3654; f) T. Clark, J. Chandrasekhar, G. W. Spitznagel, P. v. R. Schleyer, *J. Comp. Chem.* **1983**, *4*, 294; g) M. J. Frisch, J. A. Pople, J. S. Binkley, *J. Chem. Phys.* **1984**, *80*, 3265.

Experimental section Chapter 2

Compound a1

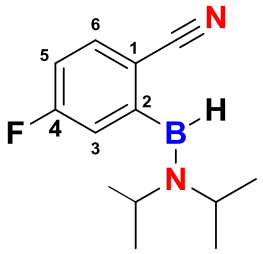

*n*BuLi 1.6 M in hexanes (3.15 mL; 5.02 mmol) was added dropwise to a THF/diethylether solution (1/1, V/V; 25 mL) of 4-fluoro-2-bromobenzonitrile (1.00 g; 5.00 mmol) below − 100°C. The solution turned pale yellow and was stirred for 30 min. Chloro(diisopropylamino)borane (0.778 g, 5.27 mmol) was then added and the reaction solution was stirred for 30 min at − 78°C and then 90 min at room temperature. The mixture was evaporated to dryness, dissolved in cold pentane at −10°C and passed through a small plug of Celite®. The filtrate was dried in vacuo. **a1** was isolated without further purification as a pale yellow oil in 82% yield. **^{1}H NMR (**C_6D_6**,** 300.13 MHz**,** 298K**):** 0.82 and 1.20 (d, 6H, $^{3}J_{H\text{-}H}$ = 8.8 Hz , C*H*$_3$ ^{i}Pr); 2.98 and 3.54 (sept, 1H, $^{3}J_{H\text{-}H}$ = 8.8 Hz, C*H* ^{i}Pr); 5.35 (br, 1H, B*H*); 6.35 (m, 1H, C*H*$_{ar\text{-}5}$); 6.74 (m, 1H, C*H*$_{ar\text{-}3}$); 6.95 (m, 1H, C*H*$_{ar\text{-}6}$).**^{11}B NMR (**C_6D_6**,** 96.29 MHz**,** 298K**)**: 37.1 (d, $^{1}J_{B\text{-}H}$ ≈ 110Hz). **^{13}C{^{1}H} NMR (**C_6D_6**,** 100.64 MHz**,** 298K**):** 21.86 and 27.06 (s, *C*H$_3$ ^{i}Pr); 45.40 and 51.21 (s, *C*H ^{i}Pr); 111.23 (d, $^{4}J_{C\text{-}F}$ = 3.1Hz, C^{1}); 114.99 (d, $^{2}J_{C\text{-}F}$ = 22.8 Hz, *C*H$_{ar\text{-}5}$); 117.87 (d, $^{2}J_{C\text{-}F}$ =20.4 Hz, *C*H$_{ar\text{-}3}$); 118.75 (s, *C*≡N); 134.96 (d, $^{3}J_{C\text{-}F}$ = 8.9 Hz, *C*H$_{ar\text{-}6}$); 151.11 (br, ipso-*C*^{IV}-B); 164.51 (d, $^{1}J_{C\text{-}F}$ = 255 Hz, ipso-*C*^{IV}-F). **^{19}F NMR** (C_6D_6**,** 376.31 MHz**,** 298K**):** 105.5 (m). **IR: ν$_{BH}$ =** 2495 (s), 2482 (sh) cm^{-1}; $\nu_{C\equiv N}$ = 2219 cm^{-1} (s). **HRMS** ASAP^{+} (100°C) [M+H]$^{+}$ calcd for $C_{13}H_{19}BN_2F$: m/z = 233.16198. Found 233.1621 (0 ppm) calculated on the monoisotopic peak.

Compound a2

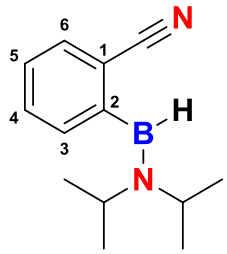

*n*BuLi 1.6 M in hexanes (3.5 mL; 5.6 mmol) was added dropwise to a THF (25 mL) solution of 2-bromobenzonitrile (1.00 g; 5.50 mmol) at −78°C and stirred for 30 min. The solution turned first yellow and then brown. Chloro(diisopropylamino)borane (0.923 mg; 6.26 mmol) was then added. The reaction mixture was stirred for 30 min at −78°C and then 90 min at room temperature. The mixture was evaporated to dryness, re-dissolved in cold pentane at −10°C and passed through a small plug of Celite®. The filtrate was pumped to dryness and the resulting oil was purified by Kugelrohr distillation (110°C / 0.01 mm Hg) to yield a colorless oil of **a2** in 70% yield. **^{1}H NMR** (C_6D_6, 400.18 MHz**,** 298K)**:** 0.87 and 1.25 (d, 6H, $^{3}J_{H\text{-}H}$ = 6.8Hz , C*H*$_3$ ^{i}Pr); 3.04 and 3.69(sept, 1H, $^{3}J_{H\text{-}H}$ = 6.8Hz , C*H* ^{i}Pr); 5.52 (br, 1H, B*H*); 6.75 (m, 1H , C*H*$_{ar\text{-}5}$); 7.02 (m, 1H, C*H*$_{ar\text{-}4}$); 7.06 (d, 1H, C*H*$_{ar\text{-}3}$); 7.21 (d, 1H, $^{3}J_{H\text{-}H}$ = 8 Hz, C*H*$_{ar\text{-}6}$). **^{11}B NMR** (C_6D_6**,** 128.39 MHz**,** 298K): 37.5 (d, $^{1}J_{B\text{-}H} \approx$ 115Hz). **^{13}C{^{1}H} NMR** (C_6D_6**,** 100.64 MHz**,** 298K)**:** 21.95 and 27.13 (s, *C*H$_3$ ^{i}Pr); 45.32 and 50.98 (s, *C*H ^{i}Pr); 115.46 (s, C$_{ar\text{-}1}$); 119.55 (s, *C*≡N); 127.55 (s, C$_{ar\text{-}5}$); 130.96 (s, C$_{ar\text{-}3}$); 131.28 (s, C$_{ar\text{-}4}$); 132.29 (s, C$_{ar\text{-}6}$); 147.34 (br, ipso-C^{2}-B). **IR: ν_{BH}** = 2491 (s), 2460 (sh) cm^{-1}; $\nu_{C\equiv N}$ = 2219 cm^{-1} (s); **HRMS** DCI $[M+H]^+$ calcd for $C_{13}H_{20}BN_2^+$: m/z = 215.1720. Found 215.1721 (0.5 ppm), calculated on the monoisotopic peak.

Compound a3

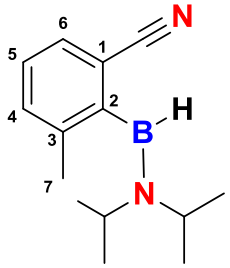

Same procedure as for **a2** using *n*BuLi 1.6M in hexanes (3.2 mL; 5.2 mmol) and 2-bromo-3- methyl benzonitrile (1.00 g; 5.10 mmol). **a3** was isolated as a colorless oil in 89% yield. **^{1}H NMR (**C_6D_6, 400.16 MHz**,** 298K**):** 0.73, 1.08, 1.18 and 1.39 (d, 3H, $^{3}J_{H\text{-}H}$ = 6Hz, C*H*$_3$ ^{i}Pr);

2.02 (s, 3H, C*H*$_3$ Me); 3.06 and 3.49 (sept, 1H, $^3J_{H\text{-}H}$ = 6Hz, C*H* ^{i}Pr); 5.49 (br, 1H, B*H*); 6.73 (m, 1H, $^3J_{HH}$ = 7.70 Hz, C*H*$_{ar\text{-}5}$); 6.87 (d, 1H, $^3J_{HH}$ = 6.87 Hz, C*H*$_{ar\text{-}4}$); 7.12 (d, 1H, $^3J_{HH}$ = 7.12 Hz, C*H*$_{ar\text{-}6}$). **^{11}B NMR (**C_6D_6**,** 128.39 MHz**,** 298K**)**: 37.8 (d, $^1J_{B\text{-}H}$ ≈ 120Hz). **^{13}C{^{1}H} NMR (**C_6D_6**,** 100.64 MHz**,** 298K**):** 21,58 (s, *C*^{7}H$_3$); 21.58, 21.85 , 26.97, 27.05 (s, *C*H$_3$ ^{i}Pr); 45,10 and 51.76 (s, *C*H ^{i}Pr); 114.01 (s,C^1); 119.84(s, *C*≡N); 127.54 (s, *C*H$_{ar\text{-}5}$); 129.49 (s, *C*H$_{ar\text{-}6}$); 132.58(s, *C*H$_{ar\text{-}4}$); 139.84(s, *C*^{3}); 147.35 (br, ipso-*C*^{2}-B). **IR: ν$_{BH}$** = 2470 (s), 2450 (sh) cm^{-1}; ν$_{C≡N}$ = 2220 cm^{-1} (s). **HRMS** DCI [M+H]$^+$ calcd for $C_{14}H_{22}BN_2$: m/z = 229.1876. Found 229.1886 (4.4 ppm), calculated on the monoisotopic peak.

Compound a4

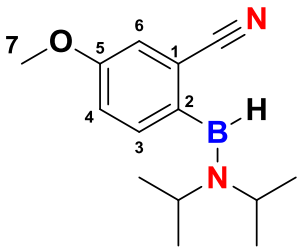

*n*BuLi 1.6 M in hexanes (3.20 mL; 5.12 mmol) was added dropwise to a THF/diethylether solution (1/1, V/V; 30 mL) of 2-bromo-5-methoxybenzonitrile (1.05 g; 4.95 mmol) below – 110°C. The solution turned turbid then extremely light yellow and was stirred for 30 min. Chloro(diisopropylamino)borane (0.807 g; 5.47 mmol) was then added and the reaction solution was stirred for 30 min at – 78°C and then 90 min at to room temperature. The mixture was evaporated to dryness, dissolved in cold pentane at –10°C and passed through a small plug of Celite®. The filtrate was pumped to dryness. **a4** was isolated without further purification as a pale yellow oil in 87% yield. **^{1}H NMR (**C_6D_6, 400.18 MHz**,** 298K**):** 0.93 and 1.27 (d, 6H, $^3J_{H\text{-}H}$ = 6.8Hz, C*H*$_3$ ^{i}Pr); 3.09 and 3.84 (sept, 1H, $^3J_{H\text{-}H}$ = 6.8 Hz , C*H* ^{i}Pr); 3.16 (s, 3H, OC*H*$_3$); 5.51 (br, 1H, B*H*); 6.81 (dd, 1H, $^4J_{H\text{-}H}$ = 2.4 Hz , $^3J_{H\text{-}H}$ = 8.4 Hz , C*H*$_{ar\text{-}3}$); 6.88 (d, 1H, $^4J_{H\text{-}H}$ = 2.4Hz , C*H*$_{ar\text{-}6}$); 7.06 (d, 1H, $^3J_{H\text{-}H}$ = 8.4 Hz , C*H*$_{ar\text{-}4}$). **^{11}B NMR (**C_6D_6**,** 128.39 MHz**,** 298K**)**: 37.7 (d, $^1J_{B\text{-}H}$ ≈ 115 Hz, B*H*). **^{13}C{^{1}H} NMR (**C_6D_6**,** 100.64 MHz**,** 298K**):** 22.05 and 27.20 (s, *C*H$_3$ iPr); 45.30 and 50.63 (s, *C*H ^{i}Pr); 54.87(s, O*C*H$_3$); 116.59 (s, *C*H$_{ar\text{-}6}$); 117.02 (s, *C*^{1}); 119.05(s, CH$_{ar\text{-}4}$); 119.54 (s, *C*≡N); 132.93 (s, C$_{ar\text{-}3}$); 138.41 (br, ipso-C^{IV}-B); 159.30 (s, ipso-C^{IV}-O). **IR: ν$_{BH}$ =** 2488 (s), 2454 (sh) cm^{-1}, ν$_{C≡N}$ = 2222 cm^{-1} (s). **HRMS** ASAP$^+$ (65°C) [M+H]$^+$ calcd for $C_{14}H_{22}BN_2O$: m/z = 245.18197. Found 245.1820 (0 ppm) calculated on the monoisotopic peak.

Compounds **a1-3** were crystallized by slow evaporation from a pentane solution.

Compound b1

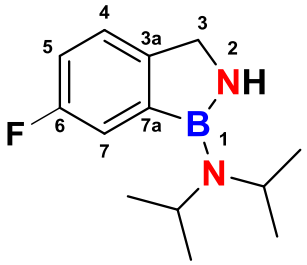

General procedure: In a Fisher-Porter bottle, the ruthenium complex $[RuH_2(\eta^2\text{-}H_2)_2(PCy_3)_2]$ (**1**) (29 mg, 0.043 mmol, 5 mol%) was added under stirring to a pentane solution (5 mL) of compound **a1** (200 mg, 0.861 mmol). The solution turned dark red and was pressurized with 1 bar(g) of dihydrogen for 5 hours. The mixture was evaporated to dryness and the crude was purified by Kügelrohr distillation (140 °C/0.01 mm Hg). Compound **b1** was isolated as a white solid in 50% yield. **^{1}H NMR (**C_6D_6, 400.18 MHz**,** 298K**):** 1.07 (d, 12H, $^3J_{H\text{-}H}$ = 6.8 Hz, C*H*$_3$ ^{i}Pr); 2.84 (s, 1H, N*H*); 3.62 (br, 2H, C*H* ^{i}Pr); 3.91 (s, 2H, C*H*$_2$); 6.97 (m, 2H, C*H*$_{ar\text{-}4}$ and C*H*$_{ar\text{-}5}$); 7.69 (m, 1H, C*H*$_{ar\text{-}7}$). **^{13}C{^{1}H} NMR (**C_6D_6**,** 100.64 MHz**,** 298K**):** 23.04 (s, *C*H$_3$ ^{i}Pr); 46.25 (s, *C*H ^{i}Pr); 50.14 (s, *C*H$_2$); 115.11 (d, $^2J_{C\text{-}F}$ = 22.8 Hz, *C*H$_{ar\text{-}5}$); 117.60 (d, $^2J_{C\text{-}F}$ = 20.3Hz, *C*H$_{ar\text{-}7}$); 123.92 (d, $^3J_{C\text{-}F}$ = 8 Hz, *C*H$_{ar\text{-}4}$); 141.85 (br, ipso-*C*^{IV}-B); 147.35 (d, $^4J_{C\text{-}F}$ = 2 Hz, *C*^{IV}-CH$_2$); 162.55 (d, $^1J_{C\text{-}F}$ = 239 Hz, ipso-C^{IV}-F). **^{11}B NMR (**C_6D_6**,** 128.39 MHz**,** 298K**)**: 30.1 (s). **^{19}F NMR** (C_6D_6**,** 376.51 MHz**,** 298K**):** −118.23 (q) **IR: ν** $_{N-H\ (solid)}$ = 3496 cm^{-1} **ν**$_{N-H\ (toluene)}$ = 3482 cm^{-1}. **HRMS** ASAP$^+$ (100°C) $[M+H]^+$ calcd for $C_{13}H_{21}BN_2F$: m/z = 235.17763. Found 235.1778 (1 ppm) calculated on the monoisotopic peak.

Compound b2

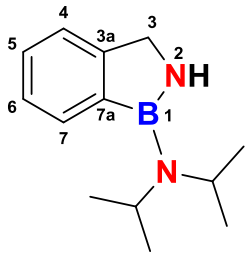

The general procedure described for **b1** was followed by using **a2** (200 mg, 0.934 mmol). The crude was purified by Kügelrohr distillation (130°C/0.01 mm Hg) and **b2** was isolated as a white solid in 82 % yield. **^{1}H NMR (**C_6D_6, 400.18 MHz**,** 298K**):** 1.15 (d, 12H, $^3J_{H\text{-}H}$ = 6.8 Hz, CH$_3$ ^{i}Pr); 2.86 (s, 1H, N*H*); 3.78 (sept, 2H, $^3J_{H\text{-}H}$ = 6.8 Hz, CH ^{i}Pr); 4.06 (s, 2H, CH$_2$); 7.28

(m, 3H, C*H*$_{ar-4,}$ C*H*$_{ar-5}$ and C*H*$_{ar-7}$); 7.92 (m, 1H, C*H*$_{ar-6}$). **^{11}B NMR (**C_6D_6**,** 128.39 MHz**,** 298K**)**: 30.6 (s). **^{13}C{^{1}H} NMR (**C_6D_6**,** 100.64 MHz**,** 298K**):** 23.18 (s, *C*H$_3$ ^{i}Pr); 46.29 (s, *C*H ^{i}Pr); 50.79 (s, *C*H$_2$); 122.89 (s, *C*H$_{ar-4}$); 126.14 (s, *C*H$_{ar-5}$); 130.96 (s, *C*H$_{ar-7}$); 131.54 (s, *C*H$_{ar-6}$); 139.19 (br, ipso-*C*^{IV}-B); 152.26 (s, *C*^{IV}-CH$_2$). **IR: ν** $_{N–H\ (solid)}$ = 3480 cm^{-1} **ν**$_{N–H\ (toluene)}$ = 3486 cm^{-1}. **HRMS** DCI [M+H]$^+$ calcd for $C_{13}H_{22}BN_2$: m/z=217.1879. Found 217.1875 (2 ppm) calculated from the mono-isotopic peak.

Compound b3

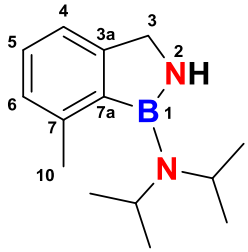

The general procedure described for **b1** was followed by using **a3** (200 mg, 0.877 mmol). The crude was purified by Kügelrohr distillation (140°C/0.01 mm Hg) and **b3** was isolated as a white solid in 57 % yield. **^{1}H NMR (**C_6D_6, 400.18 MHz**,** 298K**):** 1.16 (d, 12H, $^{3}J_{H-H}$ = 6.8 Hz, C*H*$_3$ ^{i}Pr); 2.55 (s, 3H, C*H*$_3$ Me); 3.18 (s, 1H, N*H*); 3.77 (sept, 2H, $^{3}J_{H-H}$ = 6.8 Hz, C*H* ^{i}Pr); 4.08 (s, 2H, C*H*$_2$); 7.11 (m, 2H, C*H*$_{ar}$); 7.25 (t, 1H, C*H*$_{ar}$). **^{11}B NMR (**C_6D_6**,** 128.39 MHz**,** 298K**)**: 32.3 (s). **^{13}C{^{1}H} NMR (**C_6D_6**,** 100.64 MHz**,** 298K**):** 23.44 (s, *C*H$_3$ ^{i}Pr); 24.47 (s, *C*H$_3$ Me); 46.37 (s, *C*H ^{i}Pr); 50.28 (s, *C*H$_2$); 120.00 (s, *C*H$_{ar-4}$); 127.82 (s, *C*H$_{ar-5}$); 128.84(s, *C*H$_{ar-6}$); 140.16 (s, *C*^{7}); 152.51 (s, *C*^{IV}-*C*H$_2$). **IR: ν** $_{N–H\ (solid)}$ = 3481cm^{-1} **ν**$_{N–H\ (toluene)}$ = 3496 cm^{-1}. **HRMS** ASAP$^+$ (50°C) [M+H]$^+$ calcd for $C_{14}H_{24}BN_2$: m/z=231.2027. Found 231.2028 (0 ppm), calculated on the monoisotopic peak.

Compound b4

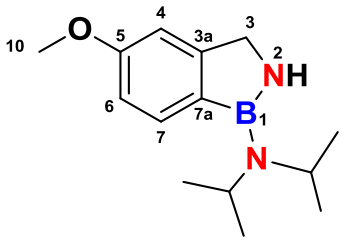

The general procedure described for **b1** was followed by using **a4** (200 mg, 0.820 mmol). The crude was purified by Kügelrohr distillation (140°C/0.01 mm Hg) and **b4** was isolated as a white solid in 54 % yield. **^{1}H NMR (**C_7D_8, 400.18 MHz**,** 298K**):** 1.16 (d, 12H, C*H*$_3$ ^{i}Pr); 2.78 (s, 1H,

N*H*); 3.42 (s, 3H, OC*H*$_3$); 3.75 (sept, 2H, C*H* ^{i}Pr); 4.04 (s, 2H, CH_2); 6.79 (m, 1H, C*H*$_{ar\text{-}4}$); 6.85 (dd, 1H, C*H*$_{ar\text{-}6}$); 7.74(d, 1H, C*H*$_{ar\text{-}7}$). **^{11}B NMR (**C_7D_8**,** 128.39 MHz**,** 298K**)**: 30.5 (s). **^{13}C{^{1}H} NMR (**C_7D_8**,** 100.64 MHz**,** 298K**):** 23.23 (s, *C*H$_3$ ^{i}Pr); 46.32 (s, *C*H ^{i}Pr); 50.28 (s, *C*H_2); 54.61 (s, O*C*H_3); 107.94 (s, *C*H$_{ar\text{-}4}$); 112.85 (s, *C*H$_{ar\text{-}6}$); 132.32 (s, *C*H$_{ar\text{-}7}$); 154.32 (s, *C*^{IV}-CH_2); 160.58 (s, *C*^{IV}-OMe)**.** **IR: ν** $_{N–H\ (solid)}$ = 3472 cm-1 **ν**$_{N–H\ (toluene)}$ = 3486 cm^{-1}. **HRMS** ASAP$^+$ (65°C) $[M+H]^+$ calcd for $C_{14}H_{24}BN_2O$: m/z = 247.19762. Found 247.1979 (1 ppm) calculated on the monoisotopic peak.

Compounds **b1-4** were crystallized by slow evaporation from a pentane solution.

Experimental section chapter 3

Catalytic procedures

Standard catalytic conditions in Fisher-Porter bottles:

a2 (100 mg, 0.467 mmol) was placed in a Fisher-Porter bottle (20 mL) and solubilized in pentane (1 mL). 5 mol% of complex **I** (15 mg, 0.023 mmol) or complex **II** (14 mg, 0.023 mmol) was added with 1.5 mL of pentane**.** After 4 min, argon was rapidly removed under vacuum and the bottle was pressurized with H_2 (1 bar(g)) along with stirring (450 rpm). To monitor the reaction, the reactive media was sampled under argon and placed into a NMR tube containing 0.25 mL of deuterated benzene. The tube was frozen in liquid nitrogen if necessary.

Standard catalytic conditions in NMR tubes for high pressure:

Deuterated toluene solutions of the ruthenium precursor **I** (8 mg, 10 mol%) and of the benzonitrile borane **a2** (26 mg; 0.12 mmol) were introduced, at room temperature, into a NMR tube for high pressure without shaking. Argon was rapidly removed under vacuum, and the tube was pressurized with 1 or 2 bar(g) of H_2. The mixture was immediately frozen in liquid nitrogen before analysis.

Stoichiometric conditions for variable temperature NMR experiments:

Complex **I** (12 mg; 0.018 mmol) was charged in a NMR tube for high pressure containing deuterated toluene (0.2 mL) and maintained at – 80°C. A cold solution of **a2** (8.0 mg; 0.036 mmol) in deuterated toluene (0.5 mL) was added at once. The tube was directly inserted in the NMR spectrometer set at the desired temperature.

Complex I

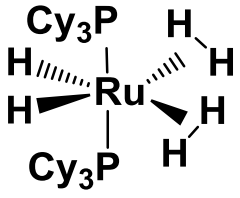

Ru(COD)(COT) (1.59 g; 5.03 mmol) and tricyclohexylphosphine (2.73 g; 9.73 mmol) were dissolved in 20 mL of pentane. The mixture was pressurized with 3 bar(g) of dihydrogen for two hours. A white solid precipitated. The solution was filtered off and the solid washed with

pentane. The ruthenium complex was recovered in 90% yield. **^{1}H NMR (**C_7D_8, 400.18 MHz**,** 298K**):** – 7.9 (pt, 6H, $^2J_{P-H}$ = 7.3Hz, hydrides), 1.23 - 2.13 (m, 66H, Cy); **^{31}P{^{1}H} NMR (**C_7D_8, 161.99 MHz**,** 298K**):** 76.43 (s)

Complex I-a

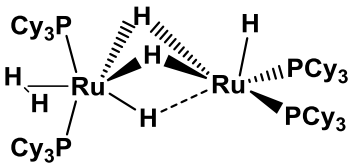

$RuH_2(H_2)_2(PCy_3)_2$ (80 mg; 0.12 mmol) was dissolved into 10 mL of THF and stirred overnight. The solution turned red. The mixture was cooled down at – 40°C to obtain a red precipitate. The solution was filtered off and the red powder dried under vacuum. **^{1}H NMR (**C_7D_8, 400.18 MHz**,** 298K**):** – 12.60 (br), 0.9 - 2.45 (m, Cy). **^{31}P{^{1}H} NMR (**C_7D_8, 161.99 MHz**,** 298K**)**: 75.6 (br)

Complex I-b

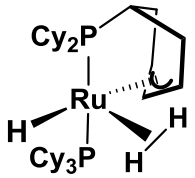

Tert-butylethylene (115 µL; 0.892 mmol) was added to a suspension of $RuH_2(H_2)_2(PCy_3)_2$ (220 mg; 0.329 mmol) in 30 mL of pentane. The mixture was stirred for 30 min. A white precipitate formed. The mixture was filtered and the solid was washed with pentane to be recovered as a white powder in 73 % yield. **^{1}H NMR (**THF d_8, 400.18 MHz**,** 298K**):** – 8.14 (t, 3H, J_{P-H} = 16 Hz); 0.87 - 2.40 (m, 63H, Cy); 3.98 (s, 2H, η^3-C_6H_8); 4.60 (q, 1H, central η^3-C_6H_8). **^{31}P{^{1}H} NMR (**THF d_8, 161.99 MHz**,** 298K**)**: 60.82 (d, J_{P-P} = 264 Hz); 109.56 (d; J_{P-P} = 264 Hz)

Complex I-c

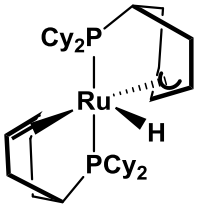

Tert-butylethylene (100 µL; 0.775 mmol) was added to a suspension of $RuH_2(H_2)_2(PCy_3)_2$ (100 mg ; 0.150 mmol) in 2.5 mL of pentane. After 2.5 hours, the mixture was filtered and the solid was washed 3 times with 2 mL of diethylether. The product was recovered as a pink powder in 75 % yield. **^{1}H NMR (**C_6D_6, 400.18 MHz**,** 298K**):** – 8.04 (dd, 1H, J_{P-H} = 24 Hz); 0.87 – 3.19 (m, 61H, Cy); 3.35 (m, 1H, η^3-C_6H_8); 3.81 (m, 1H, η^2-C_6H_9); 4.01 (m, 1H, η^3-C_6H_8); 4.38 (m, 1H, η^2-C_6H_9); 5.05 (m, 1H, η^3-C_6H_8). **^{31}P{^{1}H} NMR (**C_6D_6, 161.99 MHz**,** 298K**)**: 51.85 (d ; J_{P-P}= 267 Hz); 84.69 (d ; J_{P-P}= 267 Hz).

Complex I-e

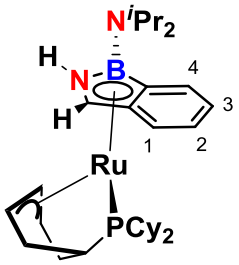

$[RuH_3\{(\eta^3\text{-}C_6H_8)PCy_2\}(PCy_3)]$ **I-b** (148 mg; 0.224 mmol) and aryl(cyano)(aminoborane) **a2** (96 mg; 0.45 mmol) were dissolved in 4 mL of THF. The solution instantly turned dark red. After 2 hours of stirring at room temperature, the yellow-brown solution was evaporated under vacuum. A mixture of ether and acetonitrile was used to afford a yellow precipitate. The solution was filtered off and the solid further dried under vacuum. The solid was recovered in 45% yield. The same reaction performed in toluene or pentane led to the same result. **^{1}H NMR (**C_7D_8, 500.33 MHz**,** 298K**):** 1.04 – 2.50 (Cy); 1.06 (d, $^3J_{H-H}$ = 6.8 Hz, C*H*$_3$ ^{i}Pr); 1.20 (d, $^3J_{H-H}$ = 6.8 Hz, C*H*$_3$ ^{i}Pr); 1.44 (η^3-C_6H_8); 3.46 (1H, N*H*); 3.58 (sept, 2H, $^3J_{H-H}$ = 6.8 Hz, C*H* ^{i}Pr); 3.76 (t, 1*H*, η^3-C_6H_8); 3.91 (br, 1H, η^3-C_6H_8); 5.90 (pt, 1H, NC*H*C, $J_{(P-H)}$= 4Hz $J_{(N-H/C-H)}$ = 2.8 Hz); 6.69 (m, 1H, H_{ar-3}); 6.81 (m, 1H, H_{ar-2}); 7.16 (m, 1H, H_{ar-4}); 7.43 (d, 1H, $^3J_{H-H}$ = 7.4 Hz, H_{ar-1}). **^{13}C{^{1}H3 NMR (**C_6D_6, 125.82 MHz**,** 298K**):** 23.04 (s, *C*H$_3$ ^{i}Pr); 24.08 (s, *C*H$_3$ ^{i}Pr); 26.89, 26.91, 28.32, 28.34, 28.40, 28.52, 30.30, 30.34, 30.36, 30.76, 32.06, 32.66 (12 *C*H$_2$ Cy); 37.13, 38.18,

39.09 ($^1J_{P-H}$ = 23, 17 and 14 Hz, respectively, 2 *C*H Cy); 44.74 (s, η^3-*C*$_6$H$_8$); 45.97 (s, *C*H ^{i}Pr); 55.10 (s, η^3-*C*$_6$H$_8$); 64.90 (s, N*C*H); 66.87 (s, η^3-*C*$_6$H$_8$); 85.4 (br, ipso-*C*^{IV}-B), 104.59 (s, ipso-C^{IV}-CH), 120.52 (*C*H$_{ar-2}$), 121.75 (*C*H$_{ar-4}$), 123.40 (*C*H$_{ar-3}$), 131.96 (*C*H$_{ar-1}$). **^{31}P{^{1}H} NMR (**C$_7$D$_8$, 202.56 MHz**,** 298K**)**: 115.2 (br). **^{11}B NMR (**C$_7$D$_8$**,** 128.39 MHz**,** 298K**)**: 17 (br)

Complex I-f

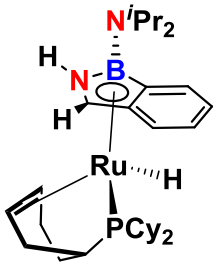

Complex **I-e** (10 -15 mg) was charged in a NMR tube for high pressure and dissolved in deuterated toluene. The tube was pressurized with 1 or 2 bar(g) of H_2. The reaction was monitored on a 500 MHz NMR spectrometer. The compound was characterized *in situ*. **^{1}H NMR** (C$_6$D$_6$, 500.33 MHz**,** 298K**):** – 17.20 (d, 1H, J_{P-H} = 33.5 Hz, Ru*H*); 3.43 (m, 1H, η^2-C$_6$*H*$_9$); 3.64 (br, 1H, N*H*); 4.43 (m, 1H, η^2-C$_6$*H*$_9$); 5.83 (d, 1H, $J_{(N-H/C-H)}$ = 1.8 Hz, NC*H*C); 6.83 (m, 1H, *H*$_{ar}$); 6.88 (m, 1H, *H*$_{ar}$); 7.45 (m, 1H, *H*$_{ar}$); 7.48 (m, 1H, *H*$_{ar}$). **^{13}C NMR (**C$_6$D$_6$, 125.82 MHz**,** 298K**)**: 53.28 (η^2-*C*$_6$H$_9$); 55.66 (η^2-*C*$_6$H$_9$); 59.22 (N*C*H); 119.2, 122.2, 126.07 (*C*H$_{ar}$). **^{31}P{^{1}H} NMR** (C$_7$D$_8$, 202.56 MHz**,** 298K): 96.7 (br). **^{31}P NMR{^{1}H cyclohexyl} :** 96.7 (d, J_{P-H} = 33.5 Hz)

Complex I-g

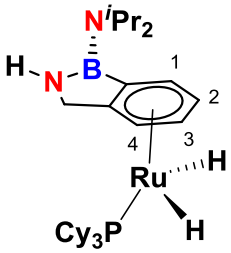

Complex **I-e** (10mg) was charged in a NMR tube for high pressure and dissolved in deuterated toluene. The tube was pressurized with 1 or 2 bar(g) of H_2. The reaction was monitored using a 500 MHz NMR spectrometer. This compound was observed at the end of the hydrogenation reaction and persisted. **^{1}H NMR** (C$_6$D$_6$, 500.33 MHz**,** 298K**):** – 10.87 (AB, J_{P-}

$_H$ = 43Hz, J_{H-H} = 6.8Hz, 1H, hydride); – 10.89 (AB, J_{P-H} = 43Hz, J_{H-H} = 6.8Hz, 1H, hydride); 2.50 (br, 1*H*, NH); 3.98 (d, J_{H-H} = 14 Hz, 1H, C*H*$_2$); 4.07 (dd, J_{H-H} = 14 Hz, J_{N-H} = 1.5 Hz, 1H, C*H*$_2$); 5.11 (t, 1H, J_{H-H} = 5 Hz, H_{ar-2} or H_{ar-3}); 5.36 (t, 1H, J_{H-H} = 5 Hz, H_{ar-2} or H_{ar-3}); 5.55 (d, 1H, J_{H-H} = 6 Hz, H_{ar-1} or H_{ar-4}); 5.90 (d, 1H, J_{H-H} = 6 Hz, H_{ar-1} or H_{ar-4}). **^{13}C NMR** (C_7D_8, 125.82 MHz**,** 298K): 50.90 (N*C*H$_2$); 79.00 (*C*H$_{ar-1}$ or *C*H$_{ar-4}$); 82.00 (*C*H$_{ar-2}$ or *C*H$_{ar-3}$); 84.61 (*C*H$_{ar-2}$ or *C*H$_{ar-3}$); 85.52 (*C*H$_{ar-1}$ or *C*H$_{ar-4}$). **^{31}P {^{1}H} NMR** (C_7D_8, 202.56 MHz**,** 298K): 78.17 (br). **^{31}P NMR{^{1}H cyclohexyl}** (C_7D_8, 202.56 MHz**,** 298K): 78.17 (t, J_{P-H} = 43Hz).

Complex I-h

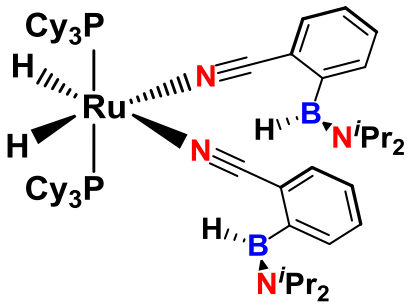

Complex **I** $RuH_2(H_2)_2(PCy_3)_2$ (12 mg; 0.018 mmol) was placed in a NMR tube for high pressure and cooled down to – 80°C. In a 5 mL reaction flask, aryl(cyano)(aminoborane) **a2** (8.0 mg; 0.036 mmol) was solubilized in 0.6 mL of C_7D_8 and cooled down to – 60°C. The solution of **a2** was transferred in the NMR tube through a cannula and kept at – 80°C. The NMR tube was quickly shaken before being inserted into the NMR apparatus set at – 80°C. Complex **I-h** was observed as a unique complex at this temperature but was characterized at – 40°C. **^{1}H NMR** (C_7D_8, 500.33 MHz**,** 233K)**:** – 14.17 (t, 2H, Hydrides, J_{P-H} = 24 Hz); 1.01 (d, $^3J_{H-H}$ = 6 Hz, CH_3 ^{i}Pr); 1.45 (d, $^3J_{H-H}$ = 6 Hz, CH_3 ^{i}Pr); 3.06 (sept, CH ^{i}Pr); 4.05 (sept, CH ^{i}Pr); 5.70 (br, B–H); 7.06 (H_{ar}), 7.09 (H_{ar}), 7.25 (d, 2H, $^3J_{H-H}$ = 8 Hz, H_{ar}), 7.80 (d, 2H, $^3J_{H-H}$ = 8 Hz, H_{ar}).**^{13}C NMR** (C_7D_8, 125.82 MHz**,** 233K): 23.3 (CH_3 ^{i}Pr); 27.3 (CH_3 ^{i}Pr); 44.88 (CH ^{i}Pr); 45.24 (CH ^{i}Pr); 120.3 (C≡N); 121.03 (ipso-*C*^{IV}- C≡N); 128.3, 132.22, 133.2 (CH_{ar}); 143.80 (ipso-*C*^{IV}-B).**^{31}P{^{1}H} NMR** (C_7D_8, 202.56 MHz**,** 233K): 64.12 (s). **^{31}P{^{1}H cyclohexyl} NMR** (C_7D_8, 202.56 MHz**,** 233K)**:** 64.12(t, J_{P-H} = 24 Hz).

Complex I-i

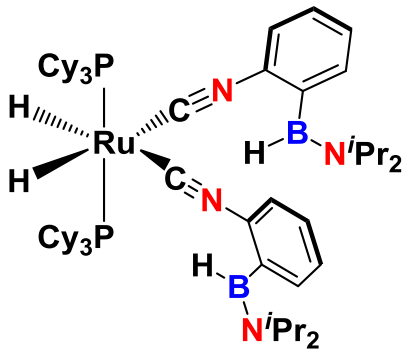

nBuLi 1.6 M in hexanes (95 µL; 0.15 mmol) was added dropwise to a THF (2.5 mL) solution of 2-bromophenyl isocyanide (27 mg; 0.15 mmol) at – 78°C. Chloro(diisopropylamino)borane (22 mg; 0.15 mmol) was then added at once. The reaction mixture was stirred while warming up until room temperature for 45 minutes. A suspension of $RuH_2(H_2)_2(PCy_3)_2$ (100 mg, 0.150 mmol) in 1.5 mL of THF was transferred to the reaction mixture. After 4 hours stirring, the solvent was removed under vacuum, the powder was re-dissolved in cold pentane at – 40°C and passed through a small plug of Celite®. **^{1}H NMR (**C_6D_6, 400.18 MHz**,** 298K**):** – 8.48 (t, 1H, $J_{P\text{-}H}$ = 24 Hz), 0.9 – 2.5 (Cy), 0.98 and 1.42 (d, $^3J_{H\text{-}H}$ = 6.6 Hz, CH_3 ^{i}Pr); 3.16 and 4.07 (sept, 1H, $^3J_{H\text{-}H}$ = 6.6 Hz, CH ^{i}Pr); 5.7 (br, 1H, BH); 6.99 (m, 1H, CH_{ar}); 7.20 (m, 1H, CH_{ar}); 7.24 (m, 1H, CH_{ar}); 7.63 (m, 1H, CH_{ar}). **^{13}C{^{1}H} NMR (**C_6D_6**,** 100.64 MHz**,** 298K**):** 22.18 and 27.06 (s, CH$_3$ ^{i}Pr); 45.08 and 49.70 (s, CH ^{i}Pr); 123.97, 127.66, 128.04 and 132.06 (s, CH$_{ar}$). **^{31}P{^{1}H} NMR :** 72.35.

Experimental section chapter 4

Compound b2[1]

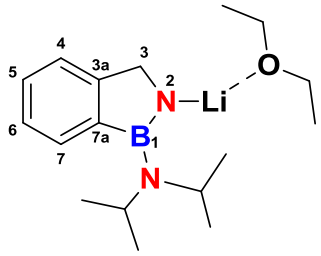

*n*BuLi 1.6 M in hexanes (610 µL; 0.976 mmol) was added dropwise to a cold (– 20°C) diethylether (1mL) solution of **b2** (200 mg, 0.925 mmol). After 10 min stirring, the solution was filtered off and the monoetherate lithium boramidinate salt **b2[1]** was isolated in 76% yield as a white solid. **^{1}H NMR (**C_7D_8, 400.18 MHz**,** 298K**):** 0.84 (t, 6H, C*H*$_3$ OEt); 1.30 (br, 12H, C*H*$_3$ ^{i}Pr); 3.09 (q, 4H, C*H*$_2$ OEt); 3.80 (br, 2H, C*H* ^{i}Pr); 4.51 (br, 2H, C*H*$_2$); 7.21 (t, 1H, $^{3}J_{H\text{-}H}$ =7.2 Hz, C*H*$_{ar\text{-}5}$); 7.29 (t, 1H, $^{3}J_{H\text{-}H}$ =7.2 Hz, C*H*$_{ar\text{-}6}$); 7.39 (br, 1H, C*H*$_{ar\text{-}4}$); 8.03 (br, 1H, C*H*$_{ar\text{-}7}$). **^{7}Li NMR** (C_7D_8, 155.53 MHz**,** 298K**):** 1.96 (s). **^{11}B NMR (**C_7D_8**,** 128.39 MHz**,** 298K**)**: 37.8 (s). **^{13}C{^{1}H} NMR (**C_7D_8**,** 100.64 MHz**,** 298K**):** 14.41 (s, *C*H$_3$ OEt); 24.28 (s, *C*H$_3$ ^{i}Pr); 46.41 (s, *C*H ^{i}Pr); 57.41 (s, *C*H$_2$N); 65.16 (s, *C*H$_2$ OEt); 122.16 (s, *C*H$_{ar\text{-}4}$); 125.48 (s, *C*H$_{ar\text{-}6}$); 126.22 (s, *C*H$_{ar\text{-}5}$); 132.13 (s, *C*H$_{ar\text{-}7}$); 142.89 (s, ipso-*C*^{IV}-B); 160.37 (s, *C*^{IV}-CH$_2$).

The same procedure could also be performed using pentane as a solvent. The reaction led to the ether-free lithium salt **b2[1']** that was as well crystallized in pentane at – 40 °C.

Compound b2[2]

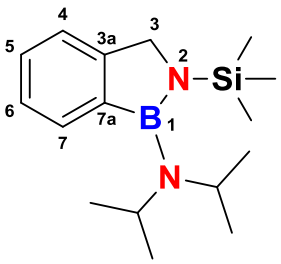

General procedure: **b2** (200 mg; 0.925 mmol) was dissolved in 1 mL of diethylether. Upon stirring at – 20°C, *n*BuLi 1.6 M in hexanes (610 µL; 0.976 mmol) was added dropwise. The reaction was left 10 min at – 20°C and then allowed to reach room temperature. A white precipitate of **b2[1]** was formed. After filtration, the solid was dissolved in 3mL of diethylether.

(chloro)(trimethyl)silane (290 µL; 2.286 mmol) was then added. After 2.30 hours stirring, LiCl was removed by filtration over celite® and the filtrate was evaporated to dryness. The resulting white oil was recovered in 76% yield. **^{1}H NMR (**C_6D_6, 400.18 MHz**,** 298K**):** 0.29 (s, 9H, Si*Me*$_3$); 1.31 (d, 12H, $^{3}J_{H\text{-}H}$ = 7 Hz, C*H*$_3$ ^{i}Pr); 4.01 (sept, 2H, $^{3}J_{H\text{-}H}$ = 7 Hz, C*H* ^{i}Pr); 4.19 (s, 2H, C*H*$_2$); 7.27 (m, 3H, C*H*$_{ar}$); 8.04 (m, 1H, C*H*$_{ar}$). **^{11}B NMR (**C_6D_6**,** 128.39 MHz**,** 298K**)**: 34.7 (s). **^{13}C{^{1}H} NMR (**C_6D_6**,** 100.64 MHz**,** 298K**):** 2.28 (s, Si*Me*$_3$); 24.73 (s, *C*H$_3$ ^{i}Pr); 48.50 (s, *C*H ^{i}Pr); 55.35 (s, *C*H$_2$); 122.41 (s, *C*H$_{ar}$); 125.88 (s, *C*H$_{ar}$); 128.14 (s, *C*H$_{ar}$); 133.06 (s, *C*H$_{ar}$); 139.83 (s, ipso-*C*^{IV}-B); 153.51 (s, ipso-*C*^{IV}-CH$_2$). **^{29}Si NMR DEPT (**C_6D_6**,** 79.51 MHz**,** 298K**):** 3.63 (s). **HRMS** ASAP^{+} (75°C) $[M+H]^{+}$ calcd for $C_{16}H_{30}BN_2Si$: m/z = 289.22658. Found 289.2266 (0 ppm) calculated on the monoisotopic peak.

Compound b2^{3}

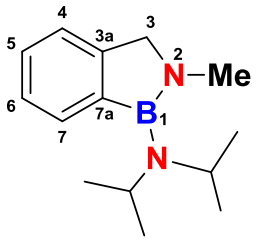

The general procedure described for **b2^{2}** was followed by using MeI (25 µL; 0.41 mmol). The reaction was stirred for 12h. The final compound was recovered as a white solid in 75% yield. Compound **b2^{3}** was crystallized in pentane at – 40°C. **^{1}H NMR** (C_6D_6, 400.18 MHz, 298K): 1.28 (d, 12H, $^{3}J_{H\text{-}H}$ = 6.9 Hz, C*H*$_3$ ^{i}Pr); 2.88 (s, 3H, NC*H*$_3$); 3.82 (sept, 2H, $^{3}J_{H\text{-}H}$ = 6.9 Hz, C*H* ^{i}Pr); 3.92 (s, 2H, C*H*$_2$); 7.17 (m, 1H, C*H*$_{ar\text{-}4}$); 7.28 (m, 2H, C*H*$_{5\text{-}ar}$ and C*H*$_{ar\text{-}6}$); 7.99 (d, 1H, $^{3}J_{H\text{-}H}$ = 6.8 Hz, C*H*$_{ar\text{-}7}$). **^{11}B NMR** (C_6D_6, 128.38 MHz, 298K): 31.0 (s). **^{13}C{^{1}H} NMR** (C_6D_6, 100.64 MHz, 298K): 24.31 (s, *C*H$_3$ ^{i}Pr); 36.57(s, NCH$_3$); 46.48 (s, *C*H ^{i}Pr); 60.98 (s, *C*H$_2$); 122.07 (s, *C*$_{ar\text{-}4}$); 126.09 and 127.59 (s, *C*$_{ar\text{-}5}$ and *C*$_{ar\text{-}6}$); 132.11 (s, *C*$_{ar\text{-}7}$); 140.32 (s, ipso-*C*^{IV}-B); 150.33 (s, ipso-*C*^{IV}-CH$_2$).

Compound b2^{4}

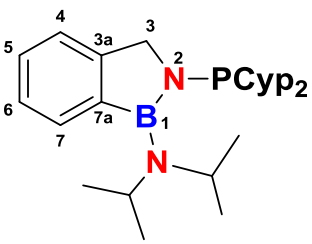

The general procedure described for **b2²** was followed by using chloro(dicyclopentyl)phosphine (Cyp_2PCl) (82 mg; 0.40 mmol). The reaction was stirred for 1h. The final compound was recovered as a white solid in 76% yield. **^{1}H NMR** (C_6D_6, 400.13 MHz, 298K): 1.1-2.1 (m, *H* Cyp); 1.39 (d, 12H, $^{3}J_{H-H}$ = 6.6 Hz, C*H*$_3$ ^{i}Pr); 4.13 (s, 2H, C*H*$_2$-N); 4.36 (sept, 2H, $^{3}J_{H-H}$ = 6.6 Hz, C*H* ^{i}Pr); 7.24 (m, 3H, C*H*$_{ar}$); 8.07 (m, 1H, C*H*$_{ar}$). **^{11}B NMR** (C_6D_6, 128.38 MHz, 298K): 34.6 (s). **^{13}C{^{1}H} NMR** (C_6D_6, 100.62 MHz, 298K): 24.16 (d, *C*H$_3$ ^{i}Pr, J_{P-C} = 2Hz); 26.13 (d, C_{cyp}, J_{P-C} = 7Hz); 27.40 (d, C_{cyp}, J_{P-C} = 7 Hz); 29.89 (d, C_{cyp}, J_{P-C}=30Hz); 26.13 (d, C_{cyp}, J_{P-C} = 7Hz); 30.77 (d, C_{cyp}, J_{P-C} = 13Hz); 38.70 (d, C_{cyp}, J_{P-C} = 17 Hz); 47.43 (d, *C*H ^{i}Pr , J_{P-C} = 13Hz); 52.69 (d, $C^{3}H_2$, J_{P-C} = 7Hz); 122.28 , 125.93 , 128.14 and 133.69 (s, *C*H$_{ar}$); 152.31(s, ipso-*C*^{IV}-CH$_2$). The ipso-*C*^{IV}-B was not observed. **^{31}P{^{1}H} NMR** (C_6D_6, 161.99 MHz, 298K): 58.9 (s). HRMS DCI $[M+H]^+$ calcd for $C_{23}H_{39}BN_2P$: m/z = 385.2944. Found 385.2957 (3.4 ppm), calculated on the monoisotopic peak.

Compound b2⁵

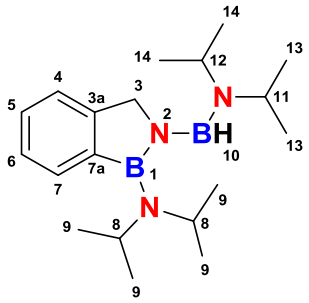

The general procedure described for **b2²** was followed by using chloro(diisopropyl)aminoborane (58 mg; 0.40 mmol). The reaction was stirred for 12 h. The final compound was recovered as a white solid in 65% yield. **^{1}H{^{11}B} NMR (**C_6D_6, 400.18 MHz**,** 298K**):** 0.88-1.30 (br d, 12H, (C*H*$_3$ ^{i}Pr^{13})); 1.37 (d, 12H, $^{3}J_{H-H}$ = 7.2 Hz, (C*H*$_3$ ^{i}Pr^{9})); 3.01 (br s, H, (C*H* ^{i}Pr^{11})); 3.88 (sept, 2H, $^{3}J_{H-H}$ = 7.2 Hz, (C*H* ^{i}Pr^{8})); 4.10 (br s, H, (C*H* ^{i}Pr^{12})) 4.36 (s, 2H, C*H*$_2$); 4.93 (s, 1H, B*H*); 7.26 (m, 3H, C*H*$_{ar}$); 7.28 (m, H, C*H*$_{ar}$); 8.13 (d, 1H, $^{3}J_{H-H}$ = 6.8 Hz, C*H*$_{ar}$). **^{11}B NMR (**C_6D_6, 96.29 MHz**,** 298K**)**: 36.2 (s, *B*^{1}); 32.4 (d, $^{1}J_{B-H}$ = 110 Hz, *B*^{10}). **^{11}B{^{1}H} NMR (**C_6D_6, 96.29 MHz**,** 298K**)**: 36.2 (s, *B*^{1}); 32.4 (s, *B*^{10}). **^{13}C{^{1}H} NMR (**C_6D_6**,** 100.64 MHz**,** 298K**):** 21.9 (br s, *(C*H$_3$ ^{i}Pr^{13},)); 23.87 (s, (C*H*$_3$ ^{i}Pr^{9})); 27.0 (br s, (C*H*$_3$ ^{i}Pr^{14})); 43.3 (br s, (*C*H ^{i}Pr^{11})); 47.41 (s, (*C*H ^{i}Pr^{8})); 54.11(s, *C*^{3}H$_2$); 122.26 (s, *C*H$_{ar}$); 125.49 (s, *C*H$_{ar}$); 127.77 (s, *C*H$_{ar}$); 133.03(s *C*H$_{ar}$); 138.50 (s, ipso-*C*^{IV}-B); 153.65 (s, ipso-*C*^{IV}-CH$_2$). **IR: ν_{BH}** = 2482cm^{-1}. **HRMS** ASAP$^+$ (65°C) $[M+H]^+$ calcd for $C_{19}H_{36}B_2N_3$: m/z = 328.30898. Found 328.3094 (1 ppm) calculated on the monoisotopic peak.

Compound b2[6]

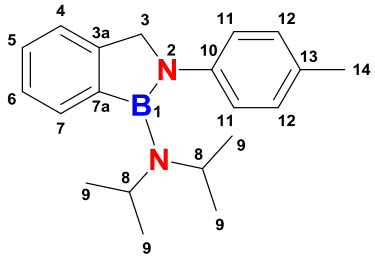

A toluene solution (1 mL) of lithium salt **b2[2]** (55 mg, 0.18 mmol) was first added to a toluene solution (1 mL) of **[1,3-bis(2,6-diisopropylphenyl)imidazol-2-ylidene](3-chloropyridyl)-palladium(II) dichloride (**PEPPSI™-IPr) (2.5 mg, 0.0037 mmol) at room temperature. The solution turned yellow and solid 4-bromotoluene (31 mg, 0.18 mmol) was then added. The resulting solution was stirred for 2.5 h and a white precipitate formed. Toluene was evaporated and replaced by pentane. The suspension was passed through a small plug of Celite® and the filtrate dried in vacuo. Compound **b2[6]** was isolated as a beige solid in 94% yield. **^{1}H NMR** (C_7D_8, 400.18 MHz**,** 298K)**:** 1.20 (d, 12H, $^{3}J_{H\text{-}H}$ = 6.8 Hz, CH_3 ^{i}Pr); 2.15 (s, 3H, CH_3[14]); 3.72 (sept, 2H, $^{3}J_{H\text{-}H}$ = 6.8 Hz, CH ^{i}Pr); 4.34 (s, 2H, CH_2); 6.96 and 7.05 (d, 2H, $^{3}J_{H\text{-}H}$ = 12Hz, C$H_{ar\text{-}11}$ and C$H_{ar\text{-}12}$); 7.10 (m, 1H, C$H_{ar\text{-}4}$); 7.23 (m, 1H, C$H_{ar\text{-}5}$); 7.28 (m, 1H, C$H_{ar\text{-}6}$); 8.06 (d, 1H, $^{3}J_{H\text{-}H}$ = 8Hz, C$H_{ar\text{-}7}$). **^{11}B NMR (**C_7D_8**,** 128.39 MHz**,** 298K**)**: 31.3(s). **^{13}C{^{1}H} NMR (**C_7D_8**,** 100.6 MHz**,** 298K**):** 20.91 (s, $C^{14}H_3$); 24.04 (s, CH_3 ^{i}Pr); 46.79 (s, CH ^{i}Pr); 61.22 (s, CH_2); 122.41 (s, $CH_{ar\text{-}4}$); 126.04 (s, $CH_{ar\text{-}11}$); 126.06 (s,$CH_{ar\text{-}6}$); 128.00 (s, $CH_{ar\text{-}5}$); 129.66 (s, $CH_{ar\text{-}12}$); 133.10 (s, $CH_{ar\text{-}13}$); 133.19 (s, $CH_{ar\text{-}7}$); 147.31 (s, ipso-C^{IV}-N); 150.50 (s, ipso-C^{IV}-CH_2). **HRMS** ASAP^{+} (80°C) $[M+H]^{+}$ calcd for $C_{20}H_{28}BN_2$: m/z = 307.234. Found 307.2347 (2 ppm) calculated on the monoisotopic peak.

Compound b2[7]

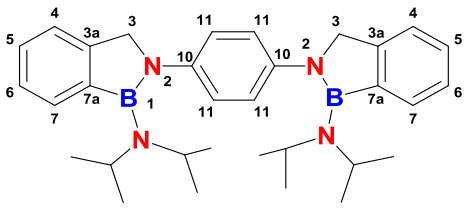

The procedure described for **b2[6]** was followed by using 1,4-dibromotoluene (20 mg, 0.085 mmol) and (5 mg, 0.007 mmol) of **(**PEPPSI™-IPr) catalyst precursor. Compound **b2[7]** was isolated as a pale yellow solid in 88% yield. **^{1}H NMR (**C_7D_8, 400.18 MHz**,** 298K**):** 1.27 (d, 12H,

$^{3}J_{H\text{-}H}$ = 6.8 Hz, C*H*$_3$ ^{i}Pr); 3.81 (sept, 2H, $^{3}J_{H\text{-}H}$ = 6.8 Hz, C*H* ^{i}Pr); 4.40 (s, 2H, C*H*$_2$); 7.09 (s, 2H, C*H*$_{ar\text{-}11}$); 7.14 (m, 1H, C*H*$_{ar\text{-}4}$); 7.28 (m, 1H, C*H*$_{ar\text{-}5}$); 7.34 (m, 1H, C*H*$_{ar\text{-}6}$); 8.17 (m, 1H, CH$_{ar\text{-}7}$). **^{11}B NMR (**C_7D_8**,** 128.39 MHz**,** 298K**)**: 31.7 (s). **^{13}C{^{1}H} NMR (**C_6D_6**,** 100.6 MHz**,** 298K**):** 24.15 (s, *C*H$_3$ ^{i}Pr); 46.83 (s, *C*H ^{i}Pr); 61.39 (s, *C*H$_2$); 122.47 (s, *C*H$_{ar\text{-}4}$); 126.20 (s,*C*H$_{ar\text{-}6}$); 126.59 (s, *C*H$_{ar\text{-}11}$); 128.15 (s, *C*H$_{ar\text{-}5}$); 133.23 (s, *C*H$_{ar\text{-}7}$); 145.76 (s, ipso-*C*^{IV}-N); 150.45 (s, ipso-*C*^{IV}-CH$_2$).

Complexes **III**, **III-a** and **III-b** were synthesized according to the literature.[128, 183, 204] Complexes **IV** and **V** were provided by the Jones' group.

Experimental section chapter 5

Compound d1

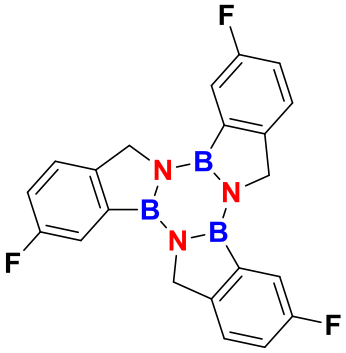

1*H*-2,1-benzazaborole **b1** (78 mg; 0.33 mmol) was placed in a sealed flask. The neat solid was heated to 130°C for 5 hours. The solid was washed once with toluene and twice with pentane. The white powder of **d1** was recovered in 82 % yield. **^{1}H NMR (**C_7D_8, 400.18 MHz**,** 298K**):** 4.38 (s, 2H, CH_2); 7.52 (m, 1H, CH_{ar}). . **^{1}H NMR (**THF d_8, 400.18 MHz**,** 298K**):** 5.01 (s, 2H, CH_2); 7.27 (m, 1H, CH_{ar}); 7.60 (m, 1H, CH_{ar}); 7.74 (m, 1H, CH_{ar}). **^{11}B NMR (**THF d_8**,** 128.39 MHz**,** 298K**)**: 35 (s). **^{19}F NMR** (C_6D_6**,** 376.51 MHz**,** 298K**):** – 118.5 (m). **^{19}F{^{1}H} NMR** (C_6D_6**,** 376.51 MHz**,** 298K**):** – 118.5 (s). **^{13}C{^{1}H} NMR (**THF d_8**,** 100.64 MHz**,** 298K**)**: 51.62 (s, CH_2); 116.41 (d, CH_{ar}, J_{C-F} = 19.5 Hz), 116.95 (d, CH_{ar}, J_{C-F} = 23.8 Hz), 124.41 (d, CH_{ar}, J_{C-F} = 6.6 Hz), 149.65 (d, ipso-C^{IV}-CH_2, $^{4}J_{C-F}$ = 2 Hz), 162.30 (d, C^{IV}-F, $^{1}J_{C-F}$ = 245 Hz). **HRMS** ASAP^{+} (165°C) $[M+H]^{+}$ calcd for $C_{21}H_{19}N_3F_3{}^{11}B_3$: m/z = 400.157. Found 400.1603 (8 ppm) calculated on the monoisotopic peak.

Compound d2

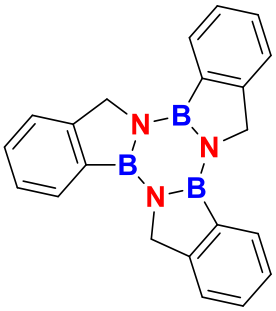

1*H*-2,1-benzazaborole **b2** (124 mg; 0.57 mmol) was refluxed in 1mL of toluene for 3 hours. At room temperature, the solution was filtered off and the remaining white solid was washed with twice 0.5 mL of pentane. The white solid was recovered in 66% yield. **^{1}H NMR (**C_7D_8, 400.18 MHz**,** 298K**):** 4.69 (s, 2H, CH_2); 7.36 (m, 3H, CH_{ar}); 7.87 (m, 1H, CH_{ar}). **^{11}B NMR**

(C_7D_8**,** 128.39 MHz**,** 298K**)**: 35.1 (s). **$^{13}C\{^1H\}$ NMR (**C_7D_8**,** 100.64 MHz**,** 298K**)**: 52.63 (s, *C*H_2); 123.3, 126.7, 129.9 and 131.4 (s, *C*H_{ar}) **HRMS** ASAP$^+$ (165°C) $[M+H]^+$ calcd for $C_{21}H_{19}N_3O_3{}^{11}B_3$: m/z = 346.18581. Found 346.18526 (2 ppm) calculated on the monoisotopic peak.

Intermediate in the formation of d3

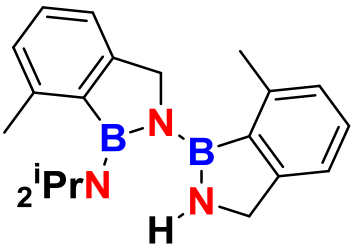

This compound was observed during the synthesis of **d3**. In the middle of the reaction, typically after 10 hours in refluxing toluene, 1*H*-2,1-benzazaborole was fully converted. However, the trimerization was not complete. The reaction mixture was filtered. The filtrate was recovered and the solvent was removed in vacuum. The intermediate species was extracted with pentane and dried to be analyzed by spectroscopy. **^1H NMR (**C_7D_8, 400.18 MHz, 298K**)**: 0.82 (d, 3H, $^3J_{H\text{-}H}$ = 6.8 Hz, CH_3 ^{i}Pr); 1.03 (d, 3H, $^3J_{H\text{-}H}$ = 6.8 Hz, CH_3 ^{i}Pr); 1.30 (d, 6H, $^3J_{H\text{-}H}$ = 6.8 Hz, CH_3 ^{i}Pr); 2.12 (s, 3H,Me); 2.27 (s, 3H,Me); 3.58 (dd, 1H, CH_2, $^2J_{H\text{-}H}$ = 13.5 Hz, $^3J_{H\text{-}H}$ = 8 Hz); 3.64 (br, 1H, CH ^{i}Pr); 3.8 (1H, N*H*); 3.81 (sept, 1H, CH ^{i}Pr, $^3J_{H\text{-}H}$ = 6.8 Hz); 4.32 (dd, 1H, CH_2, $^2J_{H\text{-}H}$ = 13.5 Hz, $^3J_{H\text{-}H}$ = 5 Hz); 4.36 (d, 1H, CH_2, $^1J_{H\text{-}H}$ = 16 Hz); 4.79 (d, 1H, CH_2, $^1J_{H\text{-}H}$ = 16 Hz); 6.88-7.17 (m, Char). **$^{11}B\{^1H\}$** NMR (C_7D_8, 128.39 MHz, 298K): 34.1 (s), 37.7 (s).

Compound d3

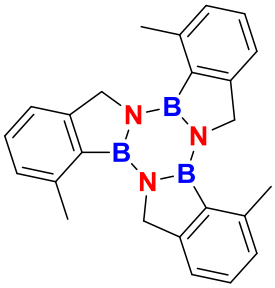

1*H*-2,1-benzazaborole **b3** (21 mg; 0.033 mmol) was refluxed in 1mL of toluene for 24 hours. At room temperature, the solution was filtered off and the remaining white solid was washed with twice 0.5 mL of pentane. The white solid was recovered in 53% yield. **^1H NMR (**C_7D_8, 400.18 MHz**,** 298K**):** 2.74 (s, 3H, *C*H_3), 4.94 (s, 2H, *C*H_2); 6.6 - 7.3 (m, *C*H_{ar}). **HRMS** ASAP$^+$

(180°C) $[M+H]^+$ calcd for $C_{24}H_{25}N_3{}^{11}B_3$: m/z = 388.23221. Found 388.2328 (2 ppm) calculated on the monoisotopic peak.

Compound d4

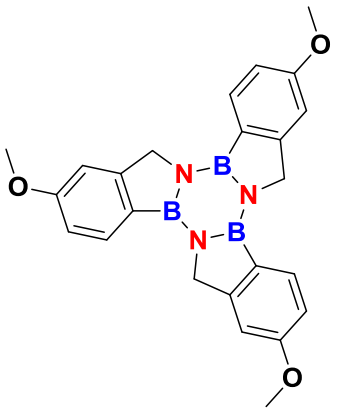

1*H*-2,1-benzazaborole **b4** (104 mg; 0.141 mmol) was refluxed in 1mL of toluene for 3 hours. At room temperature, the solution was filtered off and the remaining white solid was washed with twice 0.5 mL of pentane. The white solid was recovered in 85% yield. **^{1}H NMR (**C_7D_8, 400.18 MHz**,** 298K**):** 3.50 (s, 3H, C*H*$_3$), 4.74 (s, 2H, C*H*$_2$); 6.6 – 8.0 (m, C*H*$_{ar}$). **HRMS** ASAP$^+$ (195°C) $[M+H]^+$ calcd for $C_{24}H_{25}N_3O_3{}^{11}B_3$: m/z = 436.21696. Found 436.2176 (2 ppm) calculated on the monoisotopic peak.

UV-vis measurements

UV-Vis absorption spectra were recorded on a Specord 205 UV-Vis-NIR spectrophotometer using quartz cuvettes of 1 cm pathlength. All absorption measurements were performed at 25 °C.

Emission measurements

Steady-state luminescence spectra were measured using an Edinburgh FS920 Steady State Fluorimeter combined with a FL920 Fluorescence Lifetime Spectrometer. The emitted light was detected at 90° using a Peltier-cooled R928 PMT after passage through a monochromator. The spectra were corrected for the wavelength dependence of the detector, and the quoted emission maxima refer to the values after correction. Measurements were performed at room temperature, under air atmosphere. We worked with diluted solution (A < 0.1 at the excitation wavelength) to avoid the inner-filter effect.

Cyclic voltammetry

Electrochemical solutions: 1 mg of borazine was sonicated for 1 hour in 2.5 mL of anhydrous N,N-dimethylformamide (DMF). Tetrabutylammonium hexafluorophosphate ($TBAPF_6$)(100 mg; 0.1M) was added to the solution as supporting salts.

Electrochemical analysis. Cyclic voltammetry experiments were recorded at room temperature with an Autolab electrochemical analyzer (PGSTAT 30 potentiostat/galvanostat from Eco Chemie B.V). The experiments were performed in glovebox using a three-electrode setup. The electrochemical cell is specifically designed for allowing the measurement of small volume of solution, typically 0.5 mL. The working electrode consisted of a glassy carbon electrode (1 mm diameter), the counter electrode was a Pt wire and another Pt wire was used as quasi-reference electrode. Working electrode was polished on a felt pad with 0.05 or 0.3 µm alumina suspension; the Pt wire was flame-cleaned. Tetrabutylammonium hexafluorophosphate ($TBAPF_6$) is added to the solution as a supporting electrode at 0.1M. Ferrocene ($E_{Fc/Fc+}$ 0.405 V vs SCE) or decamethylferrocene ($E_{Fc/Fc+} = -0.14$ V vs SCE) are used as internal reference. HOMO-LUMO gap were calculated from onset redox potentials.

APPENDICES

Appendices Chapter 2

NMR spectra

Compound a1:

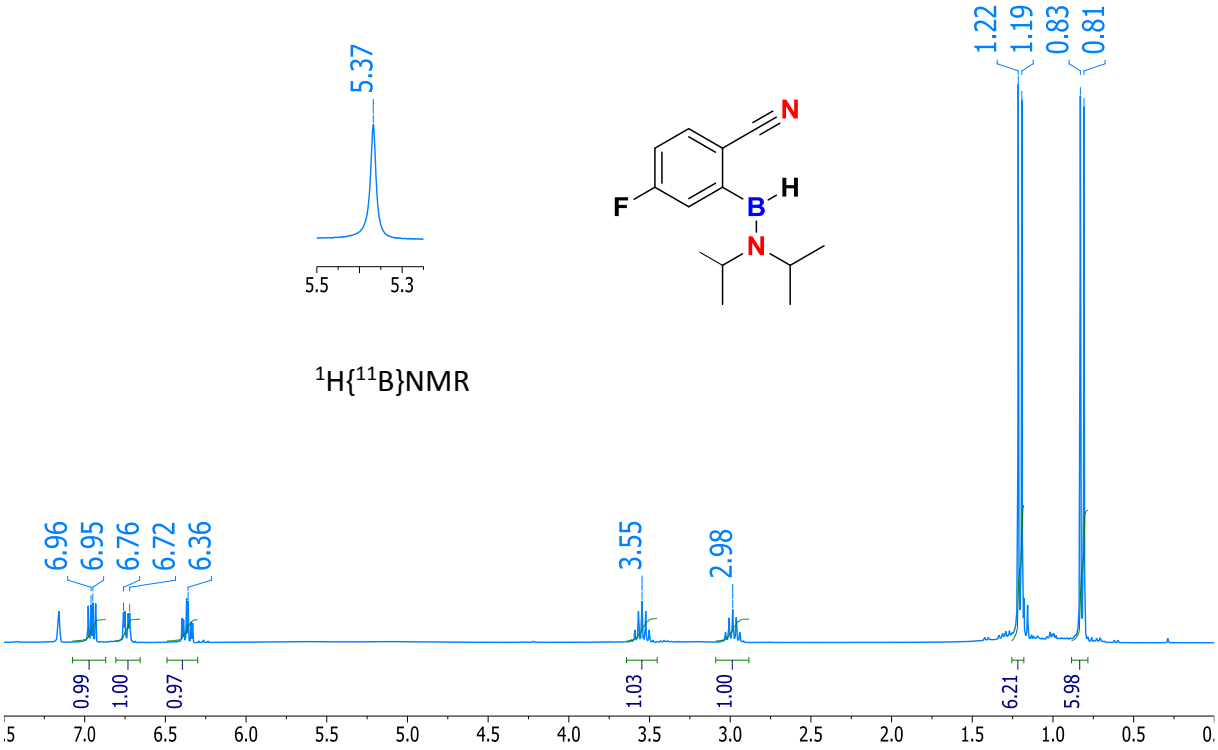

$^{1}H\{^{11}B\}$NMR

^{1}H NMR spectrum of **a1** (C_6D_6, 400.16 MHz, 298K)

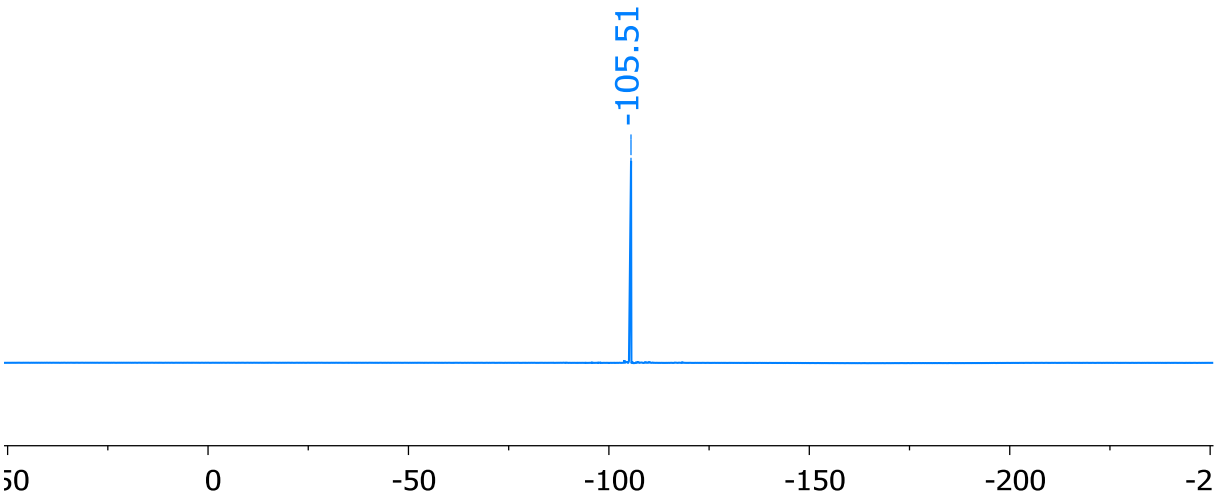

^{19}F NMR spectrum of **a1** (C_6D_6, 376.49 MHz, 298K)

Compound a2:

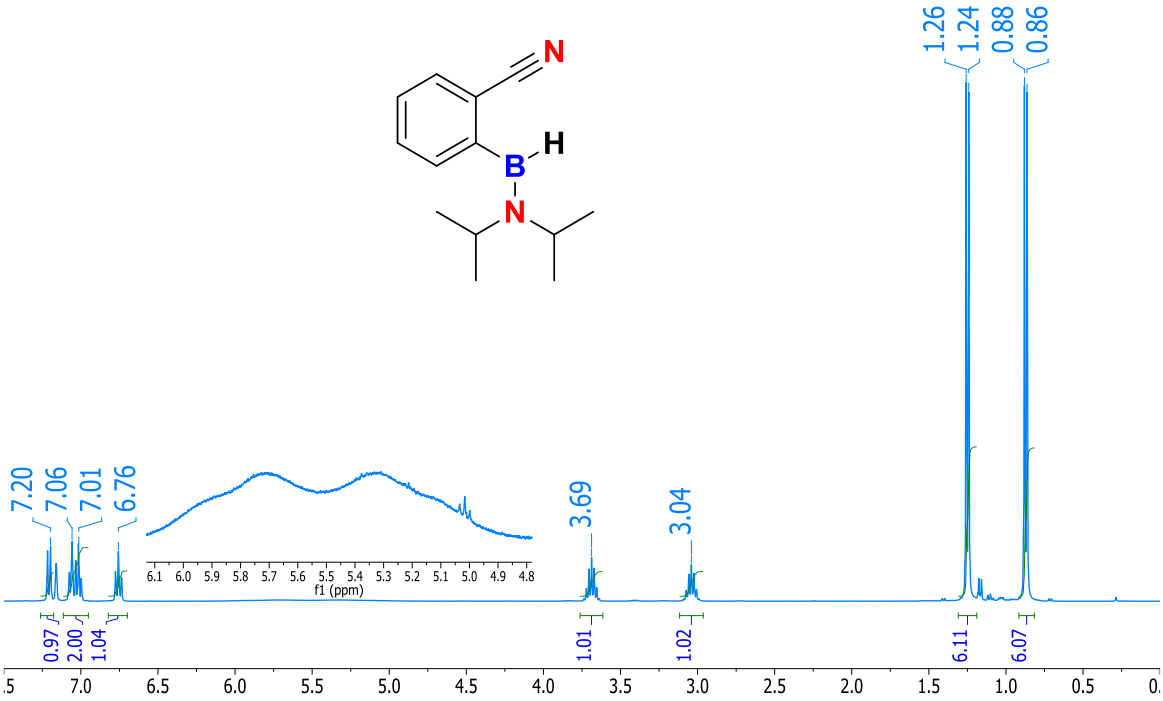

^{1}H NMR spectrum of **a2 (**C_6D_6, 400.18 MHz, 298K**)**.

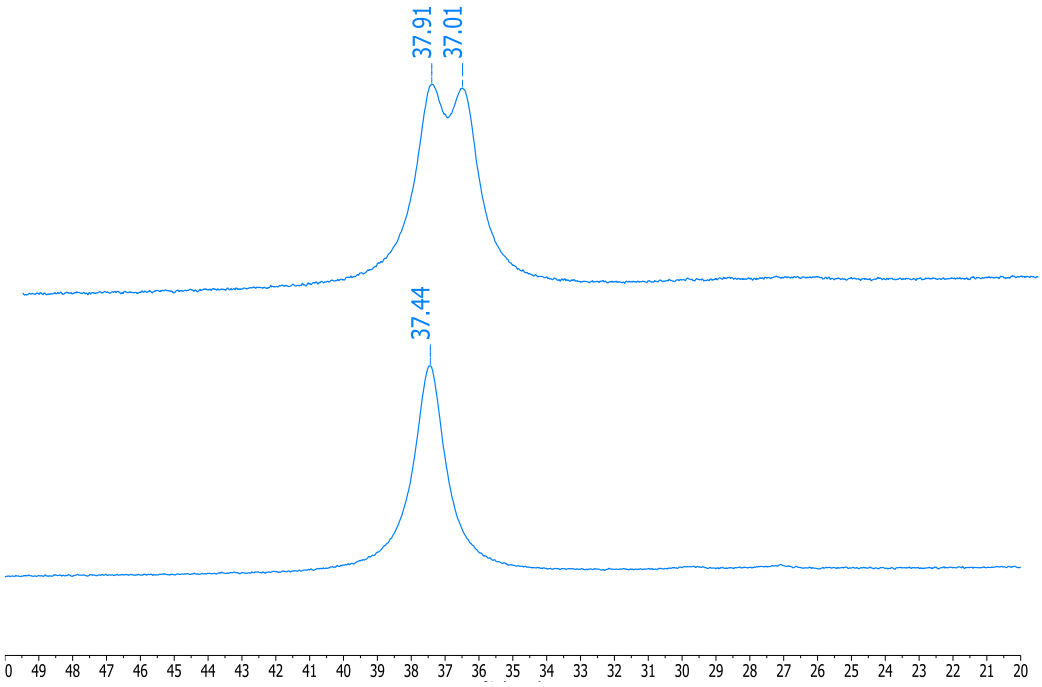

^{11}B NMR and **(**top**)** ^{11}B{^{1}H} NMR **(**bottom**)** spectra of **a2 (**C_6D_6**,** 128.39 MHz**,** 298K**).**

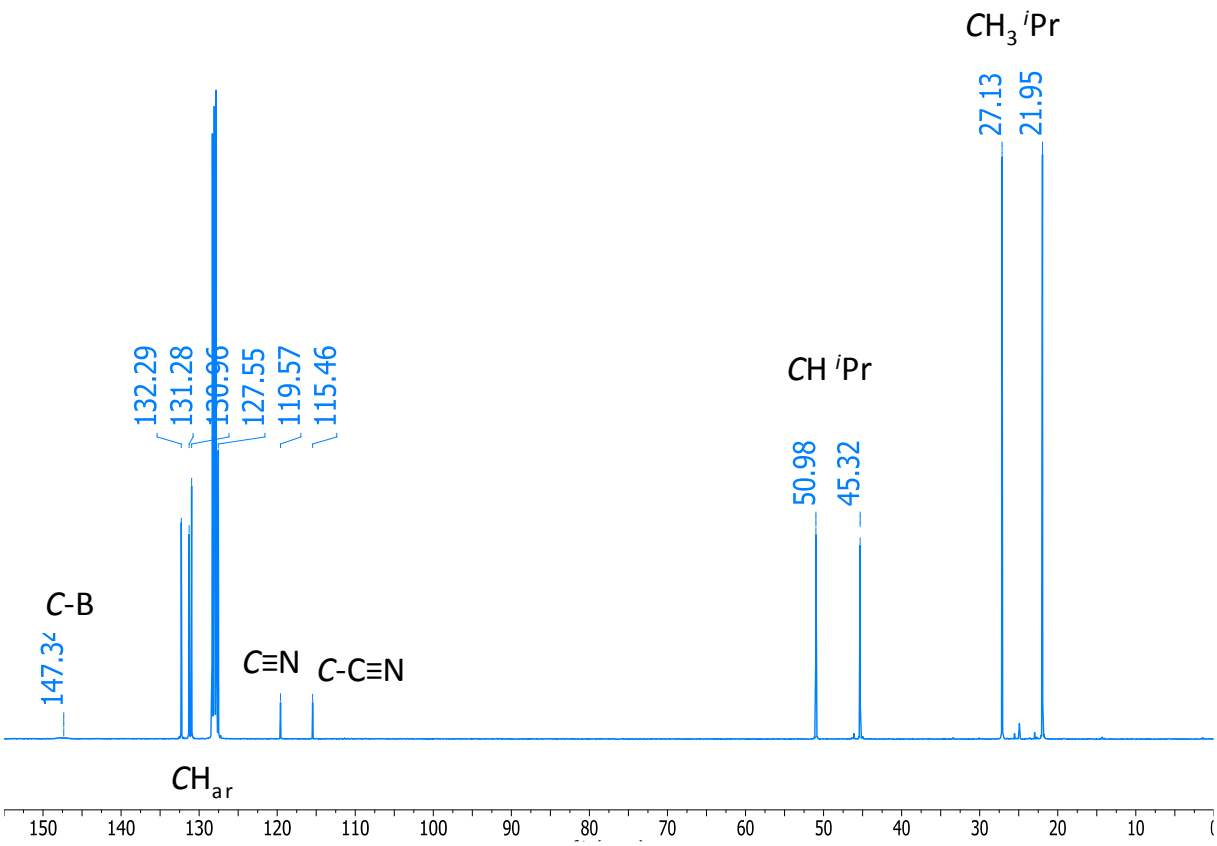

$^{13}C\{^{1}H\}$ NMR spectrum of **a2** (C_6D_6, 100.64 MHz, 298K)

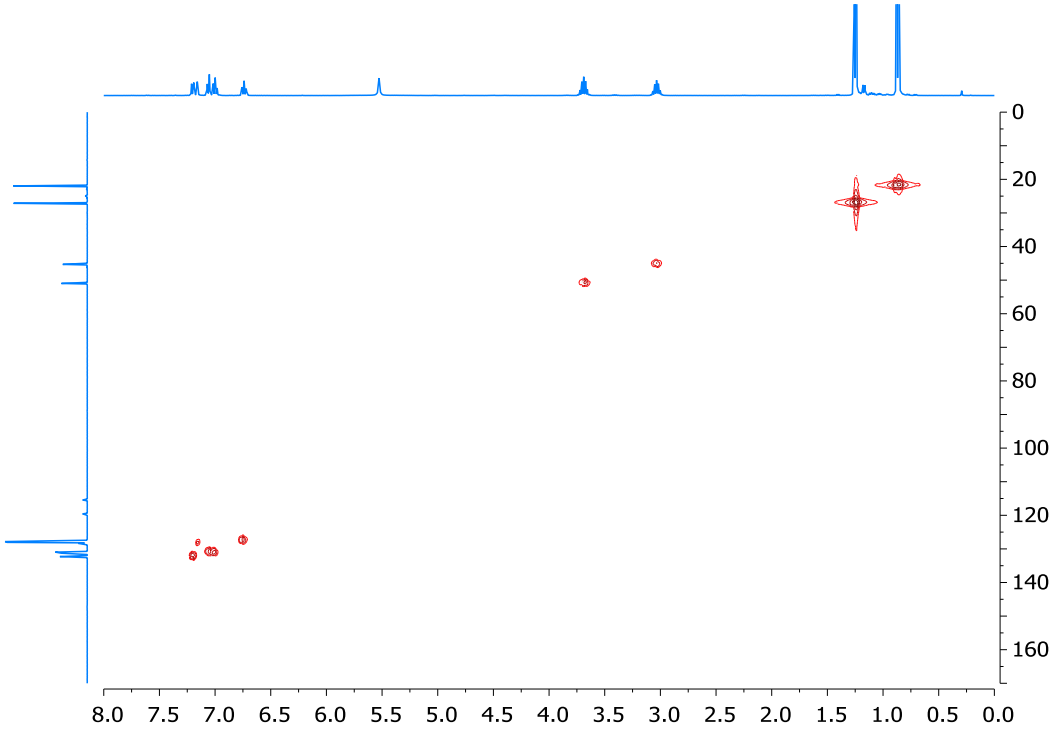

2D $^{1}H/^{13}C\{^{1}H\}$ HMQC NMR spectrum of **a2** (C_6D_6, 100.64 MHz, 298K)

Compound a3:

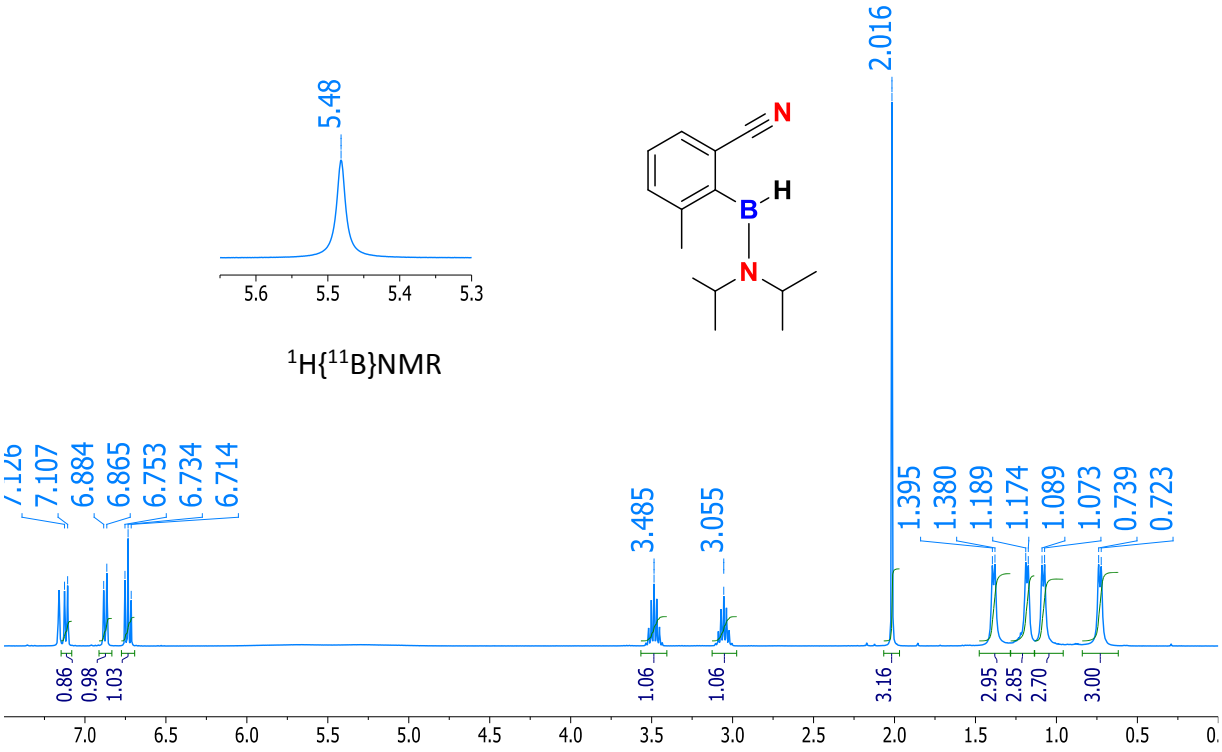

$^{1}H\{^{11}B\}$NMR

^{1}H NMR spectrum of **a3** (C_6D_6, 400.16 MHz, 298K)

Compound a4 :

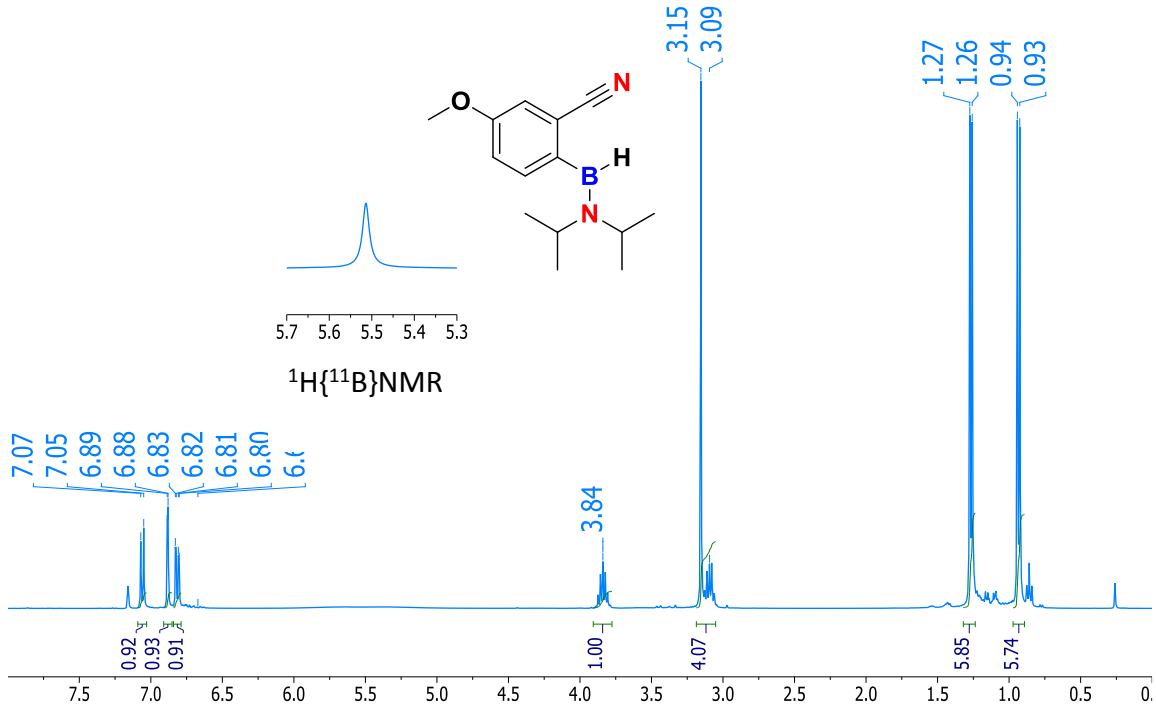

$^{1}H\{^{11}B\}$NMR

^{1}H NMR spectrum of **a4** (C_6D_6, 400.16 MHz, 298K)

Compound b1:

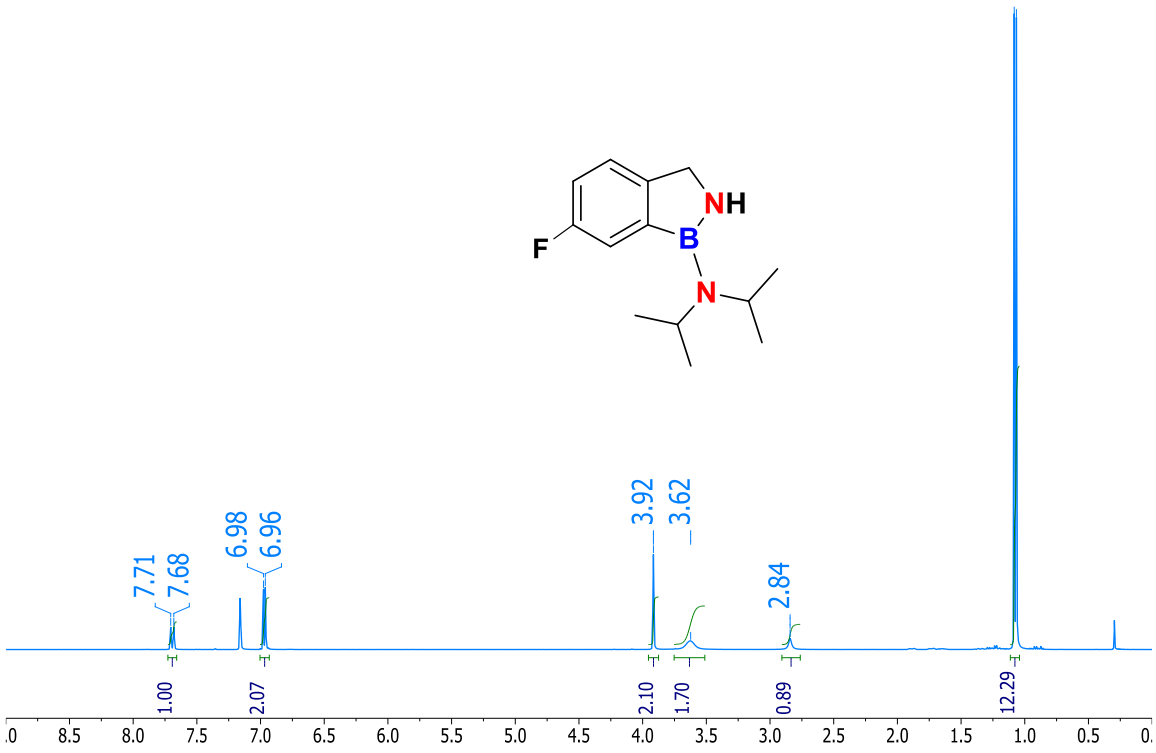

^{1}H NMR spectrum of **b1** (C_6D_6, 400.18 MHz**,** 298K**)**

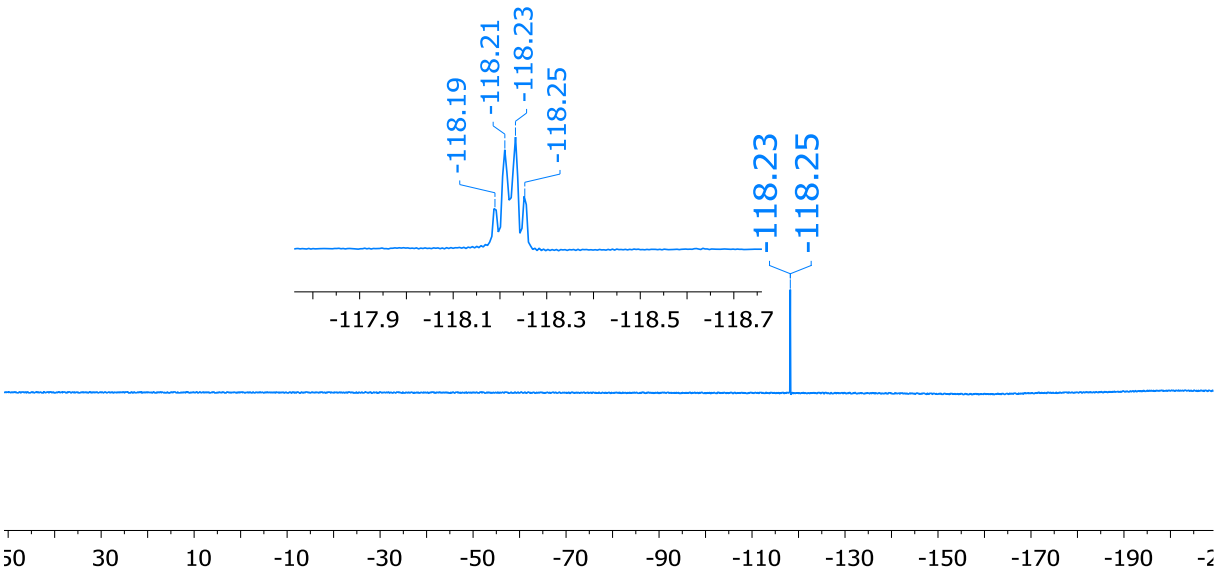

^{19}F NMR spectrum of **b1** (C_6D_6, 376.49 MHz, 298K**)**

Compound b2:

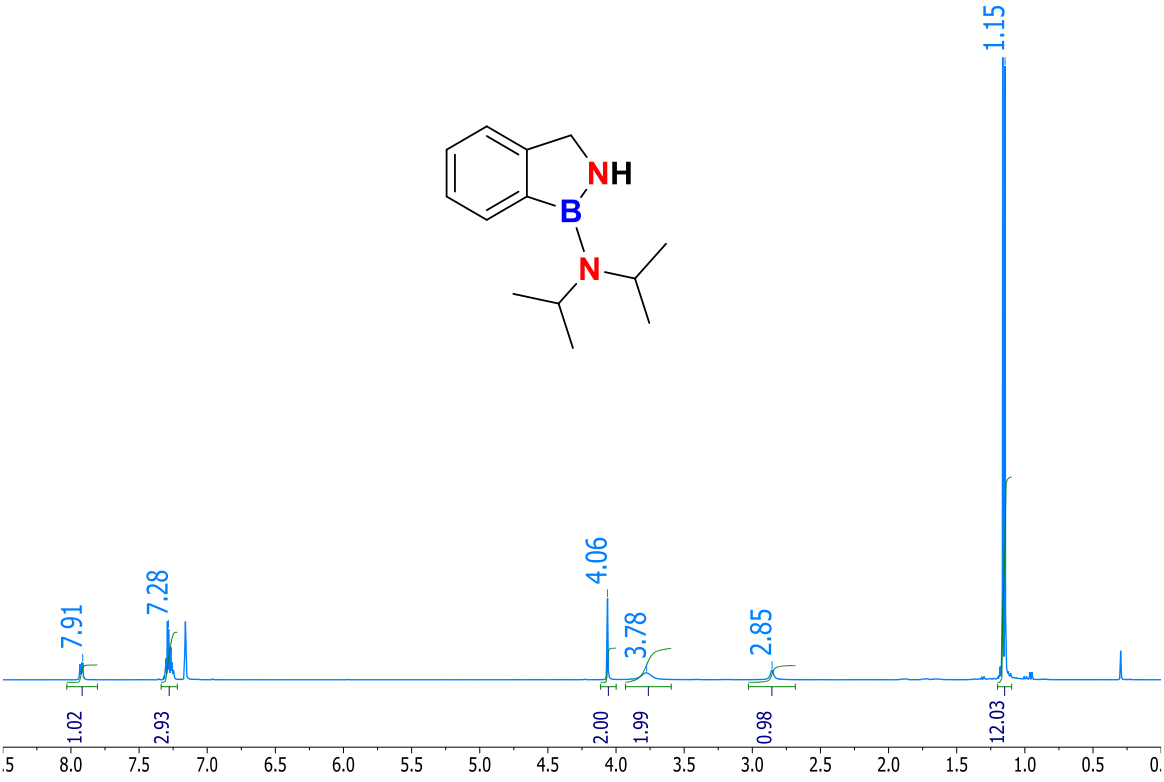

^{1}H NMR spectrum of **b2** (C_6D_6, 400.18 MHz, 298K)

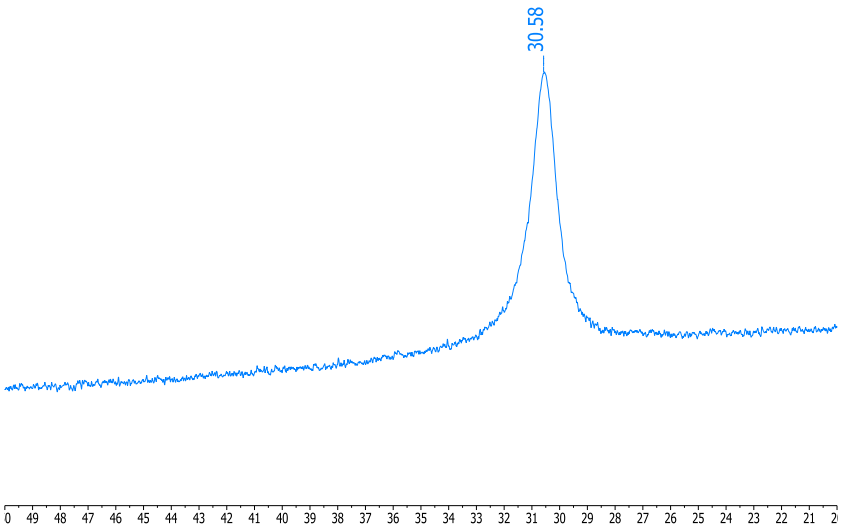

^{11}B NMR spectrum of **b2** (C_6D_6, 128.39 MHz, 298K)

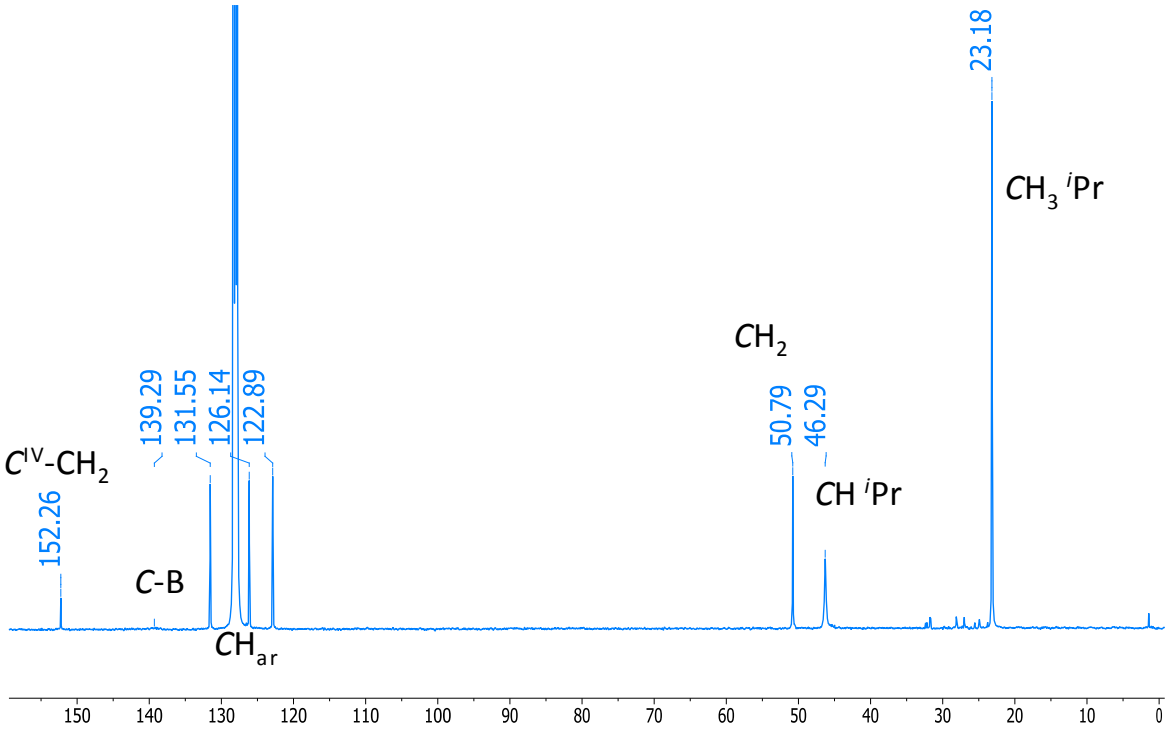

$^{13}C\{^{1}H\}$ NMR spectrum of **b2** (C_6D_6, 100.64 MHz, 298K)

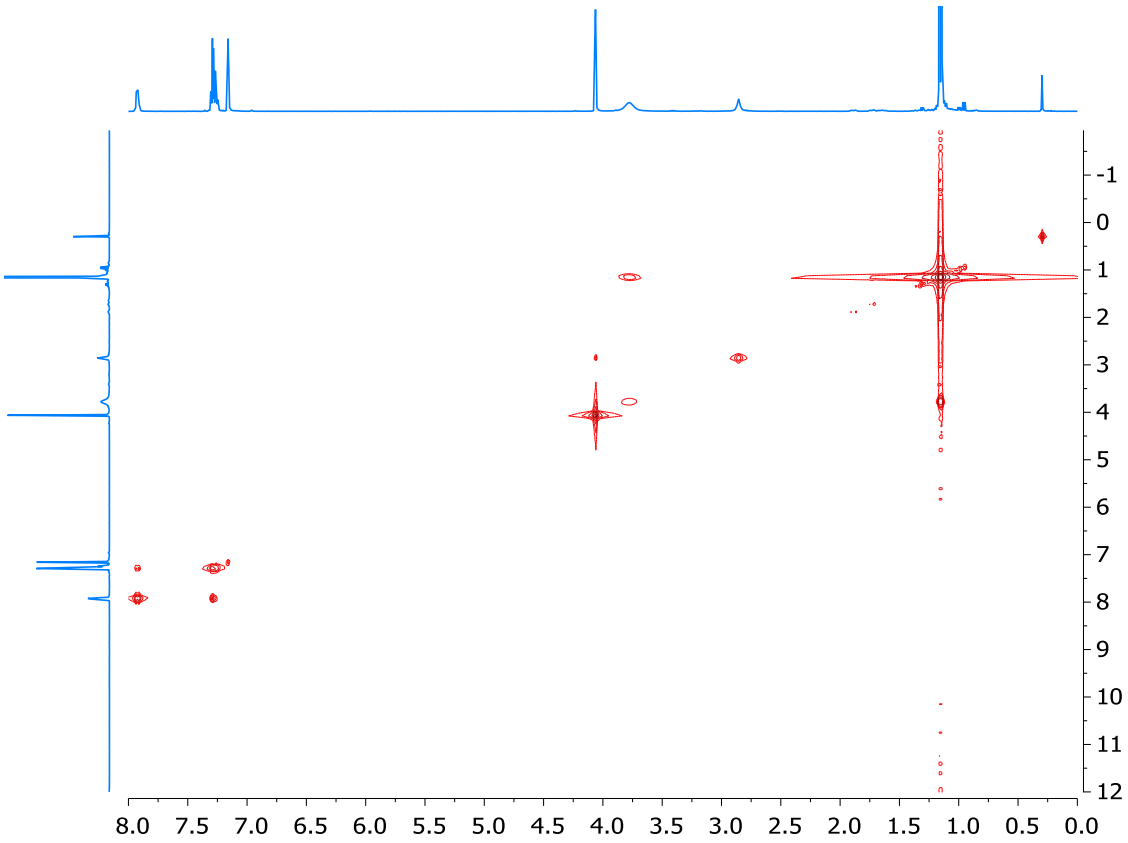

2D ^{1}H COSY NMR spectrum of **b2** (C_6D_6, 400.18 MHz, 298K)

Compound b3

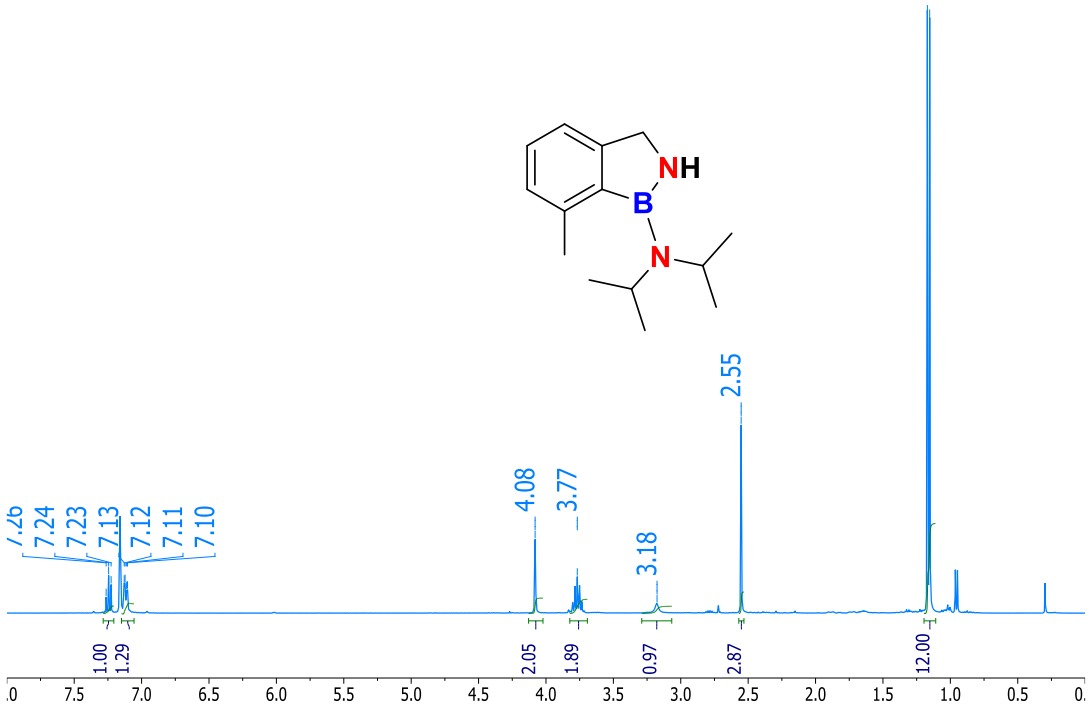

^{1}H NMR spectrum of **b3** (C_6D_6, 400.18 MHz, 298K)

Compound b4:

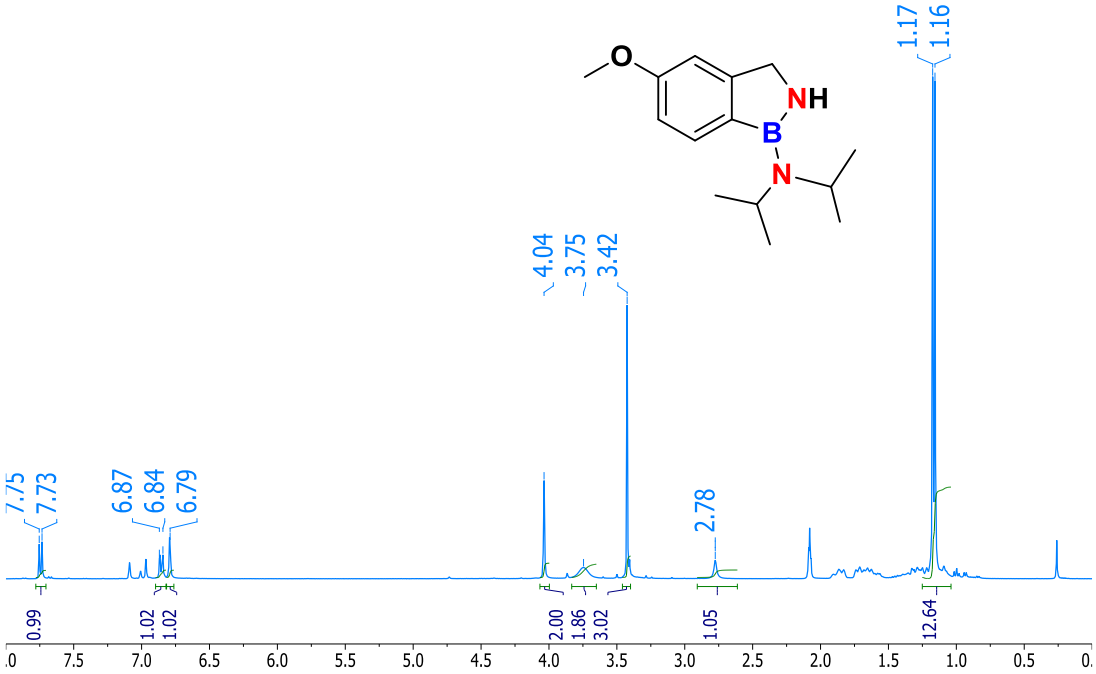

^{1}H NMR spectrum of **b4** (C_7D_8, 400.18 MHz, 298K)

Infrared spectra

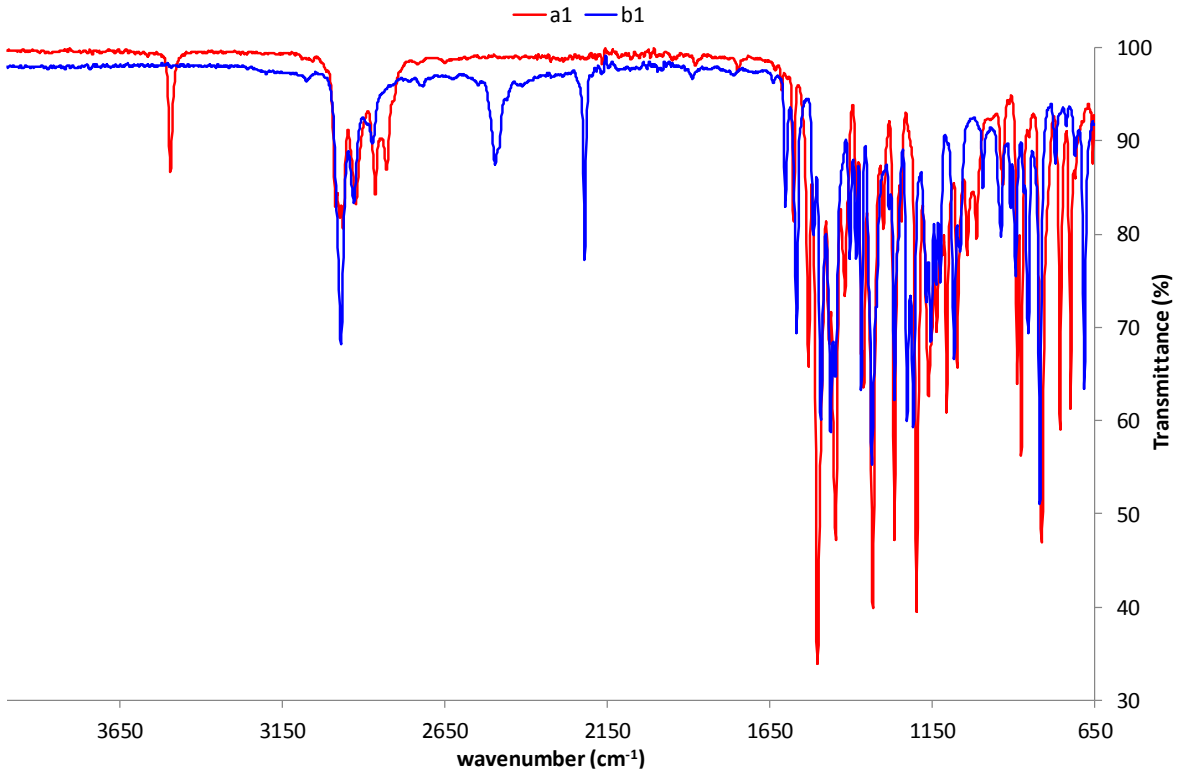

Superimposed infrared spectra of **a1** and **b1**

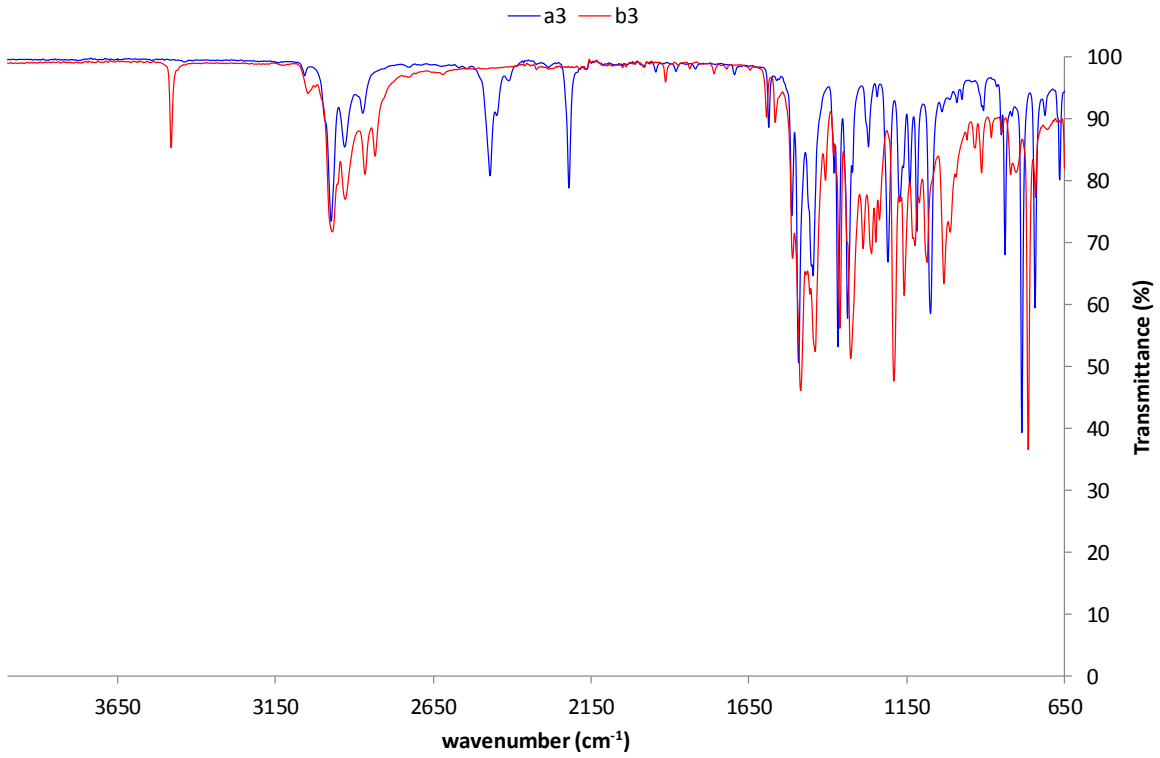

Superimposed infrared spectra of **a3** and **b3**

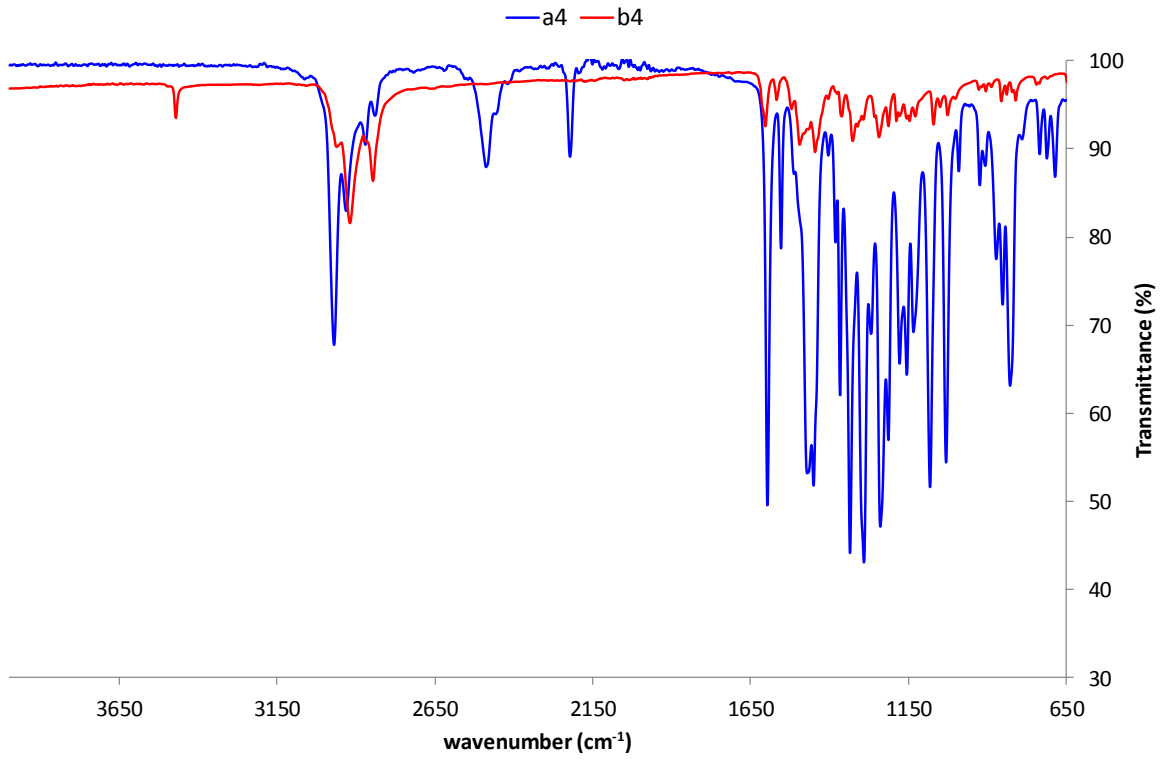

Superimposed infrared spectra of **a4** and **b4**

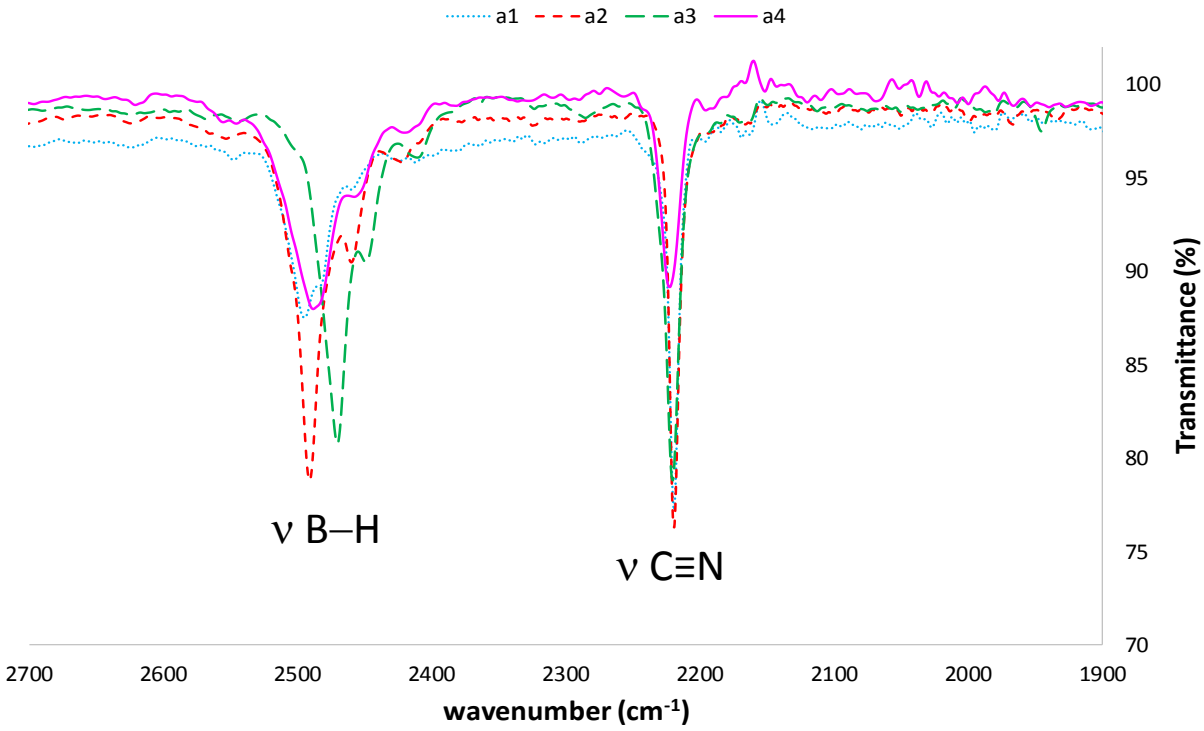

Superimposed infrared spectra of compounds **a1-4**

Crystallographic data

	a1	**a2**	**a3**
Empirical formula	C13 H18 B F N2	C13 H19 B N2	C14 H21 B N2
Formula weight	232.10	214.11	228.14
Temperature	180**(**2**)** K	180**(**2**)** K	180**(**2**)** K
Wavelength	1.54180 A	0.71073 A	0.71073 A
Crystal system, space group	Triclinic, P -1	Monoclinic, P 1 21 1	Orthorhombic, P 21 21 21
a	6.5217**(**5**)**	7.9574**(**4**)**	7.4804**(**3**)**
b	7.4977**(**5**)**	10.3796**(**5**)**	11.0509**(**4**)**
c	14.3365**(**10**)**	8.1733**(**4**)**	17.3815**(**6**)**
alpha	88.189**(**6**)**	90	90
beta	84.095**(**6**)**	100.7080**(**10**)**	90
gamma	76.210**(**6**)**	90	90
Volume $Å^3$	677.19**(**8**)**	663.32**(**6**)**	1436.84**(**9**)**
Z, Calculated density Mg/m^3	2, 1.138	2, 1.072	4, 1.055
Absorption coefficient	0.610 mm^{-1}	0.062 mm^{-1}	0.061 mm^-1
F**(**000**)**	248	232	496
Crystal size	0.15 x 0.08 x 0.02 mm	0.25 x 0.15 x 0.1 mm	0.15 x 0.06 x 0.02
Theta range for data collection	6.08 to 71.01 deg	2.54 to 26.37 deg.	2.18 to 26.37 deg.
Limiting indices	-7<=h<=6, -5<=k<=9, -17<=l<=17	-9<=h<=9, -12<=k<=12, -9<=l<=10	-9<=h<=9, -13<=k<=13, -21<=l<=20
Reflections collected / unique	3510 / 2109 [R**(**int**)** = 0.0160]	16841 / 2700 [R**(**int**)** = 0.0187]	30918 / 2945 [R**(**int**)** = 0.0318]
Completeness to theta = 25.00	99.6 %	99.4 %	99.8 %
Absorption correction	Semi-empirical from equivalents	Semi-empirical from equivalents	Semi-empirical from equivalents
Max. and min. transmission	0.9832 and 0.7701	0.957 and 0.898	0.957 and 0.898
Refinement method	Full-matrix least-squares on F^2	Full-matrix least-squares on F^2	Full-matrix least-squares on F^2
Data / restraints / parameters	2109 / 1 / 161	2700 / 2 / 152	2945 / 0 / 162
Goodness-of-fit on F^2	1.024	1.061	1.093
Final R indices [I>2sigma**(**I**)**]	R1 = 0.0432, wR2 = 0.1138	R1 = 0.0267, wR2 = 0.0709	R1 = 0.0313, wR2 = 0.0801
R indices **(**all data**)**	R1 = 0.0513, wR2 = 0.1251	R1=0.0269 wR2=0.0712	R1=0.0337 wR2=0.0817
Largest diff. peak and hole	0.191 and -0.148 e.A^-3	0.154 and -0.147 e.A^-3	0.160 and -0.152 e.A^-3

	b1	**b2**	**b3**	**b4**
Empirical formula	C13 H20 B F N2	C_{13} H_{21} B_1 N_2	C14 H23 B N2	$C_{14}H_{23}BN_2O$
Formula weight	234.12	216.13	230.15	246.15
Temperature	180**(**2**)** K	100 K	180**(**2**)** K	180**(**2**)** K
Wavelength	1.54180 A		0.71073 A	0.71073 A
Crystal system, space group	Hexagonal, P 31 2 1	Trigonal P 3_2 2 1	Orthorhombic, P 21 21 21	Monoclinic, $P2_1/c$
a	11.5177**(**7**)**	11.48050(12)	7.7535**(**10**)**	16.3999 (5)
b	11.5177**(**7**)**	11.48050(12)	8.0619**(**10**)**	8.1458 (2)
c	17.1539**(**11**)**	16.91972(19)	21.658**(**3**)**	21.6986 (6)
alpha	90	90	90	
beta	90	90	90	92.310 (3)
gamma	120	120	90	
Volume $Å^3$	1970.7**(**2**)**	1931.28(4)	1353.8**(**3**)**	2896.37 (14)
Z, Calculated density Mg/m^3	6, 1.184	6,	4, 1.129	8, 1.129
Absorption coefficient	0.629 mm^-1	0.065 mm^-1	0.065 mm^-1	
F**(**000**)**	756	708	504	1072
Crystal size mm	0.19 x 0.1 x 0.04	0.12 × 0.15 × 0.20	0.12 x 0.06 x 0.02	0.35 × 0.2 × 0.05
Theta range for data collection	4.43 to 61.93 deg	4 - 29°	2.70 to 21.06 deg.	3.6–27.4 deg
Limiting indices	-12<=h<=13, -12<=k<=12, -18<=l<=18	-16 → 16, -16 → 16, -24 → 23	-7<=h<=7, -8<=k<=8, -21<=l<=21	
Reflections collected / unique	9889 / 1986 [R**(**int**)** = 0.1170]		23514 / 1448 [R**(**int**)** = 0.0638]	
Completeness to theta = 25.00	96.4 %		98.9 %	
Absorption correction	Semi-empirical from equivalents		Semi-empirical from equivalents	
Max. and min. transmission	0.7586 and 0.4991		0.912 and 0.871	
Refinement method	Full-matrix least-squares on F^2		Full-matrix least-squares on F^2	
Data / restraints / parameters	1986 / 0 / 162		1448 / 0 / 162	
Final R indices [I>2sigma**(**I**)**]	R1 = 0.0474, wR2 = 0.1253	R1 = 0.041, wR2 = 0.099	R1 = 0.0335, wR2 = 0.0855	R1 = 0.041, wR2 = 0.099
R indices **(**all data**)**	R1 = 0.0511, wR2 = 0.1318		R1 = 0.0364, wR2 = 0.0863	
Largest diff. peak and hole	0.167 and -0.198 e.A^-3	0.154 and -0.147 e.A^-3	0.125 and -0.155 e.A^-3	

Appendices chapter 3

NMR spectra:

Complex I-e

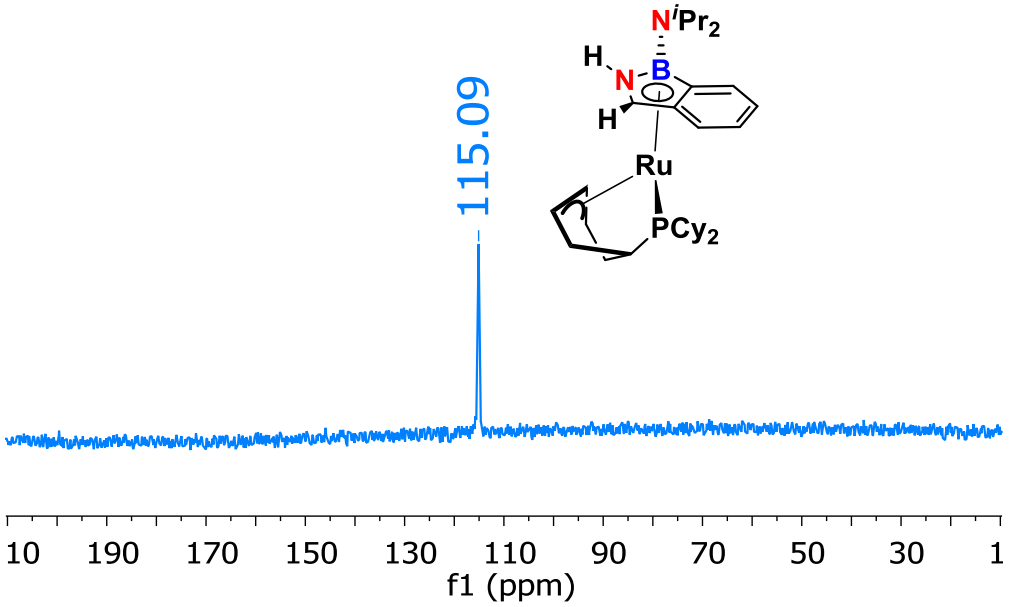

$^{31}P\{^1H\}$6NMR spectrum of complex **I-e (**C_7D_8, 202.56 MHz**,** 298K**)**

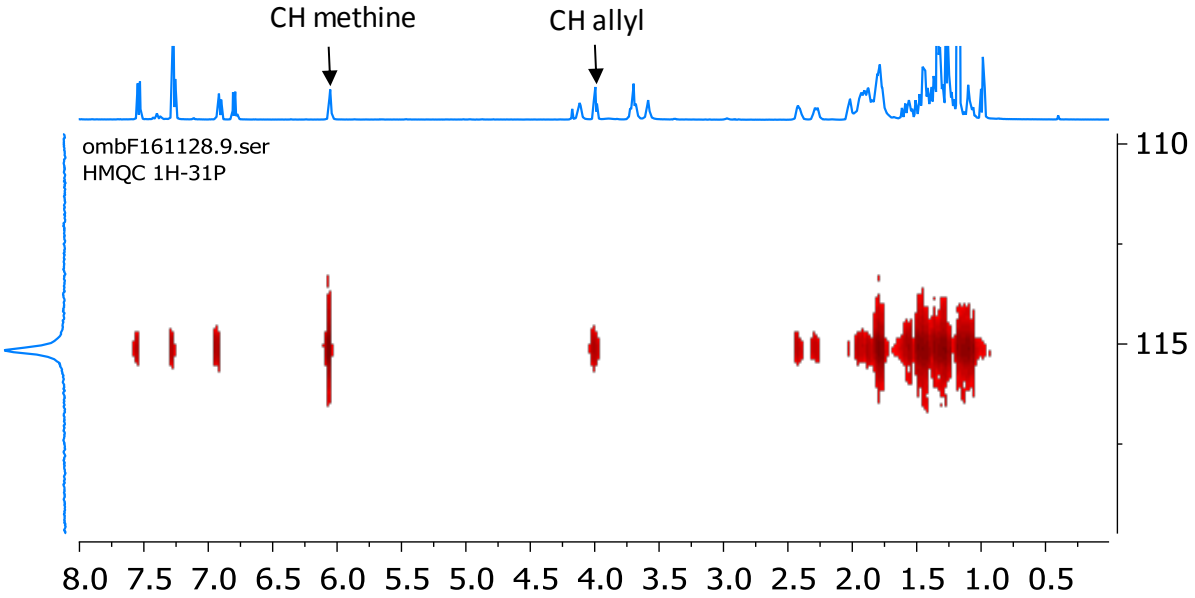

2D HMQC $^{31}P\{^1H\}/^1H$ NMR spectrum of complex **I-e (**C_6D_6, 202.56, 500.33 MHz**,** 298K**)**

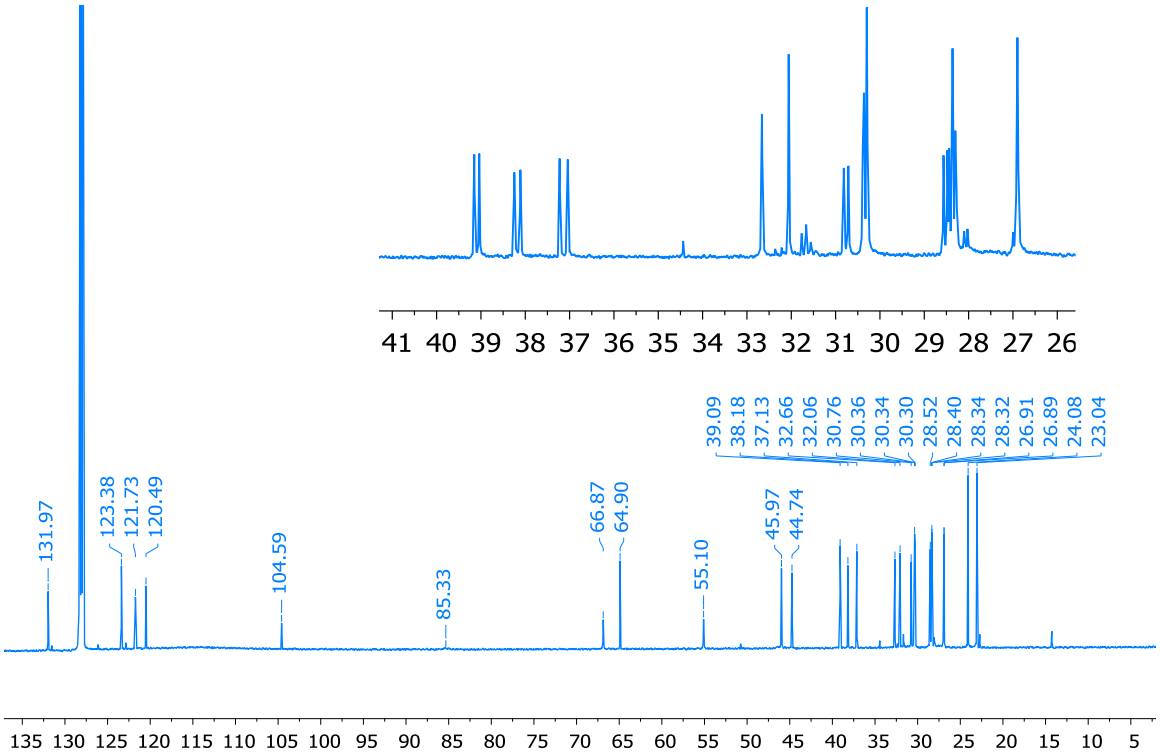

^{13}C $\{^{31}P\}\{^{1}H\}$ NMR spectrum of complex **I-e**, insert $^{13}C\{^{1}H\}$ NMR spectrum in the cyclohexyl region **(**C_6D_6, 125.82 MHz**,** 298K**)**

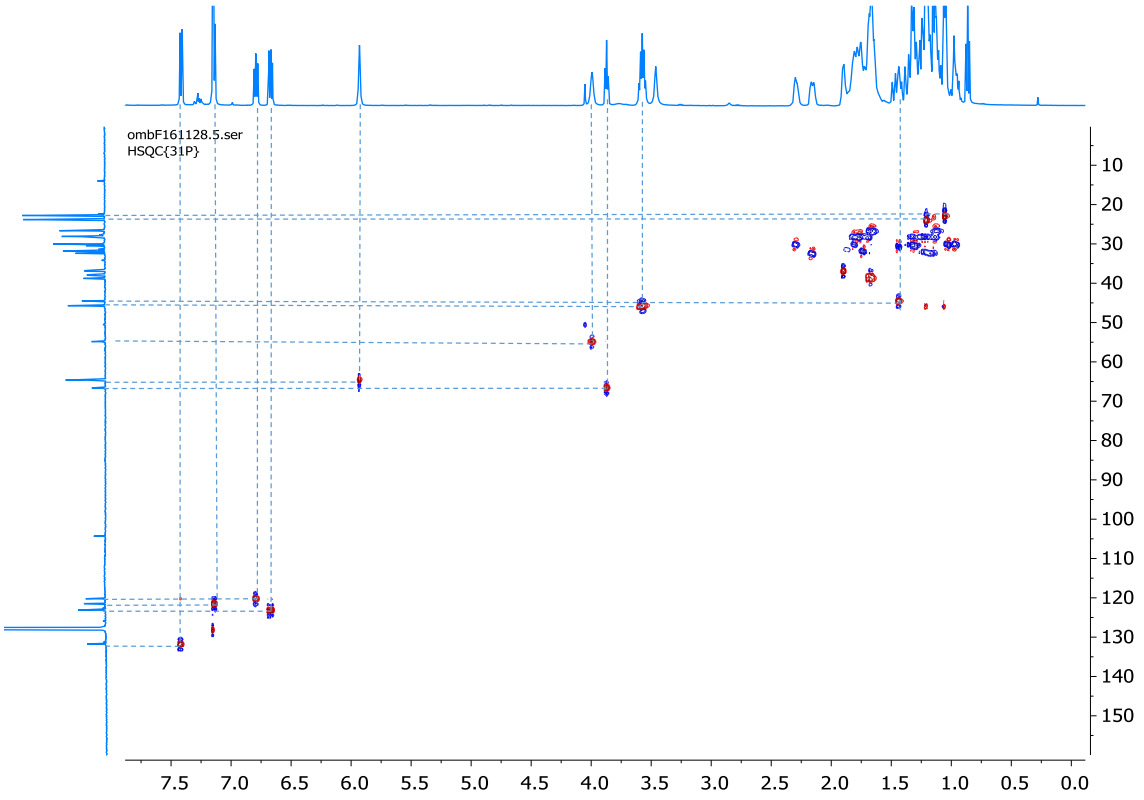

2D HSQC $^{1.3}C\{^{31}P\}/^{1}H$ NMR spectrum of complex **I-e (**red center: CH_3, CH; bleu center: CH_2**)**, **(**C_6D_6, 125.82, 500.33 MHz**,** 298K**)**

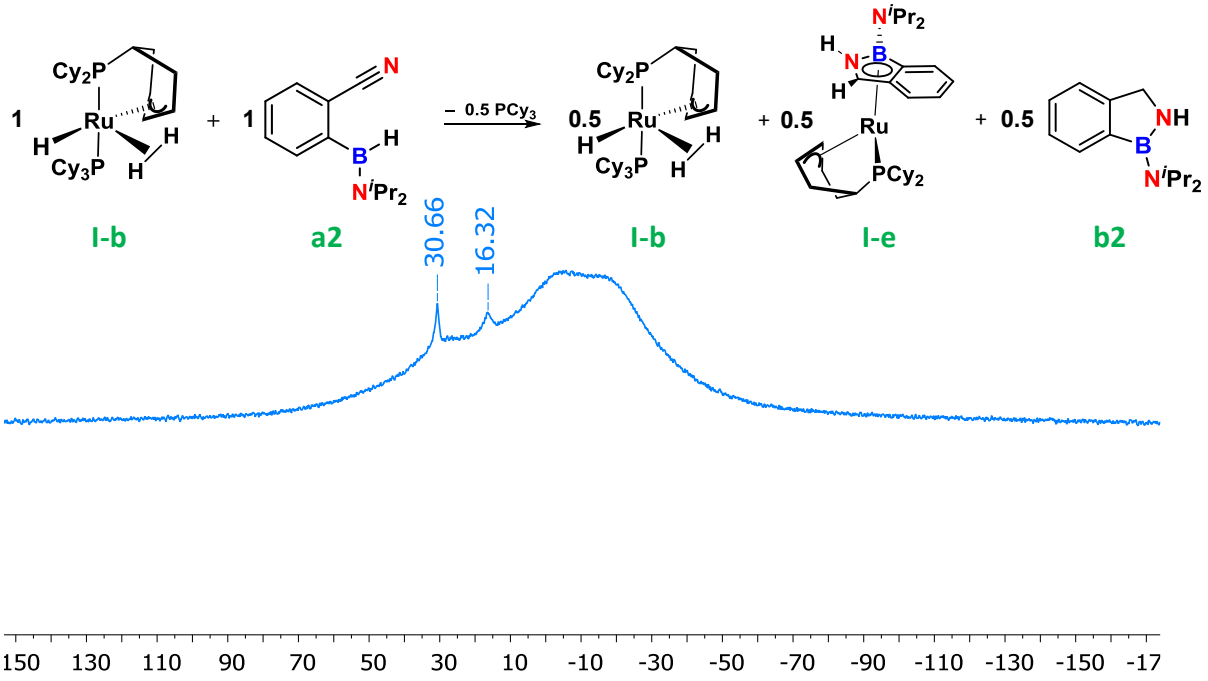

$^{11}B\{^{1}H\}$ NMR spectrum of the crude reaction mixture of **a2/I-b** in 1/1 molar ratio **(**C_7D_8, 128.39 MHz**,** 298K**)**

Complex I-f

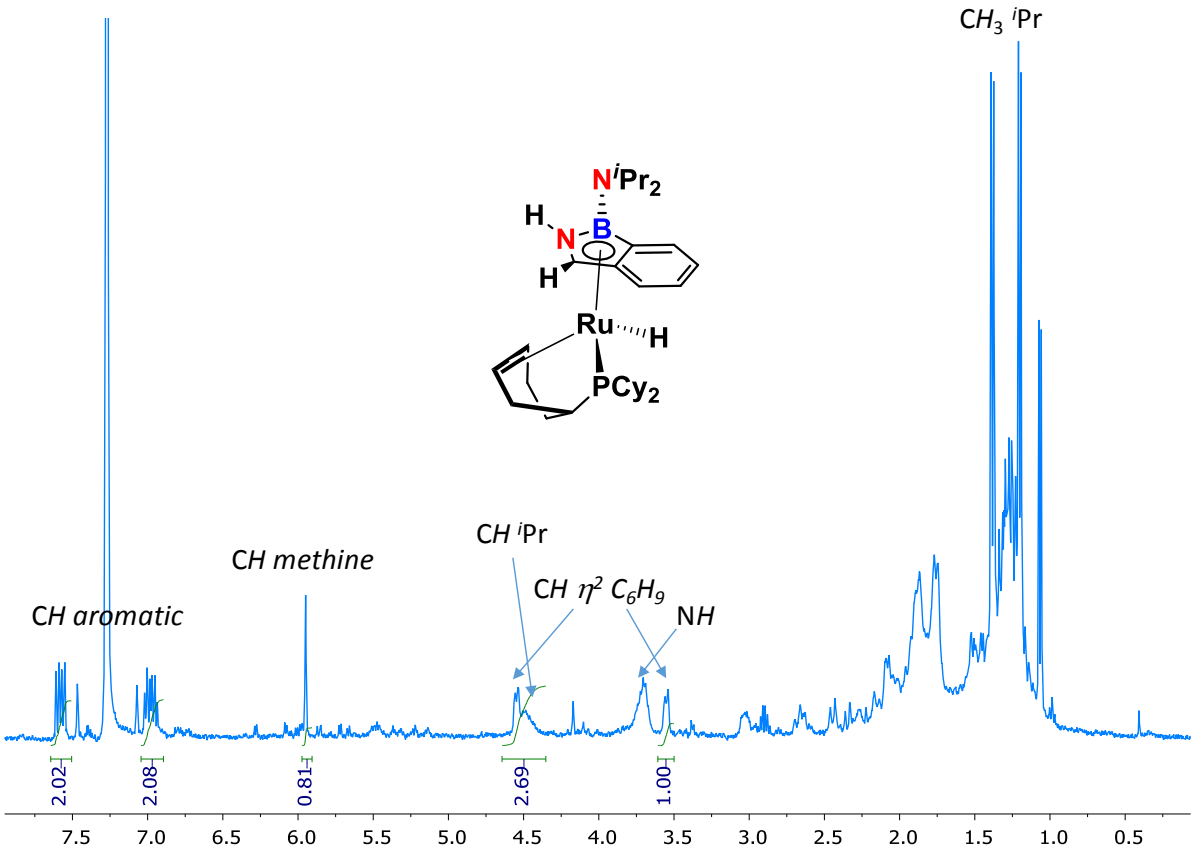

^{1}H NMR spectrum of a mixture containing complex **I-f (**C_6D_6, 500.33 MHz**,** 298K**)**

Complex I-g

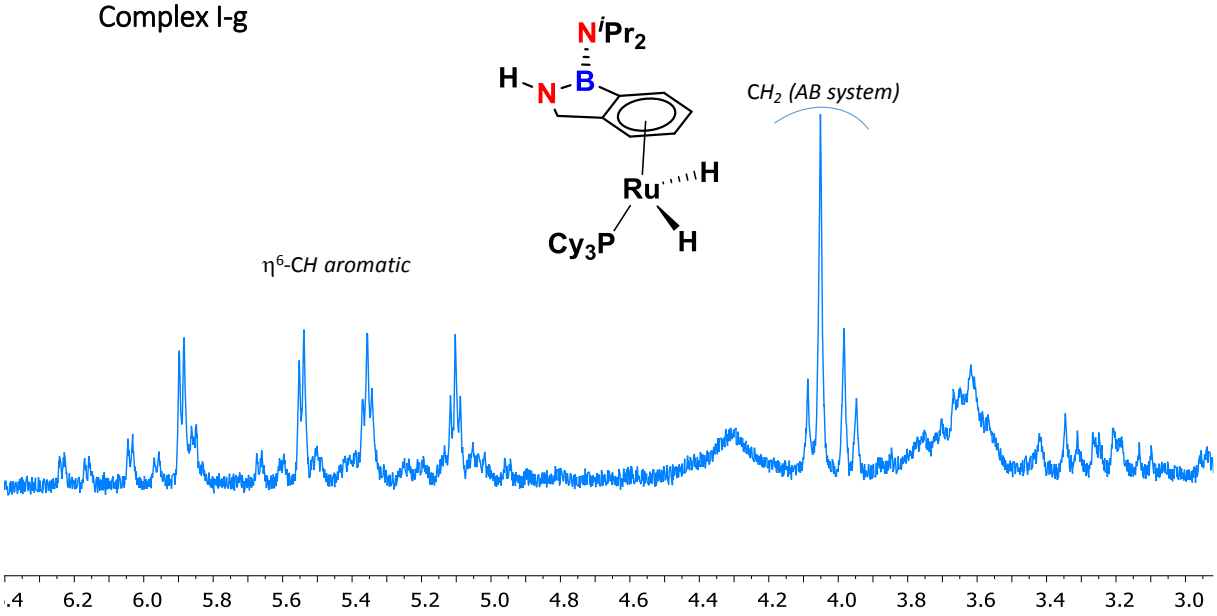

^{1}H NMR spectrum of a mixture containing complex **I-g (**C_6D_6, 500.33 MHz**,** 298K**)**

Complex I-h

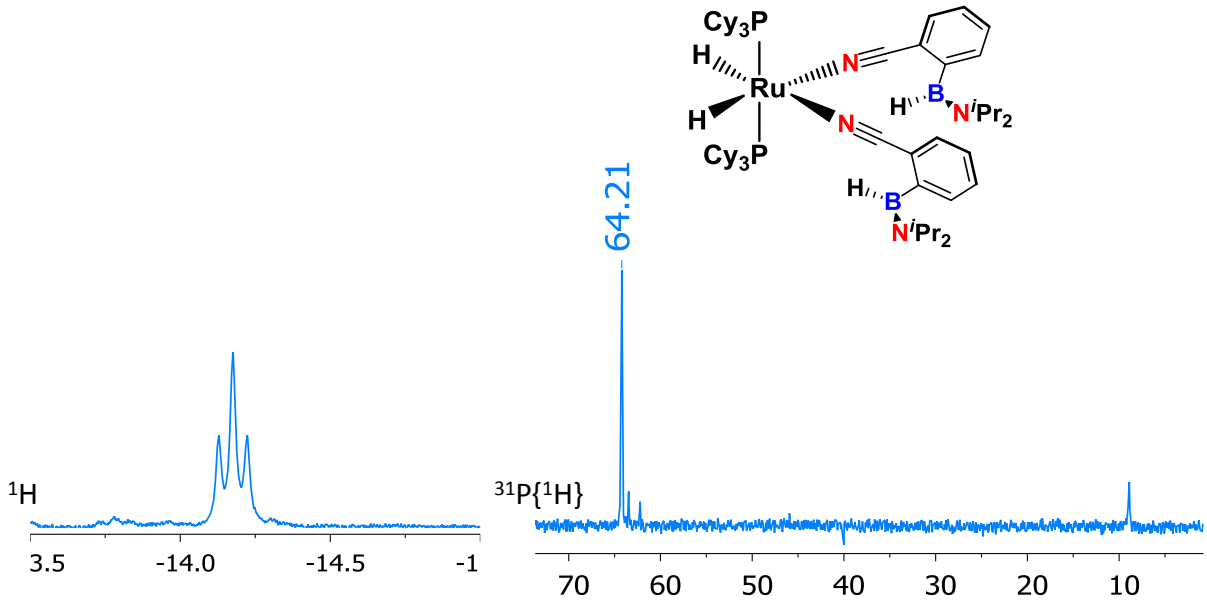

^{1}H and ^{31}P{^{1}H} NMR spectrum of a mixture containing complex **I-h (**C_7D_8, 500.33, 202.56 MHz, 233K**)**

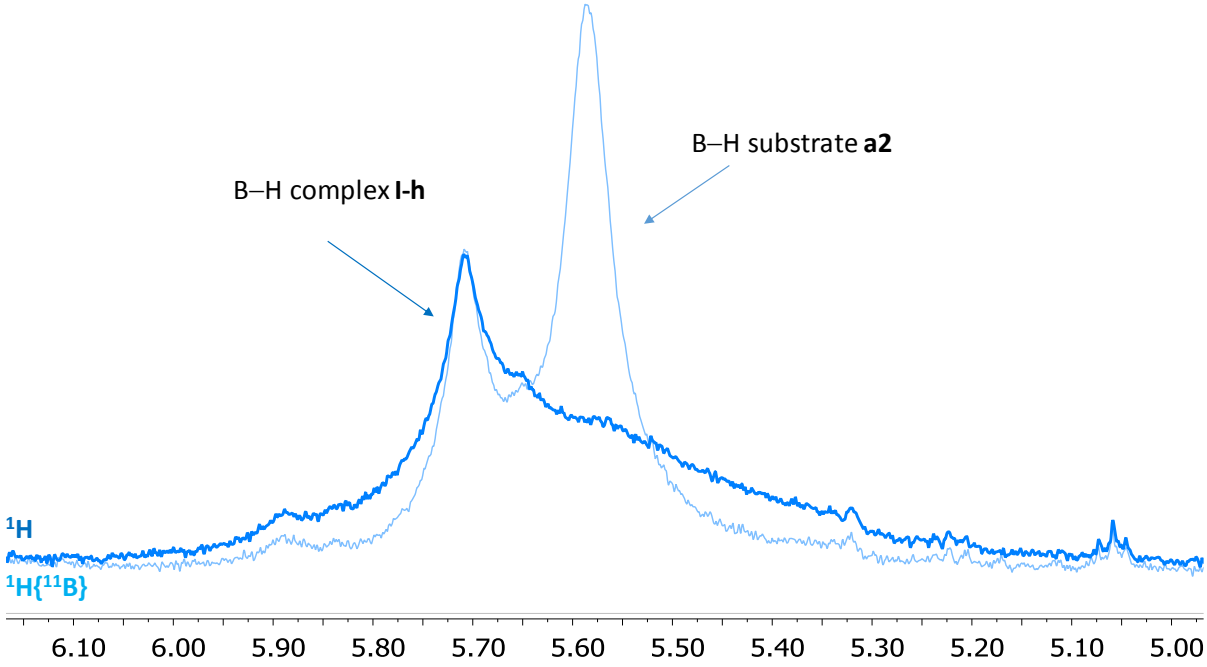

^{1}H and ^{1}H{^{11}B} NMR spectra of a mixture containing complex **I-h** and **a2** (**C_7D_8**, 500.33 MHz, 233K**)**

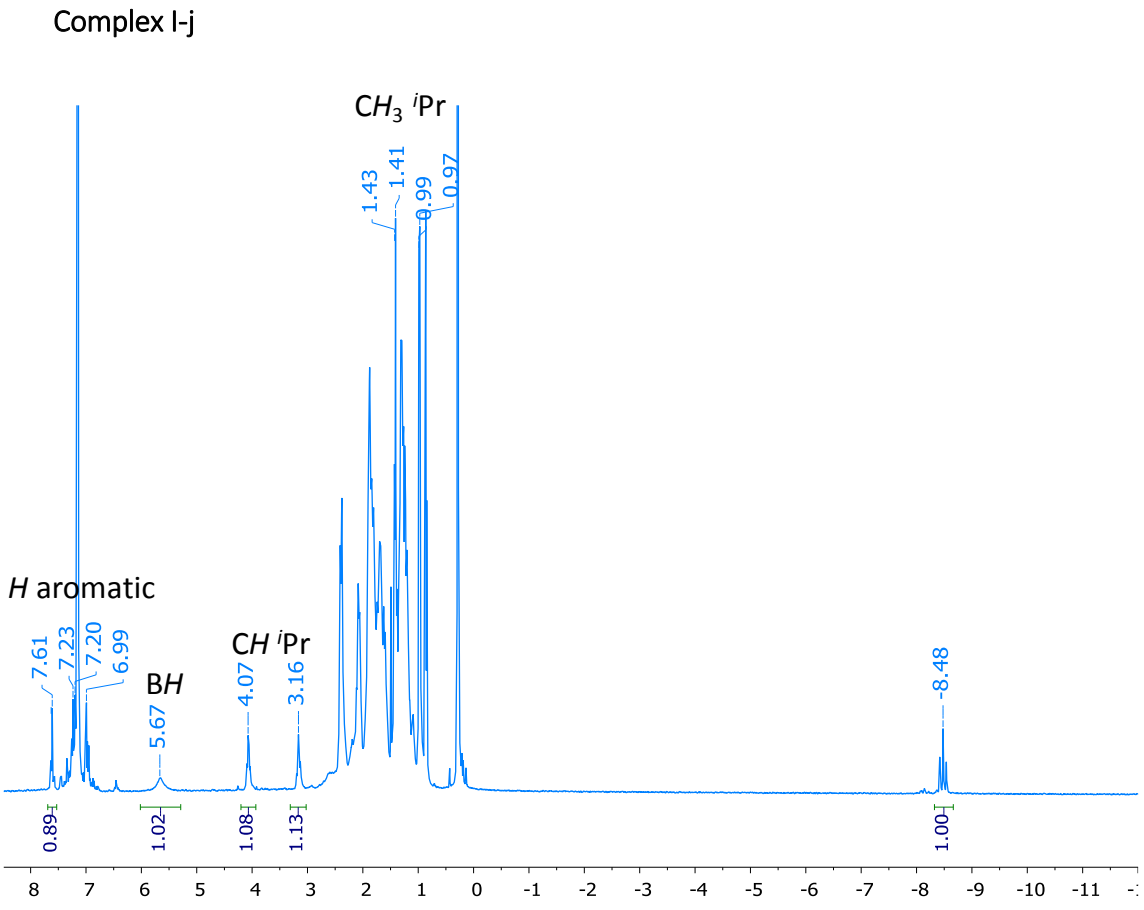

^{1}H NMR spectrum of **I-j** (**C_6D_6**, 400.18 MHz, 298K**)**

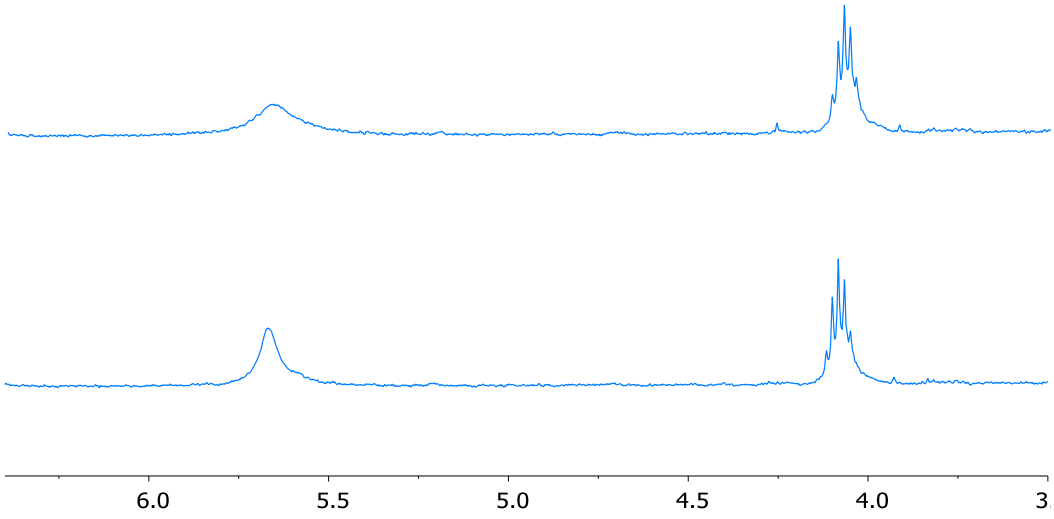

^{1}H and $^{1}H\{^{11}B\}$ NMR spectra of **I-j** (C_6D_6, 400.18 MHz, 298K)

Xray-data

Complex I-e

$C_{31}H_{50}BN_2PRu$	$F(000) = 1256$
$M_r = 593.58$	$R[F^2 > 2\sigma(F^2)] = 0.033$
Triclinic, *P*-1	$D_x = 1.33$ Mg m^{-3}
Hall symbol: -P 1	
$a = 9.9745$ (6) Å	Mo $K\alpha$ radiation, $\lambda = 0.71073$ Å
$b = 14.6282$ (9) Å	Cell parameters from 9820 reflections
$c = 21.2096$ (13) Å	$\theta = 2.5–27.5°$
$\alpha = 103.406$ (2)°	$\mu = 0.61$ mm^{-1}
$\beta = 99.818$ (2)°	$T = 100$ K
$\gamma = 90.008$ (2)°	Platelet, yellow
$V = 2963.7$ (3) Å^3	0.15 × 0.1 × 0.02 mm
$Z = 4$	$R[F^2 > 2\sigma(F^2)] = 0.033$

Appendices Chapter 4

Compound b2[1]

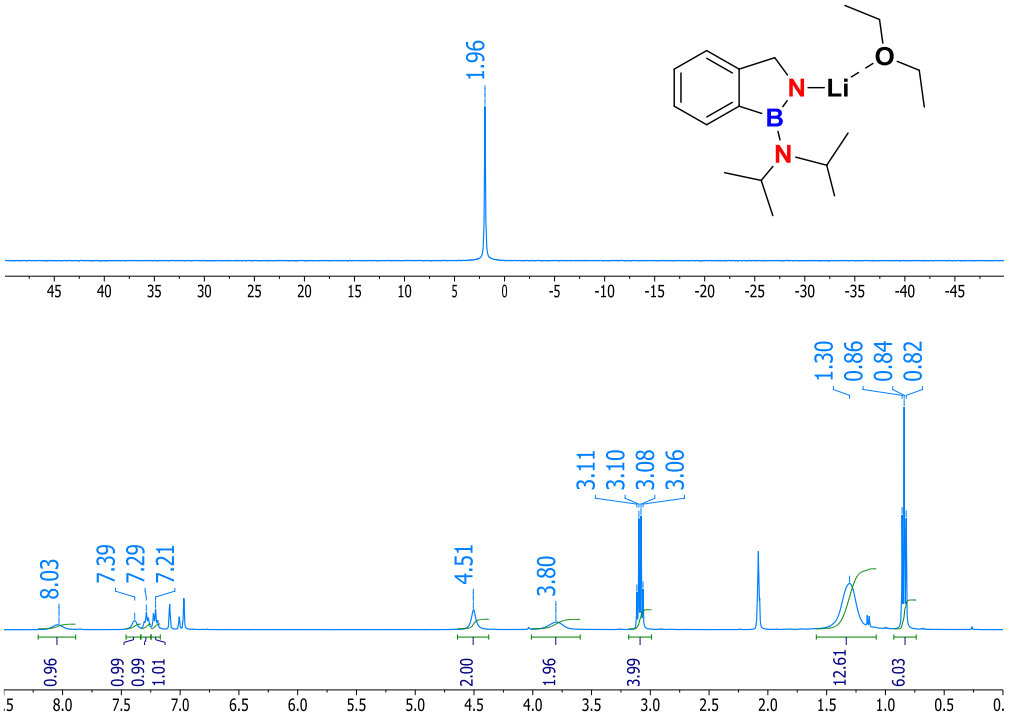

^{7}Li **(**top**)** and ^{1}H **(**bottom**)** NMR spectra of **b2[1]** **(**C_7D_8**,** 155.53 and 400.18 MHz**,** 298K**)**

Compound b2[1]

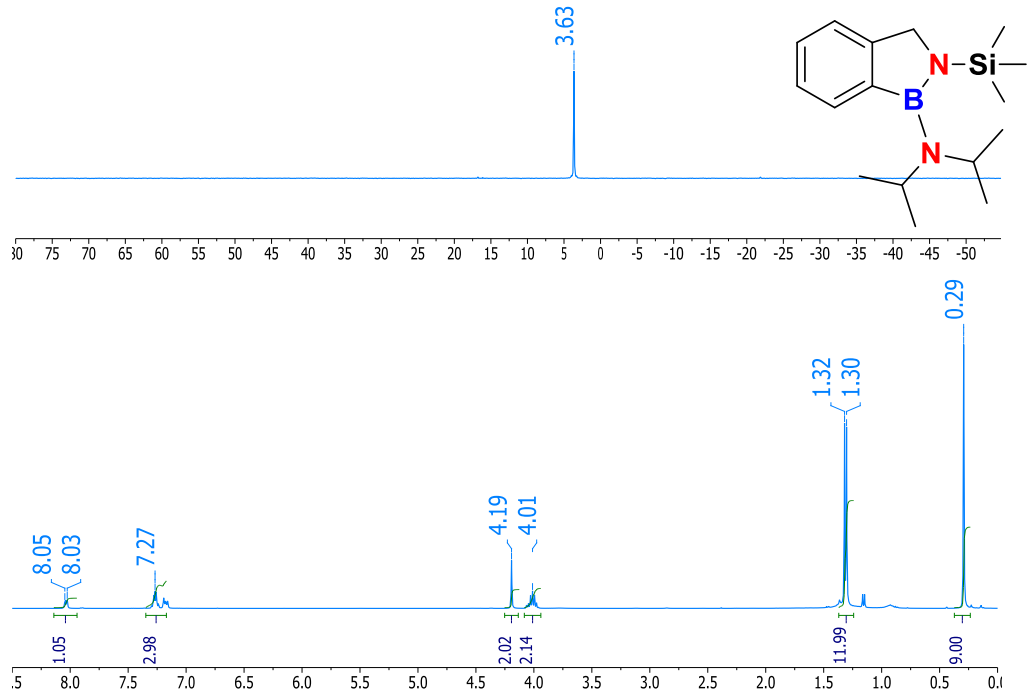

^{29}Si DEPT **(**top**)** and ^{1}H **(**bottom**)** NMR spectra of **b2[2]** **(**C_6D_6**,** 79.51 and 400.18 MHz**,** 298K**)**

Compound b2[3]

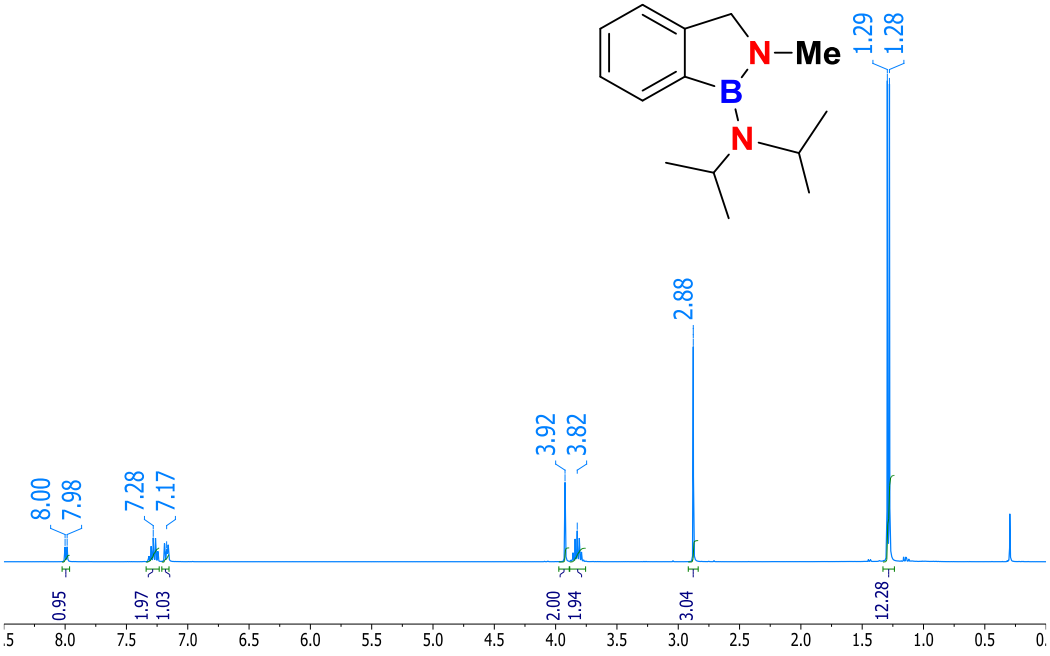

^{1}H NMR spectrum of **b2[3]** (C_6D_6, 400.18 MHz, 298K)

Compound b2[4]

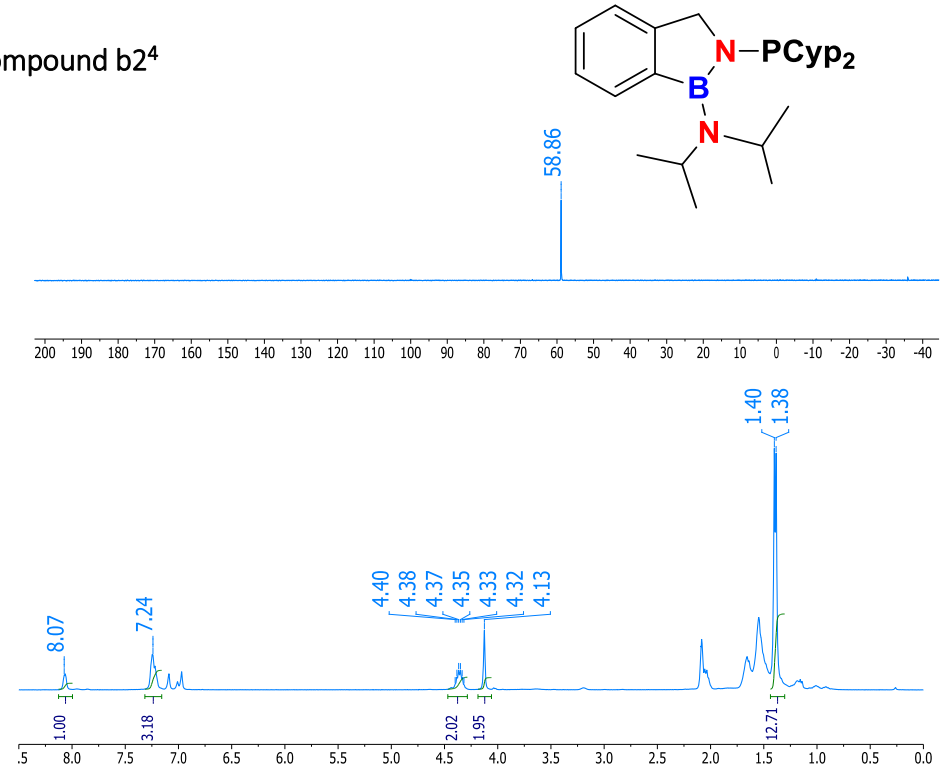

^{31}P{^{1}H} (top) and ^{1}H (bottom) NMR spectra of **b2[4]** (C_6D_6, 161.99 and 400.18 MHz, 298K)

Compound b2[5]

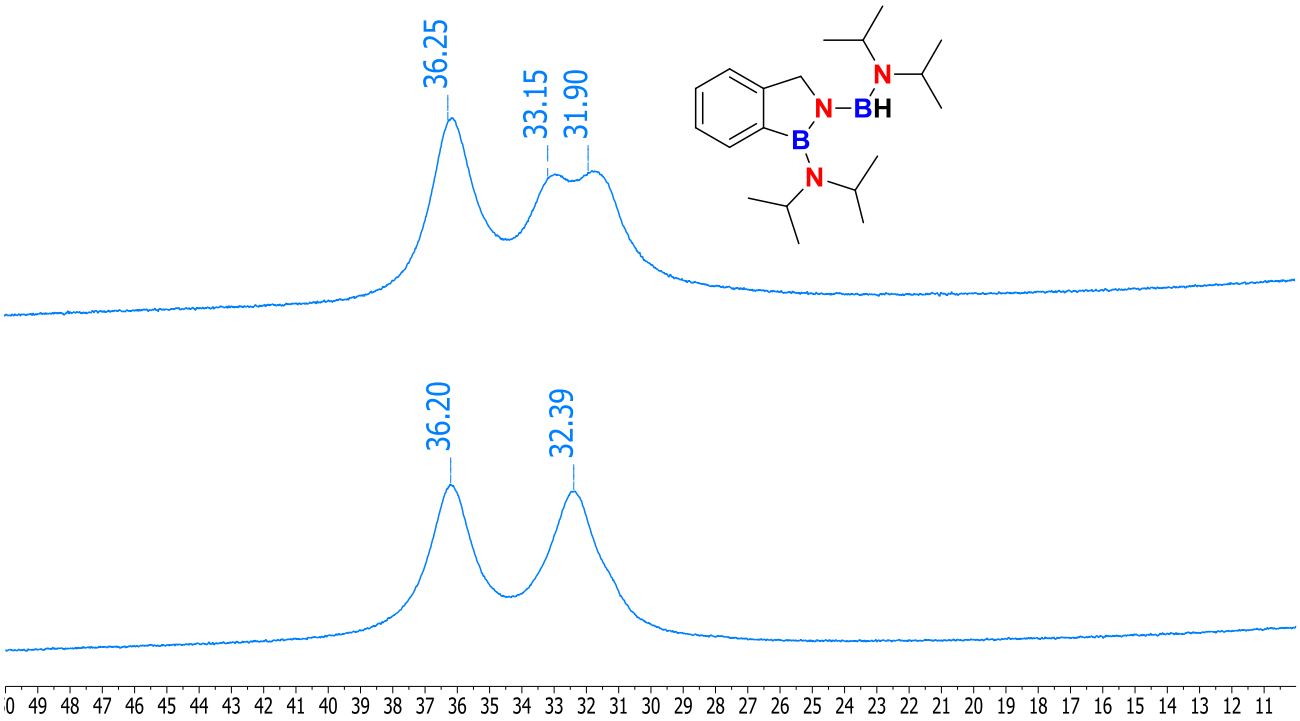

^{11}B **(**top**)** and $^{11}B\{^1H\}$ **(**bottom**)** NMR spectra of **b2[5] (**C_6D_6, 96.29 MHz**,** 298K**)**

Compound b2[6]

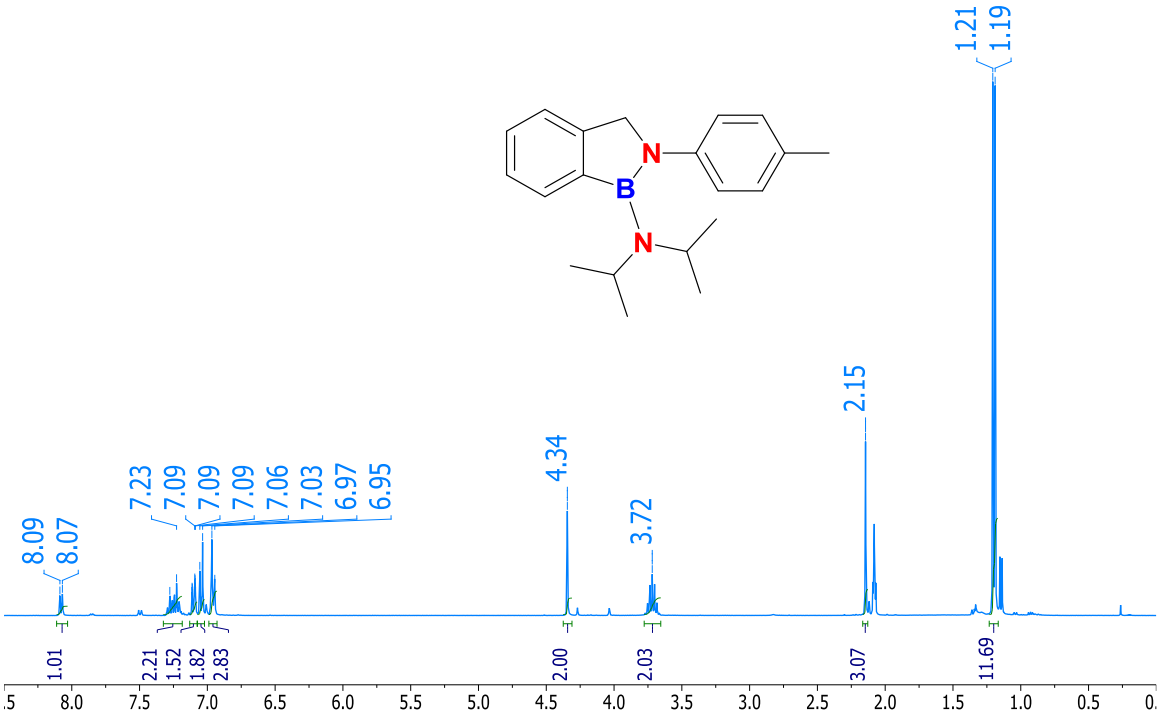

^1H NMR spectrum of **b2[6] (**C_7D_8, 400.18 MHz**,** 298K**)**

Compound b2[7]

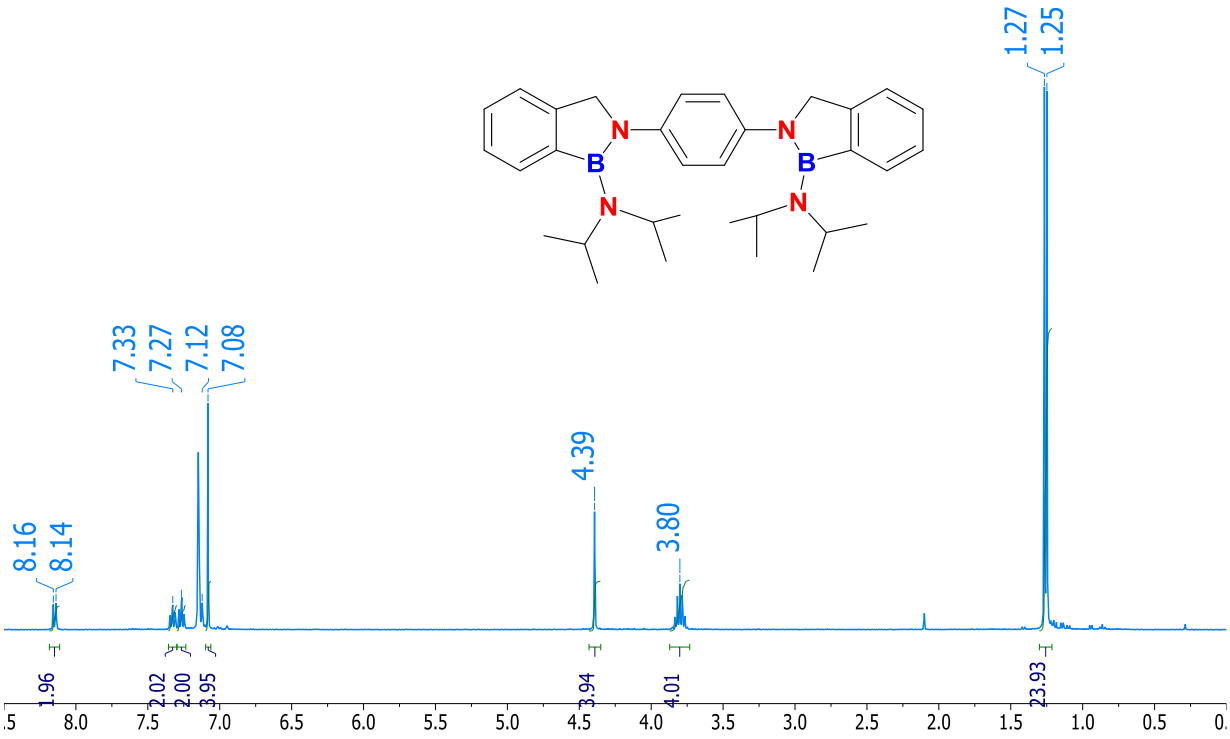

^{1}H NMR spectrum of **b2[7]** (C_7D_8, 400.18 MHz, 298K)

Appendices chapter 5

NMR spectra

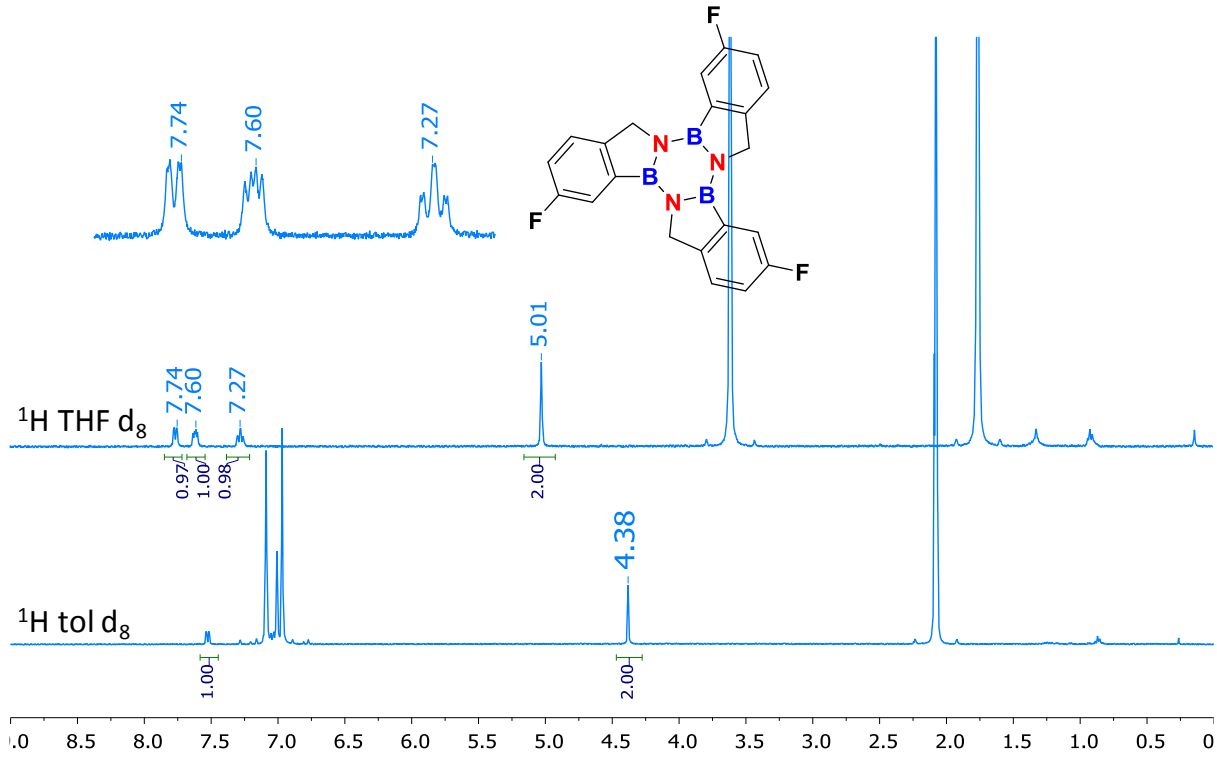

^{1}H NMR spectrum of compound **d1 (**THF d$_8$ and toluene d$_8$, 400.18 MHz**,** 298K**)**

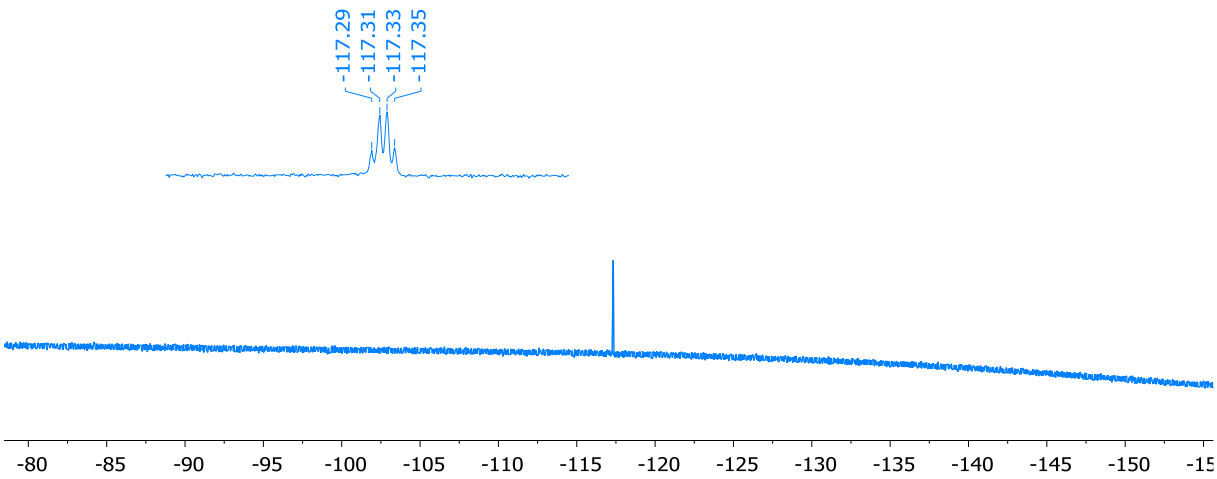

^{19}F NMR spectrum of compound **d1 (**THF d$_8$, 376.51 MHz**,** 298K**)**

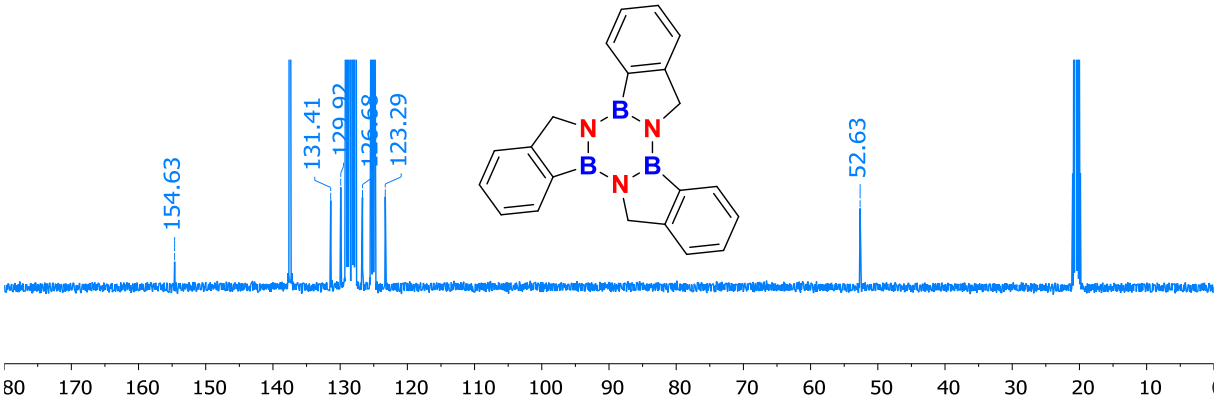

$^{13}C\{^{1}H\}$ NMR spectrum of compound **d2 (**toluene d_8, 100.63 MHz**,** 298K**)**

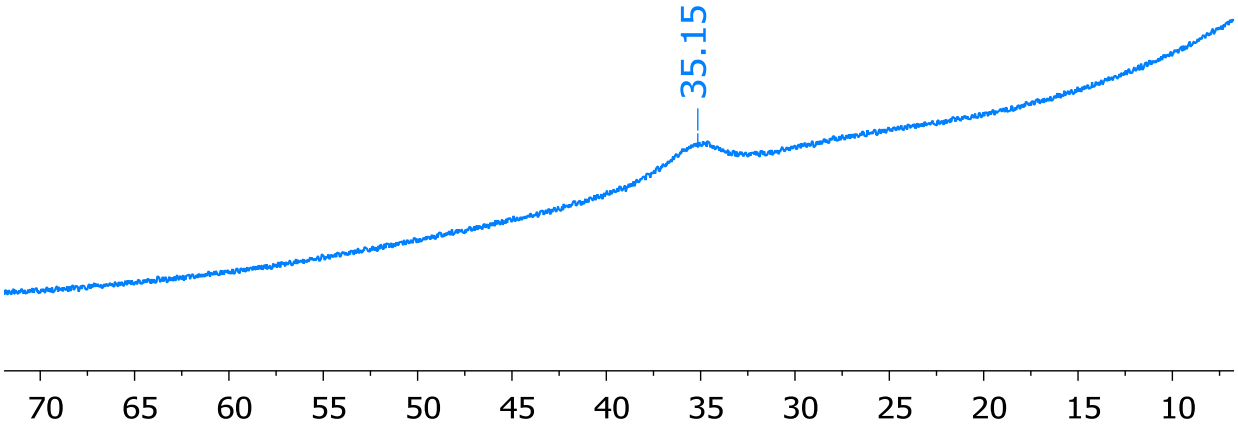

^{11}B NMR spectrum of compound **d2 (**toluene d_8, 128.39 MHz**,** 298K**)**

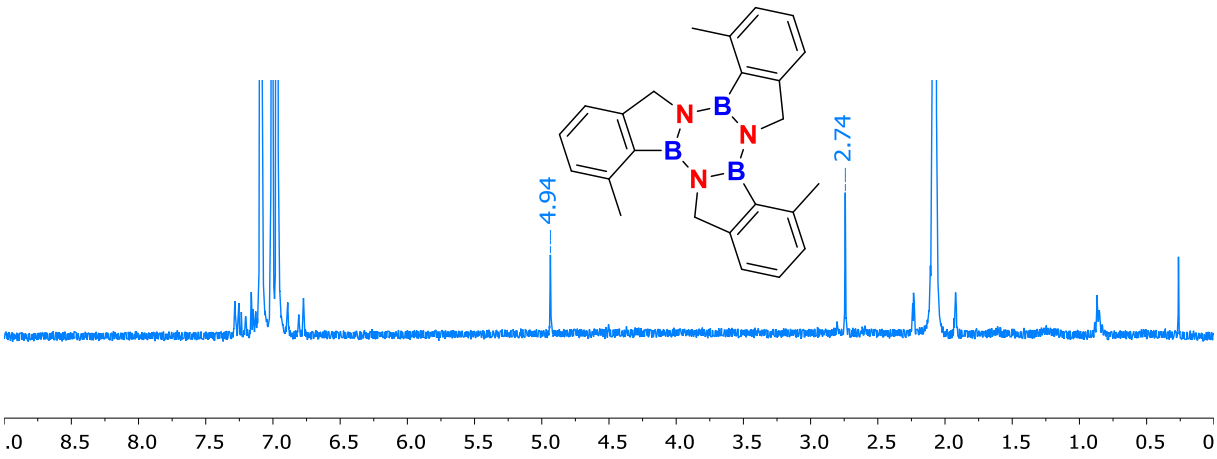

^{1}H NMR spectrum of compound **d3 (**toluene d_8, 400.18 MHz**,** 298K**)**

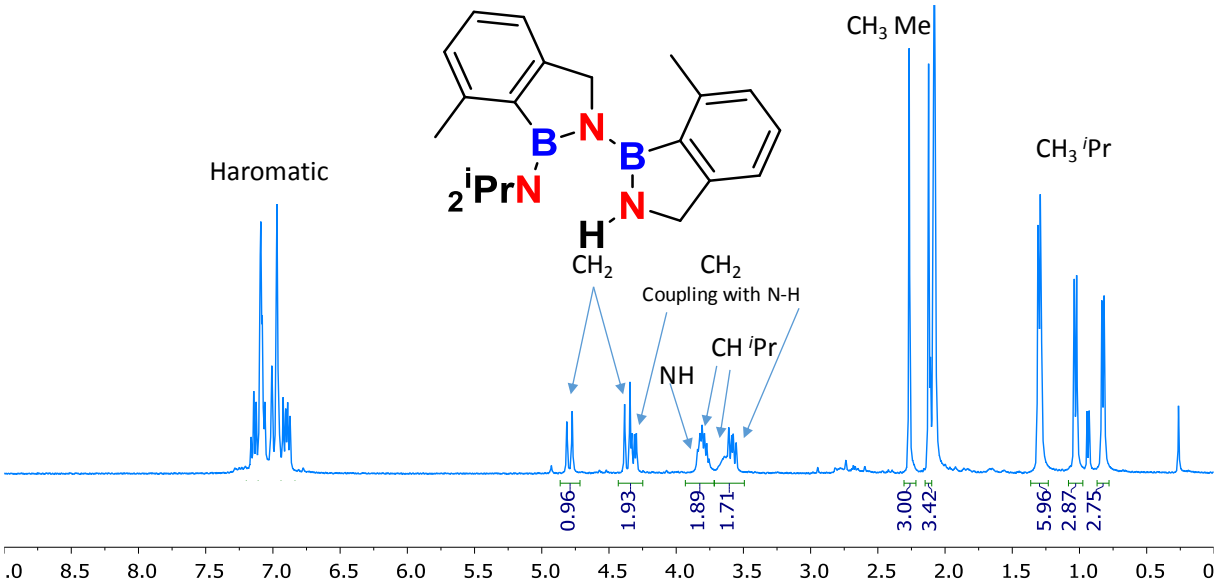

^{1}H NMR spectrum of the intermediate in **d3** formation **(**toluene d_8, 400.18 MHz**,** 298K**)**

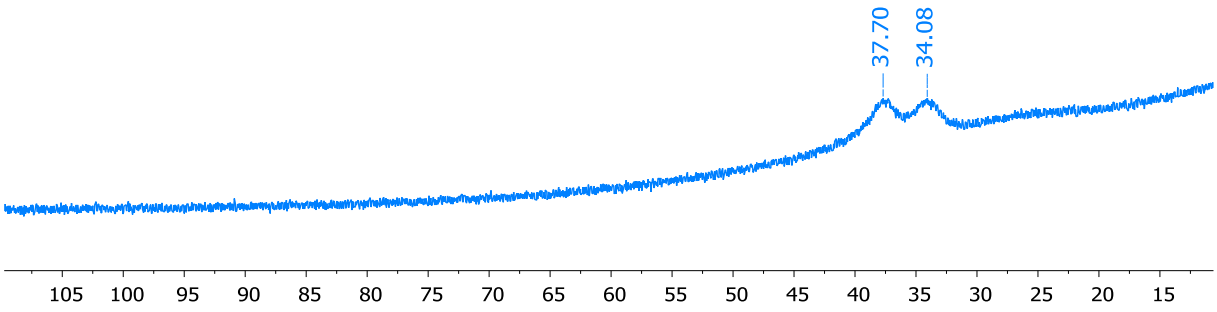

^{11}B{^{1}H} NMR spectrum of the intermediate in **d3** formation **(**toluene d_8, 128.39 MHz**,** 298K**)**

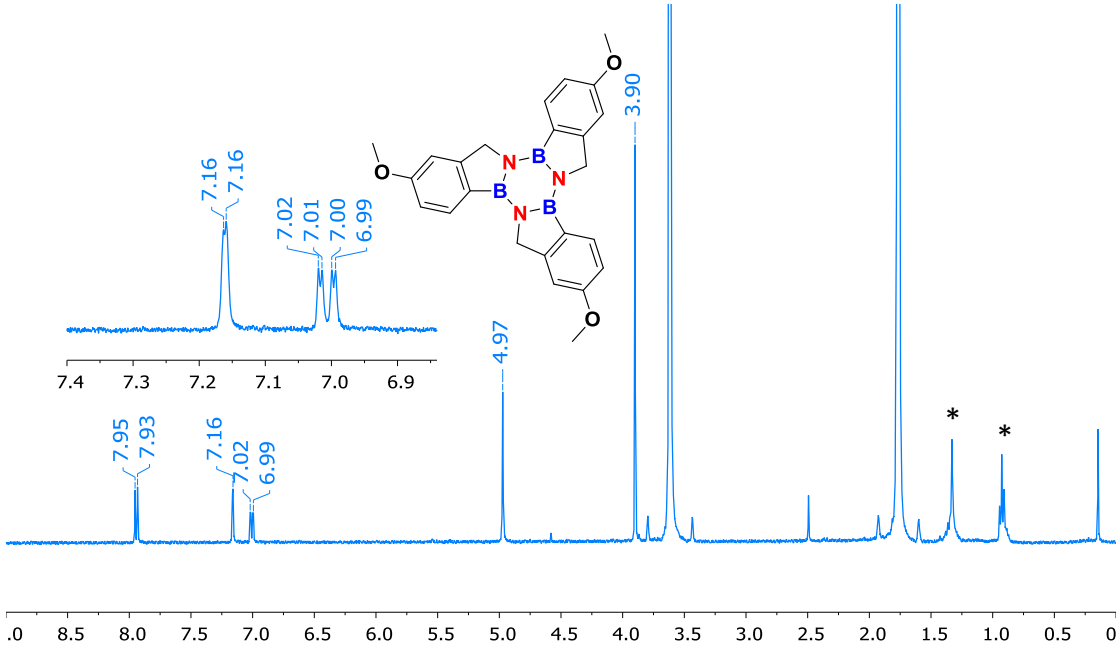

^{1}H NMR spectrum of compound **d4 (**THF d_8, 400.18 MHz**,** 298K**)** *pentane

Infrared analyses

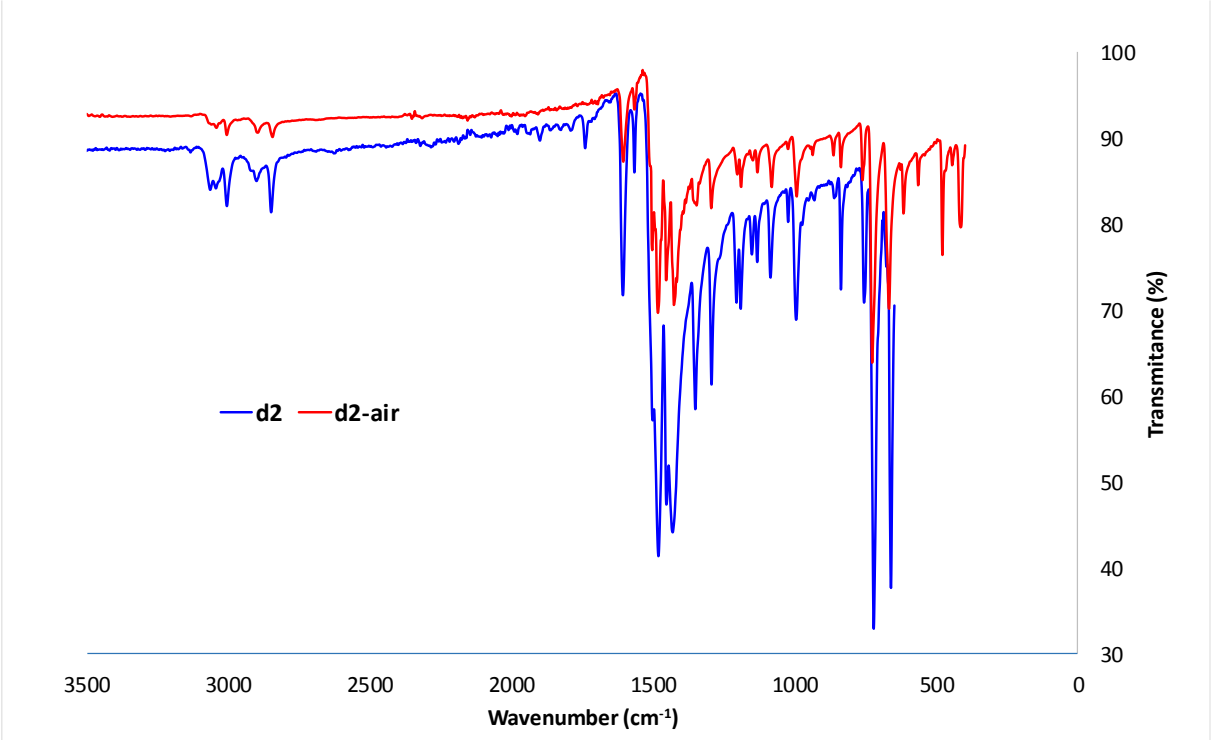

Infrared spectra of **d2** and **d2** after 6 months under ambient atmosphere

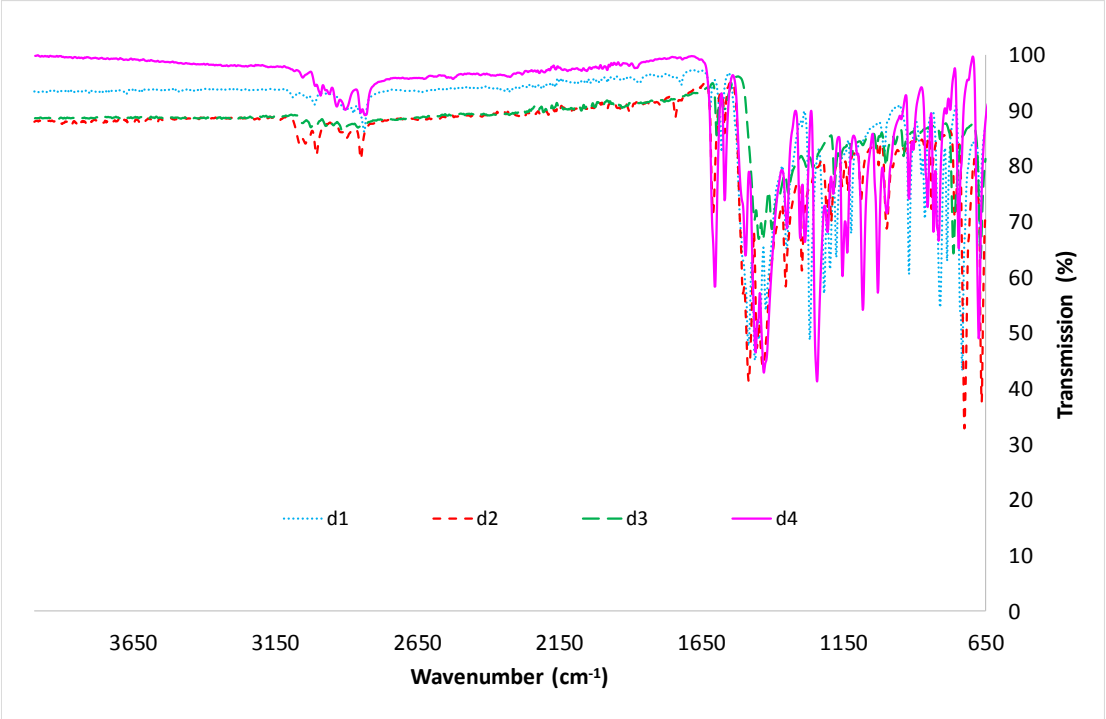

Superimposed infrared spectra of compounds **d1-4**

X-ray data

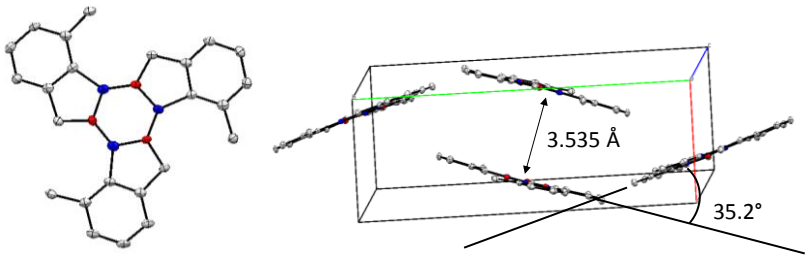

Crystal structure of compound **d3** along with the molecular packing structure

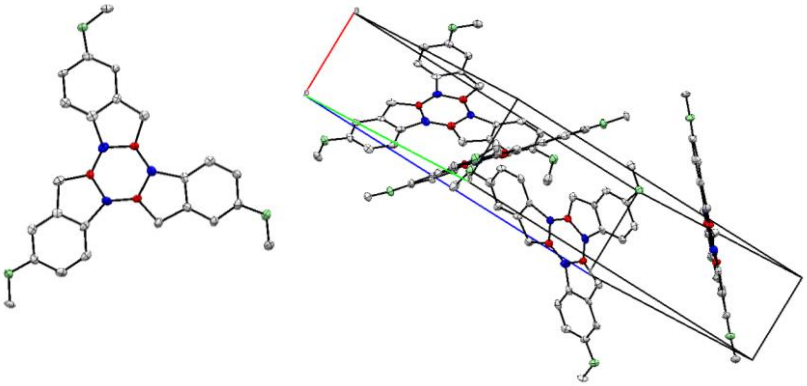

Crystal structure of compound **d4** along with the molecular packing structure

	d2	**d3**	**d4**
Empirical formula	C21 H18 B3 N3	C24 H24 B3 N3	$C_{24}H_{24}B_3N_3O_3$
Formula weight	344.81	386.89	434.89
Temperature	100(2) K	100(2) K	100 K
Wavelength	0.71073 A	0.71073 A	0.71073 A
Crystal system, space group	Monoclinic, P 1 21/c 1	Monoclinic, P 1 21/c 1	Orthorhombic, $P2_12_12_1$
a	5.1643(4)	7.4509(11)	5.1460 (16)
b	14.2468(11)	20.743(3)	19.780 (7)
c	23.4720(18)	12.8490(18)	20.684 (7)
alpha	90	90	90
beta	91.803(3)	101.145(5)	90
gamma	90	90	90
Volume $Å^3$	1726.1(2)	1948.5(5)	2105.4 (12)
Z, Calculated density Mg/m^3	4, 1.327	4, 1.319	4, 1.372
Absorption coefficient	0.077 mm^{-1}	0.076 mm^{-1}	0.09 mm^-1
F**(**000**)**	720	816	912
Crystal size	0.15 x 0.12 x 0.02 mm	0.15 x 0.05 x 0.03 mm	0.15 × 0.02 × 0.02
Theta range for data collection	2.25 to 25.74 deg.	2.54 to 26.37 deg.	2.3–19.2 deg.
Limiting indices	-5<=h<=6, -17<=k<=17, -28<=l<=28	-9<=h<=8, -25<=k<=25, -16<=l<=16	
Reflections collected / unique	36923 / 3310 [R(int) = 0.0478]	42839 / 3986 [R(int) = 0.1440]	
Completeness to theta = 25.00	99.8 %	99.9 %	
Absorption correction	Semi-empirical from equivalents	Semi-empirical from equivalents	Semi-empirical from equivalents
Max. and min. transmission	0.925 and 0.812	0.996 and 0.912	
Refinement method	Full-matrix least-squares on F^2	Full-matrix least-squares on F^2	Full-matrix least-squares on F^2
Data / restraints / parameters	3310 / 0 / 244	3986 / 0 / 274	
Goodness-of-fit on F^2	1.069	1.010	
Final R indices [I>2sigma**(**I**)**]	R1 = 0.0503, wR2 = 0.1190	R1 = 0.0559, wR2 = 0.1217	R1 = 0.068, wR2 = 0.136
R indices **(**all data**)**	R1 = 0.0711, wR2 = 0.1299	R1=0.1073 wR2=0.1448	
Largest diff. peak and hole	0.391 and -0.273 e.A^-3	0.287 and -0.280 e.A^-3	

UV-vis analyses

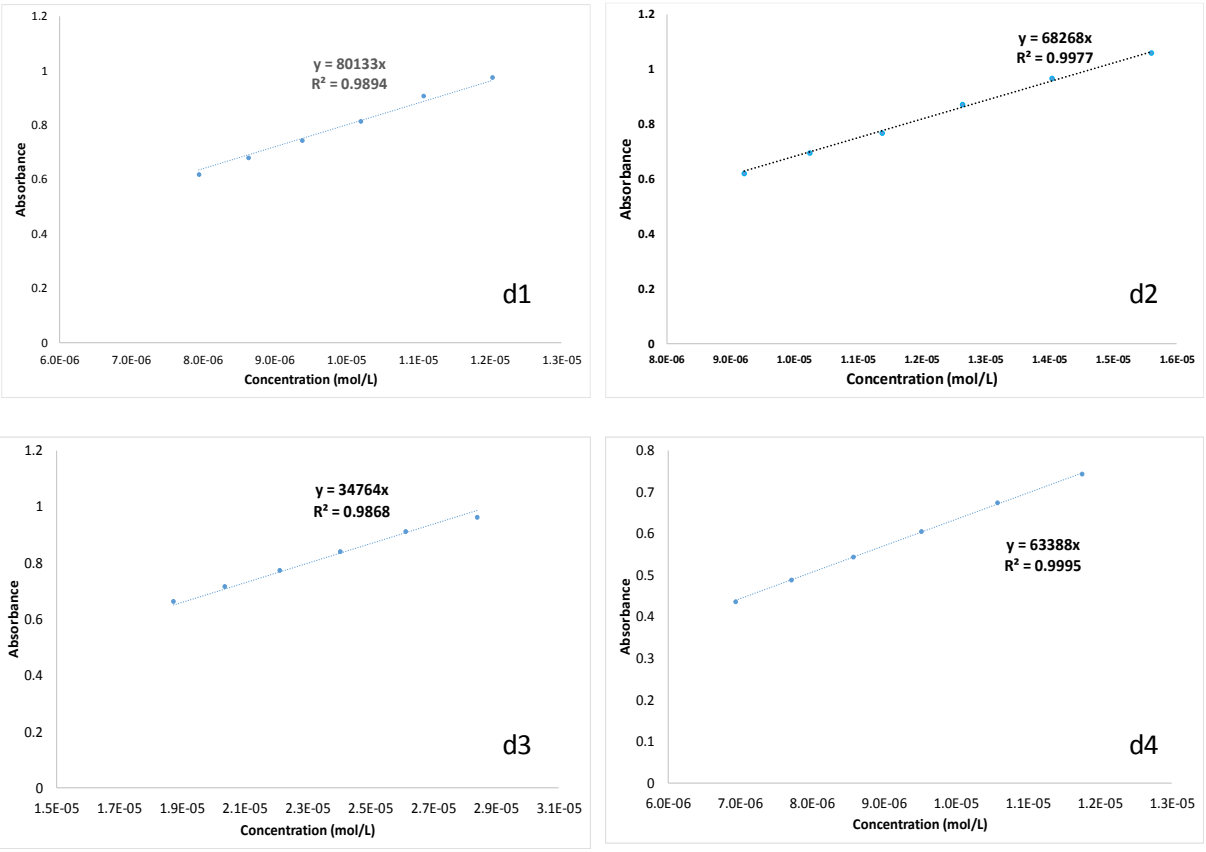

Absorbance versus concentration of compound **d1-4** in CH_2Cl_2 at RT under air atmosphere

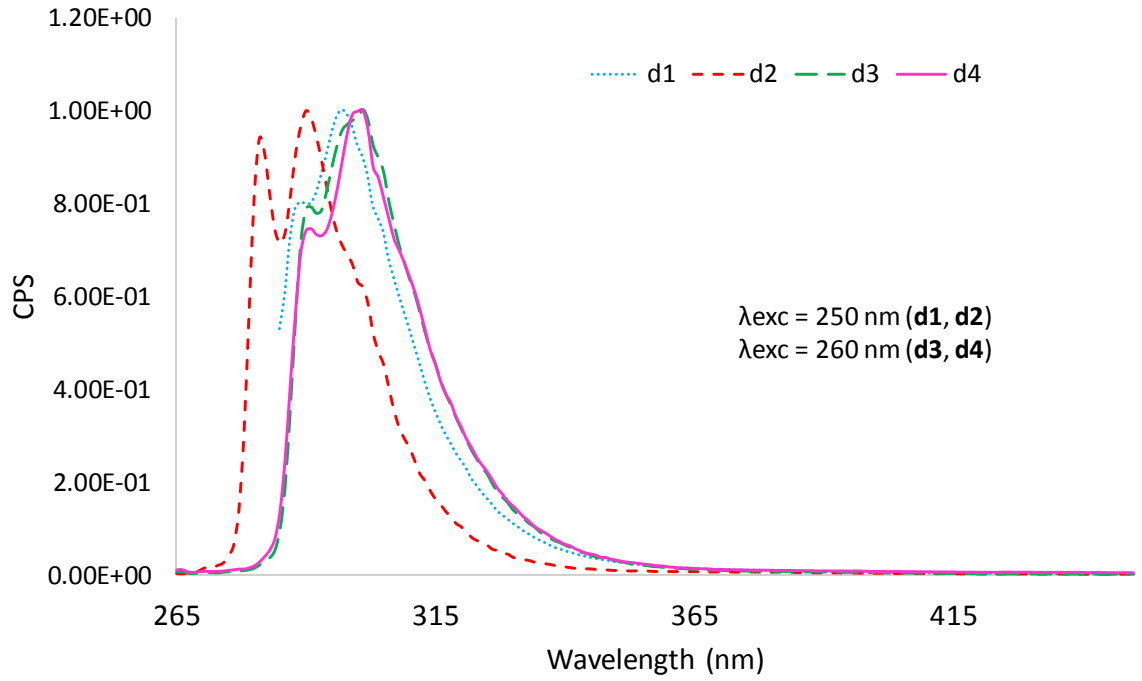

Emission spectra of compounds **d1-4** in CH_2Cl_2 at RT under air atmosphere

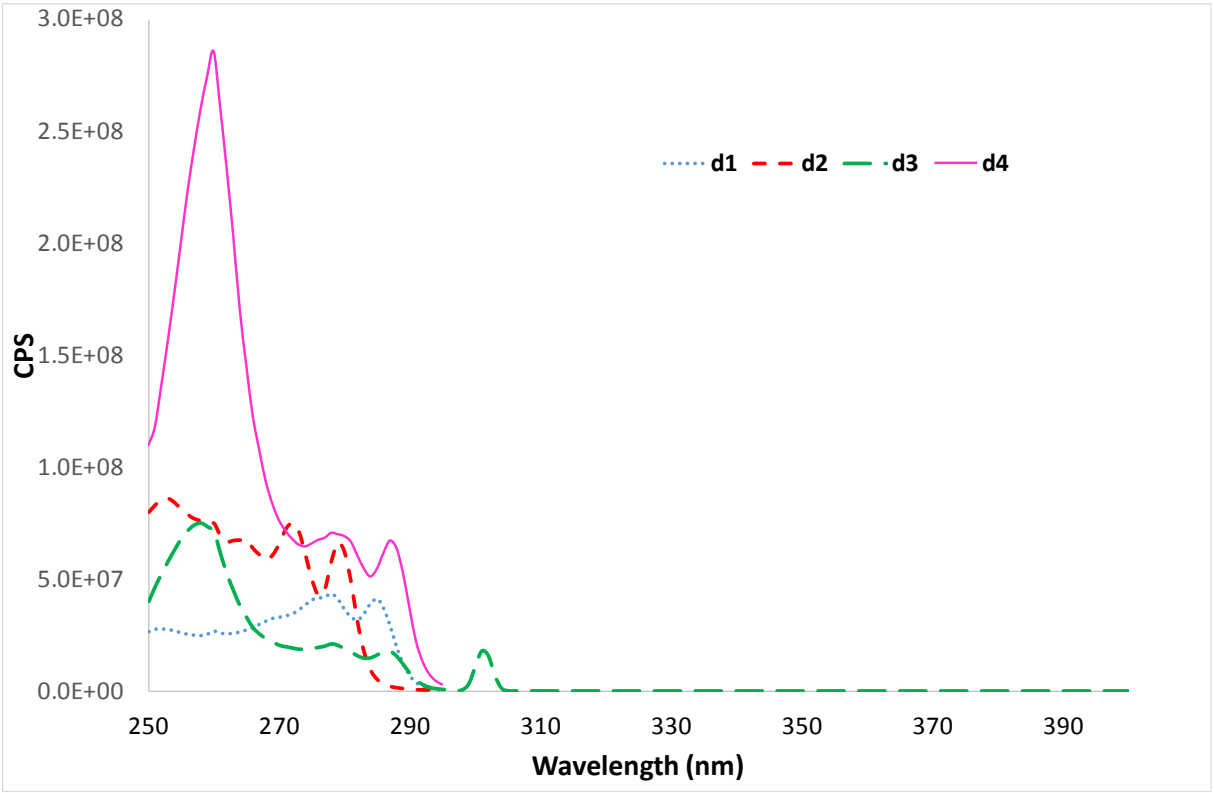

Excitation spectra of compounds **d1-4** in CH_2Cl_2 at RT under air atmosphere

Electrochemical measurements

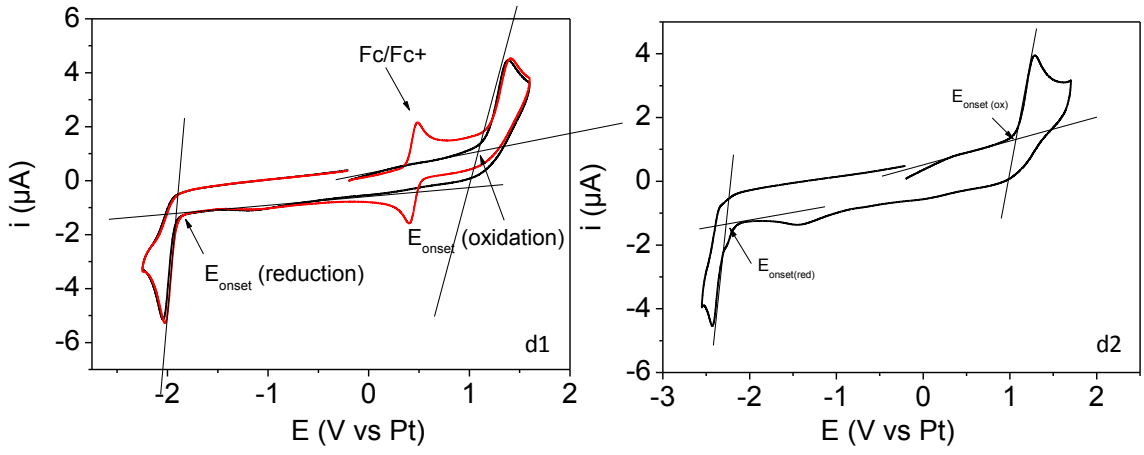

Cyclic Voltammogram of **d1** (left) **and d2** (right) **(**≈ 1 mM**)** at 0.2V/s **(**DMF + 0.1 $MTBAPF_6$, RT**)** at a glassy carbon disk electrode using decamethylferrocene as internal reference.

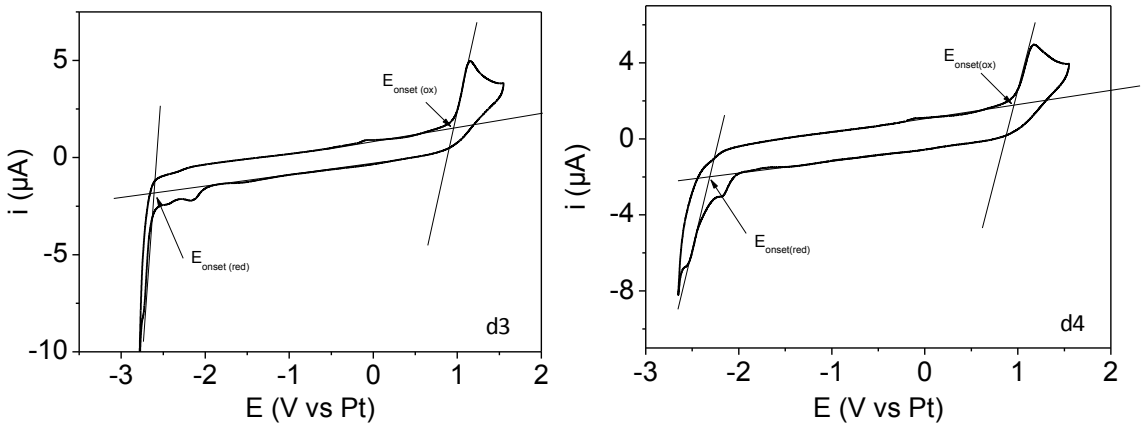

Cyclic Voltammogram of **d3** (left) and **d4** (right) **(**≈ 1 mM**)** at 0.2V/s **(**DMF + 0.1 MTBAPF$_6$, RT**)** at a glassy carbon disk electrode

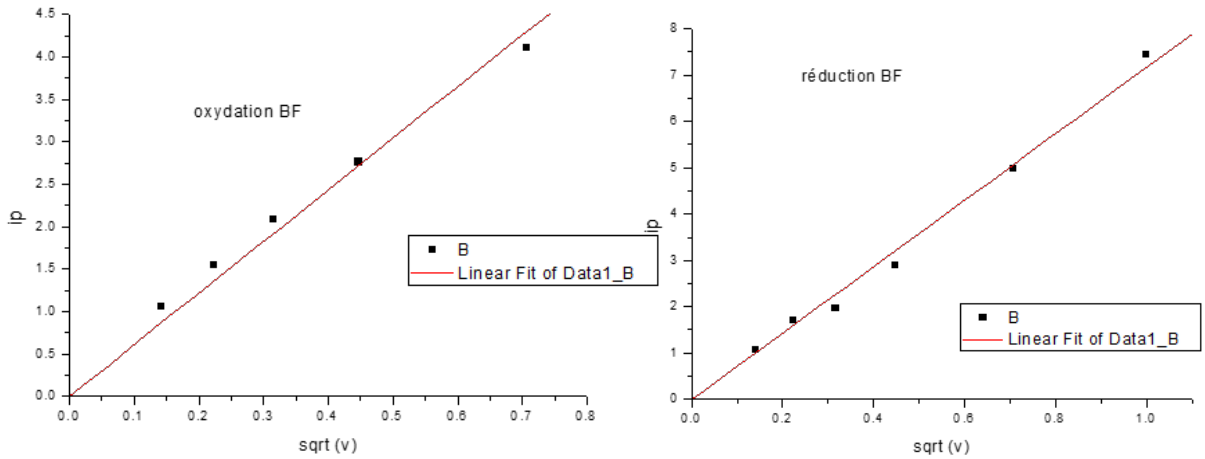

Linear variation of peak currents **(**ip**)** as a function of the square root of the scan rates

RÉSUMÉ EN FRANÇAIS

Résumé en Français

Introduction

La catalyse est un processus naturellement présent dans le monde, comme par exemple dans le corps humain. La catalyse assure le mouvement de la vie en permettant continuellement la transformation des molécules et des corps de façon efficace et sélective, faisant appel en général, à une faible demande énergétique. Pour ces raisons, la catalyse est un des principes de la chimie verte et représente un outil de choix pour répondre à des enjeux sociétaux.

La catalyse peut intervenir sur différent fronts. Notamment, il est nécessaire de diversifier les matières premières que l'on utilise pour éviter l'épuisement des ressources de la terre. La chimie de coordination a un rôle à jouer dans l'activation de molécules inertes telles que le CO_2 ou le N_2, dans la transformation de la biomasse, tout en diversifiant les systèmes catalytiques utilisés pour ces transformations. Il est aussi crucial de contrôler les déchets et de diminuer la pollution en créant des catalyseurs sélectifs et réutilisables ainsi qu'en synthétisant des matériaux biodégradables. Il est nécessaire de trouver une source d'énergie qui n'est pas basée sur le carbone telle que le dihydrogène afin de limiter l'émission de CO_2 qui contribue au réchauffement climatique. Ainsi, la production de H_2 à partir de H_2O ainsi que le stockage de l'hydrogène sont intensivement étudiés. L'utilisation de la catalyse pourrait permettre de répondre à ces enjeux. L'obtention de systèmes efficaces et sélectifs ainsi que la découverte de nouvelles transformations passent par la compréhension fondamentale des interactions entre le substrat et le catalyseur. Dans ce contexte, le bore prend de plus en plus d'importance en chimie de coordination et particulièrement dans des réactions catalysées car il permet de répondre à un vaste panel de problématiques.

Chapitre 1 :

Les travaux de recherches sur les boranes ont été trois fois récompensés par un prix Nobel, en 1976, 1979 et plus récemment en 2010 pour la réaction catalysée de Miyaura et Suzuki. Cette dernière ainsi que l'émergente fonctionnalisation de liaisons C–H par borylation sont deux exemples représentatifs de réaction catalytiques faisant intervenir les boranes. Ces réactions permettent la formation d'une très grande variété de composés à haute valeur ajoutée.

Couplage de Suzuki-Miyaura:

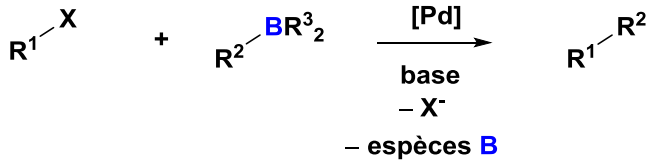

Création de liaisons C–C: conditions douces, grandes variétés de composés formés

Selective functionalization C–H:

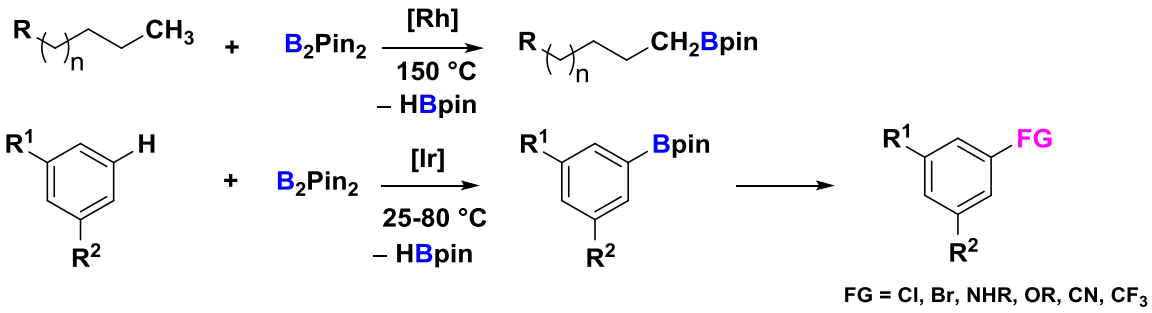

Création de liaisons C–FG: selectif, une route unique pour différentes liaisons formées

Les boranes contenant une liaison B–H sont aussi très largement étudiés. En effet, l'électronégativité respective des atomes de bore (2.04 sur l'échelle de Pauling) et d'hydrogène (2.10 sur l'échelle de Pauling) ainsi que le caractère acide de Lewis du bore fait que l'atome de bore agit comme l'électrophile et l'atome d'hydrogène comme le nucléophile. Ces propriétés permettent en partie la réduction de liaisons multiples par la réaction d'hydroboration. Utiliser la catalyse a permis l'obtention de réactions sélectives au niveau de de la fonction chimique, du site, ainsi que de la stéréochimie, tout cela dans des conditions douces. L'utilisation de la catalyse pour les réactions d'hydroboration a également permis de réduire des liaisons très fortes comme les liaisons C=O du CO_2. Cette stratégie permet la réduction du CO_2 dans des conditions douces et ainsi l'étude et la compréhension des étapes élémentaires du mécanisme de réduction. Un défi actuel dans le domaine de l'hydroboration est l'obtention de composés Z-alcenylboranes issus de l'hydroboration *trans* qui est observé uniquement lorsque la réaction est catalysée. Enfin, une stratégie émergente est l'utilisation d'hydroborane afin de réduire des liaisons multiples polaires et particulièrement la fonction nitrile. Cela permet une réduction des nitriles très sélective vers les amines dans des conditions douces. Un des avantages d'utiliser l'hydroboration plutôt que l'hydrogénation pour réduire les fonctions multiples est la diversité des systèmes catalytiques qui peuvent être utilisés.

hydroboration:

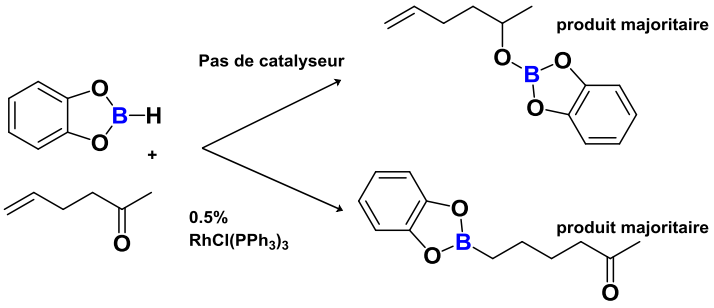

Réduction de liaisons multiples

CO_2	-C≡C-	-C≡N-
Réduction de molécule inerte	*Trans* hydroboration Z-alcenylboranes	Réduction sélective

Les boranes en catalyses sont principalement étudiés comme médiateur de la réaction et sont comptabilisés comme déchets. Cependant, quelques récents exemples montrent qu'il est possible d'utiliser la stratégie d'hydroboration pour produire des molécules d'intérêt contenant du bore. Par exemple, le groupe de Figueroa a décrit l'hydroboration d'isonitrile pour générer le *syn* (boryl)iminométane pouvant activer les petites molécules.

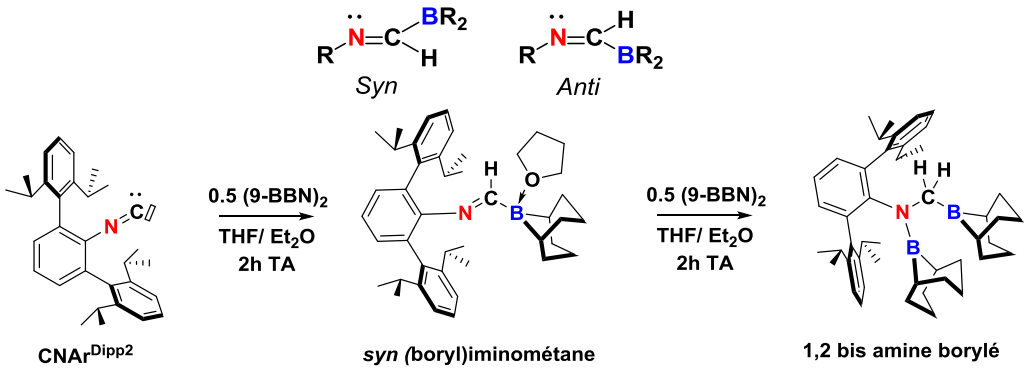

Activation de petites molécules

Le groupe de Shi a démontré l'hydroboration intramoléculaire pour former des composés BN cycliques.

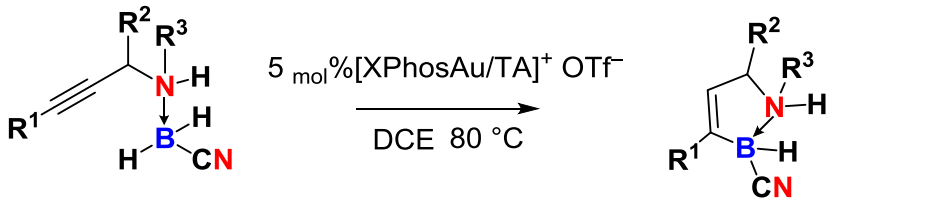

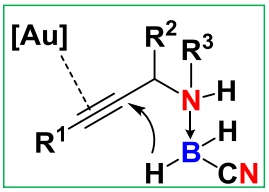

Ils ont mis au point la synthèse de composés bifonctionnels contenant une fonction alcyne ainsi qu'une liaison B–H. Lors de l'hydroboration intramoléculaire catalysée par un complexe d'or, ils proposent un mécanisme impliquant principalement l'activation de l'alcyne.

Dans ce manuscrit, nous avons utilisé les connaissances acquises dans les processus d'activation de la liaison B–H pour permettre la synthèse de molécules peu communes contenant du bore. Dans une étude précédente, l'équipe a montré que l'activation de la liaison B–H d'un aryl(phosphino)(aminoborane) avec le complexe bis(dihydrogène) $RuH_2(H_2)_2(PCy_3)_2$ a conduit à la caractérisation d'un mode de coordination à 3-centre-2 électrons (σ-B–H) avec un bore sp^2. Dans une autre étude, il a été montré que $RuH_2(H_2)_2(PCy_3)_2$ peut hydrogéner sélectivement le benzonitrile en benzylamine. Par conséquent, afin de pousser l'étude de coordination vers un système catalytique, nous avons conçu un nouveau substrat dans lequel la phosphine est remplacée par une fonction nitrile réactive :

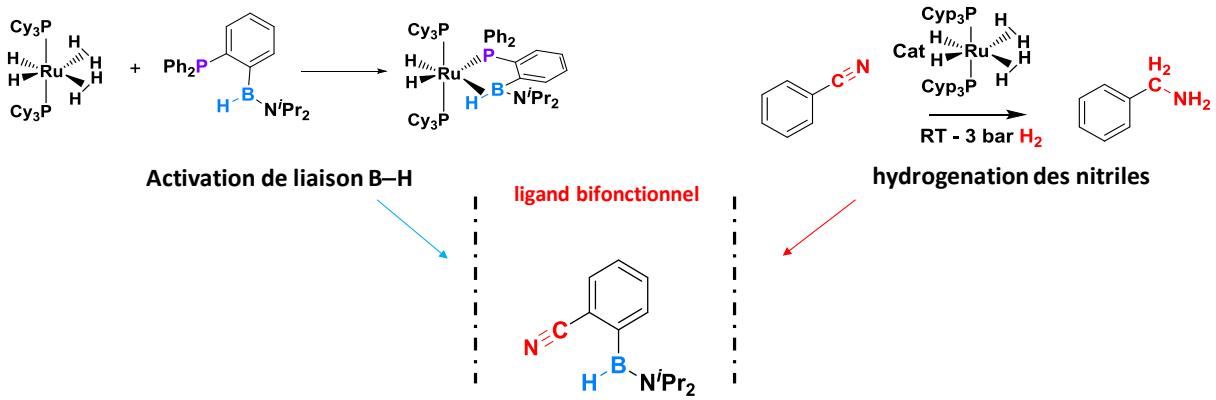

CHAPITRE 2 :

Une série d'aryl(cyano)(aminoborane) a été synthétisée via une stratégie de lithiation/borylation efficace.

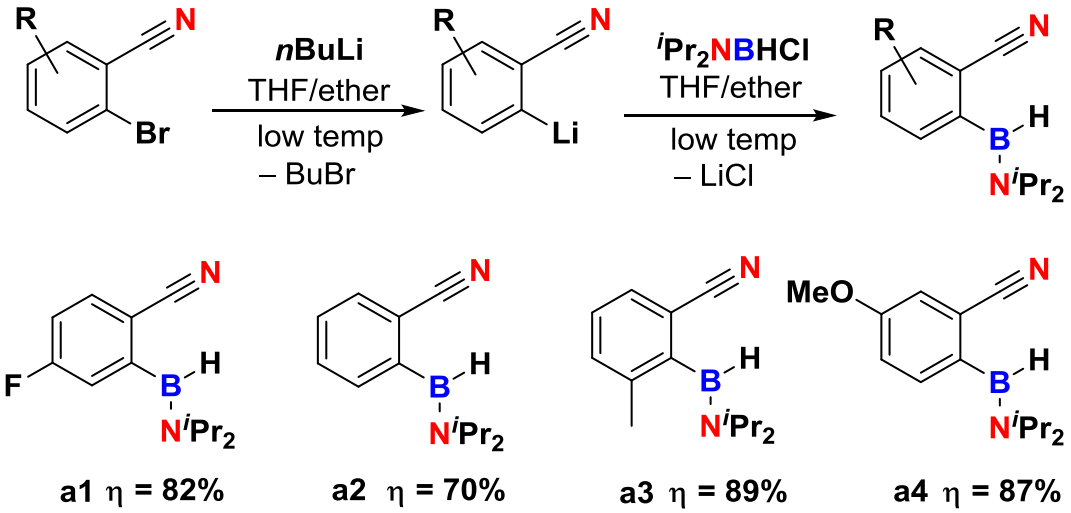

a1 η = 82% **a2** η = 70% **a3** η = 89% **a4** η = 87%

Le composé **a2** a été isolé sous la forme d'une huile incolore, stable à température ambiante. Le composé a été entièrement caractérisé par RMN, HRMS et IR. Spécifiquement, la RMN ^{11}B est un outil puissant pour la caractérisation des boranes. Le singulet à δ 37,5 dans la RMN du ^{11}B $\{^{1}H\}$ devient un doublet dans la RMN ^{11}B avec une constante de couplage de 115 Hz. Le déplacement chimique est caractéristique d'un bore trivalent alors que la grande constante de couplage est dans la gamme typique pour un couplage direct B–H. Le spectre RMN ^{1}H associé montre un large quartet à δ 5,5 attribué à la résonance B–H (voir Figure suivante). L'isotope ^{11}B a un spin 3/2, de sorte que le proton B–H doit être un quartet en fonction de la règle de multiplicité. Le signal est large en raison du grand moment quadrupolaire des noyaux ^{11}B. Dans le spectre RMN ^{1}H $\{^{11}B\}$, la résonance B–H est associée à un singulet bien défini.

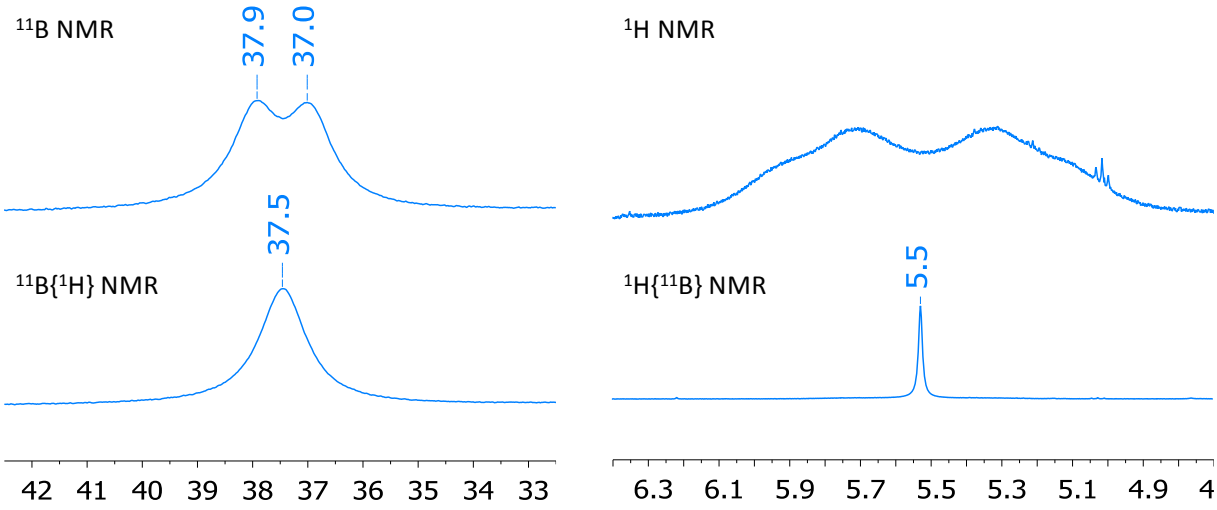

La réactivité des précurseurs avec $RuH_2(H_2)_2(PCy_3)_2$ a été évaluée. Le borane de départ subit une hydrogénation/cyclisation intramoléculaire catalytique impliquant à la fois une réduction du nitrile et une activation de la liaison B–H, sous dihydrogène. La réaction se produit dans des conditions douces (RT, PH_2 = 1 bar). Les produits résultants de la transformation, les 1H-2,1-benzazaboroles, sont des analogueues BN de l'indène avec un caractère de double liaison B–N. Pour la première fois, la synthèse est réalisée directement à partir d'une fonction nitrile ainsi que d'une manière catalysée.

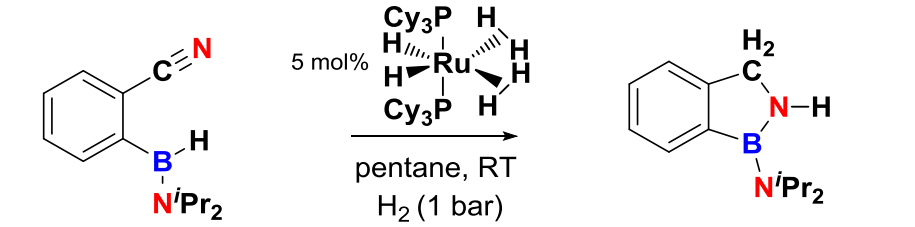

aryl(cyano)(aminoborane)

a2

1*H*-2,1-benzazaborole

b2

Les composés présentent une liaison N–H, en raison de la méthode de synthèse mise en œuvre. La réaction a été étendue avec succès à trois substrats comportant des groupes plus ou moins électroattracteurs sur l'aryle.

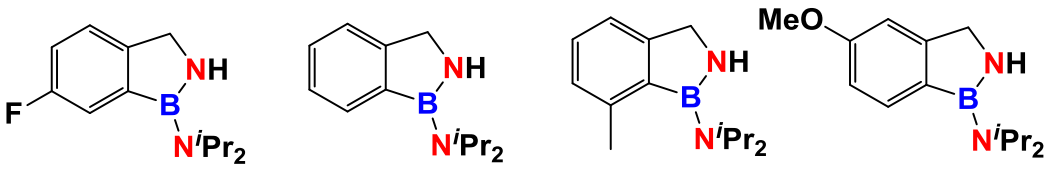

b1 b2 b3 b4

Rendement RMN (borazine)	7	7	24	ND
Rendement RMN (b)	84	85	73	ND
Rendement isolé (b)	50	82	57	54

Peu d'impact des substituants sur les données spectroscopiques a été observé. Cependant, la substitution par un méthyle en ortho du borane induit un changement dans la sélectivité de la réaction. Les précurseurs et les produits sont entièrement caractérisés par RMN, infrarouge et spectrométrie de masse ainsi que par diffraction des rayons X (sauf pour a4). Dans le chapitre suivant, nous étudierons le mécanisme de cette nouvelle réaction catalytique.

CHAPITRE 3 :

Comme point de départ, nous avons fait quelques hypothèses sur le mécanisme sur la base des travaux précédents. Notre première hypothèse repose sur deux études principales menées avec $RuH_2(H_2)_2(PCy_3)_2$.

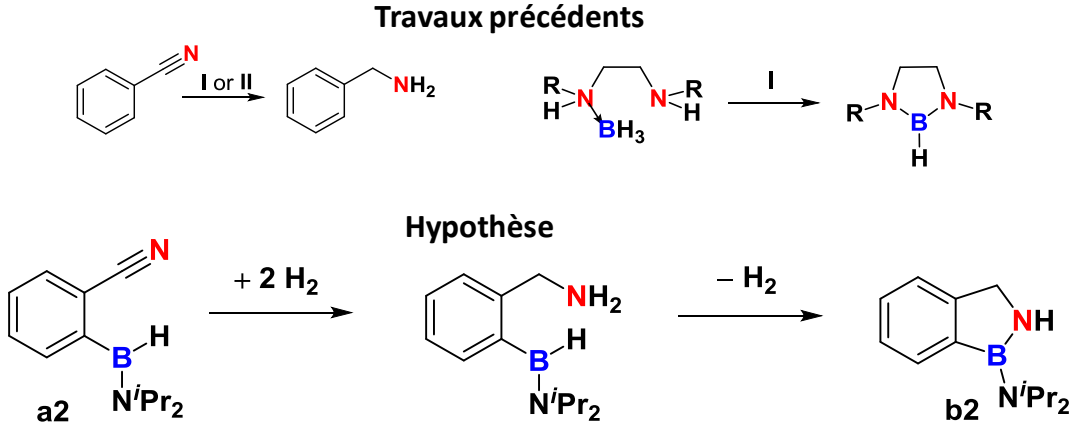

Nous savions que les complexes $RuH_2(H_2)_2(PR_3)_2$ (R = Cy, **I** et Cyp, **II**) pouvaient catalyser l'hydrogénation du benzonitrile en benzylamine. Nous pourrions donc envisager une première étape dans laquelle la fonction nitrile de l'aryl(cyano)(aminoborane) **a2** serait totalement hydrogénée, en laissant de côté la partie borane. L'équipe a également démontré la déshydrogénation de composés diaminemonoborane en utilisant **I** comme catalyseur. Ils ont

montré une activation séquentielle des liaisons B–H et N–H pour libérer H_2 et former la liaison B–N. Nous pourrions imaginer le même processus avec le benzylamine borane pour former b2. Globalement, la réaction nécessiterait encore un équivalent de dihydrogène, mais le procédé impliquerait une étape de déshydrogénation. Il a également été établi que le complexe **I** peut catalyser l'hydroboration intermoléculaire des alcènes. De plus, les aminoboranes peuvent hydroborer le benzonitrile avec un catalyseur à base de lithium. Par conséquent, une seconde hypothèse serait de considérer l'hydroboration intramoléculaire de la fonction nitrile. Une fois que la liaison B–N est formée, le 2,1-benzazaborole subirait une hydrogénation du fragment imine.

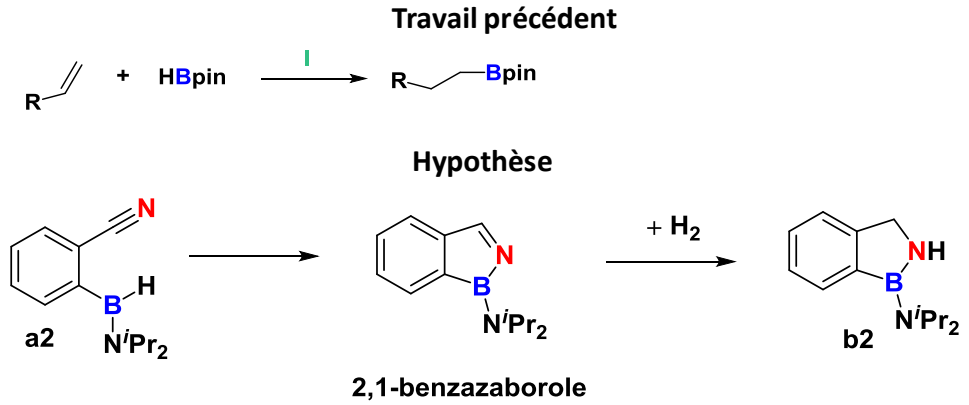

La dernière option que nous avons considérée est la séquence d'hydrogénation/hydroboration. Dans ce cas, une hydrogénation partielle de la fonction nitrile produirait une fonction imine, plus susceptible de subir une hydroboration intramoléculaire qu'une hydrogénation intermoléculaire.

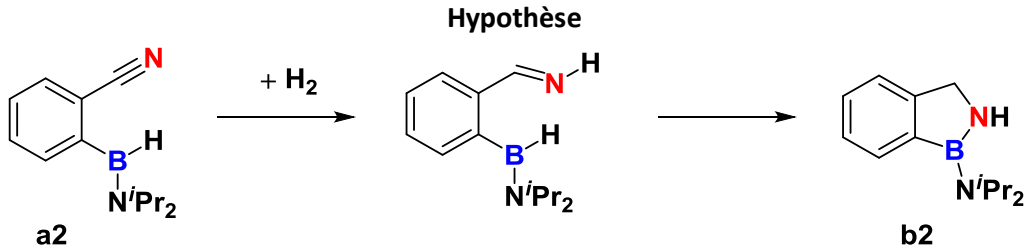

En résumé, nous pouvons proposer trois voies de transformation. Nous suggérons pour la formation de **b2** à partir de **a2** soit formellement:

• une séquence d'hydrogénation / déshydrogénation (1)

• une séquence d'hydroboration / hydrogénation (2)

• une séquence d'hydrogénation / hydroboration (3)

Nous supposons que les intermédiaires proposés dans ces séquences ne sont pas nécessairement libérés dans le milieu en raison de leur possible instabilité ou réactivité. Au-delà de la sélection d'une séquence, nous souhaitons analyser la coordination du substrat sur le catalyseur ainsi que les processus d'activation des liaisons C≡N et B–H. Sur la base d'études antérieures concernant la synthèse du ruthénium agostique aryle(phosphino)(aminoborane), nous pouvons proposer un mode de coordination agostique η2-C≡N, σ-B–H sur le ruthénium.

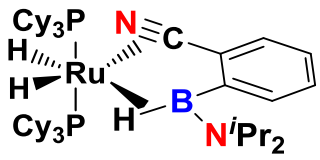

η^2-C≡N, agostique σ-B–H

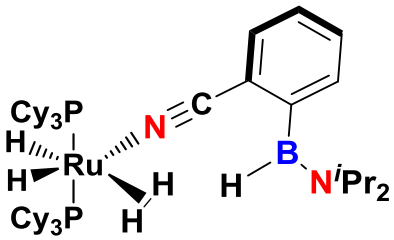

η^1-C≡N, σ-B–H pendante

Cette proposition se réfère à une activation simultanée de la liaison C≡N et B–H. Une activation supplémentaire de la liaison B–H pourrait conduire à la formation de liaison B–N. Une autre perspective, qui rappelle l'hydrogénation du benzonitrile, engagerait le nitrile dans un mode de coordination η^1 avec le centre métallique. Dans ce cas, la liaison C≡N serait activée avec le dihydrogène sur le métal et serait plus susceptible de réagir indépendamment du fragment B–H non activé.

Afin d'obtenir des informations sur le mécanisme de la transformation catalytique, nous avons mené une série d'expériences à la fois aux niveaux stœchiométrique et catalytique. Le suivi RMN en utilisant des tubes RMN basse pression s'est révélé être un moyen efficace pour identifier des intermédiaires. Notre étude approfondie a permis d'identifier plusieurs intermédiaires catalytiques et en particulier, nous avons pu isoler un complexe benzazaborolyl-ruthénium qui a piégé le produit BN à un stade intermédiaire avant sa libération finale en 1*H*-2,1-benzazaborole. Des calculs DFT ont permis de compléter les données expérimentales.

Suivi de la réaction :

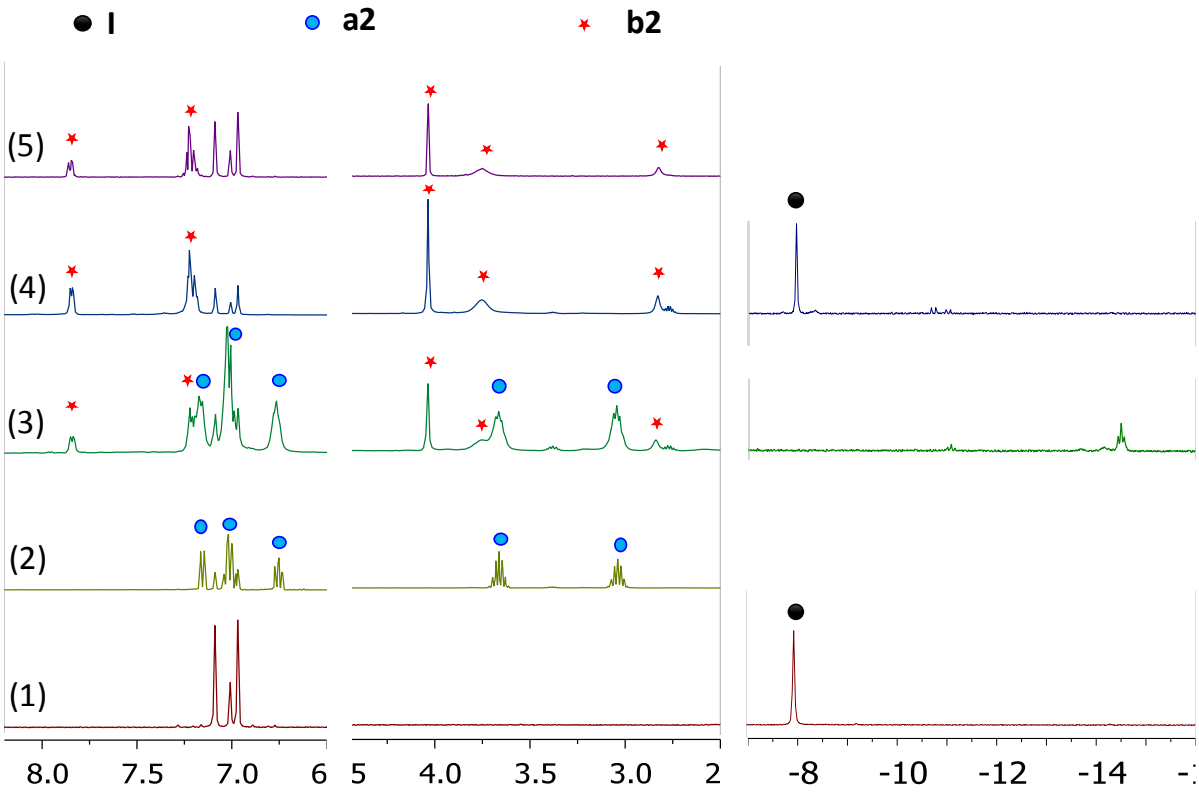

Lorsque la réaction a été effectuée dans un tube RMN sous pression, en utilisant 5% molaire de catalyseur **I** dans une solution de C_7D_8, nous avons remarqué, avant d'ajouter H_2, un changement de couleur au rouge accompagné d'un dégagement de gaz. A ce point, l'analyse RMN du mélange brut indique la consommation du précurseur de catalyseur **I** et déjà la formation de 1H-2,1-benzazaborole **b2** malgré le fait que nous n'ayons pas encore introduit de gaz H_2 (entrée (3)). Une nouvelle espèce hydrure a été détectée, en particulier caractérisée par un triplet à −14 ppm et un signal à 64 ppm dans les spectres RMN ^{1}H et ^{31}P {1H}, respectivement (voir ci-dessous). A la fin de la réaction catalytique, **a2** a été converti en **b2** et le précurseur catalytique **I** a été récupéré (figure 1 entrée (4)). A titre de comparaison, les spectres RMN ^{1}H de **I, a2** et **b2** sont également représentés (entrées (1), (2) et (5), respectivement).

RMN à basse température :

Nous avons répété la même expérience en introduisant 1 bar de dihydrogène et en congelant le tube juste après le mélange dans de l'azote liquide. Le premier spectre RMN enregistré à −80 ° C a montré la même espèce hydrure du ruthénium caractérisée par le triplet sur la figure

précédente entrée (3). La caractérisation RMN en profondeur nous a permis de la formuler comme le bis (nitrile) $[RuH_2\{NC(C_6H_4)BH(NiPr_2)\}_2(PCy_3)_2]$ (4) résultant formellement de la substitution des ligands dihydrogènes par des ligands cyano. En plus des expériences RMN DOSY, une tâche en RMN 2D-HMBC ^{13}C $\{^{31}P\}$ / ^{1}H indique une corrélation entre les hydrures et le carbone quaternaire du nitrile à 120,3 ppm. La résonance B–H (+5,7 ppm) n'est que légèrement décalée par comparaison à **a2** (+5,5 ppm), éliminant toute interaction agostique.

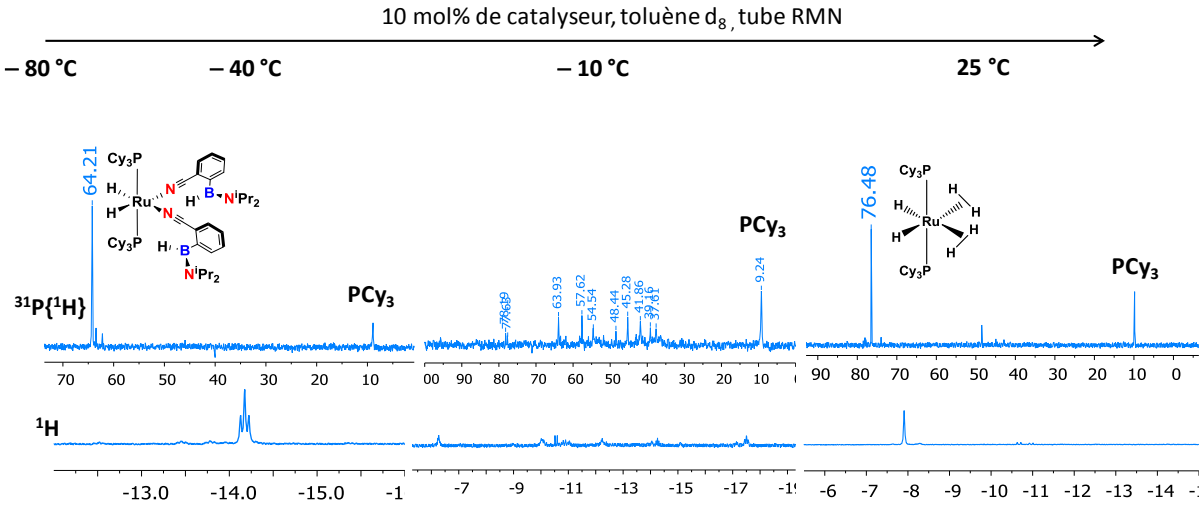

En augmentant la température jusqu'à -10 °C, le cyanoborane se transforme en benzazaborole. Cependant, beaucoup d'espèces en RMN du phosphore et du proton apparaissent, rendant impossible l'attribution de possibles intermédiaires de réaction. Après retour à température ambiante, le cyano borane est totalement converti et le catalyseur est régénéré.

Réactions stœchiométriques :

Cette étude stœchiométrique a mis en évidence la capacité du complexe $RuH_2(H_2)_2(PCy_3)_2$ (**I**) à fournir et transférer le dihydrogène au benzonitrile borane (**a2**) et à permettre la formation du 1H-2,1- benzazaborole (**b2**). Les espèces de ruthénium ont été caractérisées à différents stades de déshydrogénation en fonction de la quantité de **a2** que nous avons ajoutée. Les différentes espèces de ruthénium déshydrogénées sont représentées sur le schéma suivant.

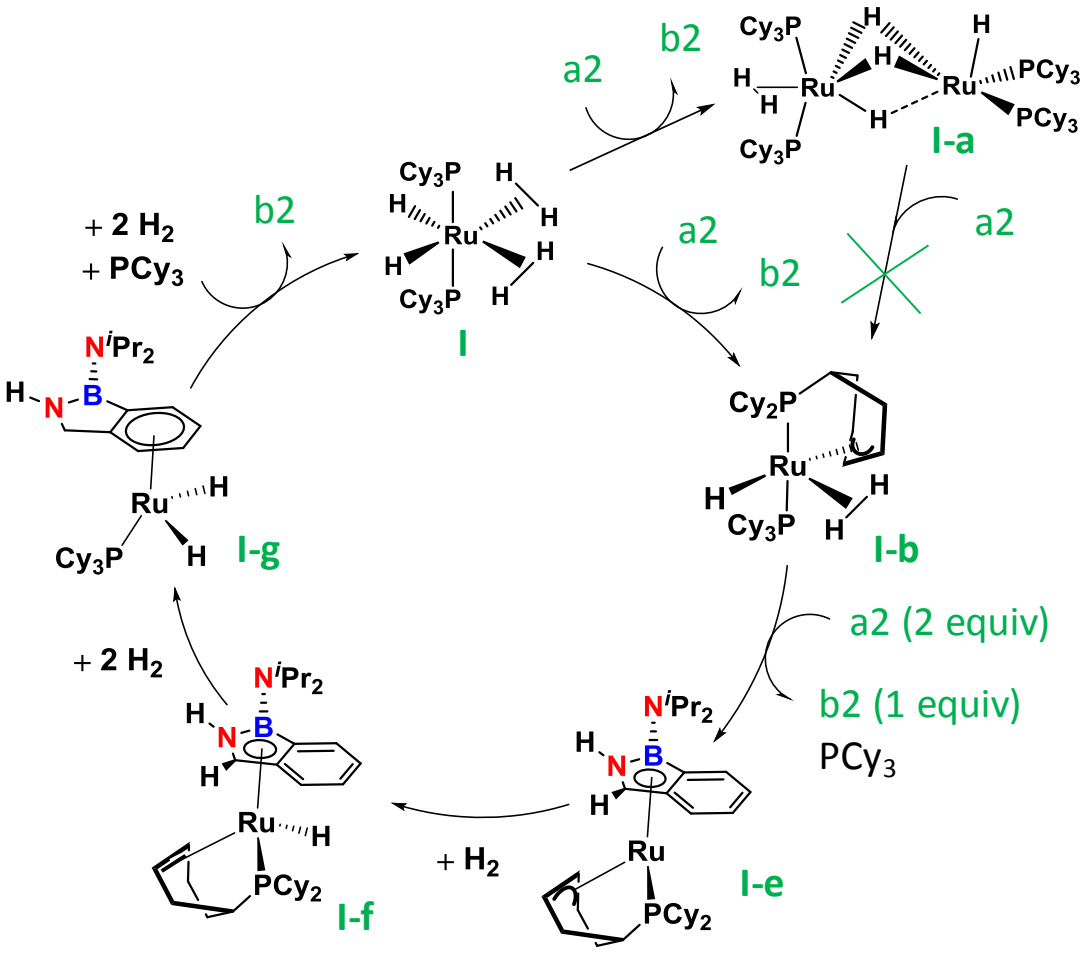

Les atomes d'hydrogène fournis peuvent provenir des ligands σ-H_2 donnant le complexe dimère **I-a**. Une fois les σ-H2 consommés, le cyclohexyle de la phosphine peut également fournir de l'hydrogène par activation C–H pour donner le complexe déshydrogéné **I-b**. Cependant, nous avons remarqué que le complexe **I-a** ne conduit pas à **I-b** lors de l'addition supplémentaire de **a2**. Le mélange 2/1 molaire de **a2** et le complexe isolé **I-b** a conduit à la libération d'un équivalent de **b2** et à la génération du complexe de ruthénium dans le stade le plus avancé de déshydrogénation, le complexe **I-e**, conjointement avec la libération de PCy_3. Le substrat a ainsi été capturé lors de sa transformation chimique sur le centre du ruthénium. Il a été capturé sous la forme du ligand 1H-2,1-benzazaborolyle, coordonné par le cycle BN au centre ruthénium. **I-e** a été préparé indépendamment et caractérisé par diffraction des rayons X et RMN multi noyaux.

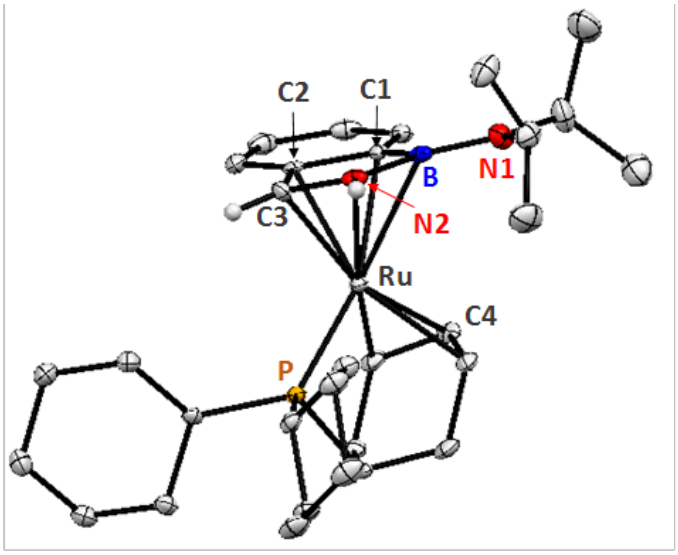

Ru–B	2.456 (3)	Ru–C1	2.369 (2)
Ru–N2	2.273 (2)	Ru–P	2.246 (1)
Ru–C3	2.127 (2)	Ru–C4	2.093 (2)
Ru–C2	2.295 (2)	B–N1	1.425 (4)
		B–N2	1.469 (4)

I-e est réactif vis-à-vis de l'hydrogène. Il subit une hydrogénation par étapes commençant par, le cyclohexényle de la phosphine produisant le monohydrure **1-f** et puis hydrogénant le carbone méthine du substrat pour compléter la formation du 1H-2,1-benzazaborole **b2** comme indiqué dans **I-g**. Le produit peut ensuite être libéré en même temps que la récupération du complexe de catalyseur précurseur hydrogéné **I** lorsque de la phosphine libre et le H_2 sont ajoutés au milieu.

Etude théorique par DFT :

Afin de compléter et d'affiner toutes nos découvertes expérimentales, des calculs DFT ont été réalisés au niveau de théorie DFT-B3PW91. Ainsi, les voies possibles impliquant l'activation de la liaison B–H, la réduction de la fonction nitrile et la formation de la liaison B–N conduisant à l'ultime bicyclique 1*H*-2,1-benzazaborole **b2** ont été théoriquement étudiées. Nous avons d'abord considéré l'interaction du cyanoborane **a2** de départ avec **I**. Nous avons vu ci-dessus qu'en présence d'un grand excès de **a2**, le complexe de bis (nitrile) **I-h** correspondant a été identifié dans le mélange catalytique. La figure ci-dessous schématise la géométrie de plusieurs espèces résultant de la substitution de 1 ou 2 ligands dihydrogénés dans **I** (**I** calc pour

la géométrie optimisée) par un ou deux équivalents de cyanoborane **a2**, ainsi que leurs valeurs relatives d'énergie libre de Gibbs.

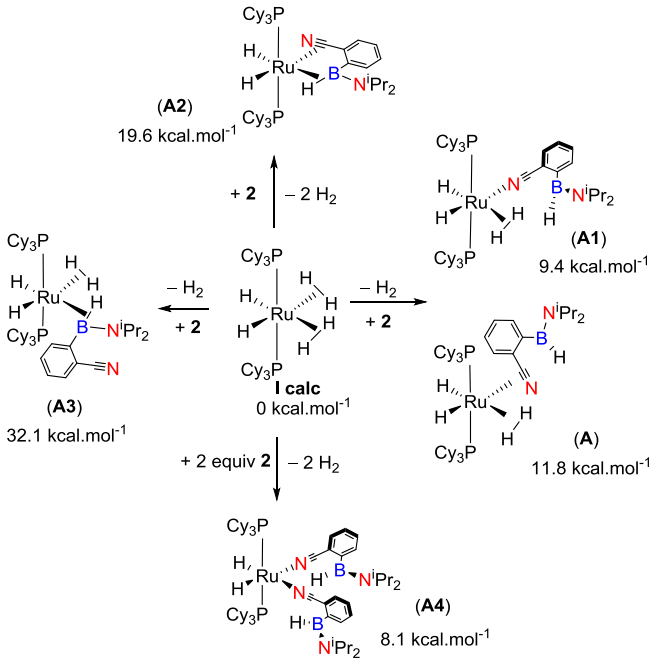

La coordination par la fonction nitrile est grandement favorisée par rapport à l'interaction B–H (9,4 vs 32,1 kcal mol^{-1}). La formation d'un complexe agostique η^2-CN, σ-B–H est aussi plus énergétique (19,6 kcal mol^{-1}). L'interaction entre le substrat **a2** et le complexe **I** est dominée par l'influence de la fonction nitrile. Par conséquent, **a2** interagit différemment de l'aryl (phosphino)(aminoborane) avec **I**. L'aryl(cyano)(aminoborane) coordonne le ruthénium par la fonction nitrile, laissant d'abord la liaison B–H inactivée, comme observée expérimentalement et confirmée par calcul. Le nitrile réagit d'abord avec le dihydrogène, ce qui conduit à l'élimination du processus d'hydroboration postulé dans la proposition 2. Par rapport au mécanisme décrit antérieurement dans la bibliographie pour l'hydroboration de nitriles avec des complexes d'hydrure métallique, ici la fonction nitrile est coordonnée et le transfert d'hydrogène sur l'azote peut être possible par coupure hétérolitique du ligand σ-H_2. Il apparaît que, dès que la liaison nitrile commence à être réduite, la liaison B–N se forme. L'interaction intramoléculaire B–N est favorisée par rapport à un transfert d'hydrogène intermoléculaire. Contrairement à l'hydrogénation classique du nitrile, la liaison C≡N ne peut pas être entièrement hydrogénée rejetant ainsi la proposition 1. Une fois le fragment imine formé, la liaison B–H est activée via une coordination du cycle BN au centre métallique, avec la perte d'un ligand phosphine. Une version déshydrogénée de l'intermédiaire après la rupture de la

liaison B–H (complexe **I-e**) a été capturée et complètement caractérisée en tant que premier ligand 1H-2,1-benzazaborolyle isolé sur un métal de transition. Nous avons démontré qu'un tel intermédiaire conduit ensuite au produit final et à la régénération du complexe **I** sous H_2 par hydrogénation progressive. Les calculs théoriques soutiennent nos résultats expérimentaux avec la présence de la version hydrogénée modélisée dans le chemin le plus favorable. Il est cependant important de noter que des voies compétitives pourraient également être calculées en particulier sans dissociation de la phosphine, en gardant à l'esprit que la libération de PCy_3 est toujours observée lors du suivi de la réaction catalytique. En conclusion, la voie mécanistique proposée est une variante de la proposition 3 où la fonction nitrile est partiellement réduite avant interaction B–N pour finalement conduire à l'activation de la liaison B–H via un intermédiaire sans précédent. Les principaux intermédiaires sont représentés dans la figure ci-dessous.

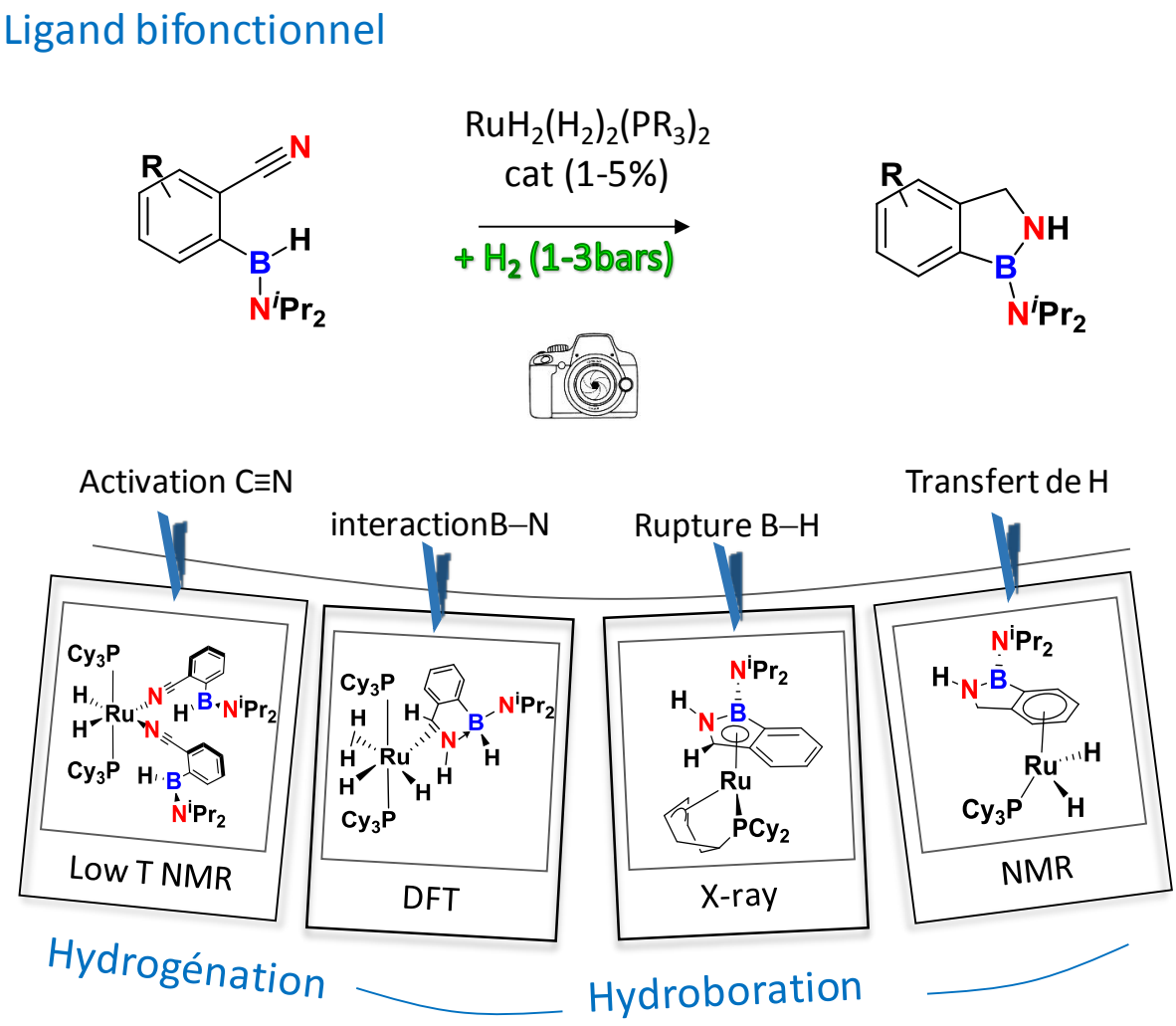

Comparaison avec l'isonitrile :

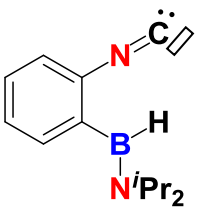

c

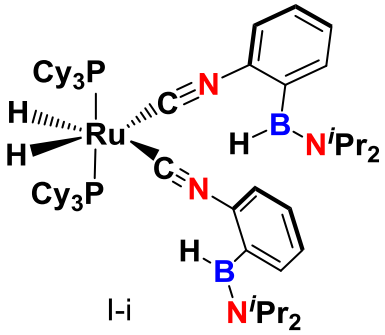

I-i

Le composé nitrile **a2** et le composé isonitrile **c** possèdent des données spectroscopiques très similaires. Le composé **c** présente une réactivité très différente de celle du composé **a2** vis-à-vis de $RuH_2(H_2)_2(PCy_3)_2$ (**I**). Un agit comme un substrat réactif (**a2**) tandis que l'autre agit comme un ligand stable (**c**). Ainsi, nous avons pu isoler à température ambiante le composé **I-i**.

CHAPITRE 4 :

Nous entrons maintenant dans la deuxième partie de ce travail visant à étudier les nouvelles molécules BN. Bien que les boranes soient souvent des molécules sacrificielles en catalyse, les composés contenant du bore sont très attractifs. En particulier, l'interaction bore-azote confère à la molécule la capacité remarquable de libérer et de transférer le dihydrogène. De plus, la liaison BN peut donner des propriétés dynamiques à la molécule, exploitables par exemple dans la chimie des capteurs de sucres. La fonction BN est isoélectronique et isostérique de la fonction C=C. Tout un panel de nouvelles molécules et matériaux peuvent être synthétisés en remplaçant la fonction CC par l'unité BN. Ces molécules ont en particulier des propriétés optoélectroniques intéressantes permettant d'élargir la bibliothèque de composés chimiques disponibles dans ces domaines. Ainsi, l'intérêt suscité par ces vieilles molécules appelle le développement de méthodes synthétiques. Des efforts importants sont faits pour accéder aux composés cycliques BN avec leur incorporation dans des systèmes électron-délocalisés.

Comme aucun autre dérivé connu du 1H-2,1-benzazaborole ne présente un fragment N–H, nous avons décidé de tirer parti de cette fonction et d'examiner la réactivité qu'elle peut offrir. Dans ce chapitre, nous décrivons la fonctionnalisation à l'azote ainsi qu'une étude de

déshydrogénation qui impliquerait l'activation de la liaison N–H et C–H du 1H-2,1-benzazaborole **b2**.

Pour commencer, dans des conditions basiques (nBuLi), nous avons démontré que nous pouvons sélectivement déprotoner N–H pour former l'amidure de lithium correspondant dans des versions éthérées ou non-éthérées. Dans de telles conditions, le borane trigonal est suffisamment stable et ne subit aucune attaque nucléophile, ce qui démontre le rôle du groupe stabilisant NiPr. La réaction de l'amidure de lithium éthéré avec divers électrophiles halogénés a conduit à la formation de liaisons N–Si, N–C, N–P et N–B suggérant qu'une grande variété de composés BN pourrait être générée.

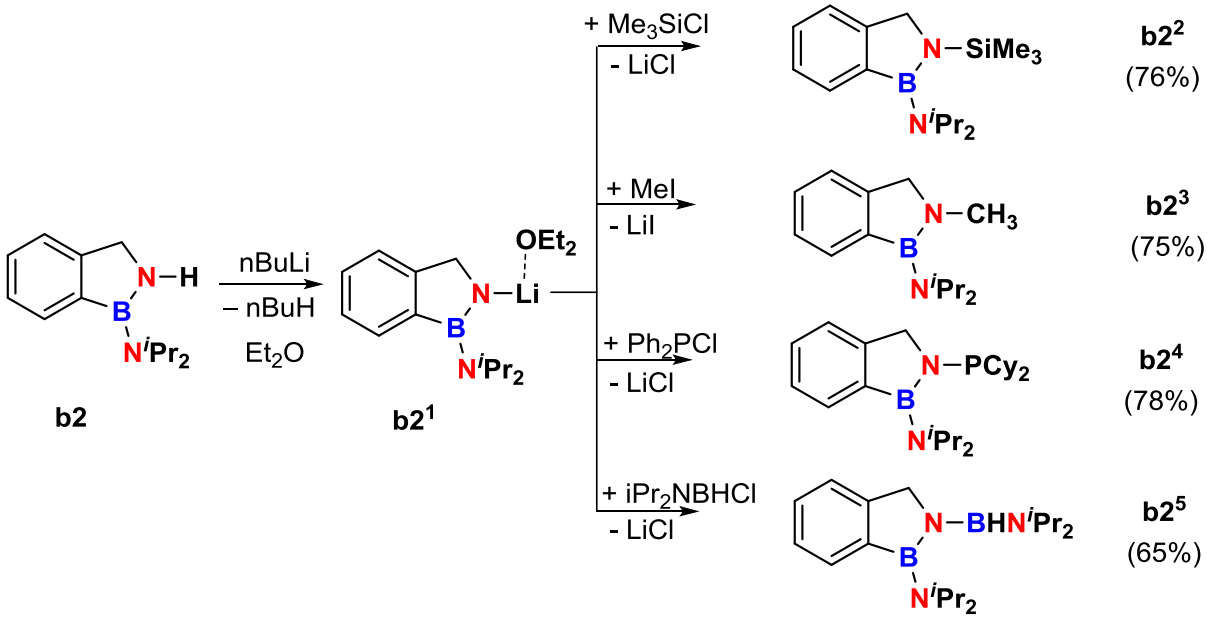

Nous avons ensuite établi la compatibilité de la molécule contenant un bore trigonal vis à vis de transformations catalytiques d'amines. Nous avons adapté avec succès la stratégie d'amination de Buchwald-Hartwig à partir du sel de lithium éthéré. Une double amination a également été obtenue et les composés ont été isolés avec un excellent rendement. Par conséquent, nous avons développé une voie efficace pour l'incorporation BN dans les systèmes délocalisés par électrons pavant la route pour les hétérocycles BN fonctionnalisés.

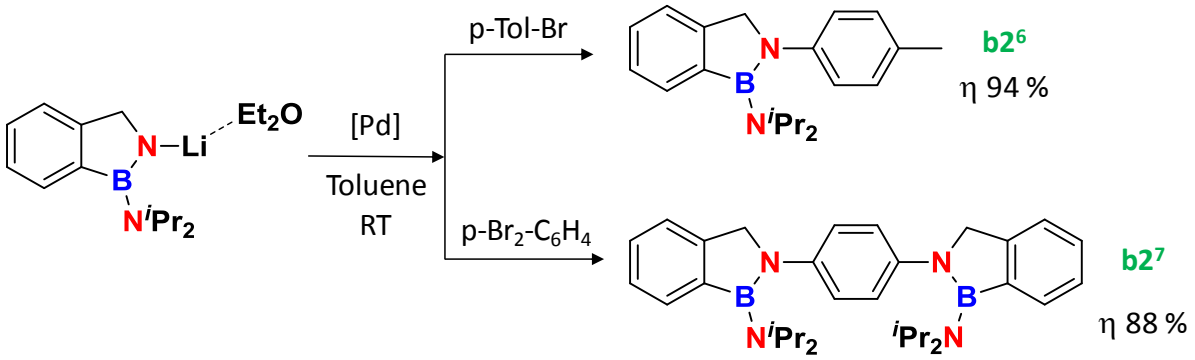

La déshydrogénation du 1H-2,1-benzazaborole **b2** qui impliquerait le clivage N–H, C–H a également été testée à l'université de Rochester dans le cadre de ma mission dans l'équipe du professeur W. Jones. A ce stade de l'étude, les essais catalytiques n'ont pas été fructueux en utilisant des pinceurs de fer, de cobalt ou d'iridium comme précurseurs catalytiques, vraisemblablement en raison à la fois de la trimérisation concurrente thermiquement activée et de l'influence du bore sur l'interaction substrat / complexe.

En résumé, après étude de la réactivité de Liu et collaborateurs sur la 1,2-dihydro-1,2-azaborine, nous avons démontré que les outils synthétiques stœchiométriques et catalytiques sont compatibles avec les anneaux BN à 5 chainons et peuvent conduire à la préparation de matériaux auparavant inaccessibles.

CHAPITRE 5 :

Comme expliqué au chapitre 1, la borazine est l'analogueue BN du benzène. Ils ont des structures très similaires mais des propriétés optoélectroniques et une stabilité très différentes. La forte polarité de la liaison BN induit un accroissement du gap orbitalaire HOMO-LUMO. L'insertion d'une telle unité BN dans des systèmes délocalisés électroniquement modifie les profils d'absorption et d'émission des composés et confère à la molécule des propriétés d'isolant électronique. La conception et la fonctionnalisation de borazines sophistiquées ont conduit aux premiers exemples de matériaux à base de borazine pour les dispositifs optoélectroniques. Les applications sont encore très peu développées et la synthèse de composés innovants est nécessaire pour le développement du domaine.

Des borazines sans précédent ont été synthétisées à partir des précurseurs de 1H-2,1-benzazaborole. La déshydroamination / trimérisation induite thermiquement des dérivés 1H-2,1-benzazaborole et dérivés substitués, conduit sélectivement à la formation des borazines

correspondantes. Les composés ont été isolés avec de très bons rendements à l'exception de la version méthylée, qui montre également une cinétique plus lente attribuée à l'effet stérique. La formation de borazine semble se produire par des réactions de condensation par étapes des unités 1H-2,1-benzazaborole, comme indiqué par la caractérisation du dimère intermédiaire. Les quatre composés ont été caractérisés par spectroscopie HRMS, RMN et IR ainsi que par diffraction des rayons X (sauf d1). Les borazines possèdent une structure remarquablement plane et sont par conséquent des molécules modèles de choix pour étudier l'incorporation du noyau BN dans des systèmes d'électrons délocalisés. Le caractère plan suggère un grand degré de conjugaison à travers la molécule qui devrait impliquer l'unité BN.

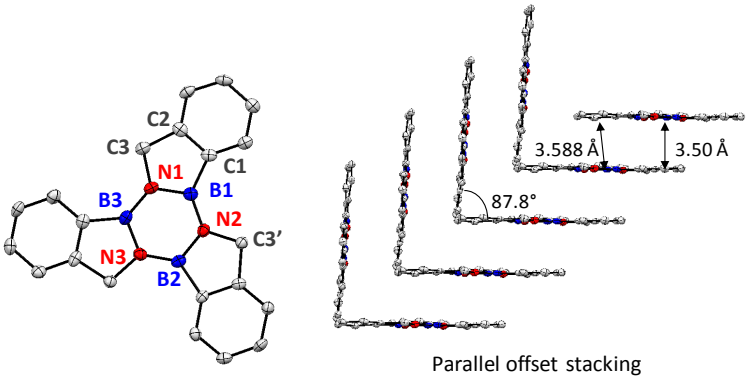

Bridged N–B (average)	1.442 (3)	N1–C3	1.472 (3)
Non-Bridged N–B (average)	1.419 (3)	B1–C1	1.564 (3)
Average N–B	1.431 (3)		
C2–C3	1.512 (3)		

Les quatre composés présentent une stabilité élevée à la température et aux conditions ambiantes à l'état solide, acceptables pour l'application en tant que matériaux. Les propriétés optoélectroniques des quatre dérivés ont été évaluées en solution. Les borazines absorbent dans la région UV avec une augmentation notable de ε par rapport aux 1H-2,1-benzazaboroles. Les composés sont émissifs avec un maximum d'absorption autour de 300 nm. Ils émettent exclusivement dans la région UV sans contamination du visible. L'émission est fortement décalée vers le bleu par rapport au truxène, l'analogueue carboné, ce qui indique la forte influence de l'incorporation de BN et suggère un élargissement de l'écart HOMO-LUMO.

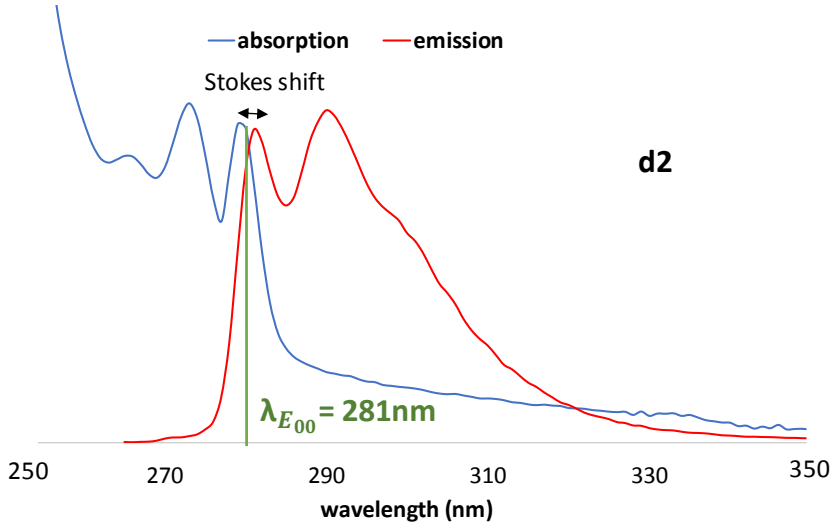

Le ΔE déterminé est grand en comparaison des composés précédemment répertoriés, une fois de plus attestant de la grande contribution de l'unité BN dans les processus optiques. Enfin, le ΔE électrochimique expérimental a été déterminé pour la première fois pour cette classe de composés en utilisant la méthode de voltammétrie cyclique. Le ΔE électrochimique se trouve être plus petit que le ΔE optique. Dans tous les cas, le ΔE est caractéristique des composés semi-conducteurs. Les calculs théoriques à venir devraient clarifier la nature des orbitales HOMO-LUMO et illustrer la contribution de l'unité BN.

Conclusion :

Le manuscrit présente une étude approfondie sur l'hydrogénation/cyclisation, catalysée par des complexes du ruthénium, de cyano-aminoboranes pour la synthèse de composés BN cycliques.Il montre également le potentiel synthétique de ces composés d
Le premier chapitre, en introduction bibliographique, a mis en évidence l'intérêt des molécules BN cycliques et décrit les étapes élémentaires clés dans les systèmes catalytiques impliquant l'activation de la liaison B–H et la réduction de la liaison CN. On s'est concentré sur la réactivité des complexes bis (dihydrogène), $RuH_2(H_2)_2(PR_3)_2$, avec des liaisons B–H et CN. Le deuxième chapitre a présenté la synthèse et la caractérisation d'une série de cyano-aminoboranes ainsi que leur transformation catalytique en utilisant $RuH_2(H_2)_2(PCy_3)_2$ sous H_2. Les 1H-2,1-benzazaboroles cycliques correspondantes sont formés de façon sélective et caractérisés par RMN, IR, rayons X et HRMS. Le troisième chapitre a détaillé une étude mécanistique sur le processus catalytique avec la découverte de quelques étapes élémentaires, l'isolement d'un complexe comportant le substrat en transformation et la

compréhension des processus de transfert d'hydrogène. Des réactions stœchiométriques, des expériences de RMN à température variable et des calculs théoriques convergent vers un mécanisme réactionnel. Dans le quatrième chapitre, nous avons étudié le potentiel synthétique du parent 1H-2,1-benzazaborole nouvellement formé. Sa réactivité dans des conditions basiques ainsi que sa transformation catalytique en utilisant des systèmes de rupture de liaison N–H bien établis ont été évaluées. Le cas spécifique de la cyclotrimérisation des 1H-2,1-benzazaboroles en borazines cycliques a été détaillé au chapitre 5 ainsi qu'une étude de leurs propriétés optoélectroniques.

REFERENCES

1. Kohno, J.; Kawahata, T.; Otake, T.; Morimoto, M.; Mori, H.; Ueba, N.; Nishio, M.; Kinumaki, A.; Komatsubara, S.; Kawashima, K., *Biosci. Biotechnol. Biochem.* **1996,** *60*, 1036-1037.
2. Dobrzhinetskaya, L. F.; Wirth, R.; Yang, J.; Green, H. W.; Hutcheon, I. D.; Weber, P. K.; Grew, E. S., *Am. Mineral.* **2014,** *99*, 764-772.
3. Grant, D. J.; Dixon, D. A., *J. Phys. Chem. A.* **2006,** *110*, 12955-12962.
4. Jonas, V.; Frenking, G., *J. Chem. Soc., Chem. Commun.* **1994**, 1489-1490.
5. Klooster, W. T.; Koetzle, T. F.; Siegbahn, P. E. M.; Richardson, T. B.; Crabtree, R. H., *J. Am. Chem. Soc.* **1999,** *121*, 6337-6343.
6. Bonifazi, D.; Fasano, F.; Lorenzo-Garcia, M. M.; Marinelli, D.; Oubaha, H.; Tasseroul, J., *Chem. Commun.* **2015,** *51*, 15222-15236.
7. Alcaraz, G.; Vendier, L.; Clot, E.; Sabo-Etienne, S., *Angew. Chem. Int. Ed.* **2010,** *49*, 918-920.
8. Alcaraz, G.; Chaplin, A. B.; Stevens, C. J.; Clot, E.; Vendier, L.; Weller, A. S.; Sabo-Etienne, S., *Organometallics* **2010,** *29*, 5591-5595.
9. Kumar, A.; Johnson, H. C.; Hooper, T. N.; Weller, A. S.; Algarra, A. G.; Macgregor, S. A., *Chem. Sci.* **2014,** *5*, 2546-2553.
10. Kumar, A.; Beattie, N. A.; Pike, S. D.; Macgregor, S. A.; Weller, A. S., *Angew. Chem. Int. Ed.* **2016,** *55*, 6651-6656.
11. MacInnis, M. C.; McDonald, R.; Ferguson, M. J.; Tobisch, S.; Turculet, L., *J. Am. Chem. Soc.* **2011,** *133*, 13622-13633.
12. Shaw, W. J.; Linehan, J. C.; Szymczak, N. K.; Heldebrant, D. J.; Yonker, C.; Camaioni, D. M.; Baker, R. T.; Autrey, T., *Angew. Chem. Int. Ed.* **2008,** *47*, 7493-7496.
13. Chakrabarty, M. R.; Thompson, C. C.; Brey, W. S., *Inorg. Chem.* **1967,** *6*, 518-520.
14. Jaska, C. A.; Temple, K.; Lough, A. J.; Manners, I., *J. Am. Chem. Soc.* **2003,** *125*, 9424-9434.
15. Pritchard, R. H.; Kern, C. W., *J. Am. Chem. Soc.* **1969,** *91*, 1631-1635.
16. Sugie, M.; Takeo, H.; Matsumura, C., *Chem. Phys. Lett.* **1979,** *64*, 573-575.
17. Zhao, P.; Nettleton, D. O.; Karki, R. G.; Zécri, F. J.; Liu, S.-Y., *ChemMedChem* **2017,** *12*, 358-361.
18. Moniz, S. J. A.; Shevlin, S. A.; Martin, D. J.; Guo, Z.-X.; Tang, J., *Energy Environ. Sci.* **2015,** *8*, 731-759.
19. Huang, Z.; Autrey, T., *Energy Environ. Sci.* **2012,** *5*, 9257-9268.
20. Staubitz, A.; Robertson, A. P. M.; Manners, I., *Chem. Rev.* **2010,** *110*, 4079-4124.
21. Chen, X.; Zhao, J.-C.; Shore, S. G., *Acc. Chem. Res.* **2013,** *46*, 2666-2675.
22. Rossin, A.; Peruzzini, M., *Chem. Rev.* **2016,** *116*, 8848-8872.
23. Bhunya, S.; Zimmerman, P. M.; Paul, A., *ACS Catal.* **2015,** *5*, 3478-3493.
24. Sutton, A. D.; Burrell, A. K.; Dixon, D. A.; Garner, E. B.; Gordon, J. C.; Nakagawa, T.; Ott, K. C.; Robinson, J. P.; Vasiliu, M., *Science* **2011,** *331*, 1426-1429.
25. Kumar, A.; Ishibashi, J. S. A.; Hooper, T. N.; Mikulas, T. C.; Dixon, D. A.; Liu, S.-Y.; Weller, A. S., *Chem. Eur. J.* **2016,** *22*, 310-322.
26. Luo, W.; Neiner, D.; Karkamkar, A.; Parab, K.; Garner Iii, E. B.; Dixon, D. A.; Matson, D.; Autrey, T.; Liu, S.-Y., *Dalton Trans.* **2013,** *42*, 611-614.
27. Chen, G.; Zakharov, L. N.; Bowden, M. E.; Karkamkar, A. J.; Whittemore, S. M.; Garner, E. B.; Mikulas, T. C.; Dixon, D. A.; Autrey, T.; Liu, S.-Y., *J. Am. Chem. Soc.* **2015,** *137*, 134-137.
28. Luo, W.; Campbell, P. G.; Zakharov, L. N.; Liu, S.-Y., *J. Am. Chem. Soc.* **2011,** *133*, 19326-19329.
29. Dallanegra, R.; Robertson, A. P. M.; Chaplin, A. B.; Manners, I.; Weller, A. S., *Chem. Commun.* **2011,** *47*, 3763-3765.
30. Johnson, H. C.; Leitao, E. M.; Whittell, G. R.; Manners, I.; Lloyd-Jones, G. C.; Weller, A. S., *J. Am. Chem. Soc.* **2014,** *136*, 9078-9093.
31. Staubitz, A.; Sloan, M. E.; Robertson, A. P. M.; Friedrich, A.; Schneider, S.; Gates, P. J.; Günne, J. S. a. d.; Manners, I., *J. Am. Chem. Soc.* **2010,** *132*, 13332-13345.
32. Shao, Z.; Fu, S.; Wei, M.; Zhou, S.; Liu, Q., *Angew. Chem. Int. Ed.* **2016,** *55*, 14653-14657.

33. Fujita, N.; Shinkai, S.; James, T. D., *Chem Asian J* **2008,** *3*, 1076-1091.
34. Sun, X.; James, T. D., *Chem. Rev.* **2015,** *115*, 8001-8037.
35. Martin, A. R.; Vasseur, J.-J.; Smietana, M., *Chem. Soc. Rev.* **2013,** *42*, 5684-5713.
36. Bosch, L. I.; Fyles, T. M.; James, T. D., *Tetrahedron* **2004,** *60*, 11175-11190.
37. Arimori, S.; Bosch, L. I.; Ward, C. J.; James, T. D., *Tetrahedron Lett.* **2002,** *43*, 911-913.
38. James, T. D.; Sandanayake, K. R. A. S.; Iguchi, R.; Shinkai, S., *J. Am. Chem. Soc.* **1995,** *117*, 8982-8987.
39. Ashe, A. J.; Fang, *Org. Lett.* **2000,** *2*, 2089-2091.
40. Fang, X.; Assoud, J., *Organometallics* **2008,** *27*, 2408-2410.
41. Dewar, M. J. S.; Kubba, V. P.; Pettit, R., *J. Chem. Soc.* **1958**, 3076-3079.
42. Hawkins, R. T.; Snyder, H. R., *J. Am. Chem. Soc.* **1960,** *82*, 3863-3866.
43. Hawkins, R. T.; Blackham, A. U., *J. Org. Chem.* **1967,** *32*, 597-600.
44. Dunn, H. E.; Catlin, J. C.; Snyder, H. R., *J. Org. Chem.* **1968,** *33*, 4483-4486.
45. Köster, R.; Iwasaki, K.; Hattori, S.; Morita, Y., *Justus Liebigs Annalen der Chemie* **1968,** *720*, 23-31.
46. Genaev, A. M.; Salnikov, G. E.; Shubin, V. G.; Nagy, S. M., *Chem. Commun.* **2000**, 1587-1588.
47. Hejda, M.; Lycka, A.; Jambor, R.; Ruzicka, A.; Dostal, L., *Dalton Trans.* **2013,** *42*, 6417-6428.
48. Rydzewska, A.; Ślepokura, K.; Lis, T.; Kafarski, P.; Młynarz, P., *Tetrahedron Lett.* **2009,** *50*, 132-134.
49. Marwitz, A. J. V.; Matus, M. H.; Zakharov, L. N.; Dixon, D. A.; Liu, S.-Y., *Angew. Chem. Int. Ed.* **2009,** *48*, 973-977.
50. Campbell, P. G.; Marwitz, A. J. V.; Liu, S.-Y., *Angew. Chem. Int. Ed.* **2012,** *51*, 6074-6092.
51. Bélanger-Chabot, G.; Braunschweig, H.; Roy, D. K., *Eur. J. Inorg. Chem.* **2017**, DOI:10.1002/ejic.201700562.
52. Morgan, M. M.; Piers, W. E., *Dalton Trans.* **2016,** *45*, 5920-5924.
53. Wang, J.-Y.; Pei, J., *Chin. Chem. Lett.* **2016,** *27*, 1139-1146.
54. Bosdet, M. J. D.; Piers, W. E., *Can. J. Chem.* **2009,** *87*, 8-29.
55. Stock, A.; Pohland, E., *Ber. dtsch. Chem. Ges.* **1926,** *59*, 2215-2223.
56. Dewar, M. J. S.; Kubba, V. P.; Pettit, R., *J. Chem. Soc.* **1958**, 3073-3076.
57. Carion, R.; Liégeois, V.; Champagne, B.; Bonifazi, D.; Pelloni, S.; Lazzeretti, P., *J. Phys. Chem. Lett.* **2010,** *1*, 1563-1568.
58. Atkinson, I. B.; Blundell, D. C.; Clapp, D. B., *J. Inorg. Nucl. Chem.* **1972,** *34*, 3037-3041.
59. Massey, A. G.; Park, A. J., *J. Organomet. Chem.* **1964,** *2*, 461-465.
60. Araneda, J. F.; Neue, B.; Piers, W. E., *Angew. Chem. Int. Ed.* **2012,** *51*, 9977-9979.
61. Kervyn, S.; Fenwick, O.; Stasio, F. D.; Shin, Y. S.; Wouters, J.; Accorsi, G.; Osella, S.; Beljonne, D.; Cacialli, F.; Bonifazi, D., *Chem. Eur. J.* **2013,** *19*, 7771-7779.
62. Wilkinson, G.; Rosenblum, M.; Whiting, M. C.; Woodward, R. B., *J. Am. Chem. Soc.* **1952,** *74*, 2125-2126.
63. Arndt, S.; Okuda, J., *Chem. Rev.* **2002,** *102*, 1953-1976.
64. Ashe, A. J., *Organometallics* **2009,** *28*, 4236-4248.
65. Liu, Z.; Xu, J.; Ruan, W.; Fu, C.; Zhang, H.-J.; Wen, T.-B., *Dalton Trans.* **2013,** *42*, 11976-11980.
66. Chen, Y.; Fang, X.; Dan, W., *Organometallics* **2016,** *35*, 15-19.
67. Trost, B. M.; Ryan, M. C., *Angew. Chem. Int. Ed.* **2017,** *56*, 2862-2879.
68. Aime, S.; Gobetto, R.; Padovan, F.; Botta, M.; Rosenberg, E.; Gellert, R. W., *Organometallics* **1987,** *6*, 2074-2078.
69. Hart-Davis, A. J.; Mawby, R. J., *J. Chem. Soc.* **1969**, 2403-2407.
70. Xu, S.; Oda, A.; Bobinski, T.; Li, H.; Matsueda, Y.; Negishi, E.-i., *Angew. Chem. Int. Ed.* **2015,** *54*, 9319-9322.
71. Ashe, A. J., III; Yang, H.; Fang, X.; Kampf, J. W., *Organometallics* **2002,** *21*, 4578-4580.
72. Krishnamurti, R.; Nagy, S.; Etherton, B. P. US 5554775 A, **1996**.
73. Zoricak, P.; Wang, Q.; Gao, X. CA 2225014 A1, **1999**.
74. Hejda, M.; Jambor, R.; Ruzicka, A.; Lycka, A.; Dostal, L., *Dalton Trans.* **2014,** *43*, 9012-9015.

75. Hejda, M.; Lyčka, A.; Mikysek, T.; Jambor, R.; Růžička, A.; Vinklárek, J.; Wilfer, C.; Hoffmann, A.; Herres-Pawlis, S.; Dostál, L., *Chem. Eur. J.* **2016,** *22*, 15340-15349.
76. Pan, J.; Kampf, J. W.; Ashe, A. J., *Organometallics* **2004,** *23*, 5626-5629.
77. Werner, H.; Prinz, R.; Deckelmann, E., *Chem. Ber.* **1969,** *102*, 95-103.
78. Carter, T. J.; Heiden, Z. M.; Szymczak, N. K., *Chem. Sci.* **2015,** *6*, 7258-7266.
79. Xu, S.; Zhang, Y.; Li, B.; Liu, S.-Y., *J. Am. Chem. Soc.* **2016,** *138*, 14566-14569.
80. McConnell, C. R.; Campbell, P. G.; Fristoe, C. R.; Memmel, P.; Zakharov, L. N.; Li, B.; Darrigan, C.; Chrostowska, A.; Liu, S.-Y., *Eur. J. Inorg. Chem.* **2017**, n/a-n/a.
81. Wang, X.-Y.; Lin, H.-R.; Lei, T.; Yang, D.-C.; Zhuang, F.-D.; Wang, J.-Y.; Yuan, S.-C.; Pei, J., *Angew. Chem. Int. Ed.* **2013,** *52*, 3117-3120.
82. Perkinson, J. C., Organic field-effect transistors. 2007.
83. Wang, X.; Zhang, F.; Liu, J.; Tang, R.; Fu, Y.; Wu, D.; Xu, Q.; Zhuang, X.; He, G.; Feng, X., *Org. Lett.* **2013,** *15*, 5714-5717.
84. Sham, I. H. T.; Kwok, C.-C.; Che, C.-M.; Zhu, N., *Chem. Commun.* **2005**, 3547-3549.
85. Weng, Q.; Wang, X.; Wang, X.; Bando, Y.; Golberg, D., *Chem. Soc. Rev.* **2016,** *45*, 3989-4012.
86. Miyaura, N.; Suzuki, A., *Chem. Rev.* **1995,** *95*, 2457-2483.
87. Lennox, A. J. J.; Lloyd-Jones, G. C., *Chem. Soc. Rev.* **2014,** *43*, 412-443.
88. Hartwig, J. F., *Acc. Chem. Res.* **2017,** *50*, 549-555.
89. Brown, H. C.; Rao, B. C. S., *J. Am. Chem. Soc.* **1956,** *78*, 5694-5695.
90. Liotta, R.; Brown, H. C., *J. Org. Chem.* **1977,** *42*, 2836-2839.
91. Thomas, S. P.; Aggarwal, V. K., *Angew. Chem. Int. Ed.* **2009,** *48*, 1896-1898.
92. Männig, D.; Nöth, H., *Angew. Chem. Int. Ed.* **1985,** *24*, 878-879.
93. Westcott, S. A.; Blom, H. P.; Marder, T. B.; Baker, R. T., *J. Am. Chem. Soc.* **1992,** *114*, 8863-8869.
94. Zhang, L.; Zuo, Z.; Leng, X.; Huang, Z., *Angew. Chem. Int. Ed.* **2014,** *53*, 2696-2700.
95. Geier, M. J.; Vogels, C. M.; Decken, A.; Westcott, S. A., *J. Organomet. Chem.* **2009,** *694*, 3154-3159.
96. Caballero, A.; Sabo-Etienne, S., *Organometallics* **2007,** *26*, 1191-1195.
97. Montiel-Palma, V.; Lumbierres, M.; Donnadieu, B.; Sabo-Etienne, S.; Chaudret, B., *J. Am. Chem. Soc.* **2002,** *124*, 5624-5625.
98. Zhang, L.; Peng, D.; Leng, X.; Huang, Z., *Angew. Chem. Int. Ed.* **2013,** *52*, 3676-3680.
99. Ohmura, T.; Yamamoto, Y.; Miyaura, N., *J. Am. Chem. Soc.* **2000,** *122*, 4990-4991.
100. Gunanathan, C.; Hölscher, M.; Pan, F.; Leitner, W., *J. Am. Chem. Soc.* **2012,** *134*, 14349-14352.
101. Obligacion, J. V.; Neely, J. M.; Yazdani, A. N.; Pappas, I.; Chirik, P. J., *J. Am. Chem. Soc.* **2015,** *137*, 5855-5858.
102. Jang, W. J.; Lee, W. L.; Moon, J. H.; Lee, J. Y.; Yun, J., *Org. Lett.* **2016,** *18*, 1390-1393.
103. Yang, Z.; Zhong, M.; Ma, X.; Nijesh, K.; De, S.; Parameswaran, P.; Roesky, H. W., *J. Am. Chem. Soc.* **2016,** *138*, 2548-2551.
104. Sundararaju, B.; Fürstner, A., *Angew. Chem. Int. Ed.* **2013,** *52*, 14050-14054.
105. Wang, Q.; Motika, S. E.; Akhmedov, N. G.; Petersen, J. L.; Shi, X., *Angew. Chem. Int. Ed.* **2014,** *53*, 5418-5422.
106. Chong, C. C.; Kinjo, R., *ACS Catal.* **2015,** *5*, 3238-3259.
107. Bontemps, S., *Coord. Chem. Rev.* **2016,** *308, Part 2*, 117-130.
108. Baker, R. T.; Calabrese, J. C.; Westcott, S. A., *J. Organomet. Chem.* **1995,** *498*, 109-117.
109. Kirton, E. H. M.; Tughan, G.; Morris, R. E.; Field, R. A., *Tetrahedron Lett.* **2004,** *45*, 853-855.
110. Koren-Selfridge, L.; Londino, H. N.; Vellucci, J. K.; Simmons, B. J.; Casey, C. P.; Clark, T. B., *Organometallics* **2009,** *28*, 2085-2090.
111. Arrowsmith, M.; Hill, M. S.; Hadlington, T.; Kociok-Köhn, G.; Weetman, C., *Organometallics* **2011,** *30*, 5556-5559.
112. Arrowsmith, M.; Hill, M. S.; Kociok-Köhn, G., *Chem. Eur. J.* **2013,** *19*, 2776-2783.
113. Xie, J.-H.; Zhu, S.-F.; Zhou, Q.-L., *Chem. Rev.* **2011,** *111*, 1713-1760.
114. Bezlada, A.; Szewczyk, M.; Mlynarski, J., *J. Org. Chem.* **2016,** *81*, 336-342.
115. Eisenberger, P.; Bailey, A. M.; Crudden, C. M., *J. Am. Chem. Soc.* **2012,** *134*, 17384-17387.

116. Wen, K.; Chen, J.; Gao, F.; Bhadury, P. S.; Fan, E.; Sun, Z., *Org. Biomol. Chem.* **2013,** *11*, 6350-6356.
117. Ramozzi, R.; Cheron, N.; Braida, B.; Hiberty, P. C.; Fleurat-Lessard, P., *New J. Chem.* **2012,** *36*, 1137-1140.
118. Barnett, B. R.; Moore, C. E.; Rheingold, A. L.; Figueroa, J. S., *Chem. Commun.* **2015,** *51*, 541-544.
119. Suginome, M.; Fukuda, T.; Nakamura, H.; Ito, Y., *Organometallics* **2000,** *19*, 719-721.
120. Weetman, C.; Hill, M. S.; Mahon, M. F., *Chem. Commun.* **2015,** *51*, 14477-14480.
121. Haddenham, D.; Pasumansky, L.; DeSoto, J.; Eagon, S.; Singaram, B., *J. Org. Chem.* **2009,** *74*, 1964-1970.
122. Khalimon, A. Y.; Farha, P.; Kuzmina, L. G.; Nikonov, G. I., *Chem. Commun.* **2012,** *48*, 455-457.
123. Weetman, C.; Anker, M. D.; Arrowsmith, M.; Hill, M. S.; Kociok-Kohn, G.; Liptrot, D. J.; Mahon, M. F., *Chem. Sci.* **2016,** *7*, 628-641.
124. Geri, J. B.; Szymczak, N. K., *J. Am. Chem. Soc.* **2015,** *137*, 12808-12814.
125. Kaithal, A.; Chatterjee, B.; Gunanathan, C., *J. Org. Chem.* **2016,** *81*, 11153-11161.
126. Lu, Z.; Williams, T. J., *Chem. Commun.* **2014,** *50*, 5391-5393.
127. Bagal, D. B.; Bhanage, B. M., *Adv. Synth. Catal.* **2015,** *357*, 883-900.
128. Bornschein, C.; Werkmeister, S.; Wendt, B.; Jiao, H.; Alberico, E.; Baumann, W.; Junge, H.; Junge, K.; Beller, M., *Nat. Commun.* **2014,** *5*, 4111.
129. Lange, S.; Elangovan, S.; Cordes, C.; Spannenberg, A.; Jiao, H.; Junge, H.; Bachmann, S.; Scalone, M.; Topf, C.; Junge, K.; Beller, M., *Catal. Sci. Technol.* **2016,** *6*, 4768-4772.
130. Chakraborty, S.; Leitus, G.; Milstein, D., *Chem. Commun.* **2016,** *52*, 1812-1815.
131. Elangovan, S.; Topf, C.; Fischer, S.; Jiao, H.; Spannenberg, A.; Baumann, W.; Ludwig, R.; Junge, K.; Beller, M., *J. Am. Chem. Soc.* **2016,** *138*, 8809-8814.
132. Adam, R.; Bheeter, C. B.; Cabrero-Antonino, J. R.; Junge, K.; Jackstell, R.; Beller, M., *ChemSusChem* **2017,** *10*, 842-846.
133. Dub, P. A.; Gordon, J. C., *ACS Catal.* **2017**, 6635-6655.
134. Kubas, G. J.; Ryan, R. R.; Swanson, B. I.; Vergamini, P. J.; Wasserman, H. J., *J. Am. Chem. Soc.* **1984,** *106*, 451-452.
135. Arliguie, T.; Chaudret, B.; Morris, R. H.; Sella, A., *Inorg. Chem.* **1988,** *27*, 598-599.
136. Grellier, M.; Vendier, L.; Chaudret, B.; Albinati, A.; Rizzato, S.; Mason, S.; Sabo-Etienne, S., *J. Am. Chem. Soc.* **2005,** *127*, 17592-17593.
137. Alcaraz, G.; Grellier, M.; Sabo-Etienne, S., *Acc. Chem. Res.* **2009,** *42*, 1640-1649.
138. Beatty, R. P.; Paciello, R. A. WO9623804A1, **1996**.
139. Reguillo, R.; Grellier, M.; Vautravers, N.; Vendier, L.; Sabo-Etienne, S., *J. Am. Chem. Soc.* **2010,** *132*, 7854-7855.
140. Toner, A.; Matthes, J.; Gründemann, S.; Limbach, H.-H.; Chaudret, B.; Clot, E.; Sabo-Etienne, S., *Proceedings of the National Academy of Sciences* **2007,** *104*, 6945-6950.
141. Hartwig, J. F.; Muhoro, C. N.; He, X.; Eisenstein, O.; Bosque, R.; Maseras, F., *J. Am. Chem. Soc.* **1996,** *118*, 10936-10937.
142. Alcaraz, G.; Clot, E.; Helmstedt, U.; Vendier, L.; Sabo-Etienne, S., *J. Am. Chem. Soc.* **2007,** *129*, 8704-8705.
143. Wallis, C. J.; Dyer, H.; Vendier, L.; Alcaraz, G.; Sabo-Etienne, S., *Angew. Chem. Int. Ed.* **2012,** *51*, 3646-3648.
144. Wallis, C. J.; Alcaraz, G.; Petit, A. S.; Poblador-Bahamonde, A. I.; Clot, E.; Bijani, C.; Vendier, L.; Sabo-Etienne, S., *Chem. Eur. J.* **2015,** *21*, 13080-13090.
145. Brookhart, M.; Green, M. L. H., *J. Organomet. Chem.* **1983,** *250*, 395-408.
146. van der Eide, E. F.; Yang, P.; Bullock, R. M., *Angew. Chem. Int. Ed.* **2013,** *52*, 10190-10194.
147. Brookhart, M.; Green, M. L. H.; Parkin, G., *Proceedings of the National Academy of Sciences* **2007,** *104*, 6908-6914.
148. Braunschweig, H.; Dewhurst, R. D.; Herbst, T.; Radacki, K., *Angew. Chem. Int. Ed.* **2008,** *47*, 5978-5980.

149. Gloaguen, Y.; Alcaraz, G.; Pecharman, A.-F.; Clot, E.; Vendier, L.; Sabo-Etienne, S., *Angew. Chem., Int. Ed.* **2009,** *48*, 2964-2968.
150. Cassen, A.; Vendier, L.; Daran, J.-C.; Poblador-Bahamonde, A. I.; Clot, E.; Alcaraz, G.; Sabo-Etienne, S., *Organometallics* **2014,** *33*, 7157-7163.
151. Cassen, A.; Gloaguen, Y.; Vendier, L.; Duhayon, C.; Poblador-Bahamonde, A.; Raynaud, C.; Clot, E.; Alcaraz, G.; Sabo-Etienne, S., *Angew. Chem. Int. Ed.* **2014,** *53*, 7569-7573.
152. Gloaguen, Y.; Alcaraz, G.; Petit, A. S.; Clot, E.; Coppel, Y.; Vendier, L.; Sabo-Etienne, S., *J. Am. Chem. Soc.* **2011,** *133*, 17232-17238.
153. Molander, G. A.; Trice, S. L. J.; Kennedy, S. M.; Dreher, S. D.; Tudge, M. T., *J. Am. Chem. Soc.* **2012,** *134*, 11667-11673.
154. Chattopadhyay, B.; Dannatt, J. E.; Andújar-de Sanctis, I. L.; Gore, K. A.; Maleczka, R. E.; Singleton, D. A.; Smith, M. R., *J. Am. Chem. Soc.* **2017**.
155. Parham, W. E.; Bradsher, C. K., *Acc. Chem. Res.* **1982,** *15*, 300-305.
156. Narasimhan, N. S.; Chandrachood, S. P.; Chandrachood, P. S.; Barve, M. V., *Proc. - Indian Acad. Sci., Chem. Sci.* **1984,** *93*, 625-34.
157. Bellamy, L. J.; Gerrard, W.; Lappert, M. F.; Williams, R. L., *J. Chem. Soc.* **1958**, 2412-2415.
158. Hejda, M.; Lycka, A.; Jambor, R.; Ruzicka, A.; Dostal, L., *Dalton Trans.* **2014,** *43*, 12678-12688.
159. Borowski, A. F.; Sabo-Etienne, S.; Christ, M. L.; Donnadieu, B.; Chaudret, B., *Organometallics* **1996,** *15*, 1427-34.
160. Sabo-Etienne, S.; Hernandez, M.; Chung, G.; Chaudret, B.; Castel, A., *New J. Chem.* **1994,** *18*, 175-7.
161. Hung, M. Y.; Ng, S. M.; Zhou, Z.; Lau, C. P.; Jia, G., *Organometallics* **2000,** *19*, 3692-3699.
162. Borowski, A. F.; Sabo-Etienne, S.; Donnadieu, B.; Chaudret, B., *Organometallics* **2003,** *22*, 1630-1637.
163. Borowski, A. F.; Sabo-Etienne, S.; Chaudret, B., *J. Mol. Catal. A: Chem.* **2001,** *174*, 69-79.
164. Wadepohl, H.; Arnold, U.; Pritzkow, H.; Calhorda, M. J.; Veiros, L. s. F., *J. Organomet. Chem.* **1999,** *587*, 233-243.
165. Lindner, H. H.; Onak, T., *J. Am. Chem. Soc.* **1966,** *88*, 1890-1894.
166. Marks, T. J.; Shimp, L. A., *J. Am. Chem. Soc.* **1972,** *94*, 1542-1550.
167. Gunanathan, C.; Hölscher, M.; Leitner, W., *Eur. J. Inorg. Chem.* **2011,** *2011*, 3381-3386.
168. Perutz, R. N.; Sabo-Etienne, S., *Angew. Chem. Int. Ed.* **2007,** *46*, 2578-2592.
169. Gloaguen, Y.; Alcaraz, G.; Petit, A. S.; Clot, E.; Coppel, Y.; Vendier, L.; Sabo-Etienne, S., *J. Am. Chem. Soc.* **2011,** *133*, 17232-17238.
170. Lygin, A. V.; de Meijere, A., *Org. Lett.* **2009,** *11*, 389-392.
171. Elmer, L.-M.; Kehr, G.; Daniliuc, C. G.; Siedow, M.; Eckert, H.; Tesch, M.; Studer, A.; Williams, K.; Warren, T. H.; Erker, G., *Chem. Eur. J.* **2017,** *23*, 6056-6068.
172. Delpech, F.; Sabo-Etienne, S.; Daran, J.-C.; Chaudret, B.; Hussein, K.; Marsden, C. J.; Barthelat, J.-C., *J. Am. Chem. Soc.* **1999,** *121*, 6668-6682.
173. Joost, M.; Alcaraz, G.; Vendier, L.; Poblador-Bahamonde, A.; Clot, E.; Sabo-Etienne, S., *Dalton Trans.* **2013,** *42*, 776-781.
174. Lamm, A. N.; Garner, E. B.; Dixon, D. A.; Liu, S.-Y., *Angew. Chem. Int. Ed.* **2011,** *50*, 8157-8160.
175. Brown, A. N.; Li, B.; Liu, S.-Y., *J. Am. Chem. Soc.* **2015,** *137*, 8932-8935.
176. Harrison-Marchand, A.; Mongin, F., *Chem. Rev.* **2013,** *113*, 7470-7562.
177. Jiang, L.; Buchwald, S. L., Palladium-Catalyzed Aromatic Carbon-Nitrogen Bond Formation. In *Metal-Catalyzed Cross-Coupling Reactions*, Wiley-VCH Verlag GmbH: **2008**; pp 699-760.
178. Surry, D. S.; Buchwald, S. L., *Chem. Sci.* **2011,** *2*, 27-50.
179. Zhang, Y.; César, V.; Storch, G.; Lugan, N.; Lavigne, G., *Angew. Chem. Int. Ed.* **2014,** *53*, 6482-6486.
180. Sunesson, Y.; Lime, E.; Nilsson Lill, S. O.; Meadows, R. E.; Norrby, P.-O., *J. Org. Chem.* **2014,** *79*, 11961-11969.
181. Abbey, E. R.; Zakharov, L. N.; Liu, S.-Y., *J. Am. Chem. Soc.* **2008,** *130*, 7250-7252.

182. Gellrich, U.; Diskin-Posner, Y.; Shimon, L. J. W.; Milstein, D., *J. Am. Chem. Soc.* **2016,** *138*, 13307-13313.
183. Chakraborty, S.; Brennessel, W. W.; Jones, W. D., *J. Am. Chem. Soc.* **2014,** *136*, 8564-8567.
184. Bellows, S. M.; Chakraborty, S.; Gary, J. B.; Jones, W. D.; Cundari, T. R., *Inorg. Chem.* **2017,** *56*, 5519-5524.
185. Xu, R.; Chakraborty, S.; Yuan, H.; Jones, W. D., *ACS Catal.* **2015,** *5*, 6350-6354.
186. Schaeffer, G. W.; Schaeffer, R.; Schlesinger, H. I., *J. Am. Chem. Soc.* **1951,** *73*, 1612-1614.
187. Wideman, T.; Sneddon, L. G., *Inorg. Chem.* **1995,** *34*, 1002-1003.
188. Framery, E.; Vaultier, M., *Heteroat. Chem* **2000,** *11*, 218-225.
189. Köster, R.; Hattori, S.; Morita, Y., *Angew. Chem. Int. Ed.* **1965,** *77*, 719-720.
190. Biswas, S.; Müller, M.; Tönshoff, C.; Eichele, K.; Maichle-Mössmer, C.; Ruff, A.; Speiser, B.; Bettinger, H. F., *Eur. J. Org. Chem.* **2012,** *2012*, 4634-4639.
191. Roberts, P. J.; Brauer, D. J.; Tsay, Y.-H.; Kruger, C., *Acta Cryst. B* **1974,** *30*, 2673-2678.
192. Krieg, M.; Reicherter, F.; Haiss, P.; Ströbele, M.; Eichele, K.; Treanor, M.-J.; Schaub, R.; Bettinger, H. F., *Angew. Chem. Int. Ed.* **2015,** *54*, 8284-8286.
193. Dosso, J.; Tasseroul, J.; Fasano, F.; Marinelli, D.; Biot, N.; Fermi, A.; Bonifazi, D., *Angew. Chem. Int. Ed.* **2017,** *56*, 4483-4487.
194. Ewald, D. US 2216001 A, **1940**.
195. Oded, Y. N.; Agranat, I., *Tetrahedron Lett.* **2014,** *55*, 636-638.
196. Shi, K.; Wang, J.-Y.; Pei, J., *Chem. Rec.* **2015,** *15*, 52-72.
197. Goubard, F.; Dumur, F., *RSC Adv.* **2015,** *5*, 3521-3551.
198. Janiak, C., *Dalton Trans.* **2000**, 3885-3896.
199. Martinez, C. R.; Iverson, B. L., *Chem. Sci.* **2012,** *3*, 2191-2201.
200. Yuan, M.-S.; Fang, Q.; Liu, Z.-Q.; Guo, J.-P.; Chen, H.-Y.; Yu, W.-T.; Xue, G.; Liu, D.-S., *J. Org. Chem.* **2006,** *71*, 7858-7861.
201. Pérez, E. M.; Sierra, M.; Sánchez, L.; Torres, M. R.; Viruela, R.; Viruela, P. M.; Ortí, E.; Martín, N., *Angew. Chem. Int. Ed.* **2007,** *46*, 1847-1851.
202. Stopel, M. H. W.; Blum, C.; Subramaniam, V., *J. Phys. Chem. Lett.* **2014,** *5*, 3259-3264.
203. Inamdar, S. N.; Ingole, P. P.; Haram, S. K., *ChemPhysChem* **2008,** *9*, 2574-2579.
204. Alberico, E.; Sponholz, P.; Cordes, C.; Nielsen, M.; Drexler, H.-J.; Baumann, W.; Junge, H.; Beller, M., *Angew. Chem. Int. Ed.* **2013,** *52*, 14162-14166.

The manuscript presents an *in-depth* study on the ruthenium-catalyzed hydrogenation/cyclization of cyano-aminoboranes for the synthesis of cyclic BN-compounds.

The first chapter is a bibliographic introduction highlighting the interest in cyclic BN-molecules and describing key elementary steps in catalytic systems involving B–H bond activation and CN bond reduction, leading in particular to B–N bond formation. A focus on the reactivity of the bis(dihydrogen) complexes, $RuH_2(H_2)_2(PR_3)_2$, with B–H and CN bonds will be provided. The second chapter presents the synthesis and characterization of a series of cyano-aminoboranes along with their catalytic transformation using $RuH_2(H_2)_2(PCy_3)_2$ under H_2. The corresponding cyclic 1*H*-2,1-benzazaboroles are cleanly formed and characterized by NMR, IR, X-ray, and HRMS. The third chapter details a mechanistic investigation on the catalytic process with the discovery of some elementary steps, the isolation of a complex featuring the substrate in transformation, and the understanding of the hydrogen transfer processes. Stoichiometric reactions, variable temperature NMR experiments and theoretical calculations will be in particular analyzed. The fourth chapter contains a study on the synthetic potential of the newly formed 1*H*-2,1-benzazaborole parent. Its reactivity in basic conditions as well as its catalytic transformation using well-established N–H bond cleavage systems are assessed. The specific case of cyclotrimerization of 1*H*-2,1-benzazaboroles into cyclic borazines is detailed in chapter 5 along with a study on their optoelectronic properties.

Le manuscrit présente une étude approfondie sur l'hydrogénation/cyclisation de cyano-aminoboranes pour la synthèse de composés BN cycliques catalysée par un complexe de ruthénium.

Le premier chapitre est une introduction bibliographique mettant en évidence l'intérêt des molécules BN cycliques et décrivant les étapes élémentaires clés dans les systèmes catalytiques impliquant l'activation de la liaison B–H et la réduction de la liaison CN menant, en particulier, à la formation d'une liaison B–N. On se concentrera sur la réactivité des complexes bis (dihydrogène), $RuH_2(H_2)_2(PR_3)_2$, avec les liaisons B–H et CN. Le deuxième chapitre présente la synthèse et la caractérisation d'une série de cyano-aminoboranes ainsi que leur transformation catalytique en utilisant $RuH_2(H_2)_2(PR_3)_2$ sous H_2. Les 1H-2,1-benzazaboroles cycliques correspondants sont formés de manière sélective et caractérisés par RMN, IR, rayons X et HRMS. Le troisième chapitre détaille l'étude mécanistique sur le processus catalytique avec la découverte de quelques étapes élémentaires, l'isolement d'un complexe comportant le substrat en transformation et la compréhension des processus d'activation des liaisons B-H et C≡N. Des réactions stœchiométriques, des expériences de RMN à température variable et des calculs théoriques seront notamment analysées. Le quatrième chapitre contient une étude du potentiel synthétique du parent 1H-2,1-benzazaborole nouvellement formé. Sa réactivité en conditions basiques ainsi que sa transformation catalytique en utilisant des procédés bien établis impliquant la rupture d'une liaison N–H sont évaluées. Le cas spécifique de la cyclotrimérisation des 1H-2,1-benzazaboroles en borazines cycliques est détaillé au chapitre 5 ainsi qu'une étude de leurs propriétés optoélectroniques.

Mots clés : Chimie de coordination – Catalyse – Boranes – Hydrogène – Activation de liaisons - Ruthénium